Università degli Studi di Palermo

AREA QUALITÀ, PROGRAMMAZIONE E SUPPORTO STRATEGICO
SETTORE STRATEGIA PER LA RICERCA
U. O. DOTTORATI

Scienze Molecolari e Biomolecolari
Dipartimento di Scienze e Tecnologie Biologiche Chimiche e Farmaceutiche (STEBICEF)
Settore Scientifico Disciplinare - SSD:CHIM/08

New indole and 7-azaindole derivatives as protein kinase inhibitors

IL DOTTORE
Dott.ssa GIOVANNA PANZECA

IL COORDINATORE
Chiar.ma Prof.ssa GIOVANNA PITARRESI

IL TUTOR
Chiar.ma Prof.ssa PATRIZIA DIANA

IL CO TUTOR
Chiar.ma Prof.ssa BARBARA PARRINO

CICLO XXXV
ANNO CONSEGUIMENTO TITOLO 2023

INDEX

1. INTRODUCTION:

1.1 The protein kinases: an overview

Nearly 2% of the human genome encodes at least 538 protein kinases. Protein kinases play important roles in regulating crucial cellular processes, such as metabolism, transcription, translation, cell cycle progression, cytoskeletal rearrangement, apoptosis, differentiation, intracellular communication, and a wide range of other cellular activities [1,2]. Kinases are a group of enzymes that transfer a phosphate group to substrates, such as proteins (tyrosine kinases, serine-threonine kinases), lipids (phosphatidylinositol kinases, sphingosine kinases), carbohydrates, and nucleic acids [3]. In this process, ATP or GTP is the phosphate group donor. Biochemically, protein kinases catalyze the following reaction:

$$MgATP^{1-} + protein{-}OH \rightarrow protein{-}O\text{-}PO_3^{2-} + MgADP + H^+$$

Although protein kinases are different in the primary amino acid sequence, they show many similarities in their tertiary structure. The function domain of the protein kinase is conservative, which usually consists of 250-300 amino acids. All protein kinases exhibit a catalytic domain that consists of a small amino-terminal N-lobe containing a β-sheet-rich structure, and a large α-helical carboxy-terminal C-lobe rich in α-helical structures, which are connected with a hinge region. ATP binds itself in the catalytic cleft between the N-terminal domain and the C-terminal domain (Figure 1) [3].

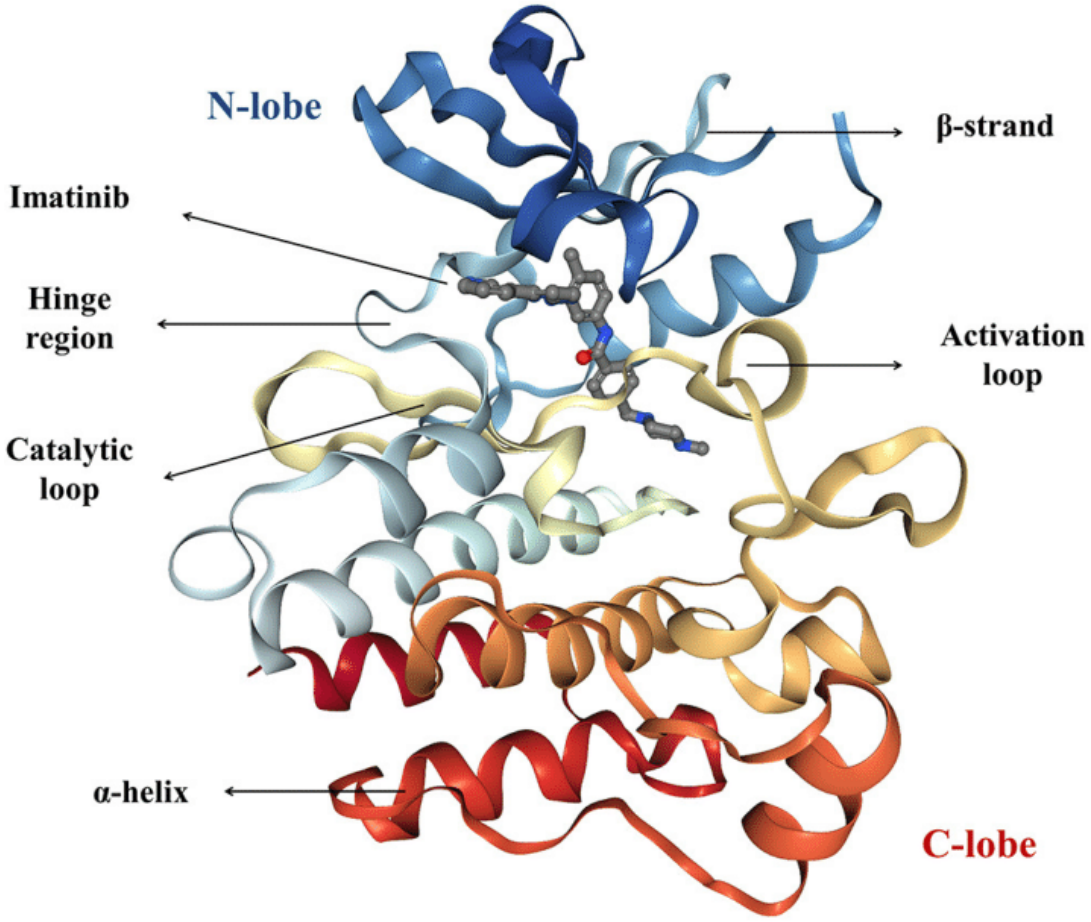

Figure 1. The crystal structure of imatinib-bound form of the Abl kinase (PDB accession code: 2HYY), colored as rainbow from N-lobe (blue) to C-lobe (red). Imatinib is represented as ball and stick [3].

Conserved residues play crucial roles in positioning ATP, stabilizing the active-conformation and in the catalytic mechanism, and they are mostly found in and around the active site but also in other parts of the protein kinase domain [4]. Almost all protein kinases possess a conserved K/E/D/D (Lys/Glu/Asp/Asp) signature that is important for the catalysis. Lysine and glutamic acid residues belong to the N-lobe, and the two aspartic acid residues are found in the C-lobe. Lysine residue binds to the α- and β-phosphates of ATP. Formation of the salt bridge between the carboxylate group of aspartic acid and the amino group of lysine stabilizes its interactions with the α- and β-phosphates, and it is required for kinase activation [3].

Protein kinases can be classified according to their **substrates**, in tyrosine kinases, serine-threonine kinases and histidine-kinases, or according to their **catalytic domains**, as AGC kinases (named after the protein kinase A, G and C families), CAMK kinases (Ca^{2+}/calmodulin-dependent protein kinases), CK1 kinases (cell kinase 1), CMGC kinases (named after set of families CDK, MAPK, GSK-3 and

CLK), STE kinases (sterile kinase), TK kinases (tyrosine kinases) and TKL kinases (tyrosine kinase-like). Most kinases act on both serine and threonine, others act on tyrosine and few kinases act on all three amino acid residues. **Serine-threonine protein kinases** phosphorylate the OH group of serine or threonine amino acid residues. These protein kinases are usually stimulated by numerous chemical signals, including cAMP/cGMP, Ca^{2+}/calmodulin, diacylglycerol. **Tyrosine kinases** that phosphorylate tyrosine amino acid residues act primarily as growth factor receptors (Figure 2) [2].

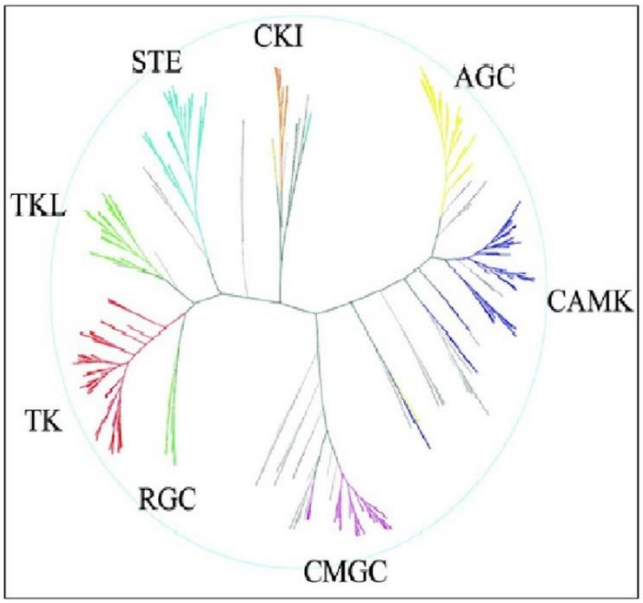

Figure 2. The "Human Kinome" as adapted from "The Protein Kinase Complement of the Human Genome". Human kinome represented as a phylogenetic tree listed in the scientific database. In addition to the eight protein kinase groups depicted in the main dendrogram, lipid, atypical and clinically relevant mutant kinases are also annotated to the human kinome. The classic kinase dendrogram includes the following eight kinase groups: TK - tyrosine kinase; TKL - tyrosine kinase-like; STE - homologs of yeast sterile 7, sterile 11, sterile kinases; CK1 - casein kinase 1; AGC - containing PKA, PKG, PKC families; CAMK - calcium/calmodulin-dependent protein kinase; CMGC - containing CDK, MAPK, GSK-3, CLK families; other - divergent kinases not represented in other groups [2].

1.2 Protein kinase inhibitors and cancer

Accumulating pharmacology and pathology evidences strongly suggest that deregulation of protein kinases activity is associated with a variety of diseases including inflammation, nervous disorders, autoimmune and cardiovascular diseases, as well as cancer. Therefore, protein kinases have become one of the most important drug targets over the past 20 years and recently also in cancer immunotherapy. The combination of protein kinase inhibitors with immune checkpoint inhibitors have achieved promising clinical results for a wide variety of cancer types [5–7]. There are 71 small

molecule protein kinase inhibitors approved by the FDA so far (see https://brimr.org/), most of them for cancer treatment, but also against metabolic and autoimmune disorders (Figure 3) [8,9].

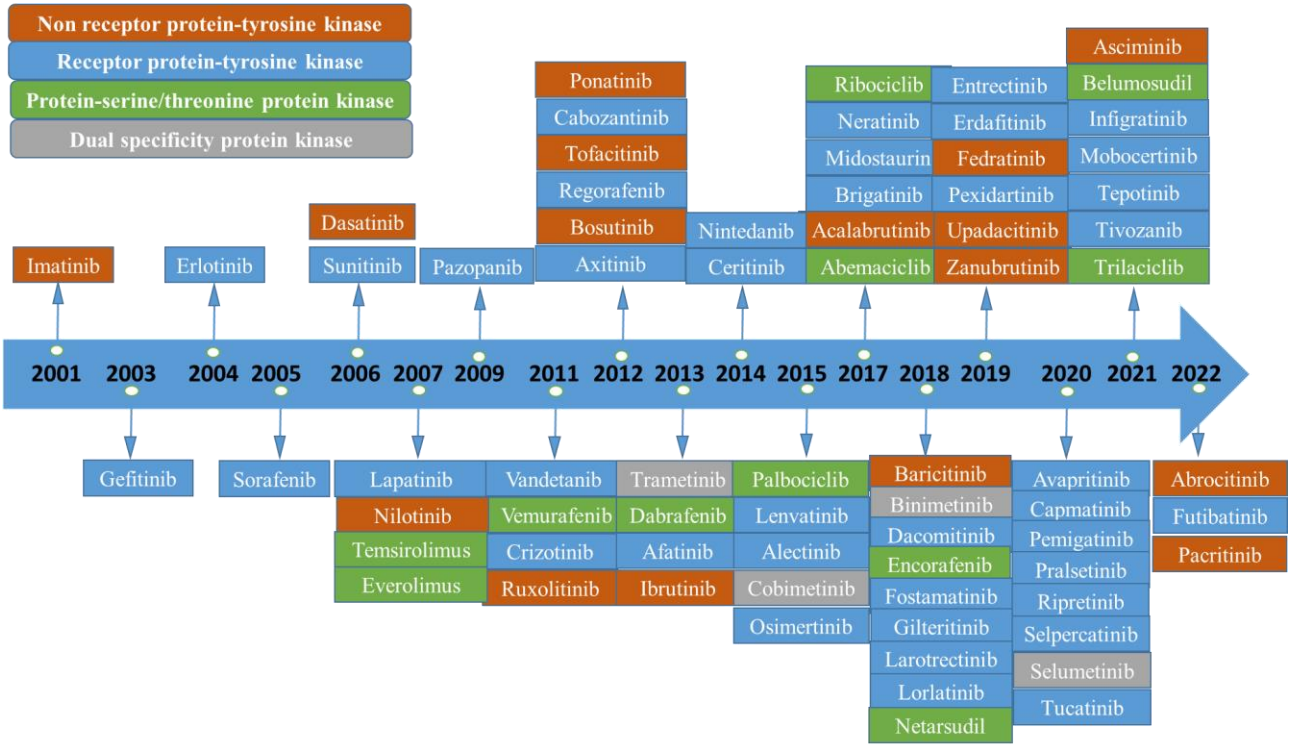

Figure 3. FDA-approved small molecule protein kinase inhibitors from 2001 to 2022.

There are 4 main categories of different kinases implicated in human cancer that can be vaguely categorized based on their hallmark roles: cytoplasmic tyrosine kinase (CTK), serine-threonine kinase (S/T Kinase), lipid kinase (LK), receptor tyrosine kinase (RTK) (Figure 4) [10].

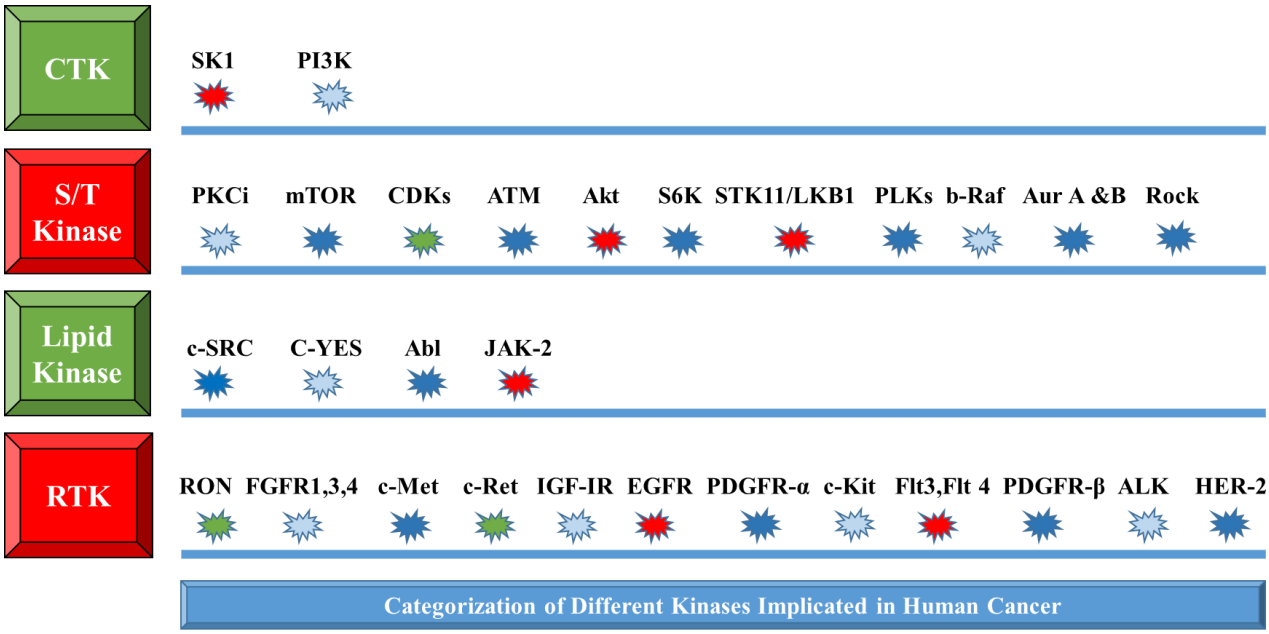

Figure 4. Categorization of different kinases implicated in human cancer. CTK: cytoplasmic tyrosine kinase, S/T Kinase: serine/threonine kinase, LK: lipid kinase, RTK: receptor tyrosine kinase. SK1: Sphingosine kinase 1, PI3K: phosphoinositide 3-kinase, PKCi: Protein kinase Ci, mTOR: mammalian target of rapamycin, CDKs: cyclin-dependent kinases, ATM: Ataxia telangiectasia mutated, Akt: protein kinase B, S6K: ribosomal protein S6 kinase, STK11/LKB1: Serine/threonine kinase 11 or liver kinase B1, PLKs: Polo-like kinases, b-Raf: B-Raf proto-oncogene, Aur A & B: Aurora Kinase A & B, c-SRC: Proto-oncogene tyrosine-protein kinase Src, c-YES: c-Yes proto-oncogene (pp62c-Yes), Abl: Abelson murine leukemia viral oncogene homolog 1, JAK-2: Janus kinase 2, RON: Recepteur d'origine nantais, FGFRs: Fibroblast growth factor receptors, c-Met: c-MET proto-oncogene, c-Ret: c-RET proto-oncogene, IGF-IR: Insulin-like growth factor 1 receptor, EGFR: Epidermal growth factor receptor, PDGFR-α: Platelet-derived growth factor receptor α, c-Kit: proto-oncogene c-Kit or Mast/stem cell growth factor receptor, Flt3,Flt-4: Fms-like tyrosine kinase 3, 4, PDGFR-β: Platelet-derived growth factor receptor β, ALK: Anaplastic lymphoma kinase, HER-2: human epidermal growth factor receptor-2 [10].

In Figure 5 the phylogenetic map of the human kinome is shown, demonstrating the development and US FDA approval of small molecules as tyrosine and serine-threonine kinase inhibitors for the treatment of a variety of solid and hematologic malignancies [2,9,11].

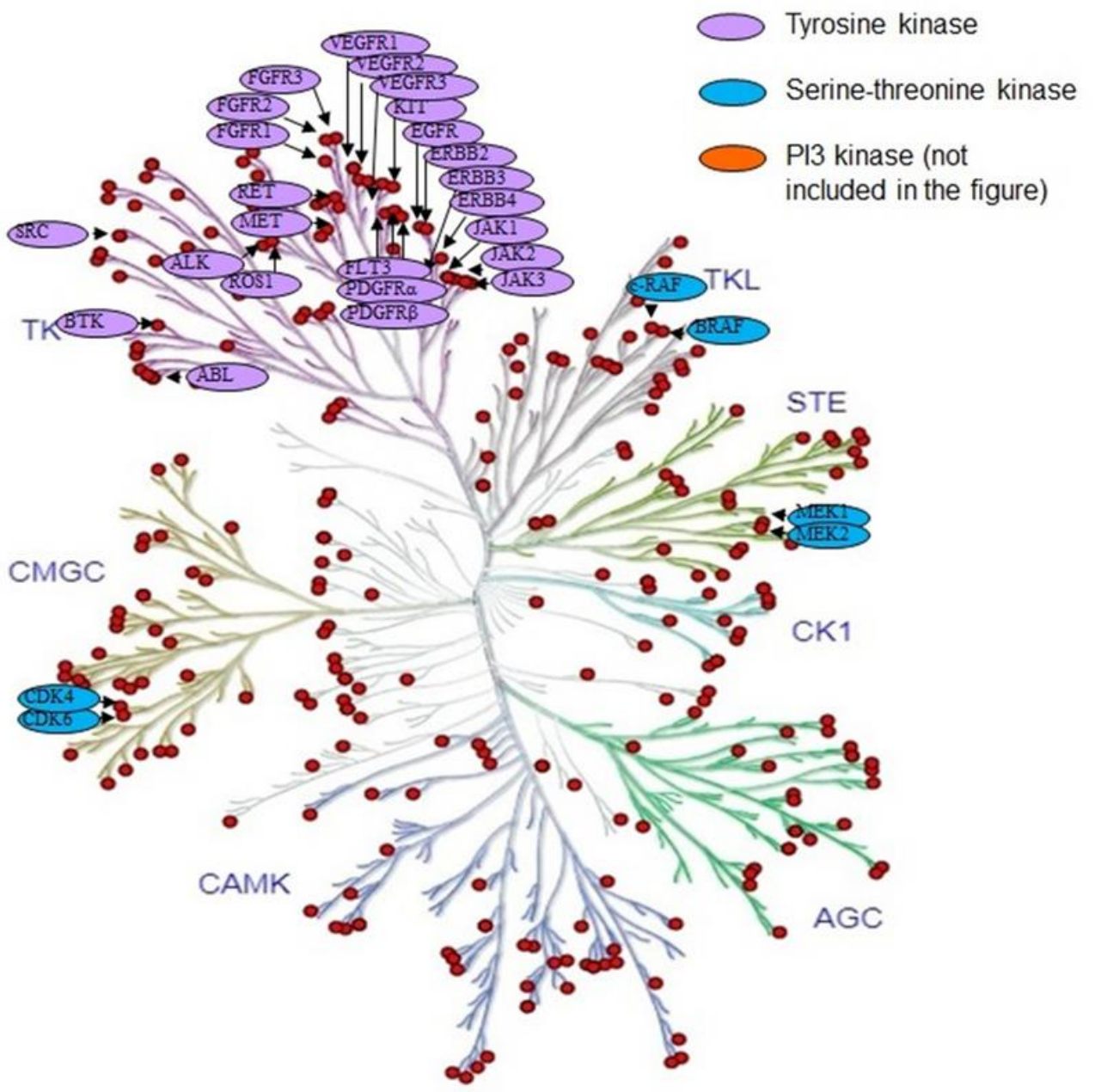

Figure 5. The phylogenetic map of the human kinome demonstrating development and US FDA approval of small molecules as tyrosine and serine-threonine kinase inhibitors for the treatment of a variety of solid and hematologic malignancies. Other kinome family members under active clinical investigation include NTRK-fusion activated kinase, CDK8, and ERK1/2 [2].

The development of kinase inhibitors for the treatment of human cancers started in mid 1970s. In 1978, the first oncogene was found to be a protein kinase. This discovery was supported in 1981 when it was found that tumor-promoting phorbol esters caused hyperactivation of protein kinase C (PKC). In the coming years, naphthalene sulphonamides, the first protein kinase inhibitors were synthesized and served as a basic design for developing further molecules. In 1984 staurosporine, an antifungal drug was identified as a nanomolar inhibitor of PKC. This drug was later used as a lead compound for

the synthesis of potential PKC inhibitors. In 2001 FDA-approved the first protein kinase inhibitor, **imatinib** (Gleevec), for treatment of chronic myeloid leukemia. Following the approval of imatinib additional inhibitors were introduced into the clinic (Figure 3) [8,10,12].

Among the 71 FDA-approved drugs, 11 target serine-threonine protein kinases, 4 are directed against dual specificity protein kinases (MEK1/2), 16 block non receptor protein-tyrosine kinases, and 40 target receptor protein tyrosine kinases. The data indicate that 58 of these drugs are prescribed for the treatment of neoplasms (49 against solid tumors including breast, lung, and colon, five against non-solid tumors such as leukemia, and four against both solid and non-solid tumors: acalabrutinib, ibrutinib, imatinib, and midostaurin). All the FDA-approved drugs are orally effective except for netarsudil, temsirolimus, and the newly approved trilaciclib. At least 25 of the approved medications are multikinase antagonists. The blockade of multiple protein kinases has potential advantages and disadvantages. Although the inhibition of two or more targets could enhance the therapeutic efficacy, on the other hand, multikinase inhibitors may act on off-target kinases leading to various side effects and contribute to adverse events [6]. Most protein kinase inhibitors reported to date are designed to bind to the ATP-binding site located in a deep cleft between N- and C-terminal lobes of the protein kinase catalytic domain, by forming hydrogen bond interactions with the hinge region that connects the two lobes. Most protein kinase inhibitors bind to the active conformation of the kinase (known as type I inhibitors); however, some inhibitors bind to the inactive state of the kinase, which has a deep allosteric pocket generated by large conformational changes in kinase [1].

This PhD project is focused on inhibitors acting on CDKs and GSK-3, protein kinases implicated in carcinogenesis and in progression of cancer.

1.2.1 CDK inhibitors as anticancer agents

Cyclin dependent kinases (CDKs) are serine-threonine protein kinases that regulate the progression of the cell cycle through the different phases. To become catalytically active, CDKs associate with specific cyclins during the different phases of the cell cycle. For example, CDK4/6-cyclin D and CDK2/cyclin E complexes sequentially phosphorylate the retinoblastoma (Rb) protein leading to its inactivation, thus facilitating progression through the G1/S checkpoint; CDK1 forms complexes either with cyclin A or cyclin B ensuring G2/M phase transition.

Tumor progression is frequently associated with genetic or epigenetic events resulting in over-expression of cyclins, constitutive activation of CDKs, loss of CDK inhibitors (such as p27 and p16), and mutations of the retinoblastoma protein. These events lead to cell cycle deregulation conferring a selective growth advantage to cancer cells.

Based on the sequence similarity, CDKs belong to CMGC kinase group. In humans, there are more than 10 CDKs and 10 cyclins involved in regulating cell division. However, CDK activity is not restricted to cell cycle proteins. CDK7/cyclin H and CDK9/cyclin T, for example, promote phosphorylation of the carboxy-terminal domain of RNA polymerase II, facilitating initiation and elongation of RNA transcription, respectively [2,13]. Different CDK antagonists are or have been in clinical phase for the treatment of a wide variety of malignancies (Figure 9), and three drugs were approved by FDA for the treatment of advanced breast cancers: palbociclib, ribociclib and abemaciclib (Figure 6) [14–16]. These drugs have IC_{50} values for CDK4/6 in the low nanomolar range. They bind in the cleft between the N-terminal and C-terminal lobes of the CDKs and inhibit ATP binding, forming hydrogen bonds with hinge residues.

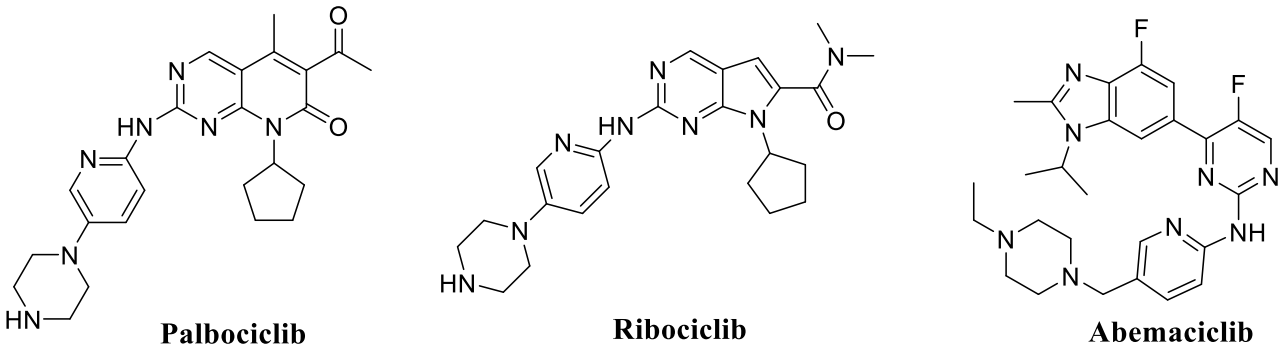

Figure 6. FDA-approved CDK inhibitors for cancer.

Palbociclib (Figure 6) is an amino-pyrido[2,3-*d*]pyrimidine derivative that initially received accelerated FDA approval for the HR-positive, HER2-negative advanced or metastatic breast cancer in 2015 in combination with letrozole [2]. The inhibitory potency of the drug has been tested against a variety of protein kinases, but its therapeutic targets (CDK4/6) are the only enzymes that are inhibited by low concentrations of the agent [15]. Palbociclib inhibits CDK4-cyclin D1 (IC_{50} value of 11 nM), CDK4-cyclin D3 (IC_{50} value of 9 nM), and CDK6-cyclin D2 (IC_{50} value of 15 nM). It is not effective against CDK2-cyclin E2, CDK2-cyclin A, and CDK1-cyclin B (IC_{50} values exceeding 10 μM) [14].

Ribociclib (Figure 6) is a 2-amino-pyrrolo[2,3-*d*]pyrimidine derivative, CDK4/CDK6 dual kinase inhibitor that was approved by the FDA in 2017 for the treatment of the post-menopausal women with HR-positive / HER2-negative advanced or metastatic breast cancer. This drug inhibits CDK4 and CDK6 with IC_{50} values of 10 and 39 nM, respectively. The inhibitor potency against CDK1 and CDK2 is significantly lower (> 50 μM) [2,14,15].

Abemaciclib (Figure 6) is an amino-pyrimidine-benzimidazole derivative, CDK4/CDK6 kinase inhibitor with more potent activity against CDK4. It was approved by FDA in 2017 for the treatment of the post-menopausal women with HR-positive, HER2-negative advanced or metastatic breast cancer in combination with fulvestrant as a frontline therapy and as monotherapy in patients who had progressed on endocrine therapy or chemotherapy in the setting of metastatic disease [2,15].

Cocrystal structures of palbociclib (PDB ID: 5L2I), ribociclib (PDB ID: 5L2T), and abemaciclib (PDB ID: 5L2S) with CDK6 revealed similar binding modes, where the aminopyrimidine moiety forms two hydrogen bonds with the backbone of valine (Val101). In addition, carbonyl group of palbociclib and ribociclib forms hydrogen bond with aspartic acid (Asp163), whilst imidazole of abemaciclib binds lysine (Lys43). The positively-charged piperazine ring of each drug is stabilized via direct interactions with a solvent-exposed ridge consisting of aspartic acid (Asp104) and threonine (Thr107) (Figure 7) [13,17,18]. Furthermore, the structure of CDK4-cyclin D3 bound to abemaciclib has also been recently reported (Figure 8, PDB 7SJ3).

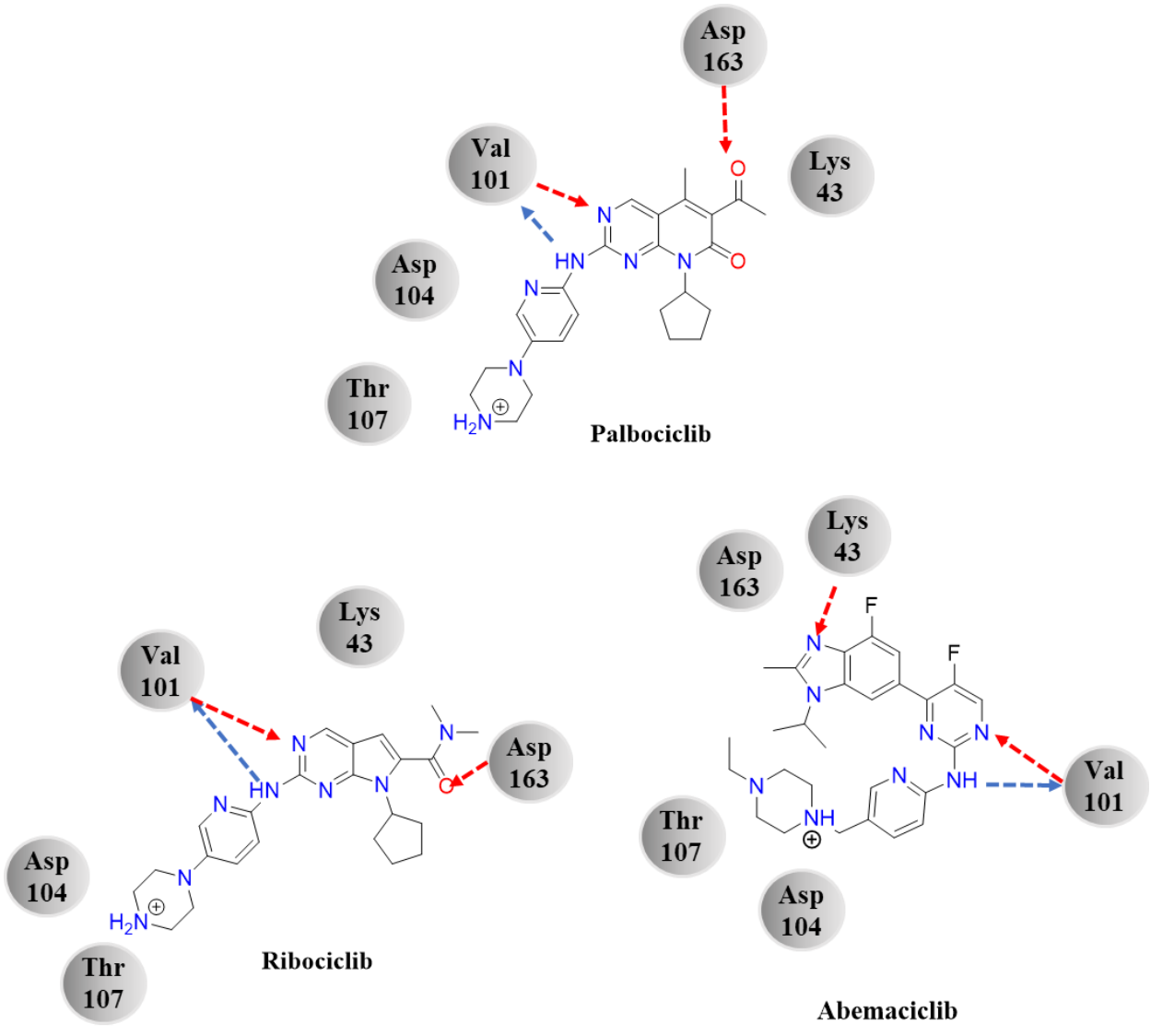

Figure 7. Binding modes for third-generation drugs. Structure of CDK6 bound to: palbociclib, ribociclib, and abemaciclib, with the binding site in a common orientation (PDB 5L2I, palbociclib; 5L2T, ribociclib; 5L2S, abemaciclib). Hydrogen bonds donor interactions are indicated by blue arrows, hydrogen bonds acceptor interactions are indicated by red arrows.

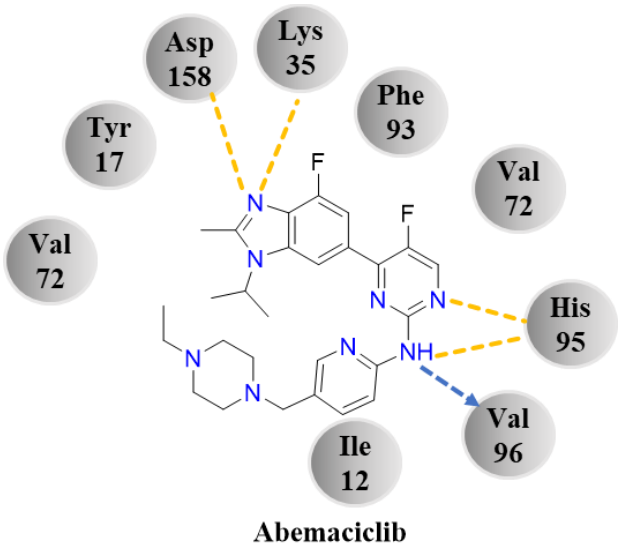

Figure 8. PDB 7SJ3: Structure of CDK4-Cyclin D3 bound to abemaciclib. Hydrogen bonds donor interaction is indicated by blue arrow, ionic interactions are indicated by yellow lines.

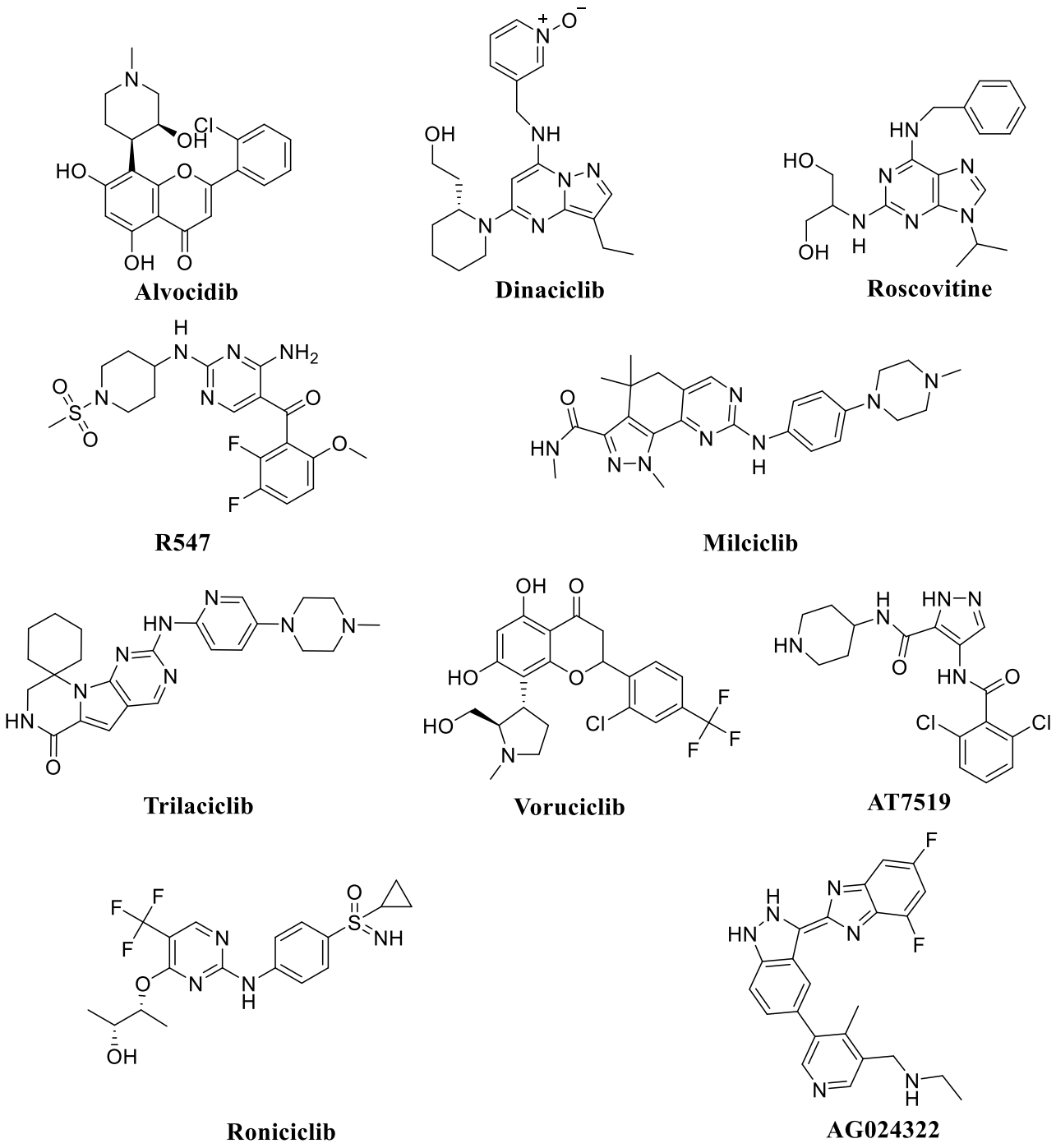

Figure 9. Representative pan-CDK inhibitors that are or have been in clinical phase.

Alvocidib (flavopiridol) (Figure 9) is a piperidine-chromenone derivative that is not FDA-approved, but it has been in clinical trials for breast, endometrial, and several other cancers and hematological malignancies. It targets CDK9 (IC_{50} = 3.2 nM), CDK4 (IC_{50} = 3.2 nM) and other CDKs (CDK1/2/3/6/7), with IC_{50} values of 1–2 orders of magnitude higher [14]. Today an oral phosphate prodrug of alvocidib (TP-1287) is in recruiting status for phase I study in patients with advanced solid tumors (NCT03604783) [19].

Dinaciclib (SCH 727965) (Figure 9) is a pyrazolopyrimidine derivative that is not FDA-approved but it has been in clinical trials for the treatment of breast and pancreatic cancer and several leukemias. This drug is a CDK inhibitor with IC_{50} values of 3.2, 1, 1, and 4 nM for CDK1/2/5/9, respectively [14]. Compared to flavopiridol, the first CDKs inhibitor to enter in clinical trials, dinaciclib exhibits superior CDK inhibitory activity with a better side effects profile. Dinaciclib has shown promising antitumor activity in preclinical studies by *in vitro* growth inhibition of a broad spectrum of cancer cell lines with median IC_{50} of 11 nM. Studies demonstrate that dinaciclib inhibits tumor growth in triple negative breast cancer (TNBC) cells from patient-derived xenografts (PDXs) and cell lines (BT549, HCC1806, MDA-MB-231), by arresting cell cycle at G2/M phase and inducing apoptosis [20]. Additionally, it produces caspase-independent downregulation of messenger RNA and protein expression of the antiapoptotic protein myeloid cell leukemia 1 (MCL1), which is essential for chronic lymphocytic leukemia (CLL) cell survival. In murine xenograft models, it exhibited a superior therapeutic index compared to flavopiridol [13,20–23]. Dinaciclib is currently in a recruiting status for phase I trials in combination with veliparib in treating patients with advanced solid tumors (NCT01434316).

Roscovitine (seliciclib) **(**Figure 9) is a member of the family of 2,6,9-trisubstituted purines, ATP competitive per CDKs. Roscovitine shows IC_{50} values below 1 µM for CDK1, CDK2, CDK5, CDK7, and CDK9; and IC_{50} values in the 1–40 µM range for few other kinases. Roscovitine has been in clinical phase for treatment of non-small cell lung cancer, metastatic breast cancer, and other advanced solid tumors [24–26]. Today it is in clinical trials (in active, not recruiting status) for Cushing disease (NCT03774446).

R547 (Figure 9) is a diaminopyrimidine with selective inhibitory activity against CDKs, such as CDK1,2,3,5,6 with IC_{50} values in nanomolar range. This inhibitor has been in phase I clinical trials for the treatment of solid tumors [27].

Milciclib (PHA-848125) (Figure 9) is a pyrazoloquinazoline, multi-CDK inhibitor with IC_{50} values in nanomolar range for CDK1,2,4,5,7. It has been in phase II clinical trial for hepatocellular carcinoma [28,29]. It is currently in clinical phase (not yet recruiting status) for advanced NSCLC in combination with gemcitabine (NCT05651269).

Trilaciclib, **AT7519**, and **voruciclib** (Figure 9) are CDK inhibitors that are currently in clinical trials for the treatment of a variety of cancers [14].

AG024322 (Figure 9) is an ATP competitive inhibitor having low kinome selectivity and broad CDK family interactions. This drug has been in phase I clinical trial for neoplasms and non-Hodgkin lymphoma [29,30].

Roniciclib (Figure 9) is an anilino-pyrimidine CDK multikinase inhibitor that has been in clinical trials for the treatment of ovarian cancer, small cell lung cancer, and thyroid cancer [14].

Cyclin-dependent kinase 1 (CDK1) plays a pivotal role for cell cycle progression. Numerous investigations have demonstrated that CDK1 dysregulation results in aggressive tumor development, chromosomal instability, and enhanced proliferation of cells. The dysregulation of CDK1 in cancer is more significant as compared to other kinases because it is the universal master kinase that is being conserved from yeast to humans. Additionally, CDK1 overexpression has been found in various cancer types, such as esophageal adenocarcinoma, gastric cancer, ovarian cancer, oral squamous cell carcinoma, colorectal cancer, liver cancer, and breast cancer, thus the development of inhibitors will have application across several malignancies. For this CDK1 has emerged as promising target for the treatment of cancer [31]. Although many pan-CDK inhibitors are under clinical studies, to date there is no molecule FDA-approved as CDK1 inhibitor. Dinaciclib is one of the most potent CDK1 inhibitors, with remarkable pharmacokinetic properties and safety profile, but as already mentioned, it also inhibits CDK2, CDK5, and CDK9 at nanomolar concentrations [29,31–33]. **CDK1 inhibitors** bind the ATP-active site showing hydrogen bond interactions in the hinge region with the leucine residue (Leu83) (donor-acceptor) and with glutamic acid (Glu81) (donor-acceptor) (Figure 10) [28].

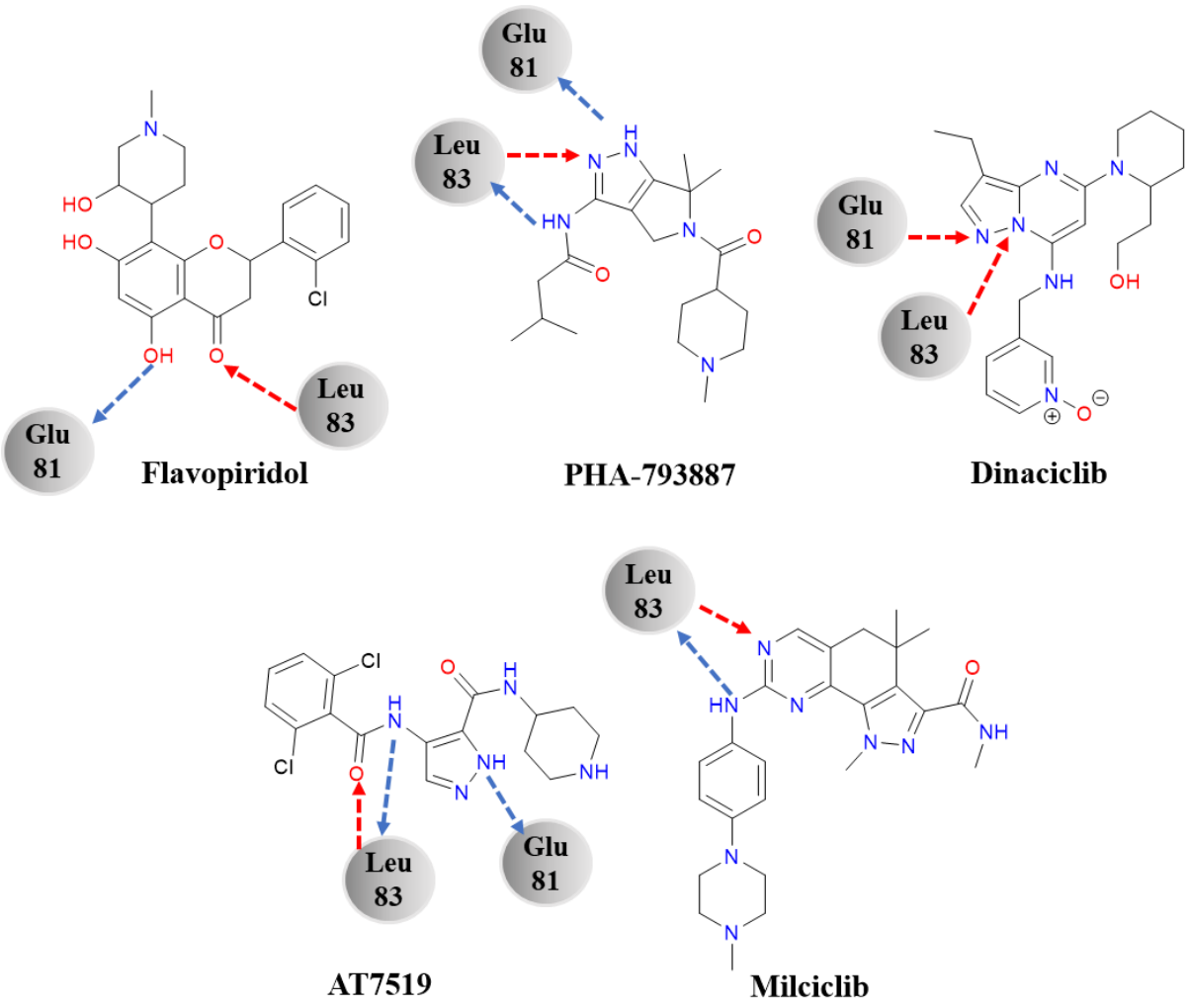

Figure 10. Structures of CDKs inhibitors and proposed binding mode of CDK1 with flavopiridol, PHA-793887, dinaciclib, AT7519, milciclib. Hydrogen bonds donor interactions are indicated by blue arrows, hydrogen bonds acceptor interactions are indicated by red arrows.

1.2.2 GSK-3 inhibitors as anticancer agents

Glycogen synthase kinase 3 (GSK-3) is a ubiquitously expressed serine-threonine protein kinase. In mammals, there are two isoforms of GSK-3, GSK-3α and GSK-3β. The most studied form of GSK-3 is GSK-3β, which has two main domains: a β-strand domain present at the N-terminus, and an α-helical domain present at the C-terminus, where protein kinase activity is located. An ATP-binding site is present at the interface of the two domains. GSK-3β activity is regulated by phosphorylation at two different sites. Phosphorylation of the serine 9 (Ser9) site inactivates GSK-3β, whereas phosphorylation at the tyrosine 216 (Tyr216) site increases its catalytic activity [34]. GSK-3, initially described as a key enzyme involved in the regulation of glycogen synthesis, is now known to regulate a diverse array of functions in many cellular processes, such as apoptosis, tumor growth, cell invasion, and metastasis [34].

Pre-phosphorylation of substrates is required for the subsequent phosphorylation by GSK-3, with only few exceptions of non-phosphorylated substrates. GSK-3β recognizes a standard amino acid sequence S/T-X-X-X-S/T in its target, inducing a functional conformational change that assists the target positioning in the active catalytic domain of the protein kinase [35]. The pre-phosphorylation of substrates is one of the mechanisms of GSK-3 regulation. In addition, GSK-3 phosphorylation, subcellular localization, and the formation of complexes containing GSK-3 are also used for regulation of GSK-3 functions. Studies have highlighted the role of GSK-3β in different oncogenic pathways, such as PI3K/Akt, Wnt β-catenin and NF-κB signaling cascades. There is scientific evidence that GSK-3β is overexpressed in various tumor types including colon, liver, ovarian, and pancreatic cancer. GSK-3 inhibitors may be appropriate for treatment of these types of tumors in which this protein kinase acts as a tumor promoter [36,37]. Notably, its aberrant expression was found in pancreatic cancer specimens with altered oncogenic KRAS status. Considering that KRAS is mutated in approximately 95% of pancreatic cancer, GSK-3β emerges as a promising new target in the war against pancreatic ductal adenocarcinoma [38].

Most of GSK-3β inhibitors, can also exert inhibitory effects towards cyclin-dependent kinases (CDKs) including CDK1/CDK2, since the amino acid sequence of GSK-3β has high homology to CDKs [39]. Therefore, GSK-3β inhibitors may indirectly impact on cell cycle regulation by CDK1-2 inhibition and enhance the antiproliferative outcome. The modulation of GSK-3β activity may form a valuable strategy to control diseases like cancer [34]. To date, no GSK-3β inhibitor has been approved by the FDA for the cancer. However, several small molecules, containing different heterocyclic rings are also under investigation (Figure 11). GSK-3 inhibitors can be divided into three main categories: non-ATP competitive inhibitors, ATP competitive inhibitors, and substrate-competitive inhibitors [34,40].

LY2090314 (Figure 11), is an ATP competitive inhibitor, which can inhibit both GSK-3 isoforms. Preclinical studies in breast cancer, non-small cell lung cancer and mesothelioma have been conducted and confirmed the antitumor potential of LY2090314 [41,42]. Moreover, it was found for the first time, in a neuroblastoma (NB) model, that LY2090314 inhibited the growth of both human MYCN amplified and non-amplified NB cells. LY2090314 has also been evaluated *in vivo* using an orthotopic xenograft nude mouse model of pancreatic cancer. LY2090314, given in combination with nab-paclitaxel, significantly prolonged the median survival of mice. However, LY2090314 and nab-paclitaxel as single agents were completely ineffective [34].

The ATP competitive inhibitor **9-ING-41** (Figure 11) has been studied as single agent or in combination with chemotherapeutic drugs in different types of solid tumors, as well as in haematologic malignancies, such as lymphoma [34].

CHIR99021 (Figure 11) is an aminopyrimidine derivative that is an ATP competitive inhibitor of both GSK-3α (IC_{50} = 10 nM) and GSK-β isoforms (IC_{50} = 6.7 nM). CHIR99021 was evaluated as a potential drug for use in epithelioid sarcoma (ES). Researchers found that CHIR99021 induced cell cycle arrest, mitotic catastrophe (MC) and autophagic response, resulting in reduced cell proliferation [43].

Tideglusib (Figure 11), a non-ATP competitive inhibitor, has been tested in xenograft and PDX murine models of human glioblastoma, resulting in reduction of colony formation and consequently increase in number of glioblastoma cancer cells in phase G0/G1 [44]. Moreover, it can reduce the phosphorylation of tau protein in Alzheimer disease, increasing the level of proapoptotic proteins in murine models of human neuroblastoma [45].

AR-A0-14418 (Figure 11), is an ATP competitive and selective GSK-3β inhibitor and preclinical studies have demonstrated its ability to reduce the proliferation and to increase the apoptosis in gastric cancer, synovial sarcoma, and fibrosarcoma cells *in vitro* and *in vivo* [46].

TWS119 (Figure 11) is a specific inhibitor of GSK-3β which has been shown to inhibit cell proliferation and induce the apoptosis of human alveolar rhabdomyosarcoma cells, while it regulates epithelial-mesenchymal transition (EMT) and cancer stem cell (CSC) properties in TNBC [34].

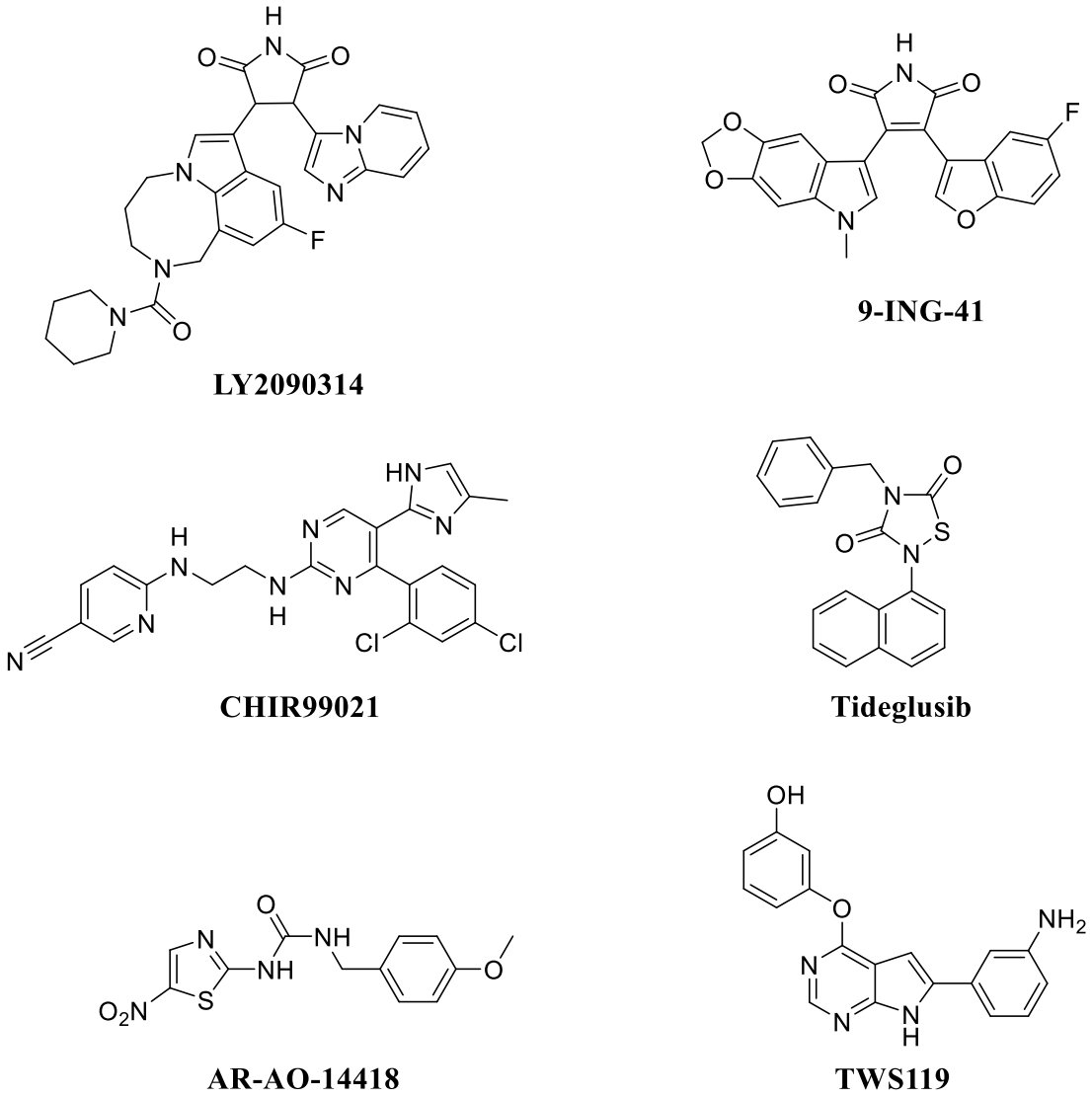

Figure 11. Representative GSK-3β inhibitors under investigation.

1.2.3 Indole and 7-azaindole scaffold in serine-threonine kinase inhibitors with anticancer activity

Most protein kinase inhibitors have been developed as ATP competitors interacting with the hinge region in ATP binding sites of protein kinases. 7-azaindole and indole have been found as privileged fragments in protein kinase inhibitors, such as serine-threonine kinases inhibitors [47,48]. In particular the 7-azaindole moiety is able to interact with the hinge region through two hydrogen bonds. As shown in Figure 12, the pyridine N atom and the pyrrole NH in the 7-azaindole ring serve as a hydrogen bond acceptor and donor, respectively. In addition, 7-azaindole has five modification sites where various substituents can be readily attached [1].

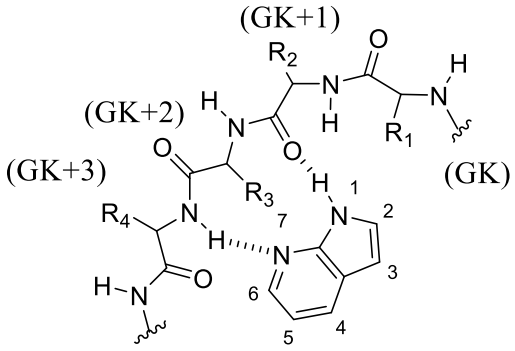

Figure 12. Hydrogen bonds between 7-azaindole fragment and the hinge region of a protein kinase are indicated by dashed line.

Comprehensive survey of a drug discovery revealed that more than 90 kinds of protein kinases have been shown sensitive to 7-azaindole-based protein kinase inhibitors, providing a broad coverage of the human kinome as shown in Figure 13 [49–52].

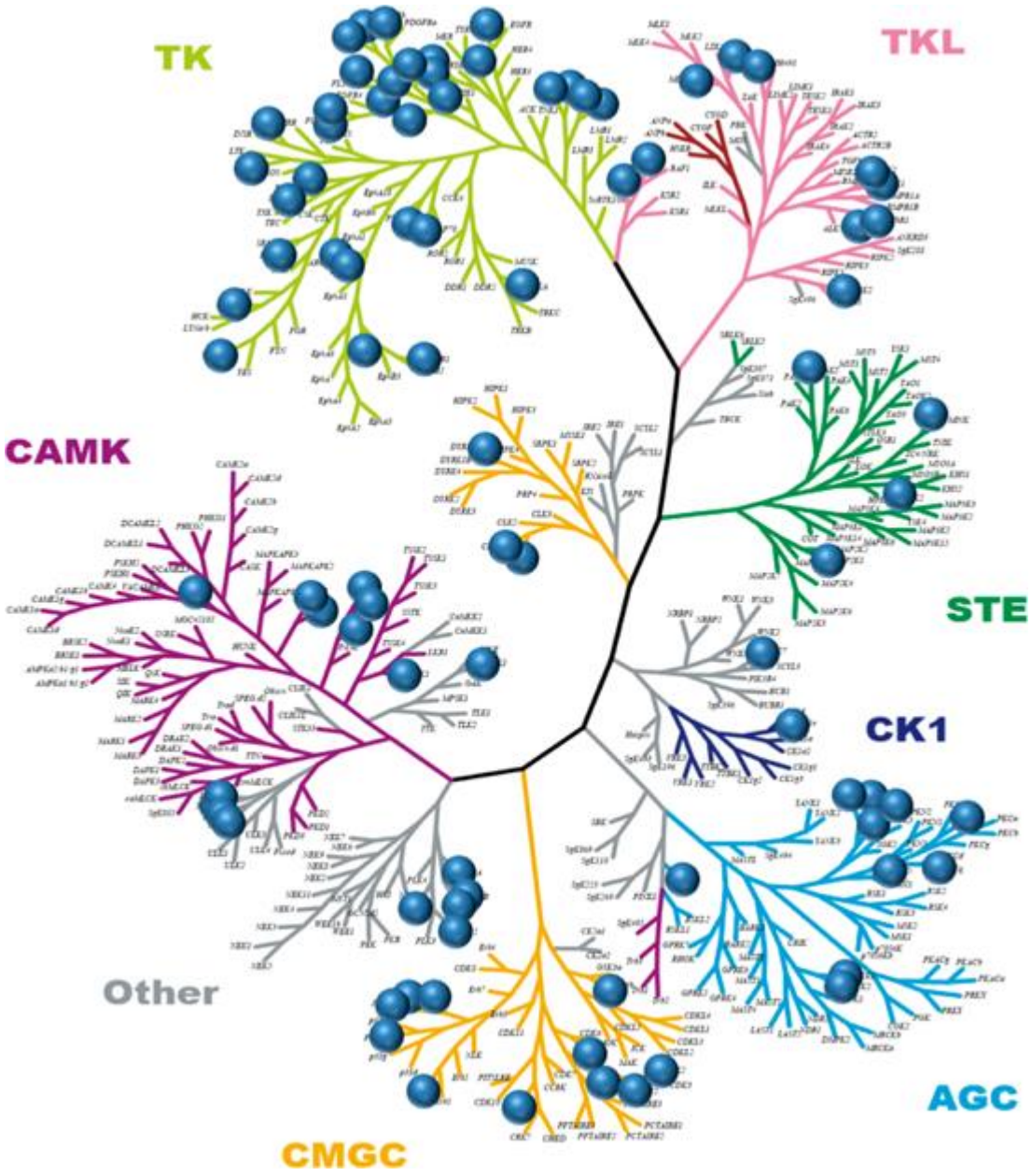

Figure 13. 7-Azaindole scaffold provides broad coverage of the human kinome [1].

Analysis of the protein kinase-inhibitors cocrystal structures revealed that the 7-azaindole moiety binds to protein kinases with different binding modes, which can be classified into three groups such as “normal” (the 7-azaindole binds to the hinge as most frequently seen), “flipped” (the 7-azaindole moiety is flipped 180° with respect to “normal” binding mode), and “non-hinge” (the 7-azaindole binds at a different site from the hinge region; Figure 14). “Normal” and “flipped” binding modes can form bidentate hydrogen bonds with the backbone amides of hinge amino acid residues, GK+1 (next to the gatekeeper residue) and GK+3 residues. Namely, the carbonyl oxygen of GK+1 interacts as a hydrogen bond acceptor while backbone N–H of GK+3 acts as a hydrogen bond donator in “normal” binding mode. On the other hand, in “flipped” binding mode, the GK+3 residue acts as both hydrogen

bond donor and acceptor. On the other hand, in the case of "non-hinge" binding mode, the 7-azaindole moiety binds at a different site from the hinge region, because such compounds have another hinge-binding motif in addition to 7-azaindole. The observation that both "normal" and "flipped" binding modes are possible in tyrosine kinases and in serine-threonine protein kinases suggests that the binding mode is not dependent on protein kinase structural features. Rather, it would depend on the ligand structure, because 2-substituted derivatives of the 7-azaindole give only "flipped" binding mode [1].

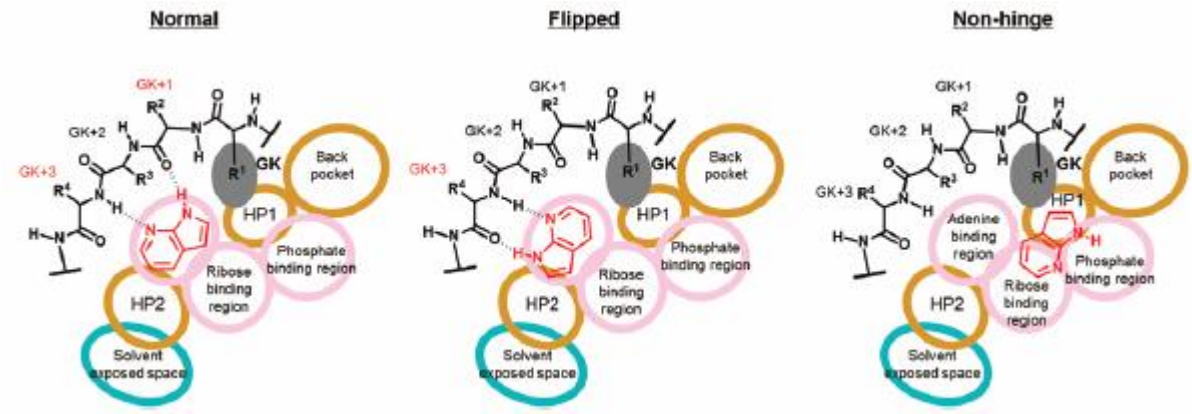

Figure 14: 7-azaindole group can bind to kinases with different binding modes HP1: hydrophobic region 1; HP2: hydrophobic region 2; GK: gatekeeper amino acid residue [1].

Figure 15 shows representative protein kinase inhibitors bearing several substituents at various positions of the 7-azaindole moiety. In particular, **vemurafenib** is the first FDA-approved 7-azaindole-based protein kinase inhibitor (for the inhibition of B-RAF kinase, a serine-threonine kinase), for the treatment of melanoma [53]. It is also currently in clinical phase for various cancers, like pancreatic cancer, leukemia and colorectal cancer; whilst compounds **GSK1070916, PLX-8394, Y-39983** have been in clinical phase for advanced solid tumors [1].

The 7-azaindole clinical candidate **AZD6738** (Figure 15) is shown to inhibit growth of ataxia telangiectasia mutation (ATM) deficient xenografts via ataxia telangiectasia mutated and Rad3 related (ATR) kinase inhibition mechanism. ATR is a serine-threonine-specific protein kinase that is involved in sensing DNA damage and activating the DNA damage checkpoint, leading to cell cycle arrest in eukaryotes. ATR is activated in response to persistent single-stranded DNA, which is a common intermediate formed during DNA damage detection and repair [54].

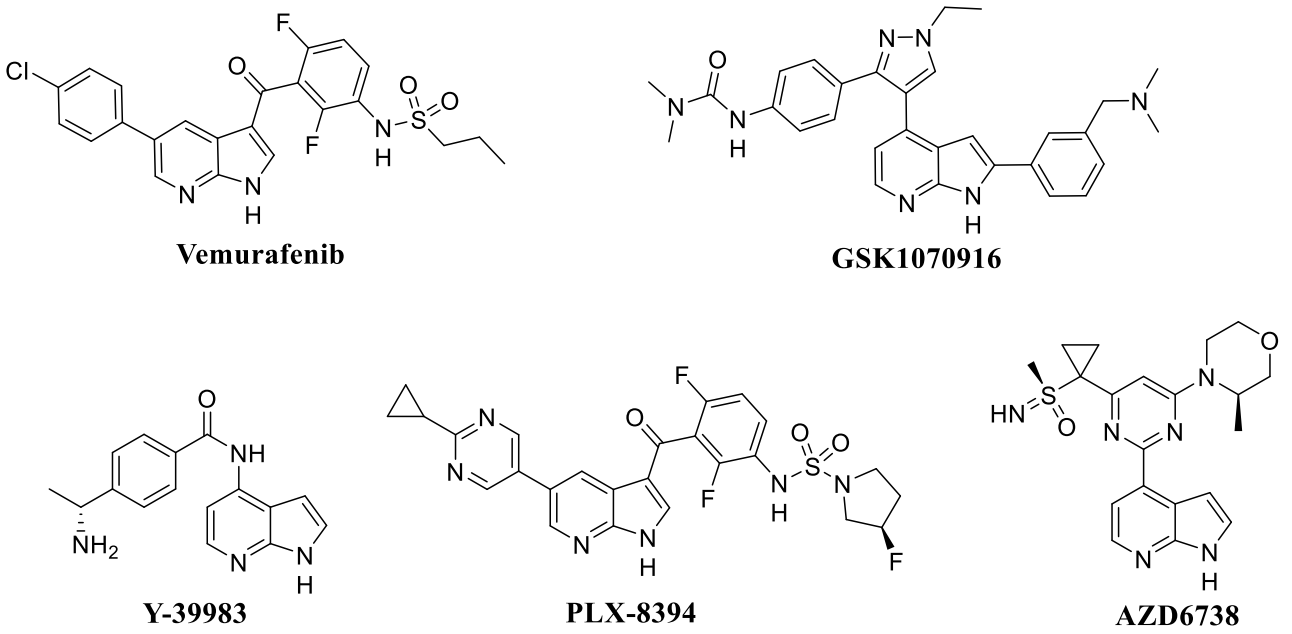

Figure 15. Representative 7-azaindole-based serine-threonine kinase inhibitors that are or have been in clinical phase.

Moreover, **2,5-disubstituted-7-azaindole 1** (Figure 16) has shown inhibition activity against multiple kinases (34 out of 104 kinases tested) and broad antiproliferative activity against various cancer cells including PC-3, Caki-2, MDA-MB-231 and NCI-H1975. A study reports that substitution of one of the amino groups in anti-mitotic drug cisplatin with 1-methyl-7-azaindole moiety affording compound **2** (*cis*-[$PtCl_2(NH_3)$(1-methyl-7-azaindole)]) (Figure 16), increased efficiency and selectivity for tumor cells in cisplatin resistant cancer cells, and this was associated with increased level of cellular DNA platination by the 7-azaindole moiety [54].

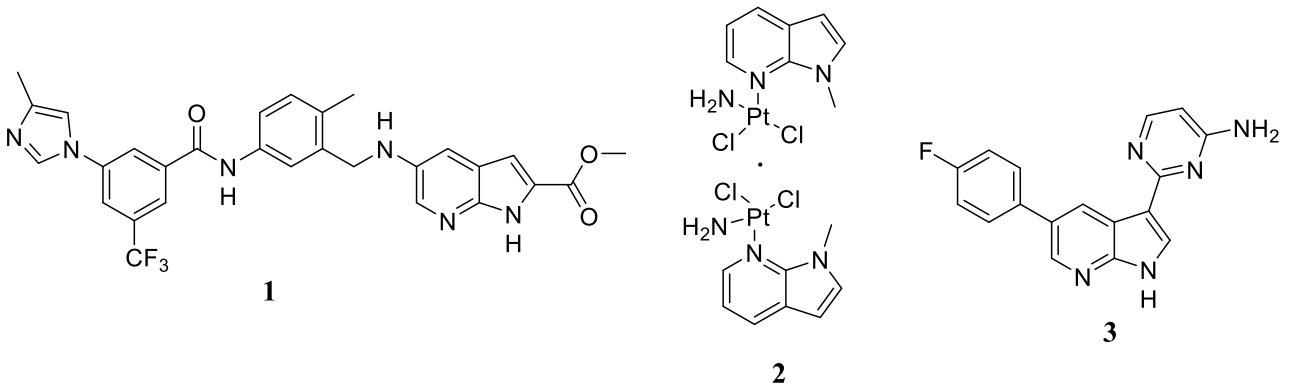

Figure 16. Representative 7-azaindole-based serine-threonine kinase inhibitors.

3,5-disubstituted-7-azaindole 3 (Figure 16) is CDK2 and CDK9 inhibitor eliciting anti-tumor activity in triple negative breast cancer mouse model [54].

Among the indole-based serine-threonine kinase inhibitors, oxindole–indole conjugates are reported as effective antitumor agents with potential **inhibitory activity against CDK4**. The most potent conjugates **4** and **5** (Figure 17) exhibited significant CDK4 inhibitory activity with IC_{50} values of 1.82 µM and 1.26 µM respectively, and *in vitro* antiproliferative activity against MCF7 and MDA-MB231 with IC_{50} values in the micromolar range [55]. Their molecular docking on CDK4 revealed that the indole structure is securely situated in a hydrophobic sub-pocket, forming a H-bonding interaction via NH with glutamic acid residue (Glu94) and hydrophobic interactions with the amino acids isoleucine (Ile12), valine (Val20), and glutamine (Gln98) (Figure 17) [55,56].

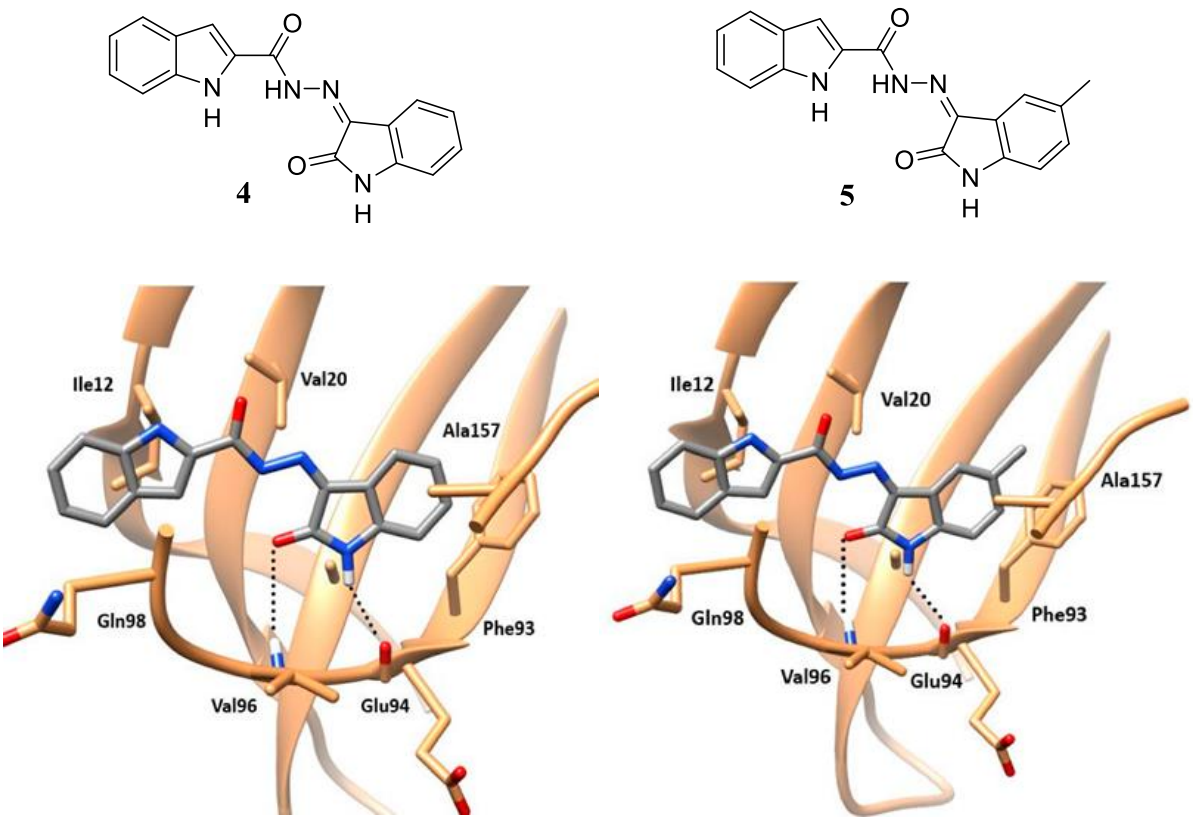

Figure 17 Indole-based CDK4 inhibitors and their binding poses [55].

Indole scaffold has also been found in **Aurora kinases inhibitors** and maternal embryonic leucine zipper kinase (**MELK**), such as amino-substituted-alkyloxy-benzo[e]pyrido[4,3-*b*]indole derivatives of formula **6** (Figure 18). Aurora kinases (members of serine-threonine kinases) play an essential role in the protein phosphorylation events that are important for the effectiveness of important mitotic activities. They have three main types as aurora A, B and C. Derivatives **6** were screened towards lung, leukemia, cervical, liver and osteosarcoma cancer cell lines in which they have provided cell

growth inhibitory effects with IC_{50}s in the nanomolar range. Moreover, compound **6a** inhibited 76% of Aurora A and 24% of Aurora B at 1 μM [57].

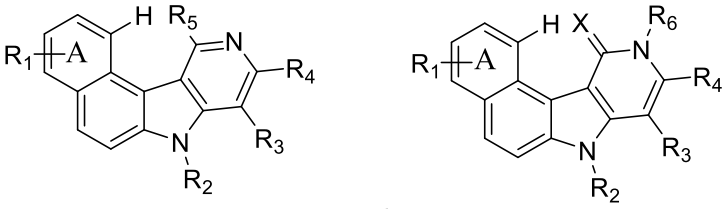

6

A=monosubstituted by R_1 in position 2/3/4
R_1=-O-(C_2-C_5)alkyl-NR_aR_b, where R_a and R_b=independently H or (un)substituted (C_1-C_4) alkyl, or NR_aR_b may be taken together to form a heterocycle
R_2=H or (un)substituted (C_1-C_3) alkyl
R_3 & R_4=independently H, (C_1-C_3) alkyl or aryl or R_3 & R_4=together form a bivalent radical
R_5= (C_1-C_4) alkoxy
R_6=H or (un)substituted (C_1-C_3) alkyl
X=O or S

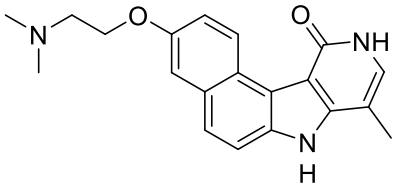

6a

Figure 18. Benzo[e]pyrido[4,3-*b*]indole derivatives **6**.

Furthermore, tricyclic indoles and (4,5-dihydro)indoles **7** (Figure 19) were developed as **inhibitors** of **CDK7** and **Akt kinases**, showing IC_{50} for Akt kinase below 500 nM. Protein kinase Akt is a serine-threonine-specific, also known as protein kinase B (PKB) [57]. Genetic mutations in Akt signalling pathway regulators are involved in oncogenesis and detected in tumors such as malignant glioma, endometrial cancer, prostate cancer, non-small cell lung cancer, melanoma, hepatocellular carcinoma, and breast cancer [58].

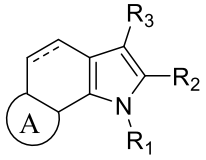

7

A = pyrrozolo, (un)substituted pyridino etc.
R_1 = H, (un)substituted alkyl, (un)substituted cycloalkyl, (un)substituted alkenyl, (un)substituted alkynyl, (un)substituted heterocyclyl, (un)substituted aryl, etc.
R_2 = H, halo, COOH and derivs., and $CONH_2$ and derivs.
--- = single bond or double bond; with the proviso that if R_2 = H, halo, (un)substituted aryl and heterocyclyl, then R_3 = not H

Figure 19. Tricyclic indoles and (4,5-dihydro)indoles **7**.

Indole moiety has also been reported in selective CDK7 (Cyclin dependent kinase 7) inhibitors, such **THZ1** (Figure 20) and **SY-1365** (covalent inhibitor) (Figure 21), and **SY-5609** (noncovalent) (Figure 22), developed by Syros Pharmaceuticals. CDK7 forms a ternary complex with MAT1 and cyclin H, called CAK (CDK-activating kinase). This plays a double role as it phosphorylates and activates several other cyclin dependent kinases, and participates to the initiation of transcription by phosphorylating the carboxy-terminal domain (CTD) of RNA polymerase II. This protein kinase is overexpressed in various types of tumors such as hepatocellular carcinoma, gastric cancer, oral squamous cell carcinoma, breast cancer, ovarian cancer, high-grade glioma, cholangiocarcinoma, pancreatic cancer, and colorectal cancer with aggressive clinicopathological features and poor prognosis. THZ1, a phenylaminopyrimidine derivative, the first irreversible ATP competitive (covalent) inhibitor, inhibited CDK7 activity with an IC_{50} of 3.2 nM and inhibited tumor growth in several murine models. The cryoelectron microscopy structure of the CAK-**THZ1** complex shows that THZ1 indole ring is rotated such that it points toward the open side of the nucleotide binding pocket (PDB ID: 6XD3 Figure 20) [59,60]. This aspect of the conformation of THZ1 more closely resembles a recent computational model for the binding of **SY-1365** to CDK7. Docking of SY-1365 binding active site of CDK7 highlights the preservation of key interactions of the indole present in THZ1, in which NH indole forms hydrogen bonds to aspartic acid (Asp155) (Figure 21) [61]. SY-1365 inhibited CDK7 with an IC_{50} of 84 nM and it was in clinical phase I for advanced solid tumors HR +, HER2-, SCLC, colorectal cancer [60]. SY-1365 has been the first selective CDK7 inhibitor in clinical trials, demonstrating the potential of CDK7 inhibition in a variety of cancer types. Nevertheless, Syros discontinued its development due to disappointing early clinical data and then focused on another similar non-covalent oral CDK7 inhibitor, **SY-5609**, that is currently being evaluated in a phase 1 clinical trial (NCT04247126) in patients with select solid tumors. This agent induced regression of the HCC70 cell line derived xenograft mouse model. Computational analysis of the putative binding mode of **SY-5609** to CDK7 confirmed that Asp155 is hydrogen bonded to the indole NH (Figure 22) [62–64].

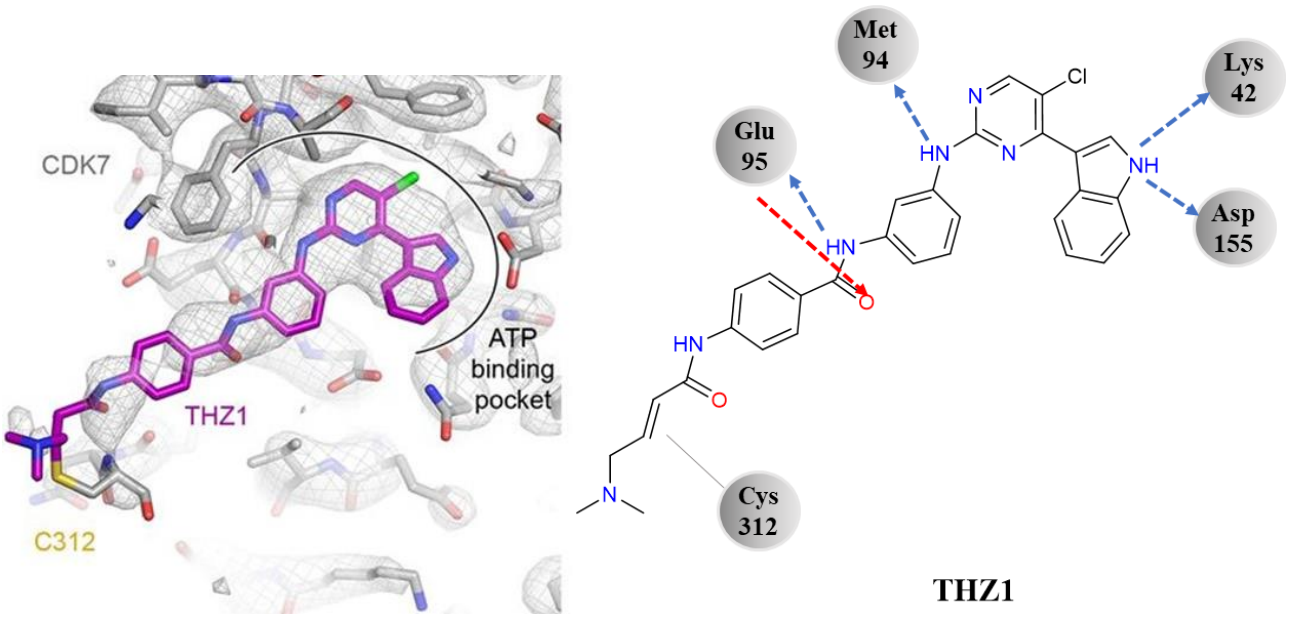

Figure 20. The cryoelectron microscopy structure of the CDK7-**THZ1 (**PDB ID: 6XD3). Hydrogen bonds donor interactions are indicated by blue arrows, hydrogen bonds acceptor interactions are indicated by red arrows, covalent bond is indicated by grey line.

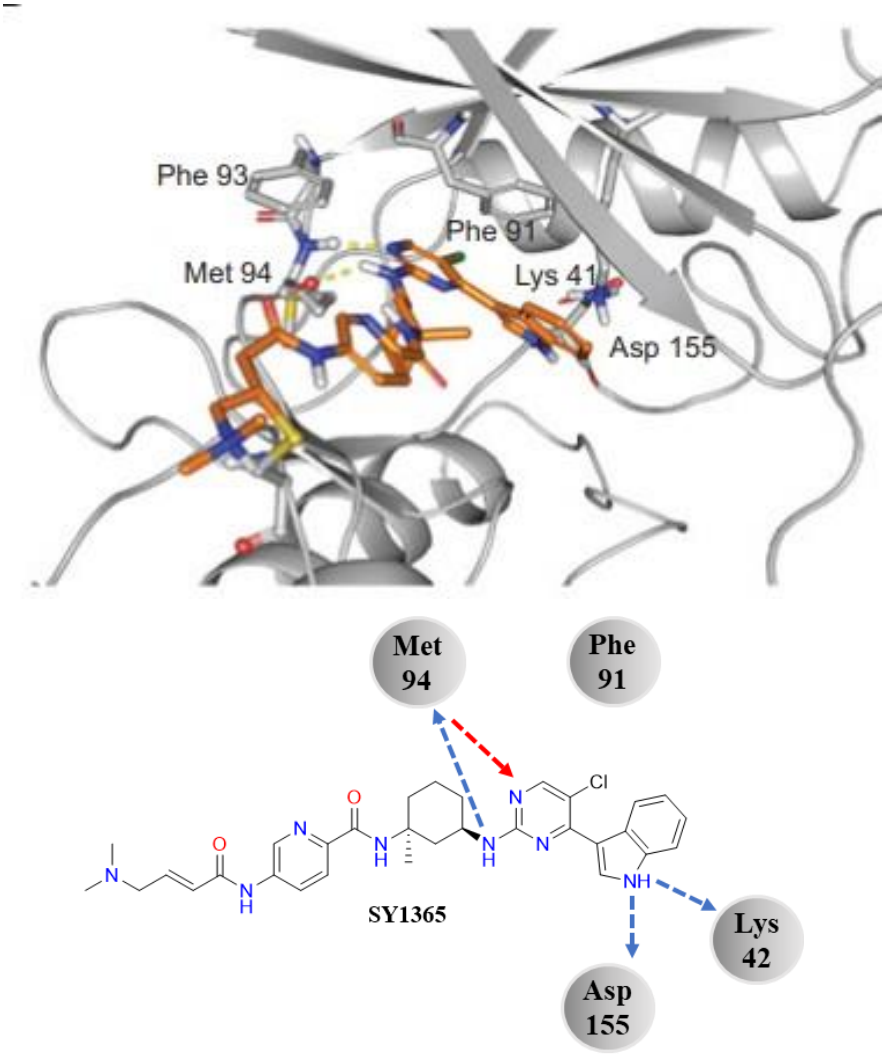

Figure 21. Model of **SY-1365** binding the active site of CDK7 and structure [61].

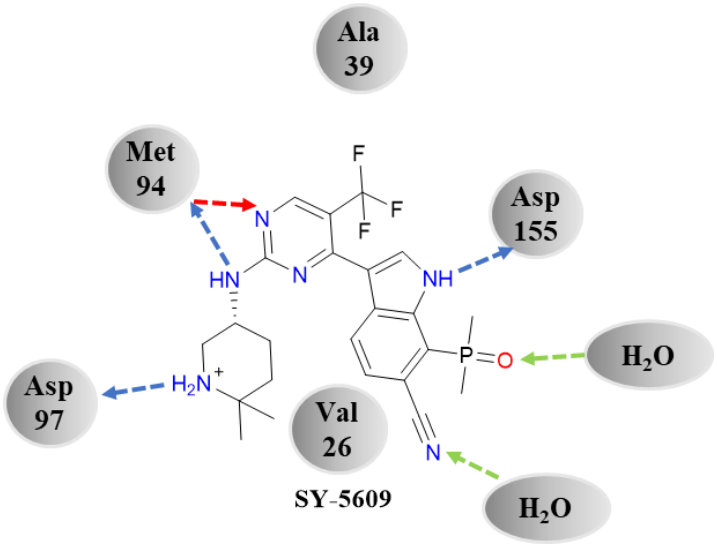

Figure 22. Computational analysis of the putative binding mode of **SY-5609** to CDK7. Hydrogen bonds donor interactions are indicated by blue arrows, hydrogen bonds acceptor interactions are indicated by red arrows while the water-mediated interactions are depicted with green dashed lines.

Indolylpyridone derivatives (compounds **8**, Figure 23) were disclosed by Stokes *et al*. for treatment of cancer and autoimmune disease. These compounds are checkpoint kinase 1 (Chk1) inhibitors, which express IC_{50s} in the range < 100 - < 1500nM. The unrelated serine-threonine kinase Chk2 and Chk1 exercise crucial role in arresting the cell cycle at the G2-M phase. This is one of the mechanisms by which various conventional melanoma chemotherapeutic drugs act [57].

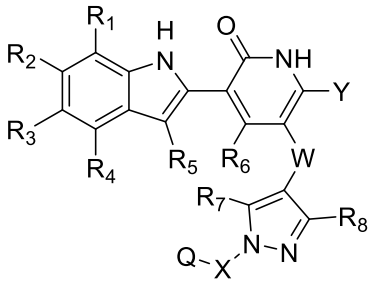

8

R_1, R_2, R_5 & R_6= H, OH, CH_3, CF_3 tec.
R_3 & R_4 = H, OH, C_{1-3} alkyl, C_{1-3} fluoroalkyl etc.
R_7 & R_8 = H, OH, or C_{1-3} alkoxy
X = (un)substituted C_{1-3} alkylene
W = CONH and derivs, or NHCO and derivs.
Y = H, C_{1-3} alkyl, C_{1-3} alkoxy, or halo
Q = (un)substituted 5-membered monocyclic heteroaryl ring

Figure 23. Indolylpyridone derivatives **8**.

Nagano et *al.* discovered 2-[(1*H*-indol-3yl)methylene]benzofuran-2(2*H*)-one derivatives and their **azaindole analogs 9** (Figure 24) as **pim-1 kinase inhibitors** with antiproliferative activity ranging from 22% to 95% at concentration of 1 µM and pim-1 kinase inhibitory potential of 14% to 100% at concentration of 0.1 µM. Furthermore, **9*H*-pyrido[3,4-*b*]indole derivatives 10** (Figure 24) developed by Babin *et al.* showed pim kinases activity inhibition with IC_{50} values ranging from 1 µM to 1000 nM. Pim kinases belong to the serine-threonine kinases and have a crucial role in cell growth, differentiation, and apoptosis. In many types of leukemia and prostate cancer, overexpression of pim-1 kinase has been observed. This suggests effectiveness of pim-1 kinase inhibitors as anticancer agents [57,65].

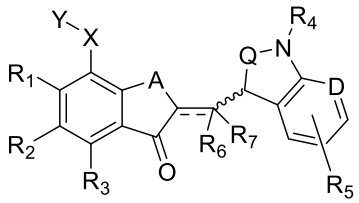

9

R_1= H, OH, C_{1-6} alkoxy, aryl-C_{1-6} alkoxy, aryloxy-C_{1-6} alkoxy, hydroxy-C_{1-6} alkoxy etc.
R_2= H, halo, C_{1-6} alkyl, C_{1-6} alkoxy, aryl, NH_2, OH, heterocyclyl or R_1 & R_2 = linked together to form C_{1-6} alkylindenedioxy
R_3 = H, halo, C_{1-6} alkyl, C_{1-6} alkoxy, aryl, NH_2, OH, heterocyclyl
R_4 = H, C_{1-6} alkyl, alkylsulfonyl, arylsulfonyl
R_5 = H or 1-4 substituens on the benzene or pyridine ring which are selected from halo, C_{1-6} alkyl, C_{2-6} alkenyl, C_{2-6} alkynyl, halo-C_{1-6} alkyl, hydroxy-C_{1-6} alkyl,amino-C_{1-6} alkyl, OH, C_{1-6} alkoxy, NH_2, NO_2, aryl, aralkyloxy, heterocyclyl etc.
---- = single or double bond
R_6 & R_7 = H, C_{1-6} alkyl, halo-C_{1-6} alkyl
A = O, S, CH_2
D = CH, N
Q = N, (un)substituted CH
X = single bond, each (un)substituted C_{1-6} alkylene, C_{2-6} alkenylene, or C_{2-6} alkynylene, O, CO
Y = (un)substituted heterocyclyl or NH_2

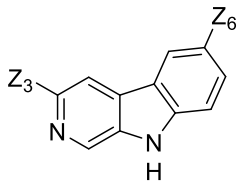

10

Z_3 = (un)substituted 5-6 membered heteroaryl contg. 1-4 heteroatoms selected from N, S or O bound to the carboline motif by a C atom or by a N belonging to Z_3
Z_6 = H, halo, OH, alkoxy, aryl etc.

Figure 24. 2-[(1*H*-indole and azaindole-3yl)methylene]benzofuran-2(2*H*)-one derivatives **9** and 9*H*-pyrido[3,4-*b*]indole derivatives **10**.

1.2.4 Indole and 7-azaindole derivatives as selective CDK1 and GSK-3β inhibitors

In the research group where I carried out my PhD, CDK1 and GSK-3β inhibitors bearing the 7-azaindole or the indole moieties, have been synthesized. In particular, bis-indoles, indolyl-7-

azaindoles and 7-azaindole-phenyl derivatives have been developed. In these compounds the two units were linked by a spacer such as a pentatomic heterocycle (1,3-thiazole or 1,2,4-oxadiazole) (Figure 25,26). Most compounds have shown antiproliferative activity on a wide spectrum of human tumor cell lines with GI_{50} values in the micro- and sub-micromolar range [66–71].

In case of compounds in which the linker was a thiazole ring interesting results were obtained, in particular, the **3-(2-phenyl-1,3-thiazol-4-yl)-7-azaindole derivatives 11** (Figure 25) showed antiproliferative activity against a wide range of human tumor cell lines with GI_{50} values in the range from micro- to sub-micromolar. The most active compounds were further tested against the pancreatic carcinoma (MiaPaCa-2) and malignant peritoneal mesothelioma (STO) with GI_{50} values in the range 4.3–41.6 μM and 0.41-17.2 μM, respectively. They were also able to inhibit the activity of cyclin-dependent kinase 1 (CDK1) with IC_{50} values less than 1 μM [69]. The **3-(2-indolyl-1,3-thiazol-4-yl)-7-azaindoles derivatives 12** (Figure 25), were tested by NCI, at the concentration of 10^{-5} M for antitumor screening against a panel of about 60 human tumor cell lines derived from 9 human cancer types. Some of them were selected by the NCI for evaluation at five concentration levels (10^{-4} -10^{-8} M), showing antiproliferative activity with GI_{50} values in the range from micro- to sub-micromolar. The five most active compounds were further tested by Istituto Nazionale dei Tumori (Fondazione IRCCS, Milano) against two additional cell lines: STO and Meso II, derived from human Diffuse Malignant Peritoneal Mesothelioma (DMPM). They showed a concentration dependent inhibition of cell proliferation in both cellular models, and they did not interfere with the proliferation of normal cells (W138). The antitumoral activity of the most active compounds was also investigated on STO cells xenotransplanted in athymic nude mice and after the treatment with each compound it was possible to observe a marked tumor growth inhibition. In order to study their mechanism of action, these compounds were tested on several protein kinases (CDK1, CDK5, EGFR, FGFR1, RET, MET, KIT, JAK2, PKCA, PKCB, ChkI, MAPK12, GSK, PKA, GSK-3α, GSK-3β). Results showed marked CDK1 activity inhibition with IC_{50} values (0.89 μM, 0.75 μM, 0.86 μM) comparable to those reported for known CDK1 inhibitors, such as roscovitine and purvalanol A (0.73 μM and 0.59 μM, respectively) and they decreased CDK1 activity in a time-dependent way. These compounds were also active against GSK-3β protein, eliciting inhibitory activity only at higher concentration [70,72].

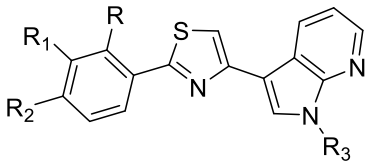

3-(2-phenyl-1,3-thiazol-4-yl)-7-azaindoles

11

R=H,Cl,F
R_1=H,CH_3,F
R_2=H,CH_3,OCH_3,Cl,Br,F
R_3=H,CH_3

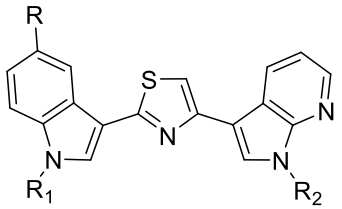

3-[2-(1*H*-indol-3-yl)-1,3-thiazol-4-yl)-1,3-thiazol-4-yl)-7-azaindoles

12

R=H,CH_3,OCH_3,Cl,Br,F
R_1=H,CH_3,Boc
R_2=H,CH_3

Figure 25. 3-(2-phenyl-1,3-thiazol-4-yl)-7-azaindole derivatives **11** and 3-(2-indolyl-1,3-thiazol-4-yl)-7-azaindole derivatives **12.**

Regarding **bis-indolyl-1,2,4-oxadiazole derivatives 13** (Figure 26)**,** they exhibited good antiproliferative activity against a panel of pancreatic ductal adenocarcinoma (PDAC) cells, such as Suit-2, Capan-1 and Panc-1, in which inhibited cell growth with IC_{50} values ranging from micromolar to sub-micromolar level. The most active compound showed cell growth inhibition with IC_{50} values in the range of 0.40–1.19 μM against all PDAC preclinical models investigated. The mechanism of the antiproliferative activity of these derivatives was pro-apoptotic, being associated with externalization of plasma membrane phosphatidylserine, a reliable marker of cell apoptosis. Furthermore, a remarkable cell migration reduction has been found in the metastatic Capan-1 cell line when treated with the most active compound. PathScan intracellular signaling and ELISA assays in Panc-1 cells also revealed a significant inhibition of GSK-3β phosphorylation. This was further supported by data from *in vitro* assay for GSK-3β activity and molecular modeling, suggesting this protein kinase as a potential downstream target of these compounds. A potential binding mode for the most active derivatives within the ATP binding site of GSK-3β is depicted in Figure 27 (PDB 1UV5) showing similar interactions to the co-crystalized ligand 6-bromoindirubin, a known potent and selective bis-indolyl inhibitor of the enzyme. These compounds established a hydrogen bond through their indole nitrogen with the peptide carbonyl oxygen of valine (Val135) [66].

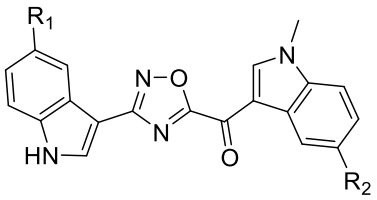

[3-(1*H*-indol-3-yl)-[1,2,4]oxadiazol-5-yl]-(1-methyl-1-*H*-indol-3-yl)-methanones

13

R_1 or R_2=H,Br,F,OCH_3

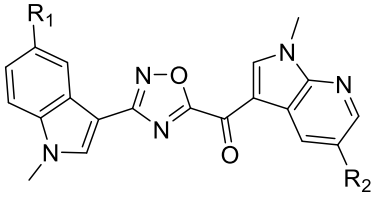

(1-methyl-7-azaindol-3-yl)-[3-(1-methyl-1*H*-indol-3-yl)-[1,2,4]oxadiazol-5-yl]-methanones

14

R_1=H,Br,F,OCH_3

R_2=H,Br

Figure 26 1,2,4-Oxadiazole derivatives **13,14**.

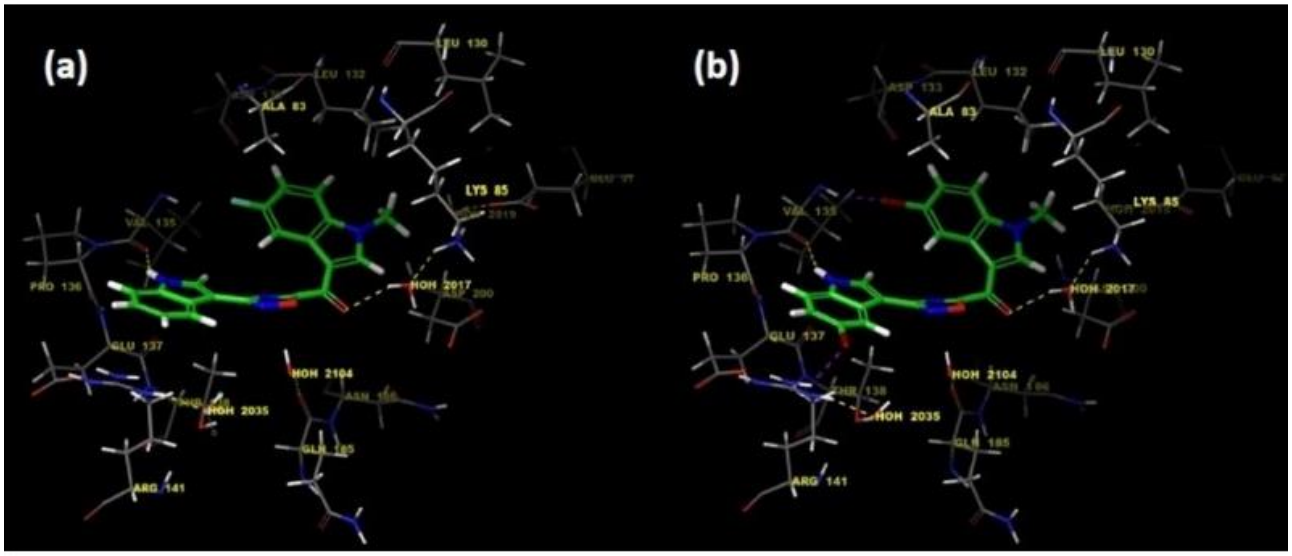

Figure 27. Proposed binding mode of the most active oxadiazole compounds with GSK3-β (PDB ID: 1UV5). H-bonds between the indole nitrogen of the compounds with the peptide carbonyl oxygen of Val135 residue, as well as the water-mediated interaction between the carbonyl group adjacent to oxadiazole ring and the Lys85 residue are shown with yellow dashed lines.

A new series of **7-azaindolyl oxadiazoles 14** (Figure 26) has also been synthesized by our research group; these compounds showed promising antiproliferative activities against a series of PDAC cells (PaTu-T, Hs766T, and HPAF-II cell lines and a primary PDAC cell culture PDAC-3). In particular the most active compound showed *in vitro* cell growth inhibition with IC_{50} values ranging from 5.7 to 10.7 μM. Molecular docking showed this compound interacting effectively with the ATP-binding site, establishing a water-mediated interaction between the nitrogen atom of the 7-azaindole moiety and the glutamine (Gln132) residue (Figure 28). This compound also induced apoptosis (which

increased 1.5- and 2-fold in PaTu-T and PDAC-3 cells, respectively), inhibited CDK1 expression (which was reduced to 45% in Hs766T) and passed the ADME prediction, showing good pharmacokinetic parameters. It respected the Lipinski rule of 5, displayed bioavailability score of 0.55, a high gastrointestinal absorption and it was not predicted to cross the blood brain barrier [67].

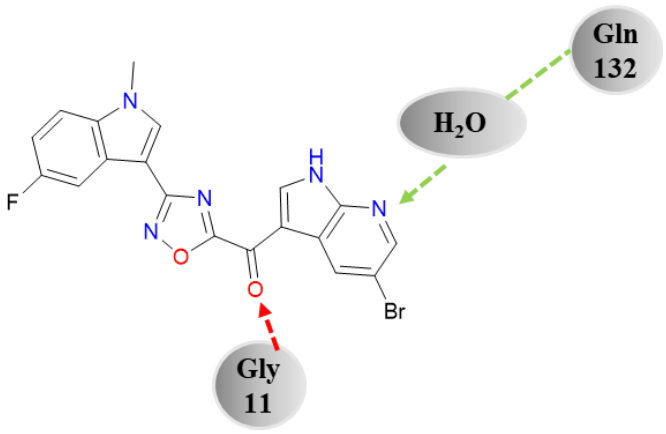

Figure 28. Proposed binding mode of the most active 1,2,4-oxadiazole compound with CDK1 (PDB ID: 4YC6). H-bond between the carbonyl group of the compound with the peptide nitrogen of Gly11 residue is shown with red dashed arrow, while the water-mediated interaction between the nitrogen atom of the 7-azaindole portion adjacent to the oxadiazole ring and the Gln132 residue is depicted with green dashed line.

2. AIM OF THE STUDY

Based on what was mentioned, eight new series of compounds of type **15-22** have been synthesized. In particular:

- 2,5-bis(1*H*-indol-3-yl)pyrazolo[1,5-*a*]pyrimidin-7-amines (**15a-e**) and 2,5-bis(1-methyl-1*H*-indol-3-yl)pyrazolo[1,5-*a*]pyrimidin-7-amines (**15f-j**), in which two same indole units are linked to the pyrazolo[1,5-*a*]pyrimidin-7-amine central ring;
- 2-(1*H*-indol-3-yl)-5-(1*H*-indol-3-yl)pyrazolo[1,5-*a*]pyrimidin-7-amines (**16a-t**), in which two differently functionalized indole units are linked to central ring;
- 2-(1*H*-indol-3-yl)-5-(1-methyl-7-azaindol-3-yl)pyrazolo[1,5-*a*]pyrimidin-7-amines (**17a-t**), in which indole and 1-methyl-7-azaindole moieties are linked to the pyrazolo[1,5-*a*]pyrimidin-7-amine in position 2 and 5 ring, respectively;
- 5-(1-benzyl-7-azaindol-3-yl)-2-(1*H*-indol-3-yl)pyrazolo[1,5-*a*]pyrimidin-7-amines (**18a-h**) in which the indole and 1-benzyl-7-azaindole moieties are linked to the central ring in position 2 and 5, respectively;
- 3-[5-(1*H*-indol-3-yl)-1,3,4-oxadiazol-2-yl]-7-azaindoles **19a-g,** in which indole and 7-azaindole units are linked to the 1,3,4-oxadiazole ring;
- 3-(5-phenyl-1,3,4-oxadiazol-2-yl)-7-azaindoles **20a-d**, in which phenyl and 7-azaindole units are linked to the 1,3,4-oxadiazole ring;
- 3-[5-(1*H*-indol-3-yl)-1,3,4-thiadiazol-2-yl]-7-azaindoles **21a-h**, in which indole and 7-azaindole moieties are linked to the 1,3,4-thiadiazole ring;
- 3-(5-phenyl-1,3,4-thiadiazol-2-yl)-7-azaindoles **22a-d,** in which phenyl and 7-azaindole moieties are linked to the 1,3,4-thiadiazole ring.

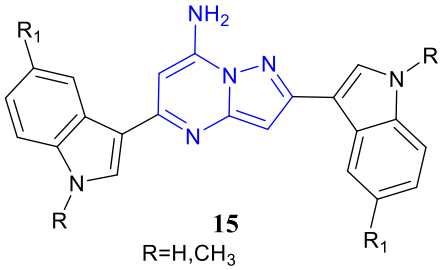

15

R=H,CH_3

R_1=H,OCH_3,Br,F,Cl

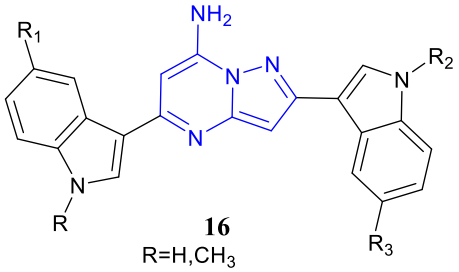

16

R=H,CH_3

R_1=H,OCH_3,Br,F,Cl

R_2=H,CH_3

R_3=H,Cl

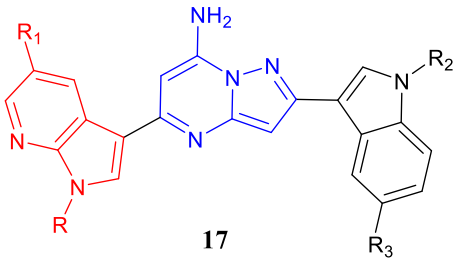

17

R=CH_3

R_1=H,Br

R_2=H,CH_3

R_3=H,OCH_3,Br,F,Cl

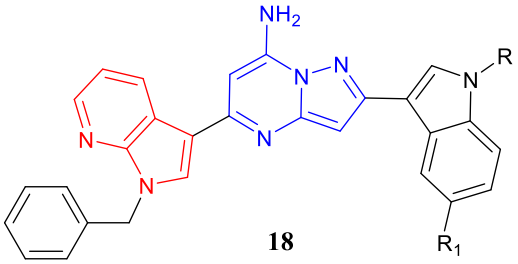

18

R=H,CH_3

R_1=H,OCH_3,Br,Cl

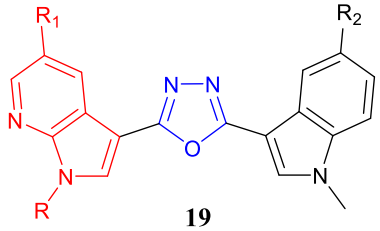

19

R=H,CH_3

R_1=H,Br

R_2=H,F,Br

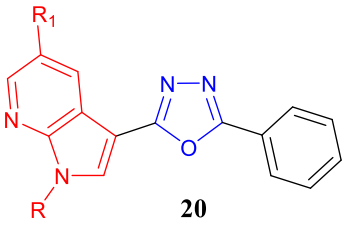

20

R=H,CH_3

R_1=H,Br

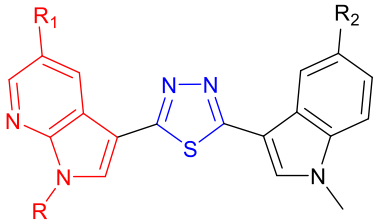

21

R=H,CH_3

R_1=H,Br

R_2=H,F,Br,OCH_3

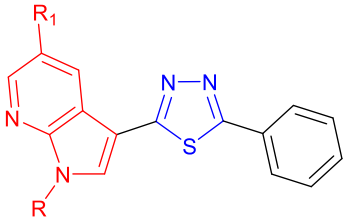

22

R=H,CH_3

R_1=H,Br

3. CHEMISTRY SECTION

The synthesis of 2,5-bis(1*H*-indol-3-yl)pyrazolo[1,5-*a*]pyrimidin-7-amines derivatives **15** was planned by *one-pot* cyclization reaction that involves key oxopropanenitrile intermediates **23,24** and *tert*-butyl carbazate (Boc-$NHNH_2$) (Scheme 1).

Scheme 1. Synthetic pathway of 2,5-bis(1*H*-indol-3-yl)pyrazolo[1,5-*a*]pyrimidin-7-amines **15**.

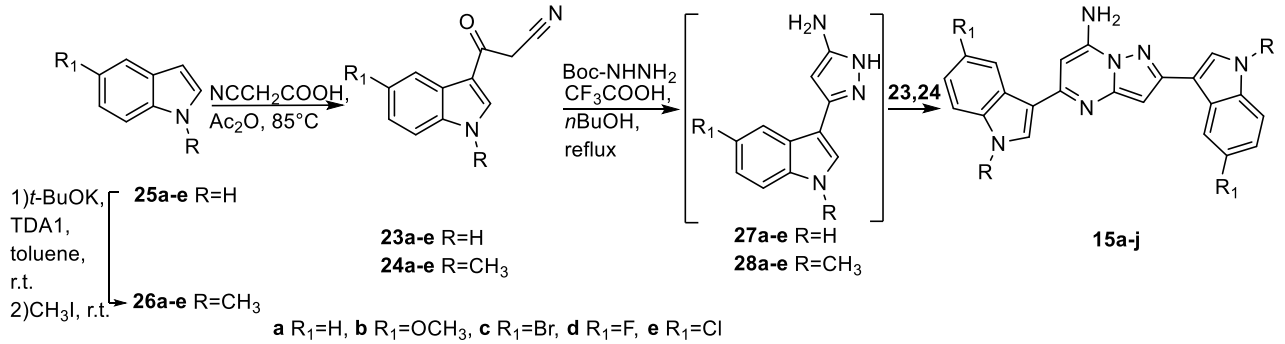

The key oxopropanenitrile intermediates **23,24** were prepared from the corresponding commercial indoles **25** or methylated indole derivatives **26**. The methylated derivatives **26** were obtained at room temperature in excellent yields (96-98%) (Table 1), from the commercial indoles **25**, using potassium *tert*-butoxide (*t*-BuOK) as base, tris[2-(2-methoxyethoxy)ethyl]amine (TDA-1) as a phase transfer catalyst, and iodomethane (CH_3I) as a methylating agent (Scheme 2). The commercial indoles **25a-e** or the indole methyl derivatives **26a-e** were reacted with a preheated solution of cyanoacetic acid ($NCCH_2COOH$) in acetic anhydride (Ac_2O) at 85°C for 10 minutes, and heating continued at the same temperature. These reaction conditions led to oxopropanenitriles **23,24** in high yields (Scheme 2) (Table 2) where the indole acylation occurred regioselectively at C-3 position. As regards the reaction mechanism, it is possible to assume that cyanoacetic acid is converted into the cyanoacetic acid anhydride or at least into the mixed anhydrides **29** (Scheme 3). These species, being more electrophilic than acetic anhydride, react with indole **25,26** to yield the 3-functionally substituted indoles **23,24** [73].

Scheme 2. Synthesis of 3-(1*H*-indol-3-yl)-3-oxopropanenitriles **23a-e** and 3-(1-methyl-1*H*-indol-3-yl)-3-oxopropanenitriles **24a-e.**

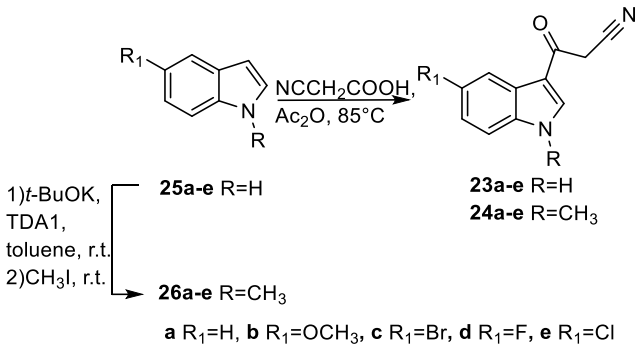

Table 1. 1-Methyl-1*H*-indoles **26**.

Compound	R	R_1	Yield%
26a	CH_3	H	96
26b	CH_3	OCH_3	97
26c	CH_3	Br	96
26d	CH_3	F	98
26e	CH_3	Cl	98

Table 2. Oxopropanenitriles **23,24**.

Compound	R	R_1	Yield%	Compound	R	R_1	Yield%
23a	H	H	95	**24a**	CH_3	H	90
23b	H	OCH_3	94	**24b**	CH_3	OCH_3	84
23c	H	Br	85	**24c**	CH_3	Br	81
23d	H	F	86	**24d**	CH_3	F	74
23e	H	Cl	86	**24e**	CH_3	Cl	88

Scheme 3. Preparation of a solution of mixed anhydrides **29**.

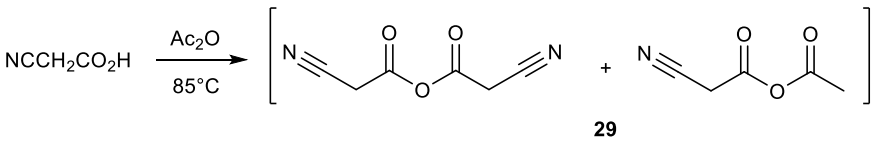

The key oxopropanenitrile intermediates **23,24** were subjected to a *one-pot* cyclization reaction in *n*-butanol under reflux, with *tert*-butyl carbazate (Boc-$NHNH_2$) and trifluoroacetic acid (CF_3COOH) for *in situ N*-Boc deprotection to give the corresponding hydrazine. The reaction of oxopropanenitrile intermediates **23,24** with the formed hydrazine led to 3-(1*H*-indol-3-yl)-1*H*-pyrazol-5-amines **27,28**, which were reacted with oxopropanenitrile intermediates **23,24** not yet consumed in the reaction mixture to give 2,5-bis(1*H*-indol-3-yl)pyrazolo[1,5-*a*]pyrimidin-7-amine derivatives **15** in high yields (Scheme 4) (Table 3) [74].

Scheme 4. *One-pot* cyclization reaction for synthesis of 2,5-bis(1*H*-indol-3-yl)pyrazolo[1,5-*a*]pyrimidin-7-amines **15a-e** and 2,5-bis(1-methyl-1*H*-indol-3-yl)pyrazolo[1,5-*a*]pyrimidin-7-amines **15f-j**.

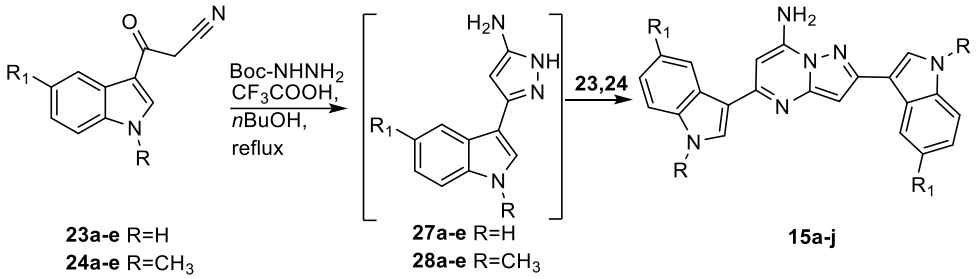

a R_1=H, **b** R_1=OCH_3, **c** R_1=Br, **d** R_1=F, **e** R_1=Cl

Table 3. 2,5-bis(1*H*-indol-3-yl)pyrazolo[1,5-*a*]pyrimidin-7-amines **15**.

Compound	R	R_1	Yield%	Compound	R	R_1	Yield%
15a	H	H	57	**15f**	CH_3	H	89
15b	H	OCH_3	48	**15g**	CH_3	OCH_3	73
15c	H	Br	63	**15h**	CH_3	Br	91
15d	H	F	64	**15i**	CH_3	F	100
15e	H	Cl	90	**15j**	CH_3	Cl	100

The plausible mechanism for the formation of the 3-(1*H*-indol-3-yl)-1H-pyrazol-5-amines **27,28** may be explained by the initial addition of the amine group of hydrazine to the carbonyl carbon of the oxopropanenitrile intermediates **23,24** resulting in the intermediates **30**, followed by elimination of water, to give β-cyanoalkylidene hydrazides **31**. The latter conveniently undergoes intramolecular cycloaddition by the nucleophilic attack of the second amine to the nitrile carbon to give the pyrazole imines **32**, which upon aromatization leads to the 3-(1*H*-indol-3-yl)-1*H*-pyrazol-5-amines **27,28** (Scheme 5).

Scheme 5. Reaction mechanism for the synthesis of 3-(1*H*-indol-3-yl)-1*H*-pyrazol-5-amines **27,28.**

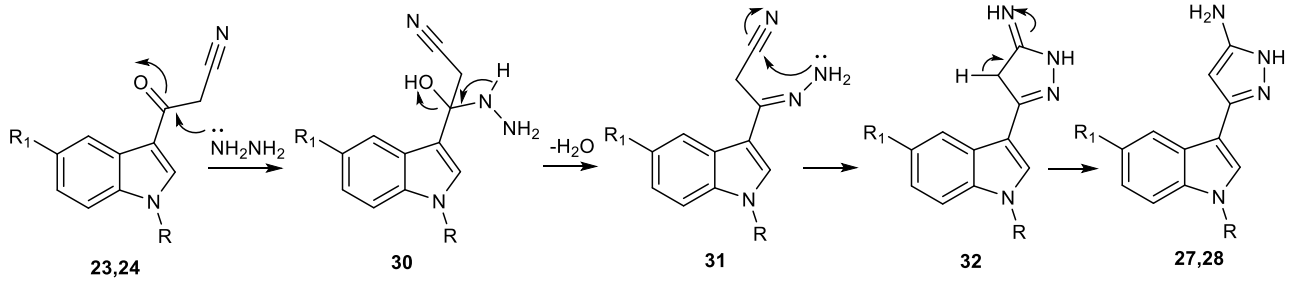

The formation of 2,5-bis(1*H*-indol-3-yl)pyrazolo[1,5-*a*]pyrimidin-7-amine derivatives **15** is believed to proceed via initial attack of the exocyclic amine group of intermediates **27,28** on the keto group of 3-cyanoacetylindoles **23,24**, followed by elimination of water, and subsequent cyclization by the nucleophilic addition of the endocyclic imino group to the nitrile function (Scheme 6).

Scheme 6. Reaction mechanism for the synthesis of pyrazolo[1,5-*a*]pyrimidin-7-amine derivatives.

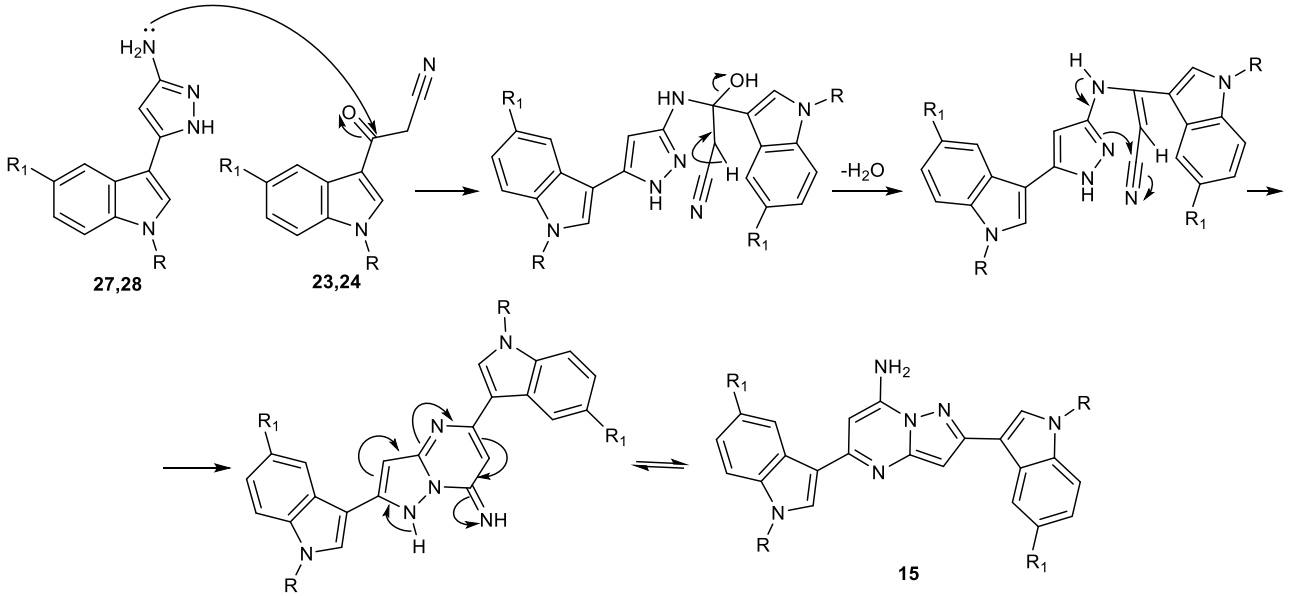

To synthesize highly functionalized 2-(1*H*-indol-3-yl)-5-(1*H*-indol-3-yl)pyrazolo[1,5-*a*]pyrimidin-7-amine derivatives **16** a different synthetic strategy was used, in order to isolate the 3-(1*H*-indol-3-yl)-1*H*-pyrazol-5-amine intermediates **27,28**.

3-(1*H*-Indol-3-yl)-1*H*-pyrazol-5-amine derivatives **27,28** were obtained from oxopropanenitrile intermediates **23,24**, which were reacted with acethydrazide ($AcNHNH_2$) in *n*-butanol (*n*-BuOH) in the presence of *p*-toluenesulfonic acid monohydrate ($PTSA \cdot H_2O$) for *in situ N*-acetyl deprotection to give the corresponding hydrazine. The reaction mixture was heated vigorously under reflux using the Marcusson apparatus to remove water from reaction equilibrium and promote the attack of hydrazine to the carbonyl carbon atom of the oxopropanenitrile intermediates **23,24** (according to the mechanism already shown in Scheme 5) leading to th**e** formation of 3-(1*H*-indol-3-yl)-1*H*-pyrazol-5-amine **27,28**, as main reaction product (Scheme 8) (Table 4).

Scheme 8. Synthesis of 3-(1*H*-indol-3-yl)-1*H*-pyrazol-5-amines **27,28.**

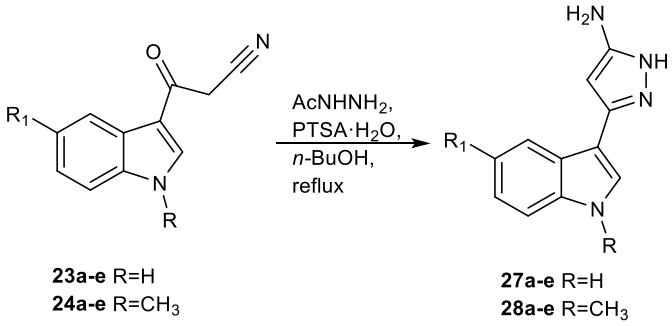

23a-e R=H
24a-e R=CH_3

27a-e R=H
28a-e R=CH_3

a R_1=H, **b** R_1=OCH_3, **c** R_1=Br, **d** R_1=F, **e** R_1=Cl

Table 4. 3-(1*H*-indol-3-yl)-1*H*-pyrazol-5-amines **27,28**.

Compound	R	R_1	Yield%	Compound	R	R_1	Yield%
27a	H	H	66	**28a**	CH_3	H	69
27b	H	OCH_3	62	**28b**	CH_3	OCH_3	66
27c	H	Br	72	**28c**	CH_3	Br	50
27d	H	F	54	**28d**	CH_3	F	55
27e	H	Cl	72	**28e**	CH_3	Cl	73

Thus, 3-(1*H*-indol-3-yl)-1*H*-pyrazol-5-amines **27,28** were reacted with 3-(1*H*-indol-3-yl)-3-oxopropanenitriles **23,24** in *n*-butanol (*n*-BuOH), in the presence of *p*-toluenesulfonic acid

monohydrate (PTSA·H_2O) catalyst at 90°C, where the subsequent cyclization afforded 2-(1*H*-indol-3-yl)-5-(1*H*-indol-3-yl)pyrazolo[1,5-*a*]pyrimidin-7-amines **16a-t** in good yields (Scheme 9) (Table 5).

Scheme 9. Cyclization reaction for the synthesis of 2-(1*H*-indol-3-yl)-5-(1*H*-indol-3-yl)pyrazolo[1,5-*a*]pyrimidin-7-amines **16a-t**.

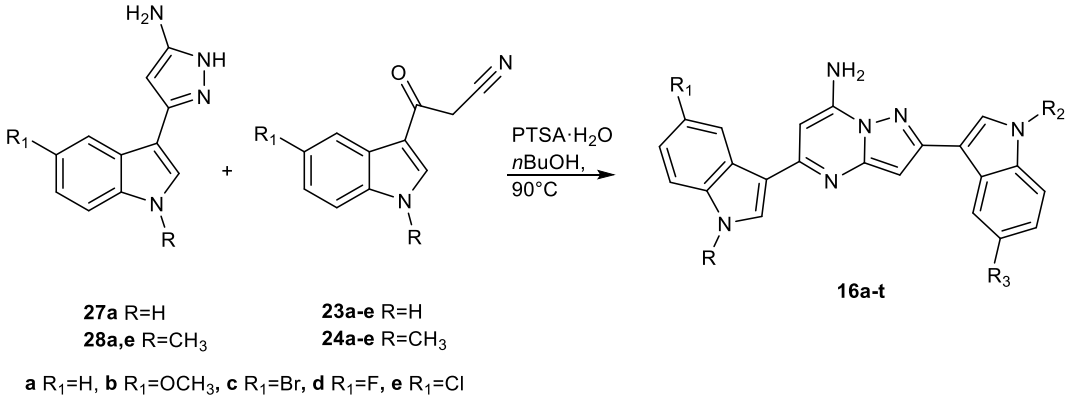

Table 5. 2-(1*H*-indol-3-yl)-5-(1*H*-indol-3-yl)pyrazolo[1,5-*a*]pyrimidin-7-amines **16a-t**.

Compound	R	R_1	R_2	R_3	Yield%	Compound	R	R_1	R_2	R_3	Yield%
16a	H	OCH_3	H	H	36	**16k**	H	OCH_3	CH_3	H	30
16b	H	Br	H	H	46	**16l**	H	Br	CH_3	H	37
16c	H	F	H	H	70	**16m**	H	F	CH_3	H	57
16d	H	Cl	H	H	36	**16n**	H	Cl	CH_3	H	34
16e	CH_3	H	H	H	70	**16o**	CH_3	OCH_3	CH_3	H	51
16f	CH_3	OCH_3	H	H	62	**16p**	CH_3	Br	CH_3	H	45
16g	CH_3	Br	H	H	35	**16q**	CH_3	F	CH_3	H	42
16h	CH_3	F	H	H	40	**16r**	CH_3	Cl	CH_3	H	40
16i	CH_3	Cl	H	H	30	**16s**	H	H	CH_3	Cl	48
16j	H	H	CH_3	H	60	**16t**	CH_3	H	CH_3	Cl	44

2-(1*H*-indol-3-yl)-5-(1-methyl-7-azaindol-3-yl)pyrazolo[1,5-*a*]pyrimidin-7-amine derivatives **17a-t** were conveniently synthesized from key intermediates: 3-(1-methyl-7-azaindol-3-yl)-3-oxopropanenitriles **33** and 3-(1*H*-indol-3-yl)-1*H*-pyrazol-5-amines **27,28.**

The oxopropanenitriles **33** were synthesized from the *N*-methyl derivatives **34** prepared by *N*-methylation of commercially available 7-azaindoles **35** using potassium *tert*-butoxide, TDA-1 and iodomethane (Table 6) (Scheme 10). The subsequent acylation of the derivatives **34**, in the presence of cyanoacetic acid and acetic anhydride at 85°C, gave the 3-oxopropanenitrile intermediates **33** (Scheme 10) (Table 7).

Scheme 10. Synthesis of 3-(1-methyl-7-azaindol-3-yl)-3-oxopropanenitriles **33a,c**.

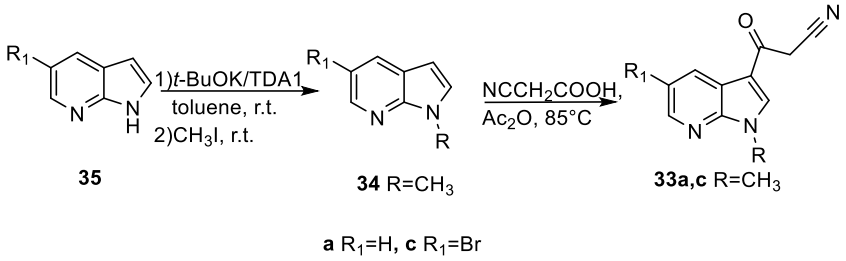

35 **34** R=CH_3 **33a,c** R=CH_3

a R_1=H, **c** R_1=Br

Table 6. 1-Methyl-7-azaindoles **34.**

Compound	R	R_1	Yield%
34a	CH_3	H	96
34c	CH_3	Br	85

Table 7. 3-(1-methyl-7-azaindol-3-yl)-3-oxopropanenitriles **33.**

Compound	R	R_1	Yield%
33a	CH_3	H	35
33c	CH_3	Br	46

Finally, the two key intermediates of type **33** and **27,28** were reacted and cyclized using the same reaction conditions already presented (Scheme 11) (Table 8).

Scheme 11. Cyclization reaction for synthesis of 2-(1*H*-indol-3-yl)-5-(1-methyl-7-azaindol-3-yl)pyrazolo[1,5-*a*]pyrimidin-7-amines **17a-t**.

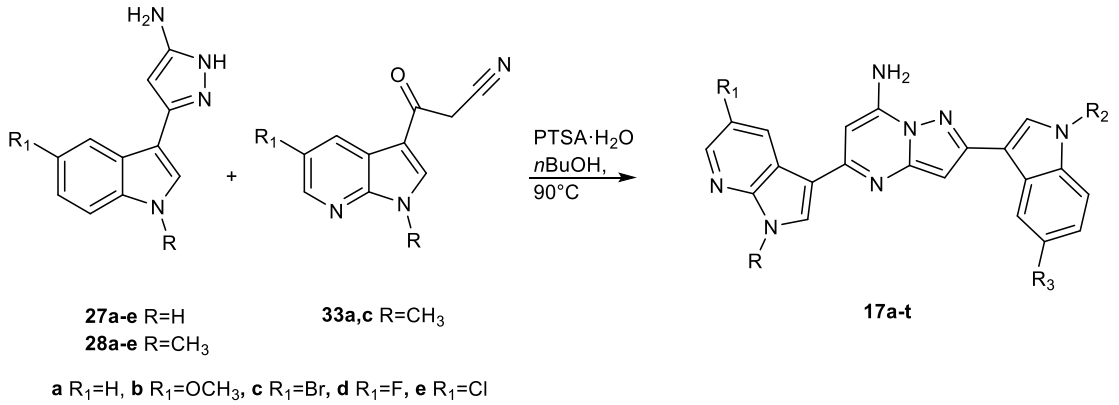

27a-e R=H
28a-e R=CH_3

33a,c R=CH_3

17a-t

a R_1=H, **b** R_1=OCH_3, **c** R_1=Br, **d** R_1=F, **e** R_1=Cl

Table 8. 2-(1*H*-indol-3-yl)-5-(1-methyl-7-azaindol-3-yl)pyrazolo[1,5-*a*]pyrimidin-7-amines **17a-t**.

Compound	R	R_1	R_2	R_3	Yield%	Compound	R	R_1	R_2	R_3	Yield%
17a	CH_3	H	H	H	47	**17k**	CH_3	H	CH_3	H	39
17b	CH_3	Br	H	H	42	**17l**	CH_3	Br	CH_3	H	34
17c	CH_3	H	H	OCH_3	58	**17m**	CH_3	H	CH_3	OCH_3	47
17d	CH_3	Br	H	OCH_3	50	**17n**	CH_3	Br	CH_3	OCH_3	39
17e	CH_3	H	H	Br	49	**17o**	CH_3	H	CH_3	Br	46
17f	CH_3	Br	H	Br	42	**17p**	CH_3	Br	CH_3	Br	46
17g	CH_3	H	H	F	29	**17q**	CH_3	H	CH_3	F	35
17h	CH_3	Br	H	F	45	**17r**	CH_3	Br	CH_3	F	35
17i	CH_3	H	H	Cl	24	**17s**	CH_3	H	CH_3	Cl	30
17j	CH_3	Br	H	Cl	35	**17t**	CH_3	Br	CH_3	Cl	32

In order to synthesize the 3-oxo-3-(7-azaindol-3-yl)propanenitrile **38** (Scheme 12) that could be reacted using the above presented procedures, it was not possible to follow the synthetic route previously described for the derivatives **33** (Scheme 10). The reaction of 7-azaindole **35a** in the presence of cyanoacetic acid and acetic anhydride did not provide the desired 3-oxo-3-(7-azaindol-3-yl)propanenitrile **38** but two undesirable reaction products **39** (yield 36%), **40** (yield 18%) deriving from *N*-acylation (Scheme 12). Other attempts were made by changing the reaction conditions, such

as the solvent (using dioxane), or the temperature, or reagents' equimolar ratios. However, in these cases the reaction yielded only *N*-acylated products.

Scheme 12

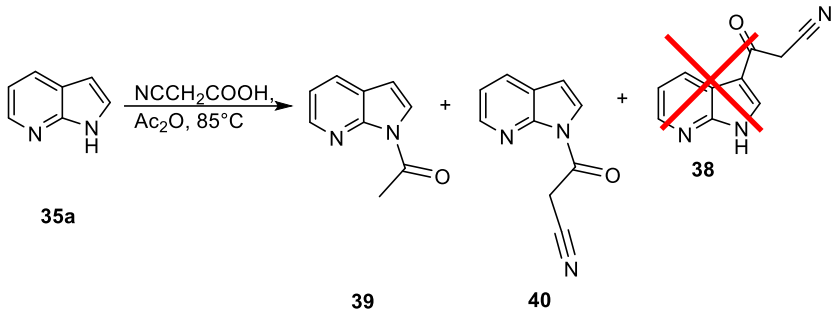

Considering the difficulties encountered, an alternative synthetic strategy was used. First a cyanoacetyl chloride **41** solution was prepared starting from a mixture of cyanoacetic acid **42** and oxalyl chloride (ClCOCOCl) in dichloromethane in the presence of anhydrous DMF as catalyst (Scheme 13). Then, a cooled mixture of 7-azaindole **35a** in dichloromethane was then added to the solution in the presence of aluminium chloride ($AlCl_3$), affording the 3-oxo-3-(7-azaindol-3-yl)propanenitrile **38** but in very low yield (10%) (Scheme 14).

Scheme 13 Preparation of a solution of cyanoacetyl chloride **41**.

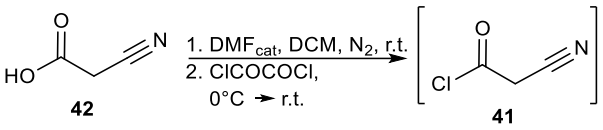

Scheme 14. 3-oxo-3-(7-azaindol-3-yl)propanenitrile **38**.

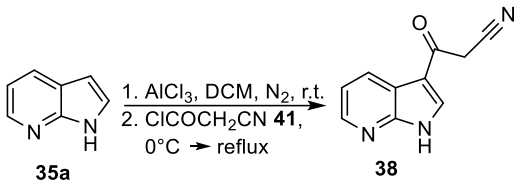

To prevent *N*-acylation, it was thought to protect the 7-azaindole nitrogen atom. Thus, compound **35a** was protected with a benzenesulfonyl group using sodium hydride (NaH) and benzenesulfonyl chloride ($PhSO_2Cl$) in tetrahydrofuran (THF) cooled at 0°C and then stirred at room temperature to obtain the derivative **43** (yield 58%) (Scheme 15.1). Nevertheless, the following 3-acylation reaction in the presence of cyanoacetic acid and acetic anhydride did not afford the desired 3-oxo-propanenitrile **44**, revealing the presence of only starting material (Scheme 15.1).

Scheme 15.1.

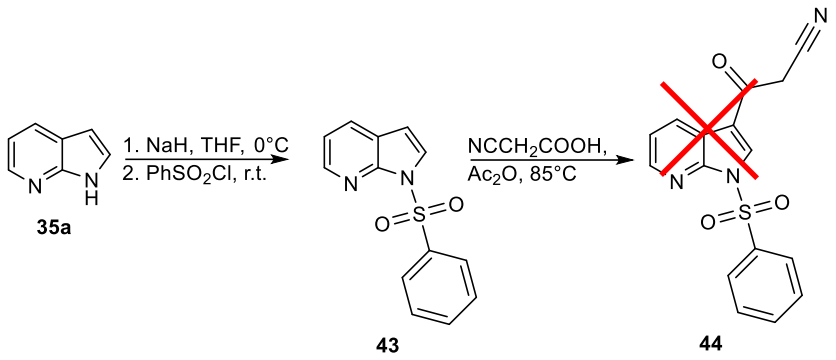

Consequently, it was necessary to protect the nitrogen of 7-azaindole with a another protecting group, such as benzyl group. The reaction was carried out using sodium hydride NaH and benzyl bromide $PhCH_2Br$, in THF, to give 1-benzyl-7-azaindole **36** (yield 58%). The subsequent acylation of the derivative **36**, in the presence of cyanoacetic acid and acetic anhydride at 85°C, gave the *N*-benzyl protected oxopropanenitrile **37** (yield 45%) (Scheme 15.2).

Scheme 15.2. Synthesis of *N*-benzyl protected oxopropanenitrile **37.**

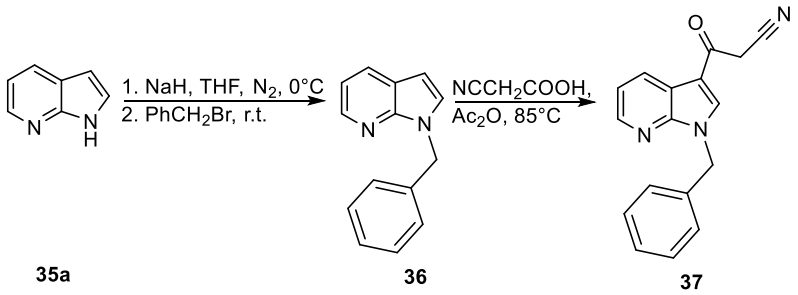

Thus, compound **37** was reacted with intermediates **27,28** in *n*-butanol (*n*-BuOH), in the presence of *p*-toluenesulfonic acid monohydrate ($PTSA \cdot H_2O$) catalyst at 90°C, to give 5-(1-benzyl-7-azaindol-3-yl)-2-(1*H*-indol-3-yl)pyrazolo[1,5-*a*]pyrimidin-7-amine derivatives **18a-h** in good yields (Scheme 16) (Table 9). A subsequent *N*-deprotection procedure of compounds **18a-h,** that was not carried out due to time constraints, could lead to the corresponding *N*-unprotected derivatives.

Scheme 16. Cyclization reaction for synthesis of 5-(1-benzyl-7-azaindol-3-yl)-2-(1*H*-indol-3-yl)pyrazolo[1,5-*a*]pyrimidin-7-amine derivatives **18a-h.**

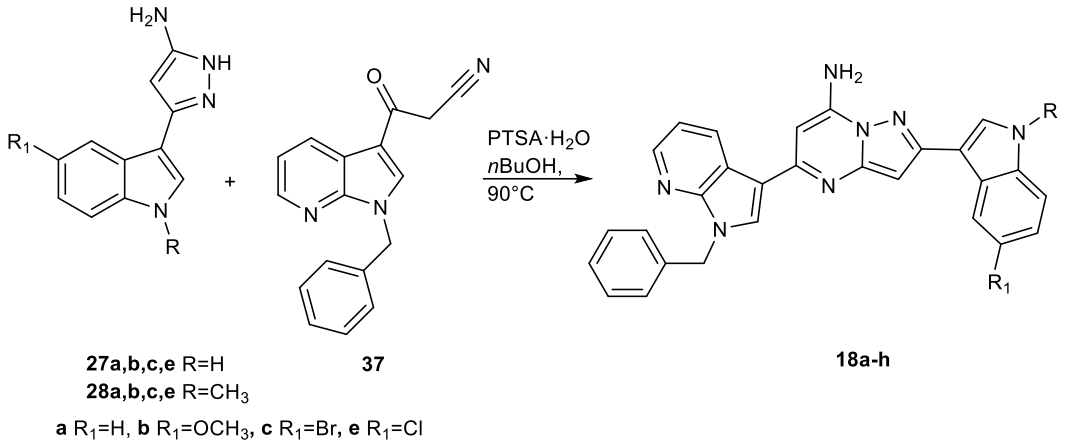

Table 9. 5-(1-benzyl-7-azaindol-3-yl)-2-(1*H*-indol-3-yl)pyrazolo[1,5-*a*]pyrimidin-7-amine derivatives **18a-h**.

Compound	R	R_1	Yield%	Compound	R	R_1	Yield%
18a	H	H	61	**18e**	CH_3	H	51
18b	H	OCH_3	62	**18f**	CH_3	OCH_3	47
18c	H	Br	41	**18g**	CH_3	Br	49
18d	H	Cl	40	**18h**	CH_3	Cl	34

On the other hand, compounds **19,20** (1,3,4-oxadiazoles) and **21,22** (1,3,4-thiadiazoles) were synthesized from the key intermediates **45** or **51.** The key intermediates **45** were prepared through the reaction of hydrazines of type **46** and acids of type **47**, commercially available (Scheme 17). The unavailable hydrazine **46c** was in turn synthesized from their corresponding carboxylic acids **48** treated with hydrazine, according to the procedure already reported in literature [52,75].

Thus, compounds **46** and **47** were reacted in the presence of 1-ethyl-3(3-dimethylaminopropyl) carbodiimide (EDCI), hydroxybenzotriazole, diisopropylethylamine (DIPEA) in dimethylformamide (DMF) to afford compounds **45** in very good yields. Compounds **45** were then cyclized using phosphoryl chloride or Lawesson's reagent in pyridine under reflux, to obtain compound **19** and **21** respectively, in yields from good to excellent (Table 10).

Analogously, compounds **20** and **22** were synthesized from commercially available carboxylic acids **48** and benzoylhydrazine **49**, reacted using the same reaction conditions used for the synthesis of the key intermediates **45** already presented, to obtain the desired compounds **51** in excellent yields (91-95%). The latter were then cyclized in phosphoryl chloride or using Lawesson's reagent in pyridine to afford compounds **20** and **22** respectively, in good yields (Table 11).

Scheme 17. Synthetic pathway of 1,3,4-oxadiazoles **19,20** and 1,3,4-thiadiazoles **21,22**.

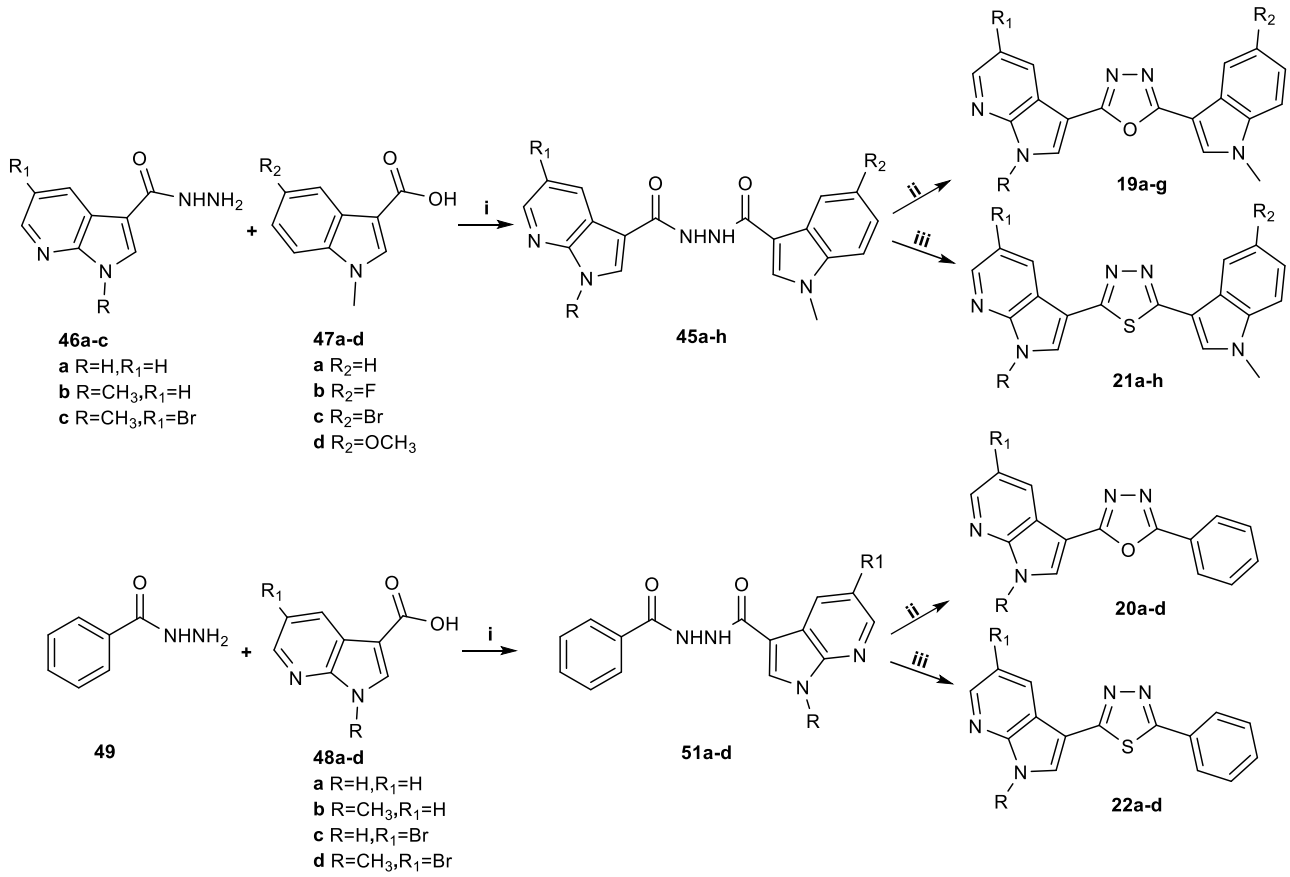

Table 10. 1,3,4-oxadiazoles **19** and 1,3,4-thiadiazoles **21**.

Compound	R	R_1	R_2	Yield%	Compound	R	R_1	R_2	Yield%
19a	H	H	H	75	**21a**	H	H	H	78
19b	CH_3	H	H	86	**21b**	CH_3	H	H	99
19c	CH_3	H	F	85	**21c**	CH_3	H	Br	78
19d	CH_3	H	Br	86	**21d**	CH_3	H	F	60

19e	CH_3	Br	H	78	**21e**	CH_3	H	OCH_3	60
19f	CH_3	Br	Br	90	**21f**	CH_3	Br	H	70
19g	CH_3	Br	F	45	**21g**	CH_3	Br	Br	50
					21h	CH_3	Br	F	80

Table 11. 1,3,4-oxadiazoles **20** and 1,3,4-thiadiazoles **22**.

Compound	R	R_1	Yield%	Compound	R	R_1	Yield%
20a	H	H	70	**22a**	H	H	78
20b	CH_3	H	75	**22b**	CH_3	H	95
20c	H	Br	55	**22c**	H	Br	60
20d	CH_3	Br	60	**22d**	CH_3	Br	82

Table 12. *N*'-(1-methyl-1*H*-indole-3-carbonyl)-7-azaindole-3-carbohydrazides **45** and *N'*-benzoyl-7-azaindole-3-carbohydrazides **51**.

Compound	R	R_1	R_2	Yield%	Compound	R	R_1	Yield%
45a	H	H	H	50	**51a**	H	H	92
45b	CH_3	H	H	80	**51b**	CH_3	H	94
45c	CH_3	H	F	85	**51c**	H	Br	92
45d	CH_3	H	Br	88	**51d**	CH_3	Br	95
45e	CH_3	Br	H	80				
45f	CH_3	Br	Br	82				
45g	CH_3	Br	F	85				
45h	CH_3	H	OCH_3	88				

4. BIOLOGY SECTION

4.1 Pyrazolo[1,5-*a*]pyrimidine derivatives

All the 58 synthesized pyrazolo[1,5-*a*]pyrimidines **15a-j,16a-t,17a-t,18a-h** were submitted to the National Cancer Institute (NCI, Bethesda, MD) and selected to evaluate their antitumor activity against a panel of sixty human cancer cells derived from 9 cancer cell types and grouped into disease subpanels including leukemia, non-small cell lung, colon, central nervous system, melanoma, ovarian, renal, prostate, and breast cancers. They were initially tested according to the NCI protocol at one-dose of 10 µM. The one-dose data was reported as a mean graph of the percent growth of treated cells. The number reported for the one-dose assay is growth relative to the no-drug control, and relative to the time zero number of cells. This allows detection of both growth inhibition (values between 0 and 100) and lethality (values less than 0). For example, a value of 100 means no growth inhibition. A value of 40 would mean 60% growth inhibition. A value of 0 means no net growth over the course of the experiment. A value of -40 would mean 40% lethality. A value of -100 means all cells are dead (Table 13).

Table 13. Mean Growth Percent after exposure at one-dose of 10 µM of compounds.

	Mean Growth Percent[a]									
Compd	**15a** 52.03	**15b** -3.12	**15c** 11.34	**15d** 71.70	**15e** 50.72	**15f** 81.64	**15g** 83.20	**15h** 76.41	**15i** 30.28	**15j** 77.98
Compd	**16a** -29.78	**16b** -55.07	**16c** -9.40	**16d** -36.27	**16e** -71.06	**16f** -63.25	**16g** -63.20	**16h** 17.62	**16i** -58.73	**16j** -39.33
Compd	**16k** -66.95	**16l** -67.16	**16m** 104.74	**16n** -68.28	**16o** -57.48	**16p** -40.44	**16q** -58.16	**16r** -41.93	**16s** -75.48	**16t** 105.21
Compd	**17a** 10.66	**17b** -59.21	**17c** -12.23	**17d** -64.09	**17e** -71.93	**17f** -63.54	**17g** -65.01	**17h** 50.70	**17i** -69.70	**17j** -51.68
Compd	**17k** -4.26	**17l** -47.03	**17m** -51.32	**17n** -49.48	**17q** 37.16	**17r** 12.41	**17s** -67.32	**17t** -68.75		

[a] Data obtained from NCI's *in vitro* disease-oriented tumor cells screen.

To date, the tests at one-dose of 48 compounds (Table 13) have been completed and among these, 41 compounds (**15b-d,15g,15i,16a-l,16n-s,17a-n,17q-t**) satisfied NCI pre-determined threshold inhibition criteria in a minimum number of cell lines and progressed to further screening at five

concentrations at 10-fold dilution (10^{-4}-10^{-8} M) on the full panel (Tables 14-19). The antitumor activity of compounds is expressed for each cell line as GI_{50}, that is the molar concentration of the compound that inhibits 50% net cell growth. The GI_{50} value for each cell line tested against a compound was then converted to its pGI_{50}, that is the –log of the molar concentration that inhibits 50% net cell growth. MG_MID values (mean graph midpoint), representing the arithmetical mean value of pGI_{50} values in the full-panel are also indicated in Table 14.

Table 14. Overview of the results of the *in vitro* antitumor screening for compounds **15,16,17**.

Compounds	N° tested cell lines	N° active cell lines[a]	GI_{50} (μM) Range[b]	pGI_{50} Range	pGI_{50} MG_MID[c]
15b	59	59	0.59-5.54	6.23-5.26	5.71
15c	59	59	1.17-3.21	5.93-5.49	5.76
15d	59	59	1.60-16.3	5.80-4.79	5.66
15g	59	59	0.39-3.23	6.41-5.49	5.77
15i	59	59	1.50-20.9	5.82-4.68	5.70
16°	60	60	1.57-15.0	5.80-4.83	5.54
16b	60	60	1.63-9.32	5.79-5.03	5.58
16c	60	60	1.49-10.1	5.83-4.99	5.51
16d	60	60	1.45-6.25	5.84-5.20	5.63
16e	60	60	1.56-14.8	5.81-4.83	5.60
16f	60	60	1.31-14.0	5.88-4.85	5.69
16g	60	60	1.54-14.1	5.81-4.85	5.66
16h	60	60	1.49-17.6	5.83-4.75	5.62
16i	60	60	0.86-16.9	6.07-4.77	5.48
16j	60	60	1.50-19.7	5.82-4.71	5.69
16k	60	60	0.34-2.05	6.46-5.69	5.78
16l	60	60	1.32-3.00	5.88-5.52	5.75
16n	59	59	1.26-3.12	5.90-5.51	5.76
16o	59	59	0.29-2.18	6.54-5.66	5.79
16p	59	59	1.44-25.1	5.84-4.60	5.69
16q	59	59	1.51-21.7	5.82-4.66	5.62
16r	59	58	1.60-18.0	5.80-4.74	5.49
16s	59	59	1.52-16.9	5.82-4.77	5.66
17a	59	59	1.69-23.0	5.77-4.64	5.29
17b	59	59	1.64-5.91	5.79-5.23	5.63
17c	58	58	1.48-52.8	5.83-4.28	5.33
17d	58	58	1.35-2.91	5.87-5.54	5.73
17e	59	59	1.29-22.8	5.89-4.64	5.68
17f	59	59	1.36-2.54	5.87-5.59	5.74
17g	58	58	1.64-18.1	5.79-4.74	5.49
17h	58	49	1.96-80.8	5.71-4.09	4.80
17i	58	58	1.49-20.1	5.83-4.70	5.70
17j	58	58	1.32-18.6	5.88-4.73	5.56
17k	59	59	1.68-21.0	5.77-4.68	5.44
17l	57	57	2.46-21.8	5.61-4.66	5.00
17m	59	59	1.36-5.18	5.87-5.29	5.63
17n	59	59	1.32-4.19	5.88-5.38	5.71
17q	58	52	2.43-65.6	5.61-4.18	4.88

17r	58	58	1.80-19.2	5.74-4.72	5.22
17s	59	59	1.50-3.23	5.82-5.49	5.72
17t	59	59	1.32-13.8	5.88-4.86	5.73

[a] Active cell line means that compound causes cell growth inhibition with GI_{50} < 100 μM; [b] range is calculated only for GI_{50} of active cell lines; [c] arithmetical mean value of pGI_{50} values in the full-panel.

Table 15. *In vitro* inhibition (μM) of cancer cell lines growth by compounds **15**.

Cell line	Cytotoxicity (GI_{50}[a] in μM)				
	15b	**15c**	**15d**	**15g**	**15i**
Leukemia					
CCRF-CEM	2.81	3.21	3.13	0.44	2.75
HL-60(TB)	1.92	2.27	1.94	1.31	1.83
K-562	2.40	2.81	2.92	0.39	2.79
MOLT-4	2.07	1.34	2.33	1.95	2.31
RPMI82226	2.54	3.17	3.05	1.78	2.64
RS	2.09	1.67	2.08	0.52	1.97
Non-small Cell Lung Cancer					
A549/ATCC	0.59	1.64	1.72	1.70	1.56
EKVX	1.73	1.55	1.76	1.84	1.73
HOP-62	1.93	1.72	2.06	1.81	1.99
HOP-92	1.69	1.51	1.79	1.88	1.90
NCI-H226	2.00	2.14	2.28	2.06	6.50
NCI-H23	ND[b]	ND[b]	ND[b]	ND[b]	ND[b]
NCI-H322M	2.20	1.44	2.09	1.84	1.81
NCI-H460	1.78	1.86	1.87	1.79	1.90
NCI-H522	1.72	1.43	1.65	1.74	1.62
Colon Cancer					
COLO 205	1.65	1.76	1.74	1.70	1.75
HCC-2998	1.97	1.80	1.95	1.87	1.74
HCT-116	1.75	1.45	1.72	1.50	1.85
HCT-15	1.99	1.36	1.79	1.15	1.85
HT29	1.79	1.71	1.80	1.73	1.64
KM12	1.88	1.48	2.00	1.85	1.84
SW-620	1.68	1.92	1.78	1.02	1.78
CNS Cancer					
SF-268	2.13	1.66	1.89	2.03	1.89
SF-295	1.87	1.89	2.10	1.88	1.94
SF-539	1.77	1.46	1.77	1.78	1.90
SNB-19	3.25	1.66	3.03	2.50	2.01
SNB-75	1.63	1.17	16.3	2.13	2.29
U251	1.79	1.49	1.71	1.82	1.68
Melanoma					
LOX IMVI	2.23	2.01	2.44	2.04	2.57
MALME-3M	1.91	1.93	1.84	1.87	1.84
M14	1.81	1.64	1.71	1.74	1.68
MDA-MB-435	1.74	1.71	1.74	1.91	1.73
SK-MEL-2	1.79	1.67	14.6	1.83	2.11
SK-MEL-28	1.82	1.62	1.83	1.85	1.79

SK-MEL-5	1.70	1.70	1.84	1.79	1.71
UACC-257	1.73	1.64	1.69	1.78	1.78
UACC-62	1.84	1.48	1.78	1.96	1.71
Ovarian Cancer					
IGROV1	2.26	1.52	2.11	2.00	1.95
OVCAR-3	1.95	1.80	1.75	1.75	1.74
OVCAR-4	2.28	2.03	1.95	2.04	1.90
OVCAR-5	2.44	1.53	1.83	1.84	1.93
OVCAR-8	1.84	1.98	1.84	1.75	1.82
NCI/ADR-RES	3.09	2.51	1.99	2.07	2.06
SK-OV-3	2.08	1.71	1.81	2.15	20.9
Renal Cancer					
786-0	1.62	1.53	1.63	1.64	1.50
A498	1.92	1.57	1.66	1.84	1.94
ACHN	1.85	1.56	1.88	1.79	1.74
CAKI-1	1.84	1.43	2.03	1.79	2.04
RXF 393	1.67	1.83	1.88	1.87	1.83
SN12C	1.98	1.84	1.92	2.02	1.90
TK-10	2.27	1.80	2.22	1.81	1.62
UO-31	1.65	1.47	1.68	1.66	1.52
Prostate Cancer					
PC-3	1.85	1.67	2.11	1.84	1.89
DU-145	1.93	1.72	2.21	1.80	1.80
Breast Cancer					
MCF7	1.68	1.45	1.60	1.25	1.67
MDA-MB-231/ATCC	2.08	1.89	1.85	1.84	2.00
HS 578T	2.22	2.30	2.35	2.57	2.45
BT-549	5.54	1.68	13.3	3.23	1.76
T-47D	1.91	1.45	1.75	1.70	1.75
MDA-MB-468	1.73	1.59	2.01	1.87	1.59

[a] Data obtained from NCI's *in vitro* disease-oriented tumor cells screen; [b] ND = Not Determined.

Table 16. *In vitro* inhibition (μM) of cancer cell lines growth by compounds **16**.

Cell Line	Cytotoxicity (GI_{50}[a] in μM)								
	16a	**16b**	**16c**	**16d**	**16e**	**16f**	**16g**	**16h**	**16i**
Leukemia									
CCRF-CEM	2.60	3.05	2.65	2.99	2.77	2.14	2.23	2.23	3.22
HL-60(TB)	1.73	2.84	2.18	2.09	1.99	1.76	2.86	1.72	2.91
K-562	1.95	2.49	2.15	2.15	2.34	1.79	3.44	2.53	2.27
MOLT-4	2.25	2.40	2.44	1.86	2.50	2.05	2.48	2.32	1.87
RPMI82226	2.37	2.88	2.64	2.29	2.51	2.37	2.98	2.48	3.42
RS	1.90	2.23	2.09	1.74	2.01	1.43	5.95	2.01	0.86

Non-small Cell Lung Cancer									
A549/ATCC	3.14	2.91	3.81	2.76	3.01	1.86	1.91	2.84	3.15
EKVX	3.93	2.92	3.49	2.44	2.48	1.70	1.83	1.99	2.80
HOP-62	3.14	3.52	4.55	3.10	3.09	2.02	3.10	2.83	2.84
HOP-92	3.04	2.06	2.42	2.10	2.29	1.87	2.25	2.06	2.73
NCI-H226	11.5	6.13	5.57	3.52	11.4	2.13	4.76	10.7	14.1
NCI-H23	3.15	2.36	3.80	2.23	2.36	1.72	1.86	1.91	2.45
NCI-H322M	4.25	3.63	6.05	3.28	2.81	1.85	2.13	2.46	4.54
NCI-H460	2.74	2.07	2.27	1.98	1.95	2.23	1.77	2.20	2.35
NCI-H522	1.64	1.68	1.88	1.74	1.69	1.78	1.65	1.78	1.64
Colon Cancer									
COLO 205	2.12	1.73	1.60	1.75	1.72	2.02	2.10	2.17	2.17
HCC-2998	1.77	1.85	2.02	1.86	1.79	1.63	1.78	1.69	1.80
HCT-116	1.75	1.77	1.91	1.67	1.90	1.72	1.70	1.71	1.84
HCT-15	1.66	1.74	1.71	1.61	1.64	1.31	1.54	1.79	1.72
HT29	1.68	1.98	2.09	2.04	1.69	1.77	1.77	1.89	1.76
KM12	2.21	2.21	2.35	2.02	1.94	2.05	1.94	2.12	2.55
SW-620	2.08	1.87	2.11	1.79	1.77	2.06	1.61	1.95	2.00
CNS Cancer									
SF-268	9.10	3.72	4.15	2.75	4.25	2.35	2.13	2.60	5.21
SF-295	1.83	1.90	1.86	1.81	1.78	1.58	1.74	1.71	1.87
SF-539	1.68	1.74	2.00	1.81	1.81	1.63	1.75	1.63	1.81
SNB-19	4.25	3.67	4.59	2.95	3.14	2.61	2.02	2.38	4.32
SNB-75	11.2	2.17	2.88	1.71	7.65	1.75	2.05	5.15	4.00
U251	2.08	2.00	3.53	1.80	2.04	1.64	1.81	1.97	2.01
Melanoma									
LOX IMVI	1.64	1.69	1.94	1.75	1.81	1.68	1.71	1.74	1.71
MALME-3M	1.70	1.91	2.24	1.78	1.56	1.79	1.87	1.75	3.93
M14	1.79	2.09	1.98	1.85	1.79	1.72	1.79	1.86	2.15
MDA-MB-435	2.04	2.95	3.67	2.42	1.92	1.83	2.07	1.93	3.69
SK-MEL-2	1.83	2.44	3.96	2.28	4.72	1.86	1.88	2.06	6.75
SK-MEL-28	1.72	2.23	2.96	1.87	1.66	1.73	1.85	1.70	7.16
SK-MEL-5	1.70	2.70	3.79	2.05	1.77	1.68	1.92	1.85	7.16
UACC-257	1.73	3.86	4.28	2.99	1.84	1.84	1.95	1.90	10.6
UACC-62	1.73	1.88	6.03	1.72	1.74	1.80	1.65	1.71	5.36
Ovarian Cancer									
IGROV1	4.52	3.55	4.26	3.34	2.64	2.03	1.99	2.18	3.61
OVCAR-3	3.27	3.44	4.17	2.90	2.10	2.02	1.86	2.30	4.75
OVCAR-4	5.06	3.97	4.20	3.65	3.26	2.42	3.06	2.76	7.30
OVCAR-5	3.86	2.08	3.30	1.90	2.05	2.05	1.91	1.97	2.09
OVCAR-8	4.12	4.06	4.30	3.19	2.66	2.05	2.84	3.35	3.53
NCI/ADR-RES	5.84	3.33	3.82	3.45	2.65	2.08	2.22	2.35	2.85
SK-OV-3	15.0	7.75	10.1	6.25	11.8	2.58	6.31	6.82	15.9
Renal Cancer									
786-0	1.57	1.63	1.49	1.67	1.68	1.61	1.88	1.49	1.60
A498	11.4	2.42	2.79	2.09	7.63	14.0	2.06	11.6	10.1
ACHN	2.62	2.77	3.22	2.76	2.22	1.70	2.03	2.07	2.98
CAKI-1	2.32	2.20	2.74	1.99	1.91	1.82	1.59	1.97	2.96
RXF 393	1.38	2.66	2.19	2.23	1.69	1.50	1.85	1.90	2.47
SN12C	10.1	4.02	6.94	3.64	3.47	1.87	1.91	2.44	5.30

TK-10	3.53	2.56	5.54	2.90	2.15	1.76	2.08	2.02	4.34
UO-31	1.86	2.74	3.02	2.59	1.64	1.61	1.71	1.71	4.22
Prostate Cancer									
PC-3	3.33	2.57	3.18	2.59	3.38	2.56	2.09	2.48	3.15
DU-145	5.19	3.88	4.30	3.56	3.61	3.29	3.33	3.70	5.69
Breast Cancer									
MCF7	1.68	2.05	2.54	1.83	1.81	1.68	1.64	1.95	1.65
MDA-MB-231/ATCC	1.91	1.90	2.01	1.96	1.90	2.07	1.91	1.98	1.90
HS 578T	6.69	3.11	3.73	3.25	5.53	3.11	2.56	3.91	4.06
BT-549	13.3	9.32	8.60	4.98	14.8	12.8	14.1	17.6	16.9
T-47D	3.05	3.15	3.54	2.61	2.02	1.85	1.97	2.05	4.44
MDA-MB-468	1.66	1.75	1.70	1.45	1.63	1.36	1.56	1.52	1.89

[a] Data obtained from NCI's *in vitro* disease-oriented tumor cells screen.

Table 17. *In vitro* inhibition (μM) of cancer cell lines growth by compounds **16**.

Cell Line	**Cytotoxicity (GI_{50}[a] in μM)**								
	16j	**16k**	**16l**	**16n**	**16o**	**16p**	**16q**	**16r**	**16s**
Leukemia									
CCRF-CEM	1.95	1.86	2.67	3.12	0.86	2.87	3.19	3.21	4.40
HL-60(TB)	1.50	1.39	1.84	2.02	1.40	2.08	2.10	2.35	1.94
K-562	1.74	0.61	2.29	2.58	0.40	2.42	2.72	2.97	2.26
MOLT-4	1.77	1.59	1.67	1.62	1.69	1.60	2.44	2.58	2.71
RPMI82226	2.11	1.94	2.73	2.62	2.08	2.48	2.93	3.27	2.94
RS	1.95	0.34	1.65	1.66	0.29	1.70	2.16	2.03	2.61
Non-small Cell Lung Cancer									
A549/ATCC	1.97	1.54	1.53	1.59	1.81	2.44	2.17	2.68	1.91
EKVX	1.65	1.80	1.66	1.48	1.46	1.75	3.02	12.6	2.12
HOP-62	1.89	1.89	1.65	1.52	1.73	2.24	1.96	5.29	2.12
HOP-92	1.94	1.68	1.51	1.76	1.76	1.48	2.06	2.23	1.99
NCI-H226	2.20	1.87	1.96	1.89	2.04	25.1	21.7	>100	16.9
NCI-H23	1.75	1.97	1.84	1.79	1.97	2.36	2.08	3.75	2.26
NCI-H322M	3.12	1.58	1.36	1.53	1.64	1.82	2.09	5.14	2.21
NCI-H460	1.86	1.90	2.06	1.92	1.90	1.96	2.02	2.20	2.36
NCI-H522	1.79	1.52	1.50	1.60	1.65	1.55	1.65	1.60	1.75
Colon Cancer									
COLO 205	1.75	1.79	1.89	1.80	1.92	1.95	1.89	1.97	1.89
HCC-2998	1.65	1.94	1.79	1.71	2.09	1.81	1.78	1.78	1.87
HCT-116	1.80	1.54	3.00	1.62	1.16	1.59	1.76	1.87	1.75
HCT-15	1.60	1.23	1.43	1.47	1.04	1.71	1.79	1.84	1.62
HT29	1.63	1.80	1.66	1.56	1.86	1.70	1.74	1.79	1.93
KM12	1.90	2.03	1.94	1.81	2.10	2.02	2.47	2.15	1.99
SW-620	1.62	1.81	1.84	1.95	1.80	2.16	2.01	2.17	2.06
CNS Cancer									
SF-268	2.40	1.94	1.89	1.89	1.97	2.66	3.35	8.07	2.16
SF-295	1.64	1.78	1.78	1.67	1.78	1.81	1.78	1.92	1.78
SF-539	1.75	1.61	1.66	1.64	1.70	1.58	1.76	1.85	1.73

SNB-19	3.43	1.66	1.67	1.68	2.18	3.24	3.09	3.45	3.29
SNB-75	1.74	1.40	1.32	1.50	1.43	2.41	12.9	10.6	1.52
U251	1.85	1.69	1.72	1.70	1.84	1.79	1.82	1.86	1.80
Melanoma									
LOX IMVI	1.86	1.76	1.68	ND[b]	ND[b]	ND[b]	ND[b]	ND[b]	1.71
MALME-3M	1.87	1.74	1.65	1.61	1.70	1.66	1.72	1.71	1.70
M14	1.75	1.79	2.29	1.68	1.85	1.82	1.83	1.95	1.77
MDA-MB-435	1.78	1.77	1.71	1.72	1.76	1.87	1.78	2.06	1.79
SK-MEL-2	1.87	1.67	1.74	1.81	1.70	1.68	1.82	1.84	2.11
SK-MEL-28	1.74	1.78	1.78	1.56	1.80	1.72	1.78	1.69	1.70
SK-MEL-5	1.95	1.76	1.71	1.67	1.81	1.89	1.87	3.50	1.98
UACC-257	1.79	1.68	1.72	1.69	1.77	1.73	1.75	2.44	1.68
UACC-62	1.64	1.62	1.54	1.63	1.73	1.58	1.68	1.64	1.80
Ovarian Cancer									
IGROV1	1.77	1.62	1.50	1.57	1.73	1.82	2.19	2.45	2.53
OVCAR-3	1.74	1.80	1.99	2.08	1.94	2.22	2.69	11.3	2.23
OVCAR-4	1.88	1.70	1.71	1.91	1.82	2.46	2.49	3.28	1.82
OVCAR-5	1.82	1.73	1.62	1.57	1.95	2.55	2.37	5.16	1.81
OVCAR-8	1.90	1.75	2.03	1.87	1.88	1.83	1.97	2.09	2.23
NCI/ADR-RES	1.78	1.89	2.07	2.11	2.03	2.45	2.41	3.03	2.46
SK-OV-3	10.5	1.81	1.98	1.91	1.92	3.72	3.32	18.0	2.24
Renal Cancer									
786-0	1.51	1.59	1.60	1.44	1.55	1.57	1.51	1.74	1.64
A498	19.7	1.73	1.67	1.60	1.76	1.74	14.6	14.3	3.16
ACHN	1.76	1.87	1.69	1.54	1.65	1.78	1.77	2.05	1.75
CAKI-1	1.68	1.73	1.50	1.45	1.71	1.44	1.84	2.00	1.66
RXF 393	1.60	1.74	1.81	1.75	1.85	1.80	1.97	1.98	1.87
SN12C	1.87	1.53	1.65	1.71	1.66	1.66	1.71	1.77	1.90
TK-10	1.77	1.89	1.43	1.26	1.91	2.19	2.01	11.7	2.03
UO-31	1.54	1.46	1.43	1.43	1.59	1.48	1.62	1.63	1.72
Prostate Cancer									
PC-3	1.81	1.67	1.64	1.64	1.80	1.87	2.20	1.93	2.97
DU-145	2.04	1.82	1.92	1.84	2.05	4.96	4.15	6.37	3.62
Breast Cancer									
MCF7	1.68	1.46	1.83	1.59	0.93	1.55	1.77	1.77	1.66
MDA-MB-231/ATCC	1.94	1.51	1.77	1.79	1.82	1.70	1.97	1.82	2.31
HS 578T	2.55	2.05	1.98	1.91	2.18	2.44	2.39	3.30	2.38
BT-549	12.4	1.83	2.07	1.66	1.87	2.29	10.5	14.6	12.9
T-47D	1.81	2.01	1.74	1.84	1.94	2.07	2.63	10.1	1.76
MDA-MB-468	1.55	1.57	1.49	1.34	1.67	1.57	1.92	2.20	1.62

[a] Data obtained from NCI's *in vitro* disease-oriented tumor cells screen; [b] ND = Not Determined.

Table 18. *In vitro* inhibition (μM) of cancer cell lines growth by compounds **17.**

Cell Line	Cytotoxicity (GI_{50}[a] in μM)									
	17a	**17b**	**17c**	**17d**	**17e**	**17f**	**17g**	**17h**	**17i**	**17j**
Leukemia										
CCRF-CEM	2.87	3.71	2.56	2.85	3.84	1.61	2.35	3.45	2.51	3.32
HL-60(TB)	1.84	2.01	1.48	2.16	1.55	1.79	1.90	9.35	1.80	2.06
K-562	2.79	2.88	1.97	2.59	2.50	1.89	3.42	4.09	2.76	2.40
MOLT-4	3.32	2.13	1.79	2.24	1.82	2.11	2.42	2.42	1.93	1.76
RPMI82226	2.42	3.07	3.05	2.91	4.04	2.23	2.43	5.67	2.60	3.88
RS	ND[b]	ND[b]	2.55	2.74	2.72	1.93	2.80	4.36	2.30	2.27
Non-small Cell Lung Cancer										
A549/ATCC	4.19	2.78	2.75	1.77	1.80	1.84	2.48	16.4	1.84	2.13
EKVX	15.3	3.14	8.55	1.66	2.34	1.76	3.47	>100	1.85	3.04
HOP-62	6.15	2.12	10.2	2.07	1.74	1.68	8.69	62.2	1.70	4.41
HOP-92	5.81	1.65	4.84	1.69	1.99	1.71	14.2	20.4	1.98	2.16
NCI-H226	14.0	3.29	20.4	1.95	1.92	2.51	1.92	24.3	1.73	2.23
NCI-H23	19.0	1.87	6.29	1.76	1.89	1.76	2.52	75.3	1.71	2.63
NCI-H322M	12.7	2.86	4.90	1.75	2.12	2.21	2.90	>100	1.91	3.47
NCI-H460	3.56	1.93	1.88	1.80	1.95	1.96	1.80	6.62	1.77	1.92
NCI-H522	5.54	1.84	4.48	1.75	1.85	1.70	13.8	5.77	1.74	1.90
Colon Cancer										
COLO 205	10.7	1.96	4.71	1.82	1.99	1.82	1.78	55.5	1.75	2.83
HCC-2998	2.23	1.65	1.80	1.74	1.82	1.76	1.79	4.20	1.76	1.76
HCT-116	2.11	1.82	3.60	1.81	1.95	1.91	1.90	32.2	1.81	2.01
HCT-15	2.13	1.70	1.91	1.35	2.71	1.69	1.82	2.55	1.79	1.61
HT29	1.95	1.80	1.98	1.96	1.83	1.97	1.91	5.04	2.00	1.93
KM12	3.34	1.79	3.41	1.99	1.78	1.59	2.50	4.00	2.03	2.17
SW-620	2.58	2.00	1.99	1.75	2.14	1.88	1.83	6.93	2.01	1.82
CNS Cancer										
SF-268	17.9	2.42	13.5	1.84	2.03	2.25	11.6	>100	2.06	7.39
SF-295	1.99	1.81	1.68	1.57	2.20	1.88	1.69	9.90	1.65	1.84
SF-539	2.58	1.67	1.63	1.64	1.58	1.64	1.78	13.7	1.62	1.66
SNB-19	14.8	2.76	8.67	2.45	2.50	2.15	4.05	37.7	2.60	3.25
SNB-75	2.44	1.70	ND[b]	ND[b]	1.29	1.46	ND[b]	ND[b]	ND[b]	ND[b]
U251	3.34	2.02	2.17	1.81	1.87	1.77	2.00	5.72	2.00	1.81
Melanoma										
LOX IMVI	2.06	1.64	2.02	1.65	1.82	1.70	1.80	1.96	1.87	1.95
MALME-3M	3.25	2.14	5.02	1.68	1.52	1.89	1.75	10.4	1.62	2.18
M14	2.63	1.91	4.56	1.83	2.02	1.69	1.88	12.3	1.81	2.37
MDA-MB-435	11.0	1.93	10.8	1.68	1.70	1.71	1.92	21.6	1.71	2.06
SK-MEL-2	12.5	1.99	19.3	1.68	17.2	1.79	12.6	26.4	12.3	2.63
SK-MEL-28	5.33	2.18	10.8	1.67	1.62	1.82	1.70	14.5	1.53	2.10
SK-MEL-5	7.04	3.46	6.18	1.78	1.75	2.08	11.6	31.3	1.65	4.35
UACC-257	13.7	3.50	21.5	1.72	1.75	2.00	14.8	23.3	1.90	12.5
UACC-62	5.71	1.66	14.2	1.55	1.73	1.60	1.77	17.7	1.63	1.69

Ovarian Cancer										
IGROV1	19.1	3.29	2.12	1.65	1.70	1.96	2.24	14.3	1.75	1.94
OVCAR-3	2.93	1.74	12.5	1.81	1.67	1.67	1.82	>100	1.68	3.23
OVCAR-4	3.42	2.70	2.06	1.84	1.83	1.95	11.6	22.5	1.79	2.98
OVCAR-5	11.0	1.82	4.66	1.59	1.41	2.03	3.33	21.9	1.73	2.01
OVCAR-8	4.63	3.22	4.93	1.86	1.99	2.01	3.18	16.8	1.81	2.29
NCI/ADR-RES	4.66	2.21	ND[b]	ND[b]	ND[b]	ND[b]	ND[b]	ND[b]	ND[b]	ND[b]
SK-OV-3	20.6	5.91	52.8	2.38	22.8	2.54	18.1	>100	2.03	18.6
Renal Cancer										
786-0	1.69	1.81	1.54	1.77	1.57	1.64	1.64	8.47	1.56	1.64
A498	23.0	4.90	25.3	2.22	1.72	1.55	17.0	>100	20.1	13.1
ACHN	3.77	2.17	3.48	1.46	1.83	1.66	1.71	6.52	1.72	1.87
CAKI-1	3.85	1.69	4.03	1.41	1.80	1.49	2.21	6.42	1.64	3.07
RXF 393	2.28	2.54	1.67	1.73	1.65	1.89	1.77	2.63	1.49	1.72
SN12C	11.6	5.02	6.93	1.70	1.82	1.72	13.1	>100	1.52	10.1
TK-10	17.1	2.69	19.1	2.48	2.11	1.78	2.95	26.5	2.02	2.27
UO-31	5.41	2.48	3.59	1.73	1.54	1.62	1.66	12.8	1.55	2.93
Prostate Cancer										
PC-3	3.83	2.41	6.67	2.54	2.48	1.69	3.26	11.4	2.54	2.27
DU-145	5.09	3.58	6.36	1.78	1.82	1.82	2.06	80.8	1.81	3.18
Breast Cancer										
MCF7	3.30	1.95	2.01	1.67	3.01	1.80	2.01	4.11	1.77	1.77
MDA-MB-231/ATCC	3.40	1.79	2.33	1.65	1.89	1.78	1.92	5.28	1.92	1.98
HS 578T	20.0	2.61	20.3	1.80	2.32	2.29	16.9	>100	1.97	12.6
BT-549	11.8	4.10	7.03	2.14	1.68	2.19	12.8	>100	1.91	13.8
T-47D	2.99	3.22	5.77	1.73	2.03	1.80	2.90	34.0	1.73	2.38
MDA-MB-468	2.21	2.23	1.53	1.42	1.59	1.36	1.66	4.64	1.56	1.32

[a] Data obtained from NCI's *in vitro* disease-oriented tumor cells screen; [b] ND = Not Determined.

Table 19. *In vitro* inhibition (μM) of cancer cell lines growth by compounds **17.**

Cell Line	**Cytotoxicity (GI_{50}[a] in μM)**							
	17k	**17l**	**17m**	**17n**	**17q**	**17r**	**17s**	**17t**
Leukemia								
CCRF-CEM	2.52	3.52	1.78	1.62	7.83	8.29	2.58	2.87
HL-60(TB)	2.33	3.53	2.17	2.07	>100	12.1	1.54	1.99
K-562	2.30	2.94	2.50	3.17	10.5	6.00	1.75	1.84
MOLT-4	2.38	3.52	1.95	1.83	20.0	5.98	2.02	1.71
RPMI82226	2.38	13.6	2.12	3.32	13.6	10.1	2.40	2.93
RS	ND[b]	2.46	ND[b]	ND[b]	2.48	4.58	ND[b]	ND[b]
Non-small Cell Lung Cancer								

A549/ATCC	4.60	9.25	3.37	2.31	7.70	3.37	2.87	1.62
EKVX	10.7	10.1	3.05	1.48	19.0	11.4	1.68	1.48
HOP-62	4.50	14.8	3.11	2.09	4.05	7.80	1.96	1.72
HOP-92	2.93	4.97	1.61	2.05	11.2	11.3	2.16	1.86
NCI-H226	2.70	15.1	2.36	4.19	4.04	5.36	2.02	1.99
NCI-H23	10.0	15.7	3.92	2.25	13.7	7.44	2.32	1.91
NCI-H322M	11.6	10.4	2.92	1.59	17.9	5.75	2.76	1.66
NCI-H460	3.75	7.78	2.05	1.83	5.43	3.44	1.88	1.79
NCI-H522	2.35	12.8	1.85	1.87	10.8	5.61	1.77	1.87
Colon Cancer								
COLO 205	3.09	16.8	1.98	1.81	6.78	12.6	1.77	2.56
HCC-2998	2.26	3.74	1.81	1.66	61.2	7.19	1.71	1.74
HCT-116	2.56	7.98	1.67	1.66	>100	15.0	1.62	1.55
HCT-15	2.17	2.53	1.76	1.48	>100	3.73	1.89	1.57
HT29	2.15	5.65	1.92	2.08	4.14	3.18	1.98	1.91
KM12	3.84	6.04	1.97	1.45	>100	12.9	2.14	1.49
SW-620	4.38	ND[b]	1.84	1.84	52.7	6.46	1.80	1.76
CNS Cancer								
SF-268	17.2	13.1	2.64	2.30	15.6	19.2	2.13	2.11
SF-295	1.73	13.5	1.81	1.77	3.22	1.80	1.77	1.75
SF-539	1.80	14.1	1.65	1.67	10.6	3.54	1.73	1.51
SNB-19	5.11	17.8	3.98	2.25	5.79	11.0	3.23	1.89
SNB-75	4.97	11.9	1.36	1.66	ND[b]	ND[b]	1.54	1.75
U251	3.16	5.65	2.48	1.94	4.12	3.23	2.18	1.94
Melanoma								
LOX IMVI	2.15	ND[b]	1.79	1.53	2.43	1.91	1.77	1.61
MALME-3M	1.86	16.8	1.74	1.92	10.6	3.43	1.71	1.74
M14	1.90	15.3	1.80	1.66	57.0	4.05	1.67	1.71
MDA-MB-435	1.95	16.4	1.72	1.80	>100	6.19	1.71	1.76
SK-MEL-2	2.17	11.2	2.83	2.07	10.4	11.4	1.91	1.93
SK-MEL-28	1.71	15.2	1.64	1.61	>100	3.90	1.65	1.72
SK-MEL-5	3.44	15.1	1.69	3.27	46.2	12.5	1.59	1.82
UACC-257	1.83	14.0	1.98	1.79	65.6	7.29	1.72	1.71
UACC-62	1.73	11.5	1.61	1.56	20.4	2.64	1.60	1.47
Ovarian Cancer								
IGROV1	2.84	11.7	2.06	2.04	4.45	3.91	1.87	1.71
OVCAR-3	3.08	13.5	1.98	1.77	14.1	11.1	1.91	1.63
OVCAR-4	2.60	17.1	2.13	2.13	4.12	4.51	2.03	2.01
OVCAR-5	8.81	14.5	4.76	1.63	25.2	12.5	1.85	1.52
OVCAR-8	5.63	21.8	3.17	2.08	4.60	6.20	2.13	2.02
NCI/ADR-RES	5.02	17.4	3.62	2.28	ND[b]	ND[b]	2.25	2.06
SK-OV-3	21.0	20.4	4.65	2.41	14.4	15.0	2.02	13.8
Renal Cancer								
786-0	1.68	13.4	1.74	1.73	4.82	4.64	1.65	1.76
A498	17.6	8.84	14.8	2.18	50.0	13.5	1.90	7.39
ACHN	2.60	13.5	2.09	1.50	4.21	3.72	1.86	1.55
CAKI-1	3.74	12.7	2.19	1.47	13.0	8.11	1.85	1.45
RXF 393	2.01	6.13	1.66	1.96	2.61	2.54	1.54	1.82

SN12C	2.97	12.8	5.18	2.11	9.61	4.41	1.63	1.72
TK-10	11.6	13.8	4.25	2.36	10.3	4.92	1.91	1.60
UO-31	4.77	13.1	1.85	1.78	31.9	12.2	1.62	1.54
Prostate Cancer								
PC-3	5.52	6.58	2.75	2.45	11.0	10.4	2.21	1.76
DU-145	9.59	21.3	2.88	2.79	8.97	5.16	2.54	1.78
Breast Cancer								
MCF7	3.38	5.31	2.27	1.77	13.4	3.60	1.83	1.64
MDA-MB-231/ATCC	2.99	13.5	1.84	1.62	9.62	2.90	1.76	1.43
HS 578T	2.48	ND[b]	2.09	2.29	11.3	10.7	2.10	1.89
BT-549	10.2	19.5	1.83	2.12	13.3	10.9	1.59	1.91
T-47D	5.77	7.38	3.24	1.66	6.15	3.25	1.80	1.58
MDA-MB-468	2.43	3.71	1.82	1.32	3.81	1.95	1.50	1.32

[a] Data obtained from NCI's *in vitro* disease-oriented tumor cells screen; [b] ND = Not Determined

All derivatives which were tested at 5 concentrations showed interesting *in vitro* antiproliferative activity with GI_{50} values ranging from micromolar to submicromolar level against all full panel NCI. The only exceptions were the derivatives **16r,17h,17q,** for which some cell lines were non-sensitive.

From structure activity relationship (SAR) analysis on all tested compounds, it was observed that the compounds that exhibited submicromolar GI_{50} values for a few cell lines were four bis-indolyl derivatives (**15b,15g,16k,16o**) bearing a methoxy group on the indole linked to C(5)-carbon of the pyrazole[1,5-*a*]pyrimidine ring. Interestingly also the presence of a methyl group at the N atom of the indole linked to C(2)-carbon of the pyrazole[1,5-*a*]pyrimidine ring seemed to play an important role for the inhibitory activity on some leukemia lines. In fact, among the 5-methoxy substituted derivatives, the derivatives **15g,16k,16o** were the most active on two leukemia cell lines K-562 and RS with submicromolar GI_{50} values. GI_{50} values against K-562 and RS were respectively: 0.39 µM and 0.52 µM for derivative **15g**, 0.61 µM and 0.34 µM for derivative **16k**, 0.40 µM and 0.29 µM for derivative **16o**. In addition, the derivatives **15g** and **16o** also selectively inhibited the cell growth of leukemia CCRF-CEM line with GI_{50} values of 0.44 µM and 0.86 µM, respectively. Derivative **16o** was shown to be also selective for MCF7 line of breast cancer (GI_{50} 0.93 µM); while the bis-5-methoxy-1*H*-indole derivative **15b** exhibited submicromolar GI_{50} value (0.59 µM) for A549/ATCC of lung cancer.

4.2 Oxadiazole and thiadiazole derivatives

4.2.1 Antiproliferative activity

During the third year of my PhD, I spent 5 months at the Cancer Center Amsterdam, under the supervision of Prof. Elisa Giovannetti, to evaluate the activity of the oxadiazole and thiadiazole derivatives against seven pancreatic ductal adenocarcinoma PDAC cell lines: BxPC-3, Suit-2, Capan-1, PaTu-T, Panc-1, gemcitabine-resistant Panc-1 (Panc-1-GR) and the primary culture PDAC-3 cell lines (Figure 29).

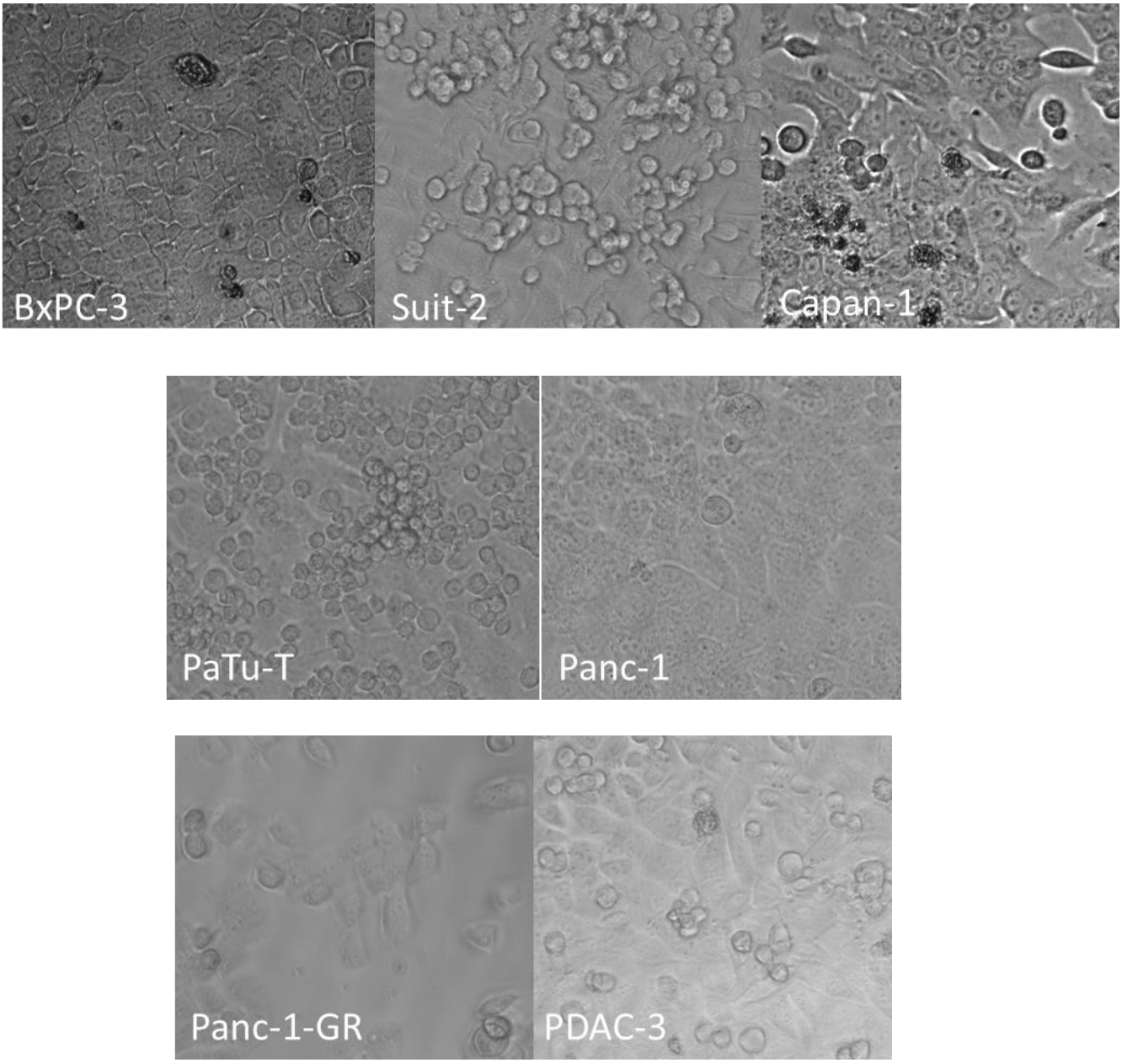

Figure 29. Microscopic observation of BxPC-3, Suit-2, Capan-1, PaTu-T, Panc-1, Panc-1-GR, and PDAC-3 cell culture after 72 hours incubation.

BxPC-3 are cells isolated from a pancreas adenocarcinoma, produce mucin, and exhibit an epithelial phenotype. BxPC-3 cells lack a KRAS mutation, although it is commonly found in pancreatic cancers. BxPC-3 cells have a high expression of tumor stem cell markers. BxPC-3 has been used in tumorigenicity studies, pancreatic cancer therapy research, and other biomedical applications. The cells have also been studied for their phenotypic and genotypic properties as they can be applied to the development of drugs against pancreatic cancer. In particular, BxPC-3 cells have a high expression of the angiogenic factors IL-8, VEGF and PGE2, which can serve as potential drug targets. BxPC-3 cells were cultured in RPMI medium supplemented with 10% NBCS (New Born Calf Serum) and 1% Pen/Strep in T-75 flasks.

Suit-2 is a cell line derived from a metastatic liver tumor of PDAC carcinoma. Suit-2 cell line produces and releases at least two tumor markers, carcinoembryonic antigen and carbohydrate antigen. Under an electron microscope, they appear to be morphologically heterogeneous (i.e., both fusiform and polygonal). Cells were cultured in RPMI-1640 (Roswell Park Memorial Institute 1640) supplemented with 10% heat-inactivated FBS (fetal bovine serum) and 1% Pen/Strep (penicillin/streptomycin) solution in T-75 flasks.

Capan-1 cells are adherent epithelial-like cells derived from a liver metastasis of a pancreatic adenocarcinoma that grown in tissue culture appeared as large epithelial-like mucin-producing cells. They are characterized by large, relatively dark stained nuclei and abundant slightly basophilic, finely granular, reticulated, or vacuolated cytoplasm. Cells were cultured in DMEM (Dulbecco's Modified Eagle's Medium) supplemented with 10% FBS and 1% Pen/Strep in T-75 flasks.

PaTu-T cells originate from liver metastases of human pancreatic adenocarcinoma, are highly invasive with significant metastatic potential. PaTu-T has the KRAS G12V mutation and a missense mutation in p53. PaTu-T cells were cultured in DMEM medium supplemented with 10% FBS and 1% Pen/Strep in T-75 flasks.

Panc-1 is an epithelioid carcinoma attached cell line, that is commonly used as an *in vitro* model to study pancreatic ductal adenocarcinoma carcinogenesis and tumor therapies, given the presence of the SSTR2 receptors, prognostic marker in pancreatic cancer. Specifically, these receptors and the presence of neuroendocrine differentiation make this cell line suitable for neuroendocrine chemotherapy of pancreatic cancer and for radionuclide therapy of the peptide receptor. Panc-1 cells appear to be morphologically heterogeneous (i.e., both cuboid and focally sarcomatoid) and typically display a perinuclear Golgi, scattered or apically localized cytoplasmic vesicles, and many apical

plasma membrane microvilli. Panc-1 cells were cultured in RPMI-1640 medium supplemented with 10% FBS and 1% Pen/Strep in T-75 flasks.

Panc-1-GR (gemcitabine-resistant Panc-1) is a gemcitabine-resistant sub-clone obtained by continuous exposure of Panc-1 to gemcitabine for 6 days, as previously described [76]. Panc-1-GR were cultured in RPMI medium supplemented with 10% NBCS and 1% Pen/Strep in T-75 flasks.

Cytotoxic chemotherapy remains the mainstay of treatment for most PDAC patients. The chemotherapeutic agent gemcitabine has been approved by the US Food and Drug Administration as a first-line therapy for pancreatic cancer since 1997. Treatment with 5-fluorouracil, leucovorin, irinotecan and oxaliplatin (Folfirinox) or with a combination of gemcitabine and nab-paclitaxel, represent the standard-of-care for unresectable patients, and recent data support the use of Folfirinox as adjuvant therapy after surgical resection. However, PDAC is broadly chemoresistant cancer, with a 5-year survival rate below 9%. Gemcitabine treatment has some disadvantages, including chemoresistance within a few weeks from treatment initiation [77,78]. It has been suggested that overcoming resistance to gemcitabine in pancreatic cancer may increase patient survival. Therefore, the identification of an agent capable to circumvent gemcitabine in pancreatic cancer may be a potential method for improving the treatment of pancreatic cancer. For this reason, we decided to extend the activity evaluation of the most active oxadiazole and thiadiazole compounds also against Panc-1-GR cells.

PDAC-3 is a primary cell line, obtained from a patient undergoing pancreaticoduodenectomy. This cellular model was chosen as previous studies showed that its genetic and histological characteristics were similar to the original tumor. Cells were cultured in RPMI medium supplemented with 10% NBCS and 1% Pen/Strep in T-75 flasks.

All the cells were maintained under conditions where they are actively growing and undergoing mitotic division, in a humidified incubator at 37°C with a supply of 5% CO_2, 95% air atmosphere and 100% relative humidity. Each compound was initially dissolved in dimethyl sulfoxide (DMSO), to obtain 10 mM stock solution, stored at +4 °C, which was then diluted in complete culture medium immediately before use at the appropriate concentration. Cells were exposed to three screening concentrations (0.1 μM, 1 μM, 10 μM) of each compound for 72 hours, and the antiproliferative activity was then evaluated by the Sulforhodamine B (SRB) chemosensitivity assay.

Graphs in the Figure 30a-f show cell growth percentage after 72 hours of treatment with each of the most active compounds **19b,19e,20c,21b,22c**, as single agent against each pancreatic cancer cell line exposed to three concentrations (0.1-10 μM). At concentration of 0.1 μM all compounds did not

appreciably impair vitality of pancreatic cancer cells, while at concentration of 10 μM all compounds showed antiproliferative activity against BxPC-3, Panc-1, Suit-2, Capan-1, and PaTu-T cells. The only compounds with antiproliferative activity against PDAC-3 and Panc-1-GR cells at concentration of 10 μM were **19b** and **21b,** with mean growth percentage values of 38.35% and 55.90% against PDAC-3, 22.47% and 40.65% against Panc-1-GR cells, respectively (Table 20). For the compounds **19e** and **22c** no growth inhibition was observed for Panc-1-GR cells, for compound **19e** also for PDAC-3 cells no growth inhibition was found (Table 20). In addition, Panc-1-GR cells were less sensitive to all compounds compared to Panc-1 cells, at the same concentration (Table 20). These results may be related to an alteration of various cell signaling pathways, transcriptional factors and enzymes, due to previous treatment with gemcitabine that cause resistance in this cell type. Studies demonstrate that Panc-1-GR cells exhibit upregulation of stem cell genes [76] and overexpression of proteins, such as pERK, and therefore an overactivation of the MAPK/ERK signaling pathway [79]. However, the mechanisms underlying the resistance to gemcitabine still lack clear explanations [78].

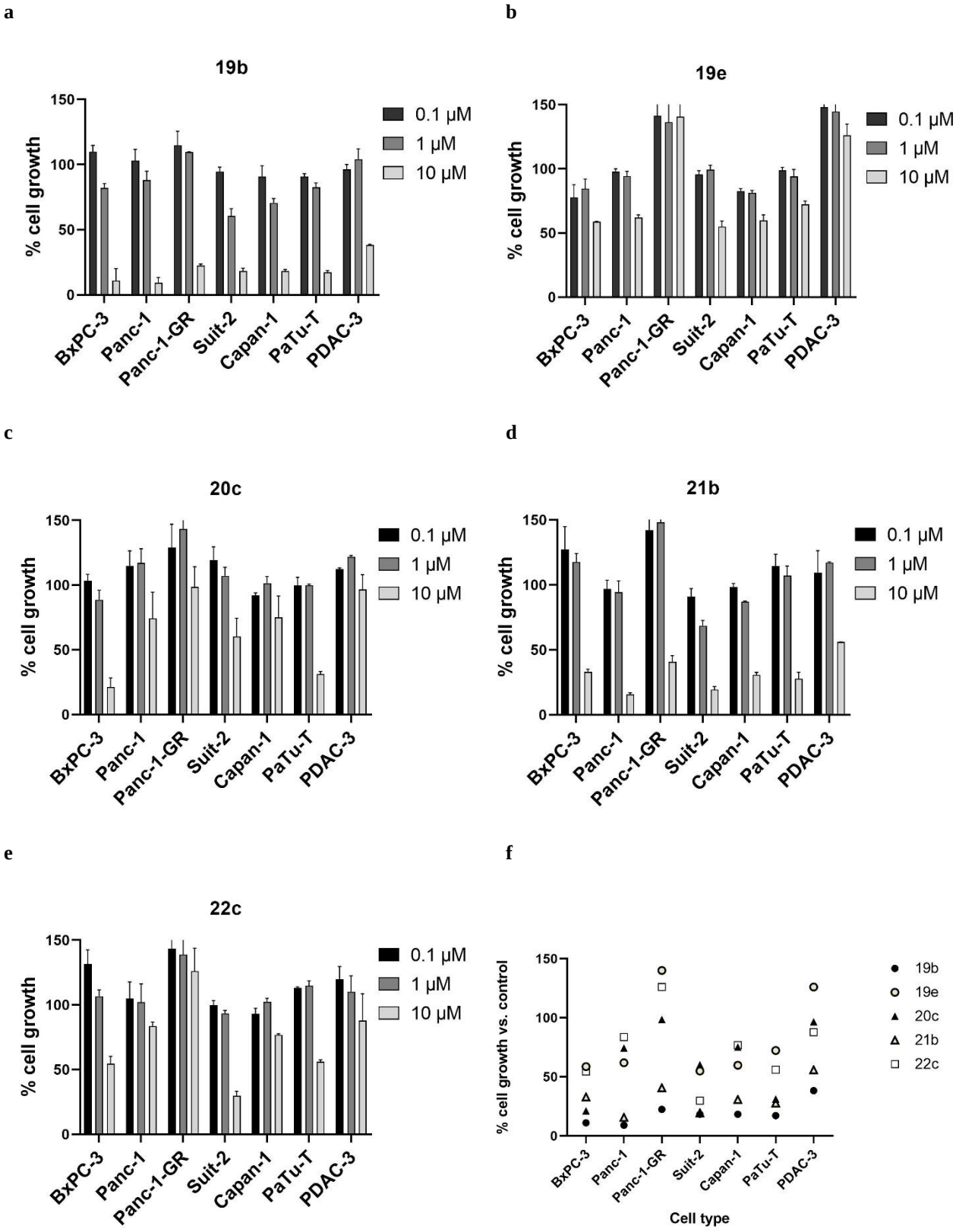

Figure 30. (a-e) Cell growth after 72 hours of treatment with each of the most active compounds **19b,19e,20c,21b,22c** against each pancreatic cancer cell lines exposed to three concentrations (0.1-10 μM). (f) Cell growth data summary after 72 hours of treatment with each of the most active compounds **19b,19e,20c,21b,22c** at concentration of 10 μM.

Table 20. Cell growth percentage after 72 hours of exposure to 10 μM of the most active compounds **19b,19e,20c,21b,22c.**

PDAC cell lines	Mean Growth Percentage[a]				
	1,3,4-oxadiazoles			1,3,4-thiadiazoles	
	19b	19e	20c	21b	22c
BxPC-3	11.10	58.64	21.13	32.88	54.59
Panc-1	9.12	61.96	74.33	15.68	83.68
Panc-1-GR	22.47	>100	98.62	40.65	>100
Suit-2	18.34	54.94	60.18	19.46	29.80
Capan-1	18.33	59.84	75.17	30.86	76.76
PaTu-T	17.13	72.33	31.22	27.73	56.09
PDAC-3	38.35	>100	96.60	55.90	87.84

[a] Data were expressed as mean values of three replicates.

SRB assays have been performed again to obtain the IC_{50} values of these five compounds. Cells were exposed to eight increasing concentrations (from 0.312 μM to 40 μM) of each compound for 72 hours. IC_{50} value, which is defined as the half maximal inhibitory concentration, was calculated by a non-linear least squares curve fitting using GraphPad PRISM software. Data were expressed as mean values ± SEM of three replicates. Concentration dependent studies revealed that for the compounds **19b,19e,** and **21b** Suit-2 cells were the most sensitive cells (with IC_{50} values of 1.4, 9.4, and 1.9 μM, respectively); for compounds **20c** and **22c** the cells found to be the most sensitive were BxPC-3 (IC_{50} value of 3.3 μM) and PaTu-T (with IC_{50} value of 3.8 μM), respectively. A weak antiproliferative activity was observed against PDAC-3 and Panc-1-GR cells, for which the only active compounds were **19b** and **21b**, with IC_{50} values of 8.1 and 10.6 μM against PDAC-3 cells, and 8.0 and 9.8 μM against Panc-1-GR cells, respectively. Among the compounds, the two most active against each cell line were 1,3,4-oxadiazole **19b** (IC_{50} 1.4-8.1 μM) and 1,3,4-thiadiazole **21b** (IC_{50} 1.9-10.6 μM) (Table 21).

Table 21. List of the half maximal inhibitory concentrations values (IC_{50}) in μM of derivatives **19b,19e,20c,21b,22c** on pancreatic cancer cells. IC_{50} calculated by a non-linear least squares curve fitting using GraphPad PRISM software. Values are reported as the Means ± Standard Error of the Mean of three separate experiments.

PDAC cell lines	Cytotoxicity IC_{50} (μM) ± SEM[a]				
	1,3,4-oxadiazoles			1,3,4-thiadiazoles	
	19b	19e	20c	21b	22c
BxPC-3	2.1 ±0.006	ND[b]	3.3±2.4	2.7 ± 0.68	ND
Panc-1	2.5 ± 0.55	ND	13.4±3.2	3.5 ± 0.01	11.5±1.2
Panc-1-GR	8.0 ± 2.8	ND	10.8±1.4	9.8 ± 0.05	ND
Suit-2	1.4 ± 0.74	9.4±4.3	ND	1.9 ± 0.27	4.1±0.9
Capan-1	2.6 ± 0.62	ND	10.8±0.67	3.3 ± 0.61	12.6±1.3
PaTu-T	3.2 ± 0.42	ND	9.7±0.17	3.4 ± 0.06	3.8±1.8
PDAC-3	8.1 ± 0.14	23±0.06	ND	10.6 ± 0.04	ND

[a] SEM: Standard Error of the Mean. [b]ND not determined.

Finally, additional experiments were performed to evaluate the *in vitro* cytotoxicity of the most active compound **19b** against the normal human skin fibroblasts Hs27 after treatment with eight different concentrations (from 0.31 μM to 40 μM) by SRB assay. As shown in Figure 31, the derivative was relatively non-toxic to normal fibroblast cells. We found only 18% growth inhibition of Hs27 cells after 72 hours exposure at the highest concentration tested (40 μM). The non-toxicity of the compound **19b** was confirmed on Hs27 cells treated with the concentrations below 10 μM, which showed a cell growth rates >100%, comparable to untreated cells, proving the absence of cytotoxicity in human normal cells.

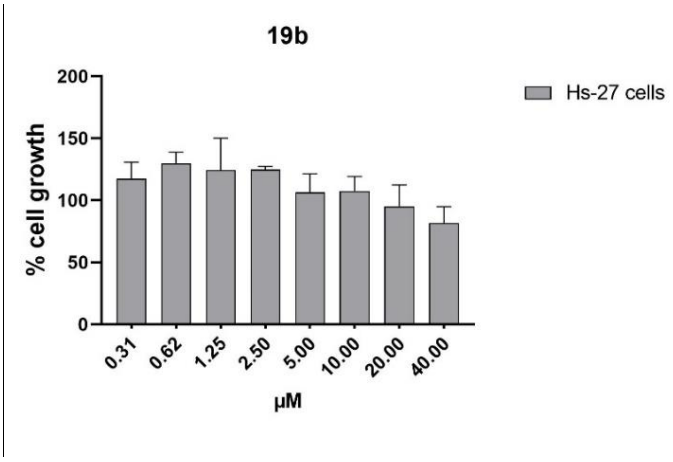

Figure 31. Toxicity evaluation of compound **19b** at different concentrations (from 0.31 μM to 40 μM) against normal human skin fibroblast Hs27 cells.

From structure activity relationship (SAR) analysis on the five most active compounds **19b,19e,20c,21b,22c**, we observe that both between 7-azaindolyl-phenyl-oxadiazoles and 7-azaindolyl-phenyl-thiadiazoles, the presence of a bromine atom at 5 position of the 7-azaindole ring and the absence of methyl group at position 1 of the 7-azaindole moiety seems to favor cytotoxic activity. Likewise, among 7-azaindolyl-indolyl-oxadiazoles and 7-azaindolyl-indolyl-thiadiazoles the absence of substituent at 5 position of the 7-azaindole and indole, and the presence of a methyl group at the 7-azaindole N-atom improve the antiproliferative activity.

4.2.2 Effect on cell cycle

Alterations in the cell cycle caused by the most active compound **19b** was evaluated in the primary cell culture PDAC-3, and the Suit-2, that was the most sensitive cell line to this compound. Cell cycle progression was analyzed by cytofluorimetry, using propidium iodide (3,8-diamino-5-[3-(diethylmethylammonio)propyl]-6phenyl- diiodide, PI) staining solution.

Cell cycle analysis showed an increase in G2-M cells and a decrease in the G1 phase. In PDAC-3 cells the compound **19b**, at concentration of 2 μM and 4-fold IC_{50}, decreased cells in G0-G1 phase from 59% to 54% and 29%, respectively, as well as in S phase from 25% to 23% and 19%. In contrast, the cells in G2-M phase increased from 16% to 23% and 52%. The cell cycle arrest in G2-M phase was most evident in Suit-2 cells. In Suit-2 cells the compound **19b**, at concentration of 2 μM and 4-fold IC_{50}, decreased cells in G0-G1 phase from 54% to 10% and 10%, respectively, as well as the S phase from 23% to 15% and 14%. In contrast, the cells in G2-M phase increased from 23% to 75% and 76% (Figure 32).

These data are consistent with the hypothesis that these new derivatives may act by protein kinases inhibition involved in the cell cycle. Further studies will be needed to affirm this, such as protein kinase activity assays. The representative cell cycle spectra are reported in the Supporting Information chapter (Figure 35-40).

a **b**

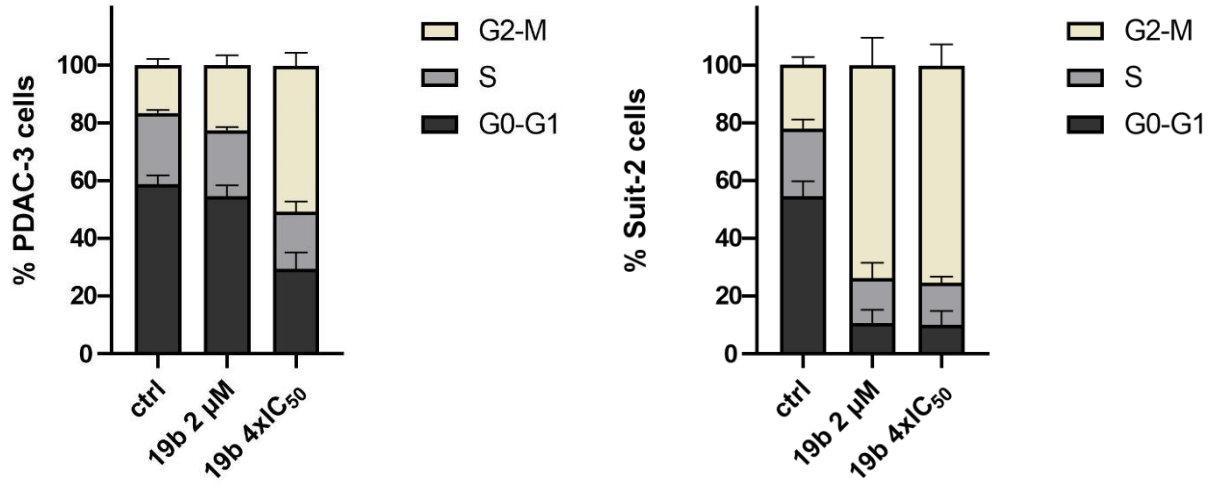

Figure 32. Effects of the oxadiazole compound **19b** on cell cycle modulation in PDAC-3 cells (a) and in Suit-2 cells (b). Cells were exposed for 24 hours to drug. Columns show the mean percentages of cells at various stages of cell cycle, G0-G1 (black), S (dark gray), and G2-M (light gray) phase, in untreated control (ctrl) and after treatment with the compound at concentration of 2 μM and 4-fold IC_{50}.

4.2.3 Anti-migration activity

Cancer cell migration is a key factor contributing to the aggressiveness of PDAC. It is therefore important to find new compounds that can counteract or stop this process. To evaluate the impact of the most active compounds **19b,21b** on *in vitro* cell migration, the *in vitro* scratch wound healing assay has been performed, using a 96-pin floating array device (Figure 34b), on the seven PDAC cell lines (BxPC-3, Suit-2, Capan-1, PaTu-T, Panc-1, Panc-1-GR, and PDAC-3). The *in vitro* scratch wound healing assay is an easy, economical, and well-developed method. It is based on the observation that, upon the creation of a new artificial space, so-called ‘‘scratch’’, on a monolayer of confluent cells, the cells on the edge of the newly created gap will move towards the opening to close the “scratch” until new cell-to-cell contacts are re-established. The basic steps therefore concern: the creation of a ‘‘scratch’’ on monolayer cells, the capture of pictures at the beginning and regular intervals during cell migration to close the scratch, and the comparison of the images to determine the rate of cell migration. The compounds were tested at concentrations of 4-fold IC_{50}.

The data (Figure 33, Table 22) showed that both compounds inhibited the cell migration rate compared with untreated cells, already after 4 hours and continued up to 24 hours. This was observed for all the cancer cell lines tested, except for BxPC-3 and Capan-1 cells. For BxPC-3 cells the

reduction of cell migration was evident only before of 20 hours, instead after 20 hours the compound **21b** allowed 100% wound closure. In this cell line the most interesting anti-migratory result was observed after 8 hours, in which the migration percentage of cells treated with each compound **19b**, and **21b** were 39% and 66%, respectively; while untreated cells achieved 100% wound closure. For Capan-1 cells anti-migratory effect occurred from 8 hours up to 24 hours, no effect was observed before 4 hours.

When cell migration percentage values of each cell line, treated with compound **19b** and **21b**, are compared to control (set at 100%) (Table 23), the most marked anti-migratory effect was observed for PDAC-3, Panc-1-GR and Capan-1 cell lines. In fact, after 24 hours, the migration percentage of cells treated with each compound **19b** and **21b** were 23% and 34% in PDAC-3, 49% and 42% in Panc-1-GR, 48% and 45% in Capan-1, respectively. For the other cell lines the inhibitory effect on cell migration of the two compounds after 24 hours was also observed but less considerable. The migration percentage of cells treated with each compound **19b** and **21b**, compared to control (set at 100%) were 71% and 100% in BxPC-3, 68% and 45% in PaTu-T, respectively; 66% in Suit-2 for both compounds (Table 23).

To sum up, between the two derivatives, compound **21b** showed the best results against all cell lines, except for BxPC-3 and PDAC-3 cells, for which compound **19b** was the most potent. In the case of Capan-1 and Suit-2 cells the two compounds showed almost the same anti-migratory effect throughout the 24-hour period.

The Figure 34a shows representative images of the wounds closure captured with the microscope at 0, 4, 8, 20 and 24 hours after scratch on PDAC-3 cells. It demonstrates that the cell density in the scratch area is reduced after treatment, compared with the control throughout the 24-hour period, as is reflected by a higher scratch area in treated wells.

a

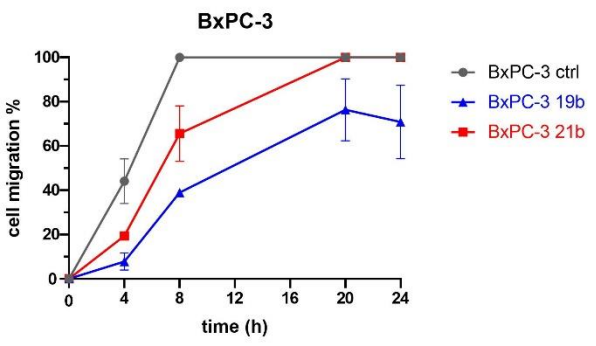

a

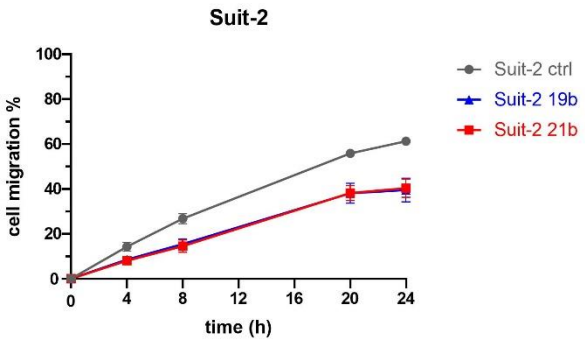

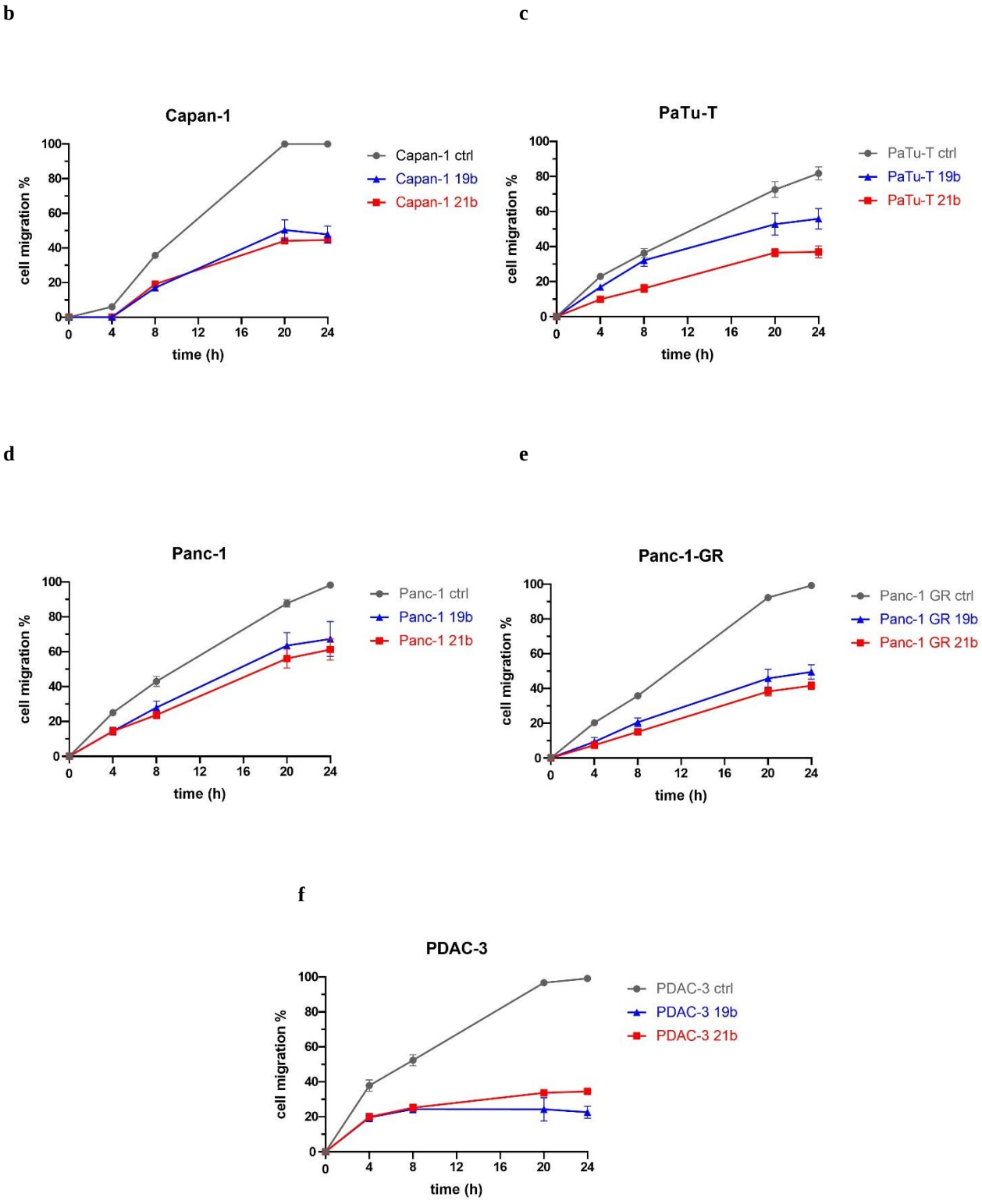

Figure 33. Cell migration percentage monitored over time (0, 4, 8, 20 and 24 hours) of BxPC-3 (a), Suit-2 (b), Capan-1 (c), PaTu-T (d), Panc-1 (e), Panc-1-GR (f), and PDAC-3 (g) cells treated with compounds **19b** and **21b** at concentration of 4 x IC_{50}. Points, mean values obtained from the means of at least three different scratch areas.

Table 22. Cell migration percentage monitored over time (0, 4, 8, 20 and 24 hours) of BxPC-3, Suit-2, Capan-1, PaTu-T, Panc-1, Panc-1-GR, and PDAC-3 cells treated with compound **19b** and **21b** at concentration 4 x $IC_{50.}$ P values were calculated with Student's t-test. ****p < 0.0001, ***p < 0.001, **p < 0.01, *p < 0.05, n.s. = not significant.

PDAC cell lines	cell migration percentage (%)											
	4h			8h			20h			24h		
	ctrl	19b	21b	ctrl	19b	21b	ctrl	19b	21b	ctrl	19b	21b
BxPC-3	44[a]	8 ***[b]	19 ***	100	39 ****	66 ***	100	76 **	100 *	100	71 **	100 n.s.
Panc-1	25	14 ****	14 ****	43	28 ****	24 ****	88	63 ****	56 ****	98	67 ****	61 ****
Panc-1-GR	20	9 ***	7 ****	36	21 ***	15 ****	92	46 ***	38 ****	99	49 ***	42 ****
Suit-2	14	8 ****	8 ****	27	15 ****	15 ****	56	38 ****	38 ****	61	40 ****	40 ****
Capan-1	6	0 ***	0 ***	36	17 ***	19 ***	100	50 ***	44 ***	100	48 ***	45 ***
PaTu-T	23	17 ***	10 ****	36	32 ****	16 ****	73	53 ****	37 ****	82	56 ****	37 ****
PDAC-3	38	20 ****	20 ****	52	24 ****	24 ****	97	24 ****	34 ****	99	23 ****	34 ****

[a] Cell migration %. [b] Cell migration % and P values.

Table 23. Cell migration percentage compared to control ctrl (untreated cells) set at 100%, of each cell line treated with compound **19b** and **21b**.

PDAC cell lines	cell migration percentage (%) compared to control set at 100%											
	4h			8h			20h			24h		
	ctrl	19b	21b	ctrl	19b	21b	ctrl	19b	21b	ctrl	19b	21b
BxPC-3	44	8	19	100	39	66	100	76	100	100	71	100
Panc-1	25	14	14	44	29	24	90	64	57	100	68	62
Panc-1-GR	20	9	7	36	21	15	93	46	38	100	49	42
Suit-2	23	13	13	44	25	25	92	62	62	100	66	66
Capan-1	6	0	0	36	17	19	100	50	44	100	48	45
PaTu-T	28	21	22	44	39	19	89	65	45	100	68	45
PDAC-3	38	20	20	52	44	24	98	24	34	100	23	34

a **b**

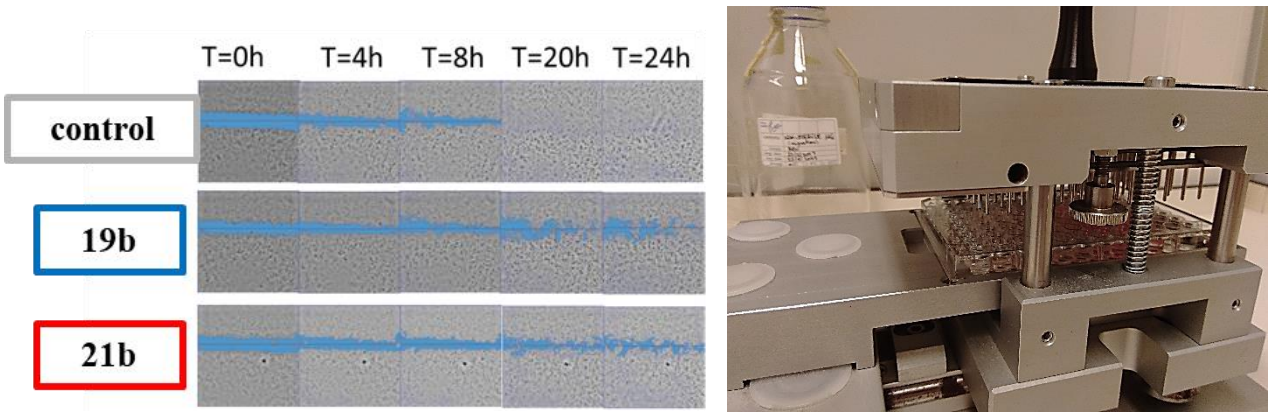

Figure 34. (a) Representative images of the wounds closure captured with the microscope at 0, 4, 8, 20 and 24 hours after scratch on PDAC-3 cells. Original magnification 5X. (b) 96-pin floating array device used to perform the scratches.

5. EXPERIMENTAL SESSION

5.1 Chemistry

The anhydrous solvents used for organic synthesis (*n*-butanol, tetrahydrofuran, *N*,*N*-dimethylformamide) and the reagents were purchased from Sigma-Aldrich Co, Alfa Aesar, VWR International and Acros Organics. Other solvents were purified and dried using standard method: toluene was distilled from calcium hydride; dichloromethane was distilled from phosphoric anhydride. All dry solvents were stored over 4 Å molecular sieves. All air- or moisture-sensitive reactions were performed using oven-dried glassware under an inert dry nitrogen atmosphere. Analytical thin layer chromatography (TLC) was performed on silica gel 60 F254 plates (0.25 mm thickness) and the develop plates were examined under ultraviolet (UV) light. All melting points were taken on a Buchi capillaries apparatus and were uncorrected. ^{1}H and ^{13}C NMR spectra were measured at 200-400 MHz and 50-101 MHz, respectively, in DMSO-d_6 or $CDCl_3$ solution, using a Bruker Avance II spectrometer. Chemical shifts were described in parts per million (δ), coupling constants (J) are expressed in Hertz (Hz), and splitting patterns were reported as singlet (s), doublet (d), triplet (t), quartet (q), multiplet (m), doublet of doublets (dd) and triplet of doublets (td). Chromatography column was performed with Merk silica gel 230-400 mesh ASTM or FLASH40i Biotage chromatography or with Buchi Sepacore Flash chromatography module (prepacked cartridge reference). Elementary analysis (C, H, N) were within ± 0.4% of the theoretical values.

Some compounds were characterized only by ^{1}H NMR spectra, for their poor solubility.

General procedure for the synthesis of 1-methyl-1*H*-indoles (26a-e):

To a solution of commercial indole **25a-e** (5.0 mmol) in anhydrous toluene (50 ml), potassium *tert*-butoxide (*t*-BuOK) (6.8 mmol) and tris[2-(2-methoxyethoxy)ethyl]amine (TDA-1) (1–2 drops) were added. After stirring overnight, methyl iodide (5 mmol) was added dropwise to the reaction mixture. Then, the resulting suspension was stirred at room temperature for 1-2 hours. After the solvent was removed *in vacuo*, the resulting residue was treated with water (15 ml) and extracted with dichloromethane DCM (3 × 15 ml), dried (Na_2SO_4) and evaporated under reduced pressure. The product obtained was purified by column chromatography, using dichloromethane or dichloromethane/ethyl acetate (9/1) as eluent.

1-Methyl-1*H*-indole (26a):

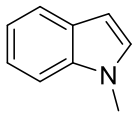

Yield: 96%; yellow oil; ^{1}H NMR (200 MHz, $CDCl_3$) δ: 3.86 (s, 3H, CH_3), 6.67-6.69 (m, 1H, H-3), 7.17 (d, 1H, *J* = 3.2 Hz, H-2), 7.29-7.35 (m, 1H, H-5), 7.39-7.49 (m, 2H, H-6 and H-7), 7.83-7.86 (m, 1H, H-4); ^{13}C NMR (50 MHz, $CDCl_3$) δ: 32.4 (q), 100.2 (d), 109.6 (d), 118.8 (d), 120.2 (d), 120.9 (d), 128.0 (s), 129.5 (d), 136.3 (s); *Anal.* Calculated for C_9H_9N (MW: 131.17): C, 82.41; H, 6.92; N, 10.68%. Found: C, 82.59; H, 6.80; N, 10.77%.

5-Methoxy-1-methyl-1*H*-indole (26b) [80]**:**

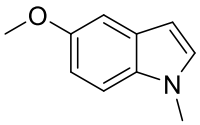

Yield: 97%; yellow solid; m.p.: 84°C; ^{1}H NMR (200 MHz, $CDCl_3$) δ: 3.67 (s, 3H, CH_3), 3.81 (s, 3H, OCH_3), 6.38 (d, *J* = 2.9 Hz, 1H, H-3), 6.87 (dd, *J* = 2.9, 8.8 Hz, 1H, H-6), 6.96 (d, *J* = 2.9 Hz, 1H, H-4), 7.07 (d, *J* = 2.9 Hz, 1H, H-2), 7.17 (d, *J* = 8.8 Hz, 1H, H-7); ^{13}C NMR (50 MHz, $CDCl_3$) δ: 32.8 (q), 55.8 (q), 100.3 (d), 102.4 (d), 109.8 (d), 111.8 (d), 128.7 (s), 129.2 (d), 132.1 (s), 153.9 (s); *Anal.* Calculated for $C_{10}H_{11}NO$ (MW: 161.08): C, 74.51; H, 6.88; N, 8.69%. Found: C, 74.76; H, 6.84; N, 8.43%.

5-Bromo-1-methyl-1*H*-indole (26c):

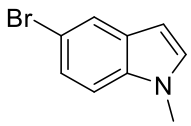

Yield: 96%; yellow solid; m.p.: 41°C; ^{1}H NMR (200 MHz, $CDCl_3$) δ: 3.47 (3H s, CH_3), 6.29 (d, *J* = 3.1 Hz, 1H, H-3), 6.84 (d, *J* = 3.1 Hz, 1H, H-2), 6.94 (d, *J* = 8.5 Hz, 1H, H-7), 7.17 (dd, *J* = 1.7, 8.5 Hz, 1H, H-6), 7.65 (d, *J* = 1.7 Hz, 1H, H-4); ^{13}C NMR (50 MHz, $CDCl_3$) δ: 32.6 (CH_3), 100.2 (CH), 110.5 (CH), 121.2 (C), 122.9 (CH), 123.9 (CH), 127.6 (C), 129.8 (CH), 135.1 (C); *Anal.* Calculated for C_9H_8BrN (MW: 210.07): C, 51.46; H, 3.84; N, 6.67%. Found: C, 51.62; H, 3.78; N, 6.89%.

5-Fluoro-1-methyl-1*H*-indole (26d) [70]**:**

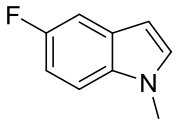

Yield: 98%; yellow solid; m.p.:55-56°C; ^{1}H NMR (200 MHz, $CDCl_3$) δ: 3.72 (3H, s, CH_3), 6.41 (d, *J* = 3.2 Hz, 1H, H-3), 6.89-7.05 (m, 2H, H-4 and H-6), 7.15-7.28 (m, 2H, H-2 and H-7); ^{13}C NMR (50 MHz, $CDCl_3$) δ: 33.0 (q), 100.7 (d, J_{C3-F} = 4.9 Hz), 105.4 (d, J_{C7-F} = 5.6 Hz), 109.6 (d, J_{C4-F} = 23.3 Hz), 109.9 (d, J_{C6-F} = 10.8 Hz), 130.3 (d), 130.4 (s x 2), 157.8 (d, J_{C5-F} = 233.0 Hz); *Anal.* Calculated for C9H8FN (MW: 149.16): C, 72.47; H, 5.41; N, 9.39%. Found: C, 72.82; H, 5.21; N, 9.12%.

5-Cloro-1-methyl-1*H*-indole (26e) [80]**:**

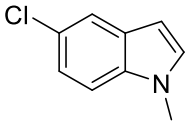

Yield: 98%; yellow solid; m.p.: 35 °C; ^{1}H NMR (200 MHz, $CDCl_3$) δ: 3.52 (s, 3H, CH_3), 6.32 (d, *J* = 3.2 Hz, 1H, H-3), 6.89 (d, *J* = 3.2 Hz, 1H, H-2), 7.05 (d, *J* = 8.4 Hz, 1H, H-7), 7.51 (d, *J* = 8.4 Hz, 1H, H-6), 7.65 (s, 1H, H-4); ^{13}C NMR (50 MHz, $CDCl_3$) δ: 32.2 (q), 100.2 (d), 110.0 (d), 119.7 (d), 121.3 (d), 124.6 (s), 129.2 (s), 129.9 (d), 134.8 (s); *Anal.* Calculated for C_9H_8ClN (MW: 165.62): C, 65.27; H, 4.87; N, 8.46%. Found: C, 65.54; H, 4.84; N, 8.69%.

General procedure for the synthesis of 3-(1*H*-indol-3-yl)-3-oxopropanenitriles (23a-e) and 3-(1-methyl-1*H*-indol-3-yl)-3-oxopropanenitriles (24a-e):

A solution of cyanoacetic acid (9 mmol) and acetic anhydride (Ac_2O) (9 ml) was heated to 85 °C for 10 minutes. Then appropriate indole **25a-e**, **26a-e** (9 mmol) was added to this solution heated at 85°C for additional 0.5 - 6 hours (the progress of the reaction was monitored by TLC). After completion, the reaction mixture was cooled and then poured into water and ice. The obtained precipitate was filtered off, dried and was triturated if necessary with DCM, to obtain the desired products (**23a-e**,**24a-e**).

3-(1*H*-indol-3-yl)-3-oxopropanenitrile (23a) [73,81]**:**

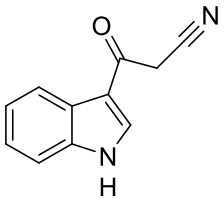

Yield: 95%; white solid; m.p.: 244-245°C; IR (cm^{-1}): 3221 (NH), 2252 (CN), 1638 (CO); ^{1}H NMR (300 MHz, DMSO-d_6) δ: 4.48 (s, 2H, CH_2), 7.23-7.25 (m, 2H, H-5, H-6), 7.51 (d, *J* = 8.4 Hz, 1H, H-7), 8.13 (d, *J* = 8.4 Hz, 1H, H-4), 8.36 (d, *J* = 2.4 Hz, 1H, H-2), 12.15 (br s, 1H, NH); ^{13}C NMR (75 MHz, DMSO-d_6) δ: d = 29.4 (t), 112.4 (d), 114.4 (s), 116.4 (s), 121.0 (d), 122.3 (d), 123.3 (d), 125.1 (s), 135.4 (d), 136.6 (s), 182.8 (s); *Anal.* Calculated for $C_{11}H_8N_2O$ (MW: 184,20): C, 71.73; H, 4.38; N, 15.21%. Found: C, 71.48; H, 4.11; N, 15.02%.

3-(5-methoxy-1*H*-indol-3-yl)-3-oxopropanenitrile (23b) [81]**:**

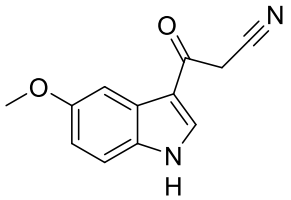

Yield: 94%; beige solid; m.p.: 288-290°C (Lit. m.p. 270°C); IR (cm^{-1}): 3223 (NH), 2258 (CN), 1631 (CO); ^{1}H NMR (300 MHz, DMSO-d_6) δ: 3.79 (s, 3H, OCH_3), 4.46 (s, 2H, CH_2), 6.88 (dd, *J* = 2.7, 8.7, 1H, H-6), 7.40 (d, *J* = 8.7 Hz, 1H, H-7), 7.63 (d, *J* = 2.7 Hz, 1H, H-4), 8.30 (d, *J* = 3.2 Hz, 1H, H-2), 12.08 (br s, 1H, NH); ^{13}C NMR (75 MHz, DMSO-d_6) δ: 29.3 (t), 55.3 (d), 102.7 (d), 113.1 (d), 113.2 (d), 114.3 (d), 116.4 (s), 126.0 (s), 131.4 (s), 135.5 (d), 155.8 (s), 182.7 (s); *Anal.* Calculated for $C_{12}H_{10}N_2O_2$ (MW:214.22): C, 67.28; H, 4.71; N, 13.08%. Found: C, 67.34; H, 4.79; N, 13.12%.

3-(5-bromo-1*H*-indol-3-yl)-3-oxopropanenitrile (23c) [82]**:**

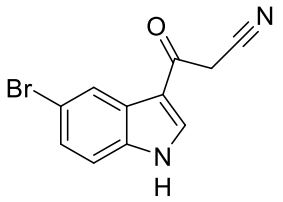

Yield: 85%; pale yellow solid; m.p.: 300-301°C (Lit. m.p. 296-298°C); IR (cm^{-1}): 3205 (NH), 2252 (CN), 1634 (CO); ^{1}H NMR (300 MHz, DMSO-d_6) δ: 4.50 (s, 2H, CH_2), 7.38 (dd, J = 8.7, 1.8 Hz, 1H, H-6), 7.49 (d, J = 9.0 Hz, 1H, H-7), 8.24 (d, J = 2.1 Hz, 1H, H-4), 8.41 (s, 1H, H-2), 12.35 (br s, 1H, NH); ^{13}C NMR (75.4 MHz, DMSO-d_6) δ: 29.48 (CH_2), 113.87 (C-3), 114.57 (C-7), 115.07 (C-Br), 116.21 (CN), 123.11 (C-2), 125.94 (C-6), 126.88 (C-3a), 135.38 (C-7a), 136.55 (C-4), 183.10 (CO); *Anal.* Calculated for $C_{11}H_7BrN_2O$ (MW: 263.09): C, 50.22; H, 2.68; N, 10.65%. Found: C, 50.10; H, 2.78; N, 10.65%.

3-(5-fluoro-1*H*-indol-3-yl)-3-oxopropanenitrile (23d):

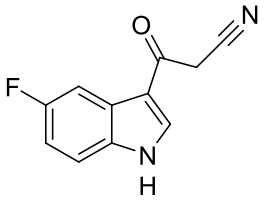

Yield: 86%; white solid; m.p. 271-272°C (Lit. m. p.: 275-280 °C); IR (cm^{-1}): 3219 (NH), 2255 (CN), 1636 (CO); ^{1}H NMR (400 MHz, DMSO-d_6) δ: 4.48 (s, 2H, CH_2), 7.11 (td, J = 9.2, 2.6 Hz, 1H, H-6), 7.52 (dd, J = 8.9, 4.6 Hz, 1H, H-7), 7.79 (dd, J = 9.8, 2.6 Hz, 1H, H-4), 8.42 (s, 1H, H-2), 12.26 (br s, 1H, NH); ^{13}C NMR (101 MHz, DMSO-d_6) δ: 29.87 (t), 106.37 (d, $J_{C4\text{-}F}$ = 24.6 Hz), 111.97 (d, $J_{C6\text{-}F}$ = 25.8 Hz), 114.26 (d, $J_{C7\text{-}F}$ = 9.7 Hz), 114.99 (d, $J_{C7a\text{-}F}$ = 4.0 Hz), 116.70 (s), 126.27 (d, $J_{C3a\text{-}F}$ = 11.1 Hz), 133.70 (s), 137.29 (d), 159.32 (d, $J_{C5\text{-}F}$ = 235.6 Hz), 183.39 (s); *Anal.* Calculated for $C_{11}H_7FN_2O$ (MW: 202,19): C, 65.35; H, 3.49; N, 13.86%. Found: C, 65.45; H, 3.51; N, 13.88%.

3-(5-chloro-1*H*-indol-3-yl)-3-oxopropanenitrile (23e) [83]**:**

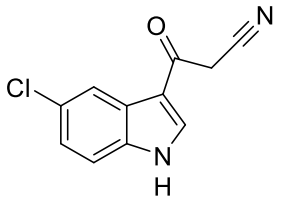

Yield: 86%; light yellow solid; m.p. 282-283°C (Lit. 299-300°C); IR (cm^{-1}): 3217 (NH), 2253 (CN), 1638 (CO); ^{1}H NMR (400 MHz, DMSO-d_6) δ: 4.51 (s, 2H, CH_2), 7.27 (dd, *J* = 8.7, 2.2 Hz, 1H, H-6), 7.53 (d, *J* = 8.6 Hz, 1H, H-7), 8.10 (d, *J* = 1.9 Hz, 1H, H-4), 8.43 (d, *J* = 2.0 Hz, 1H, H-2), 12.35 (br s, 1H, NH); ^{13}C NMR (101 MHz, DMSO-d_6) δ: 29.94(t), 114.47(s), 114.62(d), 116.68(s), 120.56(d), 123.85(d), 126.77(s), 127.50(s), 135.61(s), 137.17(d), 183.54(s); *Anal.* Calculated for $C_{11}H_7ClN_2O$ (MW:218,64): C, 60.43; H, 3.23; N, 12.81%. Found: C, 60.45; H, 3.21; N, 12.80%.

3-(1-methyl-1*H*-indol-3-yl)-3-oxopropanenitrile (24a) [81]**:**

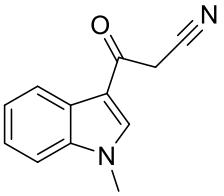

Yield 90%; white solid; m.p. 156-157°C (Lit. 154°C); IR (cm^{-1}): 2256 (CN), 1639 (CO); ^{1}H NMR (300 MHz, DMSO-d_6) δ: 3.88 (s, 3H, CH_3), 4.46 (s, 2H, CH_2), 7.37 – 7.24 (m, 2H, H-5, H-6), 7.58 (d, *J* = 7.6 Hz, 1H, H-7), 8.15 (d, *J* = 7.5 Hz, 1H, H-4), 8.38 (s, 1H, H-2); ^{13}C NMR (75 MHz, DMSO-d_6) δ: 29.3 (t), 55.3 (q), 102.7 (d), 113.1 (d), 113.2 (d), 114.3 (d), 116.4 (s), 126.0 (s), 131.4 (s), 135.5 (d), 155.8 (s), 182.7 (s); *Anal.* Calculated for $C_{12}H_{10}N_2O$ (MW: 198,23): C, 72.71; H, 5.09; N, 14.13%. Found: C, 72.75; H, 5.19; N, 14.31%.

3-(5-methoxy-1-methyl-1*H*-indol-3-yl)-3-oxopropanenitrile (24b):

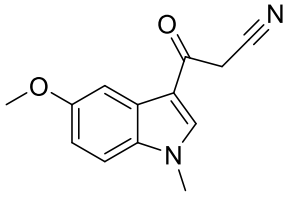

Yield 84%; white solid; m.p.: 200-201°C; IR (cm^{-1}): 2257 (CN), 1636 (CO); ^{1}H NMR (400 MHz, DMSO-d_6) δ: 3.80 (s, 3H, CH_3), 3.84 (s, 3H, OCH_3), 4.40 (s, 2H, CH_2), 6.94 (dd, *J* = 8.9, 2.5 Hz, 1H, H-6), 7.48 (d, *J* = 8.9 Hz, 1H, H-7), 7.64 (d, *J* = 2.5 Hz, 1H, H-4), 8.30 (s, 1H, H-2); ^{13}C NMR (101 MHz, DMSO-d_6) δ: 29.78 (t), 34.05 (q), 55.85 (q), 103.52 (d), 112.31 (d), 113.45 (s), 113.45 (d), 116.79 (s), 126.96 (s), 132.79 (s), 139.16 (d), 156.66 (s), 182.55 (s); *Anal.* Calculated for $C_{13}H_{12}N_2O_2$ (MW: 228,25): C, 68.41; H, 5.30; N, 12.27%. Found: C, 68.48; H, 5.33; N, 12.29%.

3-(5-bromo-1-methyl-1*H*-indol-3-yl)-3-oxopropanenitrile (24c):

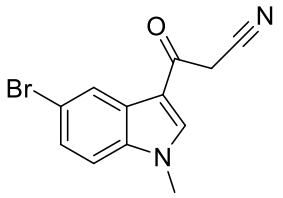

Yield 81%; white solid; m.p.: 228-228.8°C; IR (cm^{-1}): 2255 (CN), 1653 (CO); ^{1}H NMR (300 MHz, DMSO-d_6) δ: 3.88 (s, 3H, CH_3), 4.46 (s, 2H, CH_2), 7.47 (d, J = 8.7 Hz, 1H, H-6), 7.59 (d, J = 8.6 Hz, 1H, H-7), 8.26 (s, 1H, H-4), 8.42 (s, 1H, H-2); ^{13}C NMR (101 MHz, DMSO-d_6) δ: 29.98 (t), 34.13 (q), 113.12 (s), 113.74 (d), 116.08 (s), 116.58 (s), 123.66 (d), 126.41 (d), 127.66 (s), 136.63 (s), 140.25 (d), 182.99 (s); *Anal.* Calculated for $C_{12}H_9BrN_2O$ (MW: 277,12): C, 52.01; H, 3.27; N, 10.11%. Found: C, 52.13; H, 3.31; N, 10.15%.

3-(5-fluoro-1-methyl-1*H*-indol-3-yl)-3-oxopropanenitrile (24d):

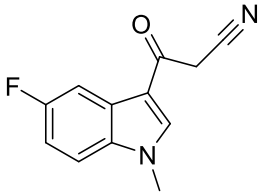

Yield: 74%; white solid; m.p.: 212°C; IR (cm^{-1}): 2256 (CN), 1647 (CO); ^{1}H NMR (400 MHz, DMSO-d_6) δ: 3.88 (s, 3H, CH_3), 4.46 (s, 2H, CH_2), 7.18 (td, J = 9.2, 2.6 Hz, 1H, H-6), 7.61 (dd, J = 9.0, 4.4 Hz, 1H, H-7), 7.80 (dd, J = 9.7, 2.5 Hz, 1H, H-4), 8.43 (s, 1H, H-2); ^{13}C NMR (101 MHz, DMSO-d_6) δ: 29.46 (t), 33.75 (q), 106.07 (d, $J_{C4\text{-}F}$ = 24.8 Hz,), 111.49 (d, $J_{C6\text{-}F}$ = 26.0 Hz), 112.57 (d, $J_{C7\text{-}F}$ = 9.8 Hz), 113.17 (d, $J_{C7a\text{-}F}$= 4.3 Hz), 116.22 (s), 126.17 (d, $J_{C3a\text{-}F}$ = 11.1 Hz), 134.02 (s), 140.04 (d), 159.19 (d, $J_{C5\text{-}F}$ = 236.1 Hz), 182.38 (s); *Anal.* Calculated for $C_{12}H_9FN_2O$ (MW: 216,22): C, 66.66; H, 4.20; N, 12.96%. Found: C, 66.60; H, 4.23; N, 12.86%.

3-(5-chloro-1-methyl-1*H*-indol-3-yl)-3-oxopropanenitrile (24e):

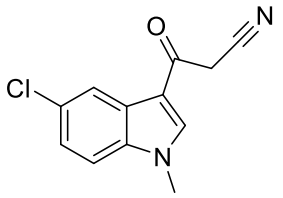

Yield: 88%; white solid; m.p.: 232.1-232.8°C; IR (cm^{-1}): 2255 (CN), 1647 (CO); ^{1}H NMR (400 MHz, DMSO-d_6) δ: 3.88 (s, 3H, CH_3), 4.47 (s, 2H, CH_2), 7.34 (dd, *J* = 8.7, 2.1 Hz, 1H, H-6), 7.63 (d, *J* = 8.7 Hz, 1H, H-7), 8.10 (d, *J* = 1.9 Hz, 1H, H-4), 8.44 (s, 1H, H-2); ^{13}C NMR (101 MHz, DMSO-d_6) δ: 29.98 (t), 34.14 (q), 113.21 (s), 113.30 (d), 116.61 (s), 120.63 (d), 123.81 (d), 127.06 (s), 128.00 (s), 136.35 (s), 140.39 (d), 182.96 (s); *Anal.* Calculated for $C_{12}H_9ClN_2O$ (MW: 232,67): C, 61.95; H, 3.90; N, 12.04%. Found: C, 61.99; H, 3.99; N, 12.24%.

General procedure for the synthesis of 2,5-bis(1*H*-indol-3-yl)pyrazolo[1,5-*a*]pyrimidin-7-amines (15a-e) and 2,5-bis(1-methyl-1*H*-indol-3-yl)pyrazolo[1,5-*a*]pyrimidin-7-amines (15f-j):

To a mixture of appropriate 3-(1*H*-indol-3-yl)-3-oxopropanenitrile (**23a-e**) or 3-(1-methyl-1*H*-indol-3-yl)-3-oxopropanenitrile (**24a-e**) (1.3 mmol) and *tert*-butyl carbazate (Boc-$NHNH_2$) (1.56 mmol) in *n*-butanol (*n*-BuOH) (7 ml), trifluoroacetic acid (CF_3COOH) (3.12 mmol) was added. The reaction mixture was heated under reflux for 0.5 - 7 hours (the progress of the reaction was monitored by TLC). A precipitate quickly formed. After completion the reaction mixture was cooled and poured into water and ice. The precipitate was filtered off to obtain the desired products (**15d**,**15f**,**15h**,**15i**,**15j**) without further purification.

If no precipitate formed the solvent was removed *in vacuo*, the resulting residue was treated with water (15 ml) and extracted with ethyl acetate (3 × 15 ml), dried (Na_2SO_4) and evaporated under reduced pressure. The product obtained was further purified by column chromatography, using cyclohexane/ethyl acetate as eluent to obtain the desired products (**15a**,**15b**,**15c**,**15e**,**15g**).

2,5-di(1*H*-indol-3-yl)pyrazolo[1,5-*a*]pyrimidin-7-amine (15a):

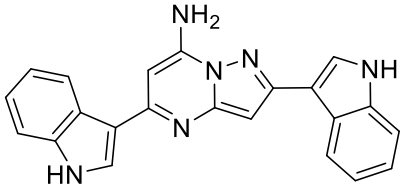

Yield: 57%; beige solid; m.p.: 232.5-233.5 °C dec; IR (cm^{-1}): 3472-3429 (NH_2), 3291-3152 (2 NH); ^1H NMR (300 MHz, DMSO-d_6) δ: 6.51 (s, 1H, pyrimidine-CH), 6.69 (s, 1H, pyrazole-CH), 7.23 – 7.09 (m, 4H), 7.39 (s, 2H, NH_2, exchangeable with D_2O), 7.46 (dd, *J* = 8.5, 4.7 Hz, 2H), 7.98 (d, *J* = 2.5 Hz, 1H), 8.02 (d, *J* = 2.7 Hz, 1H), 8.53 (dd, *J* = 11.1, 4.9 Hz, 2H), 11.41 (s, 1H, NH, exchangeable with D_2O), 11.55 (s, 1H, NH, exchangeable with D_2O); ^{13}C NMR (101 MHz, DMSO-d_6) δ: 83.73 (d, pyrimidine-CH), 90.19 (d, pyrazole-CH), 109.91 (s), 111.98 (d), 112.34 (d), 115.53 (s), 120.11 (d), 120.48 (d), 122.05 (d), 122.17 (2xd), 122.44 (d), 125.57 (s), 125.61 (d), 125.84 (s), 127.09 (d), 137.07 (s), 137.48 (s), 147.59 (s), 150.30 (s), 152.18 (s), 154.86 (s); *Anal.* Calculated for $C_{22}H_{16}N_6$ (MW: 364.41): C, 72.51; H, 4.43; N, 23.06%. Found: C, 72.61; H, 4.54; N, 23.10%.

2,5-bis(5-methoxy-1*H*-indol-3-yl)pyrazolo[1,5-*a*]pyrimidin-7-amine (15b):

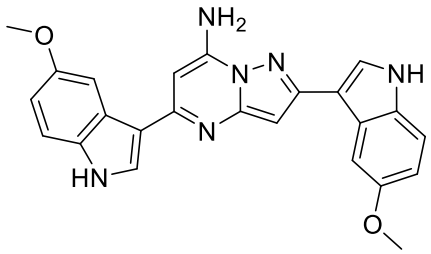

Yield: 48%; olive green solid; m.p.: 193-194°C; IR (cm^{-1}): 3447-3385 (NH_2), 3275-3238 (2 NH); ^1H NMR (300 MHz, DMSO-d_6) δ: 3.86 (s, 3H, OCH_3), 3.88 (s, 3H, OCH_3), 6.49 (s, 1H, pyrimidine-CH), 6.66 (s, 1H, pyrazole-CH), 6.84 (t, *J* = 7.4 Hz, 2H), 7.32 (s, 2H, NH_2, exchangeable with D_2O), 7.36 (d, *J* = 8.2 Hz, 2H), 7.93 (s, 2H), 7.98 (s, 1H), 8.07 (s, 1H), 11.27 (s, 1H, NH, exchangeable with D_2O), 11.42 (s, 1H, NH, exchangeable with D_2O); ^{13}C NMR (101 MHz, DMSO-d_6) δ: 55.49 (q), 55.63 (q), 83.11 (d, 1H, pyrimidine-CH), 89.75 (d, pyrazole-CH), 103.65 (d), 104.12 (d), 109.25 (s), 111.47 (d), 111.72 (d), 112.21 (d), 112.45 (d), 114.72 (s), 125.49 (s), 125.84 (d), 125.93 (s), 127.23 (d), 131.77 (s), 132.20 (s), 147.11 (s), 149.88 (s), 151.87 (s), 154.05 (s), 154.18 (s), 154.55 (s); *Anal.* Calculated for $C_{24}H_{20}N_6O_2$ (MW: 424,46): C, 67.91; H, 4.75; N, 19.80%. Found: C, 67.95; H, 4.79; N, 19.90%.

2,5-bis(5-bromo-1*H*-indol-3-yl)pyrazolo[1,5-*a*]pyrimidin-7-amine (15c):

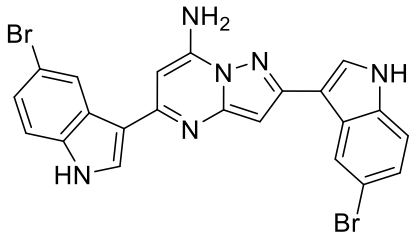

Yield: 63%; beige solid; m.p.: 313.5-314.5°C dec.; IR (cm^{-1}): 3474-3439 (NH_2), 3362-3246 (2 NH); ^{1}H NMR (400 MHz, DMSO-*d*$_6$) δ: 6.47 (s, 1H, pyrimidine-CH), 6.76 (s, 1H, pyrazole-CH), 7.29 (ddd, *J* = 8.6, 6.6, 2.0 Hz, 2H), 7.42 (t, *J* = 8.6 Hz, 2H), 7.47 (s, 2H, NH_2, exchangeable with D_2O), 8.05 (d, *J* = 2.6 Hz, 1H), 8.08 (d, *J* = 2.6 Hz, 1H), 8.67 (d, *J* = 2.0 Hz, 1H), 8.74 (d, *J* = 2.0 Hz, 1H), 11.60 (s, 1H, NH, exchangeable with D_2O), 11.72 (s, 1H, NH, exchangeable with D_2O); ^{13}C NMR (75 MHz, DMSO-*d*$_6$) δ: 83.53 (d, pyrimidine-CH), 90.55 (d, pyrazole-CH), 109.71 (s), 113.14 (s), 113.32 (s), 114.01 (d), 114.33 (d), 115.01 (s), 124.35 (d), 124.54 (d), 124.74 (d), 124.79 (d), 127.06 (s), 127.37 (d), 127.63 (s), 128.52 (d), 135.79 (s), 136.19 (s), 147.78 (s), 150.22 (s), 151.76 (s), 154.45 (s); *Anal.* Calculated for $C_{22}H_{14}Br_2N_6$ (MW: 522,20): C, 50.60; H, 2.70; N, 16.09%. Found: C, 50.66; H, 2.75; N, 16.19%.

2,5-bis(5-fluoro-1*H*-indol-3-yl)pyrazolo[1,5-*a*]pyrimidin-7-amine (15d):

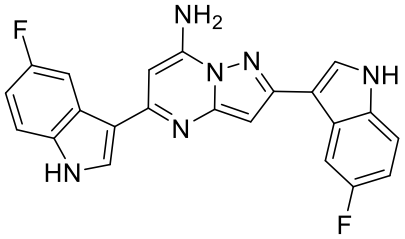

Yield: 64%; yellow solid; m.p.: 239°C; IR (cm^{-1}): 3470-3437 (NH_2), 3244-3204 (2 NH); ^{1}H NMR (300 MHz, DMSO-*d*$_6$) δ: 6.68 (s, 1H, pyrimidine-CH), 6.81 (s, 1H, pyrazole-CH), 7.06 (td, *J* = 9.2, 2.5 Hz, 1H), 7.19 (td, *J* = 9.1, 2.1 Hz, 1H), 7.48 (dd, *J* = 8.8, 4.6 Hz, 1H), 7.63 (dd, *J* = 8.9, 4.7 Hz, 1H),7.81 (d, *J* = 9.9 Hz, 1H), 8.36 (dd, *J* = 16.0, 2.6 Hz, 2H), 8.44 (dd, *J* = 10.3, 2.3 Hz, 1H), 9.18 (br s, 2H, NH_2), 11.81 (s, 1H, NH), 12.39 (s, 1H, NH); ^{13}C NMR (75 MHz, DMSO-*d*$_6$) δ: 85.27 (d, pyrimidine-CH), 87.69 (d, pyrazole-CH), 105.07 (d, *J* = 25.2 Hz), 107.50 (d, *J* = 24.3 Hz), 108.37 (d, *J* = 4.6 Hz), 110.79 (d, *J* = 26.3 Hz), 111.65 (d, *J* = 25.9 Hz), 113.22 (d, *J* = 9.9 Hz), 114.74 (d, *J* = 9.9 Hz), 125.03 (d, *J* = 10.5 Hz), 125.47 (d, *J* = 11.0 Hz), 129.86 (d), 131.55 (d), 133.86 (2xs), 134.24 (3xs), 150.46 (s), 154.10 (s), 158.42 (d, *J* = 232.3 Hz), 158.82 (d, *J* = 234.3 Hz); *Anal.* Calculated for $C_{22}H_{14}F_2N_6$ (MW: 400,39): C, 66.00; H, 3.52; N, 20.99%. Found: C, 66.15; H, 3.55; N, 20.89%.

2,5-bis(5-chloro-1*H*-indol-3-yl)pyrazolo[1,5-*a*]pyrimidin-7-amine (15e):

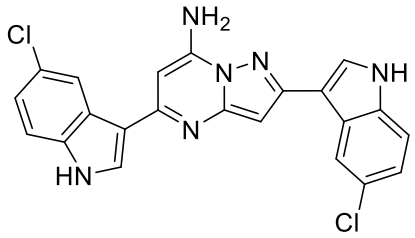

Yield: 90%; olive green solid; m.p.: 221.5-222.5°C; IR (cm^{-1}): 3462-3408 (NH_2), 3275-3244 (2 NH); ^1H NMR (300 MHz, DMSO-d_6) δ: 6.47 (s, 1H, pyrimidine-CH), 6.77 (s, 1H, pyrazole-CH), 7.18 (ddd, *J* = 8.7, 6.7, 2.1 Hz, 2H), 7.47 (dd, *J* = 8.5, 6.8 Hz, 2H), 7.52 (s, 2H, NH_2 exchangeable with D_2O), 8.08 (d, *J* = 2.5 Hz, 1H), 8.11 (d, *J* = 2.5 Hz, 1H), 8.58 (d, *J* = 1.9 Hz, 1H), 8.60 (d, *J* = 2.0 Hz, 1H), 11.61 (s, 1H, NH, exchangeable with D_2O), 11.74 (s, 1H, NH, exchangeable with D_2O); ^{13}C NMR (101 MHz, DMSO-d_6) δ: 83.53 (d, pyrimidine-CH), 90.47 (d, pyrazole-CH), 109.83 (s), 113.52 (d), 113.85 (d), 115.15 (s), 121.45 (d), 122.19 (3xd), 125.05 (s), 125.21 (s), 126.43 (s), 126.97 (s), 127.46 (d), 128.65 (d), 135.56 (s), 135.97 (s), 147.77 (s), 150.25 (s), 151.76 (s), 154.45 (s); *Anal.* Calculated for $C_{22}H_{14}Cl_2N_6$ (MW: 433,30): C, 60.98; H, 3.26; N, 19.40%. Found: C, 60.97; H, 3.24; N, 19.43%.

2,5-bis(1-methyl-1*H*-indol-3-yl)pyrazolo[1,5-*a*]pyrimidin-7-amine (15f):

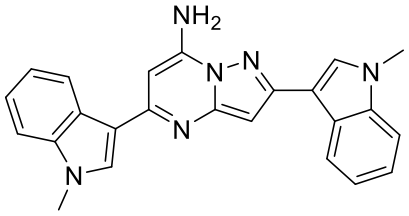

Yield: 89%; yellow solid; m.p.: 306°C; IR (cm^{-1}): 3439-3292 (NH_2); ^1H NMR (300 MHz, DMSO-d_6) δ: 3.90 (s, 3H, CH_3), 3.96 (s, 3H, CH_3), 6.69 (s, 1H, pyrimidine-CH), 6.74 (s, 1H, pyrazole-CH), 7.26 (dt, *J* = 14.8, 6.7 Hz, 2H), 7.42 – 7.33 (m, 2H), 7.54 (d, *J* = 8.0 Hz, 1H), 7.68 (d, *J* = 7.0 Hz, 1H), 8.07 (d, *J* = 7.0 Hz, 1H), 8.23 (s, 1H), 8.31 (s, 1H), 8.64 (d, *J* = 7.6 Hz, 1H), 9.15 (br s, 2H, NH_2 exchangeable with D_2O); ^{13}C NMR (75 MHz, DMSO-d_6) δ: 32.81 (q), 33.32 (q), 84.83 (d, pyrimidine-CH), 87.24 (d, pyrazole-CH), 106.75 (s), 110.05 (d), 111.37 (d), 119.51 (d), 120.40 (d), 121.75 (d), 122.17 (d), 122.30 (d), 122.99 (d), 124.51 (s), 125.09 (2xs), 131.25 (d), 132.92 (d), 137.19 (2xs), 137.59 (2xs), 149.82 (s), 153.47 (s); *Anal.* Calculated for $C_{24}H_{20}N_6$ (MW: 392,47): C, 73.45; H, 5.14; N, 21.41%. Found: 73.48; H, 5.16; N, 21.46%.

2,5-bis(5-methoxy-1-methyl-1*H*-indol-3-yl)pyrazolo[1,5-*a*]pyrimidin-7-amine (15g):

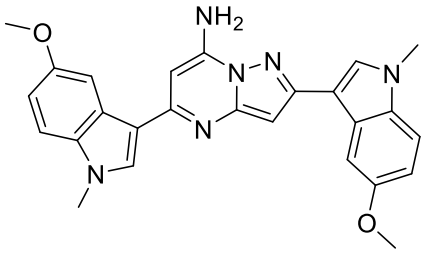

Yield: 73%; olive green solid; m.p.: 306°C; IR (cm^{-1}): 3373-3292 (NH_2); ^1H NMR (300 MHz, DMSO-d_6) δ: 3.83 (s, 3H, CH_3) 3.85 (s, 3H, CH_3), 3.86 (s, 3H, OCH_3), 3.89 (s, 3H, OCH_3), 6.45 (s, 1H, pyrimidine-CH), 6.59 (s, 1H, pyrazole-CH), 6.90 (t, *J* = 8.1 Hz, 2H), 7.36 (s, 2H, NH_2, exchangeable with D_2O), 7.40 (dd, *J* = 8.8, 5.7 Hz, 2H), 7.92 (d, *J* = 8.3 Hz, 2H), 8.00 (s, 1H), 8.07 (s, 1H); ^{13}C NMR (101 MHz, DMSO-d_6) δ: 32.86 (q), 32.97 (q), 55.50 (q), 55.66 (q), 83.03 (d, pyrimidine-CH), 89.57 (d, pyrazole-CH), 103.92 (d), 104.28 (d), 108.16 (s), 110.62 (d), 110.88 (d), 111.36 (d), 111.66 (d), 113.49 (s), 125.81 (s), 126.27 (s), 129.78 (d), 131.30 (d), 132.41 (s), 132.83 (s), 147.14 (s), 149.88 (s), 151.50 (s), 154.18 (s), 154.29 (s), 154.47 (s); *Anal.* Calculated for $C_{26}H_{24}N_6O_2$ (MW: 452,52): C, 69.01; H, 5.35; N, 18.57%. Found: C, 69.21; H, 5.39; N, 18.69%.

2,5-bis(5-bromo-1-methyl-1*H*-indol-3-yl)pyrazolo[1,5-*a*]pyrimidin-7-amine (15h):

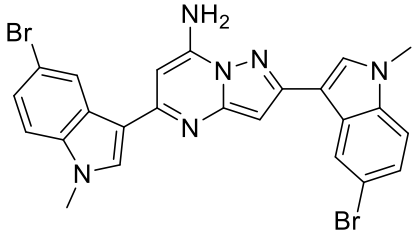

Yield: 91%; yellow solid; m.p.: 240°C; IR (cm^{-1}): 3456-3300 (NH_2); ^1H NMR (300 MHz, DMSO-d_6) δ: 3.88 (s, 3H, CH_3), 3.94 (s, 3H, CH_3), 6.59 (s, 1H, pyrimidine-CH), 6.75 (s, 1H, pyrazole-CH), 7.39 (d, *J* = 8.7 Hz, 1H), 7.51 (t, *J* = 7.0 Hz, 2H), 7.64 (d, *J* = 8.6 Hz, 1H), 8.28 (d, *J* = 7.7 Hz, 3H), 8.76 (s, 1H), 9.12 (br s, 2H, NH_2 exchangeable with D_2O); ^{13}C NMR (75 MHz, DMSO-d_6) δ: 33.03 (q), 33.46 (q), 84.89 (d, pyrimidine-CH), 87.72 (d, pyrazole-CH), 106.66 (s), 112.17 (d), 113.32 (d), 113.58 (2xs), 114.50 (s), 122.05 (d), 124.04 (d), 124.80 (d), 125.38 (d), 126.25 (s), 126.49 (s), 132.47 (d), 133.79 (d), 135.94 (2xs), 136.34 (2xs), 149.61 (s), 152.71 (s); *Anal.* Calculated for $C_{24}H_{18}Br_2N_6$ (MW: 550,26): C, 52.39; H, 3.30; N, 15.27%. Found: C, 52.43; H, 3.35; N, 15.29%.

2,5-bis(5-fluoro-1-methyl-1*H*-indol-3-yl)pyrazolo[1,5-*a*]pyrimidin-7-amine (15i):

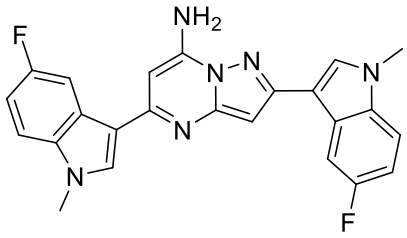

Yield: 100%; yellow solid; m.p.: 220°C; IR (cm^{-1}): 3350-3308 (NH_2); ^1H NMR (300 MHz, DMSO-d_6) δ: 3.89 (s, 3H, CH_3), 3.96 (s, 3H, CH_3), 6.62 (s, 1H, pyrimidine-CH), 6.73 (s, 1H, pyrazole-CH), 7.12 (td, *J* = 9.2, 2.4 Hz, 1H), 7.24 (td, *J* = 9.1, 2.1 Hz, 1H), 7.54 (dd, *J* = 8.9, 4.4 Hz, 1H), 7.69 (dd, *J* = 9.0, 4.6 Hz, 1H), 7.83 (d, *J* = 10.1 Hz, 1H), 8.28 (s, 1H), 8.34 (s, 1H), 8.44 (dd, *J* = 10.2, 2.3 Hz, 1H), 9.11 (br s, 2H, NH_2 exchangeable with D_2O); ^{13}C NMR (75 MHz, DMSO-d_6) δ: 33.60 (q), 34.09 (q), 85.14 (d, pyrimidine-CH), 87.63 (d, pyrazole-CH), 105.35 (d, *J* = 24.8 Hz), 107.37 (d, *J* = 4.8 Hz), 107.72 (d, *J* = 24.7 Hz),110.78 (d, *J* = 26.6 Hz), 111.57 (d, *J* = 26.0 Hz), 111.72 (d, *J* = 9.6 Hz), 113.25 (d, *J* = 10.1 Hz), 125.37 (d, *J* = 10.5 Hz), 125.74 (d, *J* = 11.0 Hz), 133.34 (d), 134.40 (3xs), 134.77 (3xs), 150.22 (s), 153.53 (s), 158.63 (d, *J* = 232.7 Hz), 159.03 (d, *J* = 234.7 Hz); *Anal.* Calculated for $C_{24}H_{18}F_2N_6$ (MW: 428,45): C, 67.28; H, 4.23; N, 19.62%. Found: C, 67.31; H, 4.25; N, 19.65%.

2,5-bis(5-chloro-1-methyl-1*H*-indol-3-yl)pyrazolo[1,5-*a*]pyrimidin-7-amine (15j):

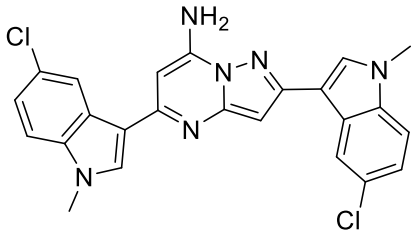

Yield: 100%; light green solid; m.p.: 231-232°C; IR (cm^{-1}): 3354-3309 (NH_2); ^1H NMR (300 MHz, DMSO-d_6) δ: 3.89 (s, 3H, CH_3), 3.95 (s, 3H, CH_3), 6.61 (s, 1H, pyrimidine-CH), 6.74 (s, 1H, pyrazole-CH), 7.27 (dd, *J* = 8.7, 1.8 Hz, 1H), 7.39 (dd, *J* = 8.8, 1.6 Hz, 1H), 7.56 (d, *J* = 8.7 Hz, 1H),7.69 (d, *J* = 8.8 Hz, 1H), 8.12 (s, 1H), 8.30 (d, *J* = 14.5 Hz, 2H), 8.65 (d, *J* = 1.7 Hz, 1H), 9.10 (br s, 2H, NH_2 exchangeable with D_2O); ^{13}C NMR (75 MHz, DMSO-d_6) δ: 33.56 (q), 34.01 (q), 85.38 (d, pyrimidine-CH), 88.05 (d, pyrazole-CH), 107.16 (s), 112.24 (d), 113.50 (d), 119.51 (d), 121.73 (d), 122.72 (d),

123.35 (d), 126.02 (2xs), 126.08 (s), 126.35 (s), 127.00 (s), 133.20 (d), 134.52 (d), 136.18 (2xs), 136.59 (2xs), 150.17 (s), 153.30 (s); *Anal.* Calculated for $C_{24}H_{18}Cl_2N_6$ (MW: 461,35): C, 62.48; H, 3.93; N, 18.22%. Found: C, 62.52; H, 3.96; N, 18.25%.

General procedure for the synthesis of 3-(1*H*-indol-3-yl)-1*H*-pyrazol-5-amines (27a-e,28a-e):

To a mixture of appropriate 3-(1*H*-indol-3-yl)-3-oxopropanenitrile (**23a-e**,**24a-e**) (5.45 mmol) and acethydrazide ($AcNHNH_2$) (6 mmol) in anhydrous *n*-butanol (*n*-BuOH) (30 ml), *p*-toluenesulfonic acid monohydrate ($PTSA \cdot H_2O$) (6 mmol) was added. The reaction mixture was heated vigorously under reflux for 1-3 hours by using the Marcusson apparatus. After completion the reaction mixture was cooled. If precipitate formed (**7d,8c,8d,8e**), it was filtered off; if no precipitate formed (**7a,7b,7c,7e,8a,8b**) the solvent was removed in vacuo. The resulting residue was neutralised by adding a few drops of saturated aqueous solution of sodium hydrogencarbonate ($NaHCO_3$), extracted with water (20 ml) and ethyl acetate (3 × 20 ml), dried (Na_2SO_4) and evaporated under reduced pressure. The product obtained was further purified by column chromatography, using ethyl acetate as eluent. If necessary, it was triturated with ethyl acetate (**7a,7b,7c,7e,8c,8d,8e**) or crystallized from ethyl acetate (**7d,8a,8b**) to obtain the desired products.

3-(1*H*-indol-3-yl)-1*H*-pyrazol-5-amine (27a):

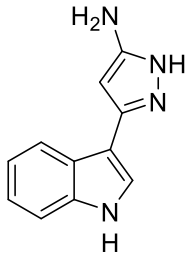

Yield 66%; white solid; m.p: 220-221°C; IR (cm^{-1}): 3414 (NH_2), 3335 (NH), 3182 (NH); ^1H NMR (400 MHz, DMSO-d_6) δ: 4.52 (br s, 2H, NH_2, exchangeable with D_2O), 5.75 (br s, 1H, pyrazole-CH), 7.07 (t, *J* = 7.1 Hz, 1H, H-5), 7.13 (t, *J* = 7.3 Hz, 1H, H-6), 7.41 (d, *J* = 7.9 Hz, 1H, H-7), 7.62 (s, 1H, H-4), 7.79 (br s, 1H, H-2), 11.27 (br s, 1H, NH, exchangeable with D_2O), 11.51 (br s, 1H, NH, exchangeable with D_2O); ^{13}C NMR (101 MHz, DMSO-d_6) δ: 112.17 (d), 119.88 (d), 121.91 (d), 123.12 (3xd), 125.11 (s), 136.78 (4xs); *Anal.* Calculated for $C_{11}H_{10}N_4$ (MW: 198,23): C, 66.65; H, 5.09; N, 28.26%. Found: C, 66.69; H, 5.15; N, 28.33%.

3-(5-methoxy-1*H*-indol-3-yl)-1*H*-pyrazol-5-amine (27b):

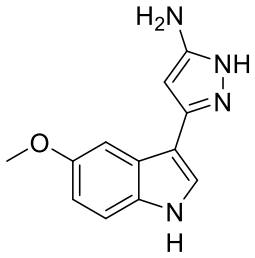

Yield: 62%; white solid; m.p.: 204-205.6°C; IR (cm^{-1}): 3462 (NH_2), 3375 (NH), 3254 (NH); ^1H NMR (400 MHz, DMSO-d_6) δ: 3.78 (s, 3H, OCH_3), 4.54 (br s, 2H, NH_2, exchangeable with D_2O), 5.70 (br s, 1H, pyrazole-CH), 6.77 (d, *J* = 8.7 Hz, 1H, H-6), 7.25 (br s, 1H, H-2), 7.29 (d, *J* = 8.7 Hz, 1H, H-7), 7.56 (s, 1H, H-4), 11.11 (br s, 1H, NH, exchangeable with D_2O), 11.47 (br s, 1H, NH, exchangeable with D_2O); ^{13}C NMR (101 MHz, DMSO-d_6) δ: 55.75 (q), 112.17 (d), 112.88 (d), 123.78 (3xd), 125.35 (s), 131.84 (3xs), 154.17 (2xs); *Anal.* Calculated for $C_{12}H_{12}N_4O$ (MW: 228,26): C, 63.15; H, 5.30; N, 24.55%. Found: C, 63.19; H, 5.35; N, 24.53%.

3-(5-bromo-1*H*-indol-3-yl)-1*H*-pyrazol-5-amine (27c):

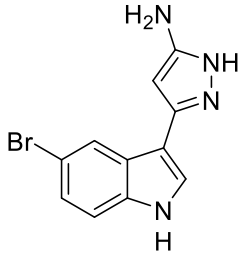

Yield: 72%; white solid; m.p.: 204.8-205.5°C; IR (cm^{-1}): 3443 (NH_2), 3399 (NH), 3254 (NH); ^1H NMR (400 MHz, DMSO-d_6) δ: 4.41-5.07 (br s, 2H, NH_2, exchangeable with D_2O, 2 tautomer peaks), 5.67 (br s, 1H, pyrazole-CH), 7.23 (d, *J* = 8.2 Hz, 1H, H-6), 7.38 (d, *J* = 8.3 Hz, 1H, H-7), 7.66 (s, 1H, H-4), 7.78-8.42 (br s, 1H, 2 tautomer peaks, H-2), 11.18-11.65 (br s, 2H, indole-NH, 2 tautomer peaks pyrazole-NH, exchangeable with D_2O); ^{13}C NMR (101 MHz, DMSO-d_6) δ: 112.41 (s), 114.12 (d), 124.33 (3xd), 124.72 (d), 126.99 (s), 135.48 (4xs); *Anal.* Calculated for $C_{11}H_9BrN_4$ (MW: 277,13): C, 47.68; H, 3.27; N, 20.22%. Found: C, 47.73; H, 3.30; N, 20.27%.

3-(5-fluoro-1*H*-indol-3-yl)-1*H*-pyrazol-5-amine (27d):

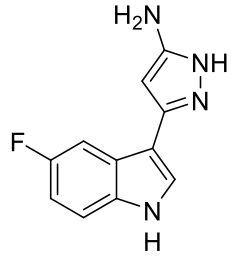

Yield: 54%; yellow needles; m.p.: 230.4-230.6°C; IR (cm^{-1}): 3404 (NH_2), 3338 (NH), 3224 (NH); ^1H NMR (400 MHz, DMSO-d_6) δ: 4.56 (br s, 2H, NH_2, exchangeable with D_2O), 5.69 (br s, 1H, pyrazole-CH), 6.97 (t, J = 8.3 Hz, 1H, H-6), 7.40 (dd, J = 8.2, 4.3 Hz, 1H, H-7), 7.57 (br s, 1H, H-2), 7.68 (s, 1H, H-4), 11.33 (br s, 1H, NH, exchangeable with D_2O), 11.50 (br s, 1H, NH, exchangeable with D_2O); ^{13}C NMR (101 MHz, DMSO-d_6) δ: 110.05 (d, $J_{C4\text{-}F}$ = 24.2 Hz), 113.16 (d, $J_{C7\text{-}F}$ = 9.7 Hz), 125.17 (2xd), 133.47 (d), 133.47 (5xs), 157.69 (d, $J_{C5\text{-}F}$ = 230.6 Hz); *Anal.* Calculated for $C_{11}H_9FN_4$ (MW: 216,22): C, 61.11; H, 4.20; N, 25.91%. Found: C, 61.16; H, 4.24; N, 25.96%.

3-(5-chloro-1*H*-indol-3-yl)-1*H*-pyrazol-5-amine (27e):

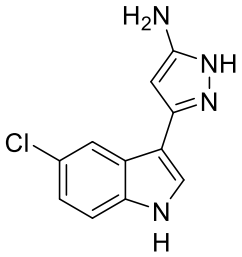

Yield: 72%; creamy white solid; m.p.: 203.6-204°C; IR (cm^{-1}): 3456 (NH_2), 3402 (NH), 3254 (NH); ^1H NMR (400 MHz, DMSO-d_6) δ: 4.71 (br s, 2H, NH_2, exchangeable with D_2O), 5.68 (br s, 1H, pyrazole-CH), 7.12 (dd, J = 8.6, 1.9 Hz, 1H, H-6), 7.42 (d, J = 8.6 Hz, 1H, H-7), 7.68 (d, J = 2.1 Hz, 1H, H-4), 7.91 (br s, 1H, H-2), 11.41 (br s, 2H, indole-NH, pyrazole-NH, exchangeable with D_2O); ^{13}C NMR (101 MHz, DMSO-d_6) δ: 113.65 (d), 119.76 (s), 121.81 (d), 124.45 (s), 124.91 (2xd), 126.24 (s), 135.26 (4xs); *Anal.* Calculated for $C_{11}H_9ClN_4$ (MW: 232,67): C, 56.78; H, 3.90; N, 24.08%. Found: C, 56.82; H, 3.95; N, 24.23%.

3-(1-methyl-1*H*-indol-3-yl)-1*H*-pyrazol-5-amine (28a):

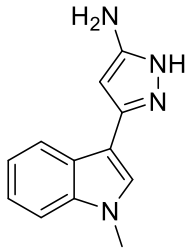

Yield: 69%; white crystals; m.p: 141.4-142°C; IR (cm^{-1}): 3447 (NH_2), 3356 (NH); ^1H NMR (400 MHz, DMSO-d_6) δ: 3.80 (s, 3H, CH_3), 4.67 (br s, 2H, NH_2, exchangeable with D_2O), 5.69 (br s, 1H, pyrazole-CH), 7.10 (t, *J* = 7.4 Hz, 1H, H-5), 7.19 (t, *J* = 7.5 Hz, 1H, H-6), 7.45 (d, *J* = 8.2 Hz, 1H, H-7), 7.58 (s, 1H, H-4), 7.88 (br s, 1H, H-2), 11.49 (br s, 1H, NH, exchangeable with D_2O); ^{13}C NMR (101 MHz, DMSO-d_6) δ: 33.01 (q), 110.40 (d), 119.98 (d), 120.56 (d), 121.99 (2xd), 125.50 (2xs), 127.30 (d), 137.20 (3xs); *Anal.* Calculated for $C_{12}H_{12}N_4$ (MW: 212,26): C, 67.90; H, 5.70; N, 26.40%. Found: C, 67.96; H, 5.69; N, 26.43%.

3-(5-methoxy-1-methyl-1*H*-indol-3-yl)-1*H*-pyrazol-5-amine (28b):

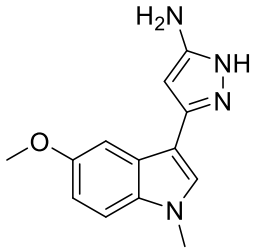

Yield: 66%; white crystals; m.p.: 146.4°C; IR (cm^{-1}): 3447 (NH_2), 3356 (NH); ^1H NMR (400 MHz, DMSO-d_6) δ: 3.76 (s, 3H, CH_3), 3.79 (s, 3H, OCH_3), 4.54 (br s, 2H, NH_2, exchangeable with D_2O), 5.66 (br s, 1H, pyrazole-CH), 6.83 (d, *J* = 8.8 Hz, 1H, H-6), 7.29 (br s, 1H, H-2), 7.34 (d, *J* = 8.8 Hz, 1H, H-7), 7.52 (s, 1H, H-4), 11.48 (br s, 1H, NH, exchangeable with D_2O); ^{13}C NMR (101 MHz, DMSO-d_6) δ: 33.15 (q), 55.84 (q), 111.14 (d), 112.14 (d), 125.75 (s), 127.86 (3xd), 132.53 (3xs), 154.38 (2xs); *Anal.* Calculated for $C_{13}H_{14}N_4O$ (MW: 242,28): C, 64.45; H, 5.82; N, 23.13%. Found: C, 64.48; H, 5.87; N, 23.21%.

3-(5-bromo-1-methyl-1*H*-indol-3-yl)-1*H*-pyrazol-5-amine (28c):

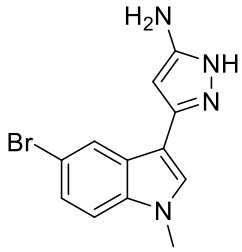

Yield: 50%; creamy white solid; m.p.: 163.7-165°C; IR (cm^{-1}): 3437-3377 (NH_2), 3356 (NH); ^1H NMR (400 MHz, DMSO-d_6) δ: 3.80 (s, 3H, CH_3), 4.83 (br s, 2H, NH_2, exchangeable with D_2O), 5.63 (br s, 1H, pyrazole-CH), 7.29 (d, J = 8.4 Hz, 1H, H-6), 7.44 (d, J = 8.6 Hz, 1H, H-7), 7.63 (s, 1H, H-4), 8.14 (br s, 1H, H-2), 11.17- 11.67 (br s, 1H, 2 tautomer peaks pyrazole-NH, exchangeable with D_2O); ^{13}C NMR (101 MHz, DMSO-d_6) δ: 33.18 (q), 112.48 (d), 112.61 (s), 124.35 (d), 127.21 (s), 128.81 (3xd), 135.98 (4xs); *Anal.* Calculated for $C_{12}H_{11}BrN_4$ (MW: 291,15): C, 49.50; H, 3.81; N, 19.24%. Found: C, 49.57; H, 3.85; N, 19.21%.

3-(5-fluoro-1-methyl-1*H*-indol-3-yl)-1*H*-pyrazol-5-amine (28d):

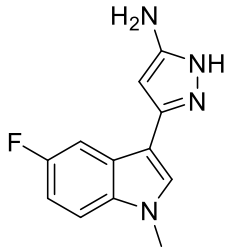

Yield: 55%; beige solid; m.p.: 166.7-167.6°C; IR (cm^{-1}): 3447 (NH_2), 3354 (NH); ^1H NMR (400 MHz, DMSO-d_6) δ: 3.80 (s, 3H, CH_3), 4.37-5.10 (br s, 2H, 2 tautomer peaks NH_2, exchangeable with D_2O), 5.64 (br s, 1H, pyrazole-CH), 7.03 (t, J = 8.4 Hz, 1H, H-6), 7.45 (s, 1H, H-7), 7.60 (br s, 1H, H-2), 7.65 (s, 1H, H-4), 11.14-11.63 (br, 1H, 2 tautomer peaks pyrazole-NH, exchangeable with D_2O); ^{13}C NMR (101 MHz, DMSO-d_6) δ: 33.29 (q), 110.05 (d, $J_{C4\text{-}F}$ = 24.9 Hz), 111.63 (d, $J_{C7\text{-}F}$ = 8.0 Hz), 125.62 (s), 129.20 (3xd), 134.03 (4xs), 157.86 (d, $J_{C5\text{-}F}$ = 231.7 Hz); *Anal.* Calculated for $C_{12}H_{11}FN_4$ (MW: 230,25): C, 62.60; H, 4.82; N, 24.33%. Found: C, 62.66; H, 4.85; N, 24.31%.

3-(5-chloro-1-methyl-1*H*-indol-3-yl)-1*H*-pyrazol-5-amine (28e):

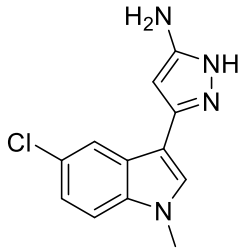

Yield: 73%; white solid; m.p.: 75-76°C; IR (cm^{-1}): 3431-3354 (NH_2), 3198 (NH); ^1H NMR (400 MHz, DMSO-d_6) δ: 3.79 (s, 3H, CH_3), 4.77 (br s, 2H, NH_2, exchangeable with D_2O), 5.63 (br s, 1H, pyrazole-CH), 7.18 (d, J = 7.6 Hz, 1H, H-6), 7.48 (d, J = 8.6 Hz, 1H, H-7), 7.64 (s, 1H, H-4), 7.96 (br s, 1H, H-2), 11.15-11.67 (br s, 1H, 2 tautomer peaks pyrazole-NH, exchangeable with D_2O); ^{13}C NMR (101 MHz, DMSO-d_6) δ: 33.21 (q), 112.05 (d), 121.83 (d), 124.74 (s), 128.98 (3xd), 135.74 (5xs); *Anal.* Calculated for $C_{12}H_{11}ClN_4$ (MW: 246,70): C, 58.42; H, 4.49; N, 22.71%. Found: C, 58.47; H, 4.52; N, 22.76%.

General procedure for the synthesis of 2-(1*H*-indol-3-yl)-5-(1*H*-indol-3-yl)pyrazolo[1,5-*a*]pyrimidin-7-amines (16a-t):

To a mixture of appropriate 3-(1*H*-indol-3-yl)-3-oxopropanenitrile (**23a-e**,**24a-e**) (0.5 mmol) and appropriate 3-(1*H*-indol-3-yl)-1*H*-pyrazol-5-amine (**27,28**) (0.5 mmol) in anhydrous *n*-butanol (*n*-BuOH) (8 ml) *p*-toluenesulfonic acid monohydrate (PTSA·H_2O) (2.5 mmol) was added. The reaction mixture was stirred to 90°C for 12 - 48 hours (the progress of the reaction was monitored by TLC). After completion the reaction mixture was left to cool, and the obtained precipitate was filtered off. Solid was neutralised by adding a few drops of saturated aqueous solution of sodium hydrogencarbonate ($NaHCO_3$) and water (20 ml), extracted with ethyl acetate (3 × 20 ml), dried (Na_2SO_4) and evaporated under reduced pressure. The product obtained was further purified by column chromatography, using dichloromethane or dichloromethane/methanol as eluent.

2-(1*H*-indol-3-yl)-5-(5-methoxy-1*H*-indol-3-yl)pyrazolo[1,5-*a*]pyrimidin-7-amine (16a):

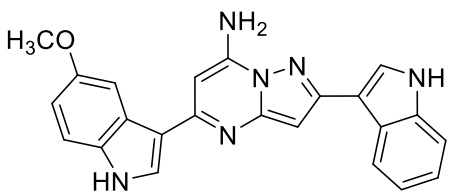

Yield: 36%; green-yellow solid; m.p.: 207°C; IR (cm^{-1}): 3441-3356 (NH_2), 3244-3123 (2 NH); ^1H NMR (400 MHz, DMSO-d_6) δ: 3.85 (s, 3H, OCH_3), 6.47 (s, 1H, pyrimidine-CH), 6.66 (s, 1H, pyrazole-CH), 6.84 (dd, *J* = 8.8, 2.5 Hz, 1H), 7.10 -7.19 (m, 2H), 7.33 (s, 2H, NH_2, exchangeable with D_2O), 7.35 (d, *J* = 8.9 Hz, 1H), 7.42 - 7.45 (m, 1H), 7.95 - 7.97 (m, 2H), 8.06 (d, *J* = 2.5 Hz, 1H), 8.53 (d, *J* = 7.1 Hz, 1H), 11.37 (s, 1H, NH, exchangeable with D_2O), 11.38 (s, 1H, NH, exchangeable with D_2O); ^{13}C NMR (101 MHz, DMSO-d_6) δ: 55.43 (q), 83.01 (d, pyrimidine-CH), 89.67 (d, pyrazole-CH), 104.03 (d), 109.45 (s), 111.47 (2xd), 112.36 (d), 114.67 (s), 119.59 (d), 121.54 (d), 121.93 (d), 125.09 (d), 125.88 (s), 127.12 (d), 129.45 (s), 132.13 (s), 136.57 (s), 147.05 (s), 149.77 (s), 151.64 (s), 154.13 (s), 154.49 (s); *Anal.* Calculated for $C_{23}H_{18}N_6O$ (MW: 394,44): C, 70.04; H, 4.60; N, 21.31%. Found: C, 70.11; H, 4.67; N, 21.36%.

5-(5-bromo-1*H*-indol-3-yl)-2-(1*H*-indol-3-yl)pyrazolo[1,5-*a*]pyrimidin-7-amine (16b):

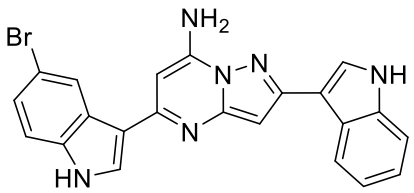

Yield: 46%; creamy white solid; m.p.: 175°C; IR (cm^{-1}): 3433-3414 (NH_2), 3283-3121 (2 NH); ^1H NMR (400 MHz, DMSO-d_6) δ: 6.45 (s, 1H, pyrimidine-CH), 6.75 (s, 1H, pyrazole-CH), 7.15 (dtd, *J* = 14.6, 7.2, 1.2 Hz, 2H), 7.30 (dd, *J* = 8.6, 2.0 Hz, 1H), 7.42 (s, 2H, NH_2, exchangeable with D_2O), 7.43 (d, *J* = 8.7 Hz, 2H), 7.99 (d, *J* = 2.4 Hz, 1H), 8.09 (d, *J* = 2.7 Hz, 1H), 8.56 (d, *J* = 7.7 Hz, 1H), 8.75 (s, 1H), 11.39 (s, 1H, NH, exchangeable with D_2O), 11.73 (s, 1H, NH, exchangeable with D_2O); ^{13}C NMR (101 MHz, DMSO-d_6) δ: 83.38 (d, pyrimidine-CH), 90.45 (d, pyrazole-CH), 109.88 (s), 111.97 (d), 113.29 (s), 114.31 (d), 115.06 (s), 120.12 (d), 122.06 (d), 122.50 (d), 124.56 (d), 124.72 (d), 125.54 (s), 125.73 (d), 127.64 (s), 128.46 (d), 136.19 (s), 137.06 (s), 147.65 (s), 150.17 (s), 152.32 (s), 154.33 (s); *Anal.* Calculated for $C_{22}H_{15}BrN_6$ (MW: 443,31): C, 59.61; H, 3.41; N, 18.96%. Found: C, 59.66; H, 3.45; N, 18.99%.

5-(5-fluoro-1*H*-indol-3-yl)-2-(1*H*-indol-3-yl)pyrazolo[1,5-*a*]pyrimidin-7-amine (16c):

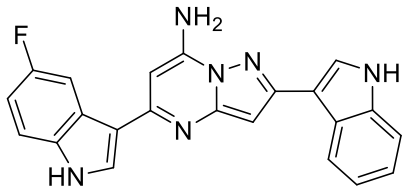

Yield: 70%; creamy white solid; m.p.: 277-278°C; IR (cm^{-1}): 3404-3318 (NH_2), 3219-3134 (2 NH); ^1H NMR (400 MHz, DMSO-*d*$_6$) δ: 6.46 (s, 1H, pyrimidine-CH), 6.72 (s, 1H, pyrazole-CH), 7.03 (td, *J* = 9.1, 2.7 Hz, 1H), 7.09 - 7.21 (m, 2H), 7.39 (s, 2H, NH_2, exchangeable with D_2O), 7.43 - 7.48 (m, 2H), 7.97 (d, *J* = 2.6 Hz, 1H), 8.10 (d, *J* = 2.8 Hz, 1H), 8.28 (dd, *J* = 10.7, 2.6 Hz, 1H), 8.54 (d, *J* = 7.2 Hz, 1H), 11.40 (s, 1H, NH, exchangeable with D_2O), 11.65 (s, 1H, NH, exchangeable with D_2O); ^{13}C NMR (101 MHz, DMSO-*d*$_6$) δ: 83.37 (d, pyrimidine-CH), 90.36 (d, pyrazole-CH), 107.02 (d, *J* = 24.7 Hz), 109.91 (s), 110.36 (d, *J* = 25.9 Hz), 111.98 (d), 113.29 (d, *J* = 9.6 Hz), 115.56 (d, *J* = 4.3 Hz), 120.11 (d), 122.05 (d), 122.41 (d), 125.58 (d),126.22 (d, *J* = 10.7 Hz), 128.84 (d), 134.14 (s), 137.08 (s), 147.63 (s), 150.25 (s), 152.22 (s), 154.53 (s), 158.07 (d, *J* = 231.6 Hz); *Anal.* Calculated for $C_{22}H_{15}FN_6$ (MW: 382,40): C, 69.10; H, 3.95; N, 21.98%. Found: C, 69.15; H, 3.98; N, 21.95%.

5-(5-chloro-1*H*-indol-3-yl)-2-(1*H*-indol-3-yl)pyrazolo[1,5-*a*]pyrimidin-7-amine (16d):

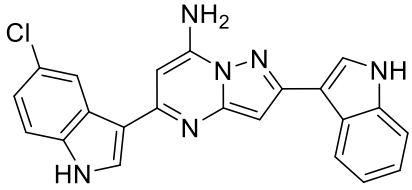

Yield: 36%; creamy white solid; m.p.: 289°C; IR (cm^{-1}): 3435-3414 (NH_2), 3283-3123 (2 NH); ^1H NMR (300 MHz, DMSO-*d*$_6$) δ: 6.46 (s, 1H, pyrimidine-CH), 6.76 (s, 1H, pyrazole-CH), 7.16 (ddd, *J* = 13.9, 7.8, 4.0 Hz, 3H), 7.44 (d, *J* = 7.9 Hz, 1H), 7.44 (s, 2H, NH_2, exchangeable with D_2O), 7.48 (d, *J* = 8.7 Hz, 1H), 7.99 (d, *J* = 2.5 Hz, 1H), 8.11 (d, *J* = 2.7 Hz, 1H), 8.56 (d, *J* = 7.0 Hz, 1H), 8.61 (d, *J* = 2.0 Hz, 1H), 11.41 (s, 1H, NH, exchangeable with D_2O), 11.74 (s, 1H, NH, exchangeable with D_2O); ^{13}C NMR (101 MHz, DMSO-*d*$_6$) δ: 83.39 (d, pyrimidine-CH), 90.43 (d, pyrazole-CH), 109.87 (s), 111.99 (d), 113.86 (d), 115.14 (s), 120.13 (d), 121.53 (d), 122.07 (d), 122.19 (d), 122.49 (d), 125.19 (s), 125.54 (s), 125.71 (d), 126.97 (s), 128.64 (d), 135.96 (s), 137.07 (s), 147.66 (s), 150.17 (s), 152.31 (s), 154.34 (s); *Anal.* Calculated for $C_{22}H_{15}ClN_6$ (MW: 398,85): C, 66.25; H, 3.79; N, 21.07%. Found: C, 66.28; H, 3.83; N, 21.12%.

2-(1*H*-indol-3-yl)-5-(1-methyl-1*H*-indol-3-yl)pyrazolo[1,5-*a*]pyrimidin-7-amine (16e):

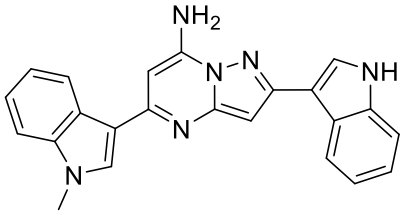

Yield: 70%; yellow crystals; m.p.: 320°C; IR (cm^{-1}): 3447-3412 (NH_2), 3244 (NH); ^1H NMR (400 MHz, DMSO-d_6) δ: 3.88 (s, 3H, CH_3), 6.48 (s, 1H, pyrimidine-CH), 6.68 (s, 1H, pyrazole-CH), 7.11 - 7.19 (m, 2H), 7.19 - 7.27 (m, 2H), 7.41 (s, 2H, NH_2, exchangeable with D_2O), 7.45 (d, *J* = 7.2 Hz, 1H), 7.50 (d, *J* = 7.3 Hz, 1H), 7.97 (d, *J* = 2.6 Hz, 1H), 8.04 (s, 1H), 8.53 (dd, *J* = 7.0, 4.1 Hz, 2H), 11.39 (s, 1H, NH, exchangeable with D_2O); ^{13}C NMR (101 MHz, DMSO-d_6) δ: 33.26 (q), 83.60 (d, pyrimidine-CH), 90.16 (d, pyrazole-CH), 109.88 (s), 110.66 (d), 112.00 (d), 114.45 (s), 120.13 (d), 120.76 (d), 122.08 (d), 122.28 (2xd), 122.45 (d), 125.56 (s), 125.66 (d), 126.20 (s), 131.28 (d), 137.07 (s), 137.93 (s), 147.65 (s), 150.23 (s), 152.25 (s), 154.43 (s); *Anal.* Calculated for $C_{23}H_{18}N_6$ (MW: 378,44): C, 73.00; H, 4.79; N, 22.21%. Found: C, 73.15; H, 4.83; N, 22.26%.

2-(1*H*-indol-3-yl)-5-(5-methoxy-1-methyl-1*H*-indol-3-yl)pyrazolo[1,5-*a*]pyrimidin-7-amine (16f):

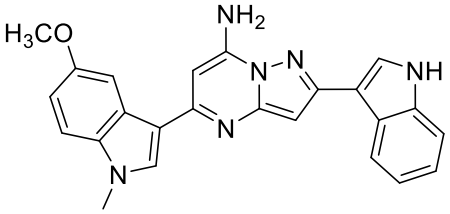

Yield: 62%; light yellow crystals; m.p.: 258°C; IR (cm^{-1}): 3433-3346 (NH_2), 3198 (NH); ^1H NMR (400 MHz, DMSO-d_6) δ: 3.84 (s, 3H, CH_3), 3.86 (s, 3H, OCH_3), 6.42 (s, 1H, pyrimidine-CH), 6.66 (s, 1H, pyrazole-CH), 6.90 (dd, *J* = 8.8, 2.5 Hz, 1H), 7.09 - 7.21 (m, 2H), 7.38 (s, 2H, NH_2, exchangeable with D_2O), 7.40 (d, *J* = 8.8 Hz, 1H), 7.42 - 7.45 (m, 1H), 7.97 (d, *J* = 2.6 Hz, 1H), 7.98 (s, 1H), 8.07 (d, *J* = 2.5 Hz, 1H), 8.54 (d, *J* = 7.0 Hz, 1H), 11.39 (s, 1H, NH, exchangeable with D_2O); ^{13}C NMR (101 MHz, DMSO-d_6) δ: 33.42 (q), 55.97 (q), 83.36 (d, pyrimidine-CH), 90.16 (d, pyrazole-CH), 104.73 (d), 109.94 (s), 111.30 (d), 111.90 (d), 111.99 (d), 113.99(s), 120.10 (d), 122.06 (d), 122.44 (d), 124.80 (s), 125.60 (d), 126.75 (s), 131.68 (d), 133.29 (s), 137.07 (s), 147.58 (s), 150.28 (s), 152.18 (s), 154.63 (s), 154.92 (s); *Anal.* Calculated for $C_{24}H_{20}N_6O$ (MW: 408,47): C, 70.57; H, 4.94; N, 20.58%. Found: C, 70.61; H, 4.90; N, 20.70%.

5-(5-bromo-1-methyl-1*H*-indol-3-yl)-2-(1*H*-indol-3-yl)pyrazolo[1,5-*a*]pyrimidin-7-amine (16g):

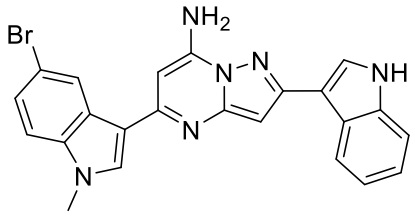

Yield: 35%; light yellow crystals; m.p.: 295-296°C; IR (cm^{-1}): 3414-3311 (NH_2), 3244 (NH); ^{1}H NMR (400 MHz, DMSO-d_6) δ: 3.89 (s, 3H, CH_3), 6.42 (s, 1H, pyrimidine-CH), 6.76 (s, 1H, pyrazole-CH), 7.11 - 7.21 (m, 2H), 7.38 (dd, *J* = 8.7, 2.0 Hz, 1H), 7.45 (d, *J* = 7.3 Hz, 1H), 7.48 (s, 2H, NH_2, exchangeable with D_2O), 7.51 (d, *J* = 8.7 Hz, 1H), 8.00 (d, *J* = 2.6 Hz, 1H), 8.11 (s, 1H), 8.57 (d, *J* = 7.3 Hz, 1H), 8.76 (d, *J* = 1.9 Hz, 1H), 11.41 (s, 1H, NH, exchangeable with D_2O); ^{13}C NMR (101 MHz, DMSO-d_6) δ: 33.49 (q), 83.25 (d, pyrimidine-CH), 90.42 (d, pyrazole-CH), 109.85 (s), 111.98 (d), 112.81 (d), 113.70 (s), 113.95 (s), 120.14 (d), 122.08 (d), 122.51 (d), 124.64 (d), 124.77 (d), 125.54 (s), 125.78 (d), 127.87 (s), 132.52 (d), 136.70 (s), 137.07 (s), 147.71 (s), 150.09 (s), 152.38 (s), 153.90 (s); *Anal.* Calculated for $C_{23}H_{17}BrN_6$ (MW: 457,34): C, 60.40; H, 3.75; N, 18.38%. Found: C, 60.45; H, 3.76; N, 18.42%.

5-(5-fluoro-1-methyl-1*H*-indol-3-yl)-2-(1*H*-indol-3-yl)pyrazolo[1,5-*a*]pyrimidin-7-amine (16h):

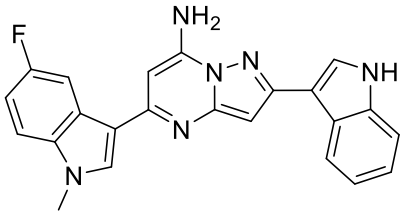

Yield: 40%; white crystals; m.p: 241°C; IR (cm^{-1}): 3447-3385 (NH_2), 3292-3236 (NH); ^{1}H NMR (400 MHz, DMSO-d_6) δ: 3.89 (s, 3H, CH_3), 6.42 (s, 1H, pyrimidine-CH), 6.72 (s, 1H, pyrazole-CH), 7.13 – 7.07 (m, 1H), 7.13 - 7.20 (m, 2H), 7.44 (s, 2H, NH_2, exchangeable with D_2O), 7.46 (d, *J* = 0.9 Hz, 1H), 7.53 (dd, *J* = 9.0, 4.6 Hz, 1H), 7.98 (d, *J* = 2.6 Hz, 1H), 8.13 (s, 1H), 8.30 (dd, *J* = 10.6, 2.6 Hz, 1H), 8.55 (d, *J* = 7.1 Hz, 1H), 11.41 (s, 1H, NH, exchangeable with D_2O); ^{13}C NMR (101 MHz, DMSO-d_6) δ: 33.57 (q), 83.18 (d, pyrimidine-CH), 90.34 (d, pyrazole-CH), 107.22 (d, $J_{C4\text{-}F}$ = 24.4 Hz), 109.87 (s), 110.38 (d, $J_{C6\text{-}F}$ = 26.4 Hz), 111.84 (d, $J_{C7\text{-}F}$ = 9.5 Hz), 111.99 (d), 114.35 (d, $J_{C7a\text{-}F}$ = 3.8 Hz), 120.13 (d), 122.07 (d), 122.44 (d), 125.55 (s), 125.65 (d), 126.53 (d, $J_{C3a\text{-}F}$ = 11.1 Hz),

132.85 (d), 134.71 (s), 137.07 (s), 147.66 (s), 150.22 (s), 152.27 (s), 154.15 (s), 158.33 (d, $J_{C5\text{-}F}$ = 231.8 Hz); *Anal.* Calculated for $C_{23}H_{17}FN_6$ (MW: 396,43): C, 69.69; H, 4.32; N, 21.20%. Found: C, 69.73; H, 4.36; N, 21.23%.

5-(5-chloro-1-methyl-1*H*-indol-3-yl)-2-(1*H*-indol-3-yl)pyrazolo[1,5-*a*]pyrimidin-7-amine (16i):

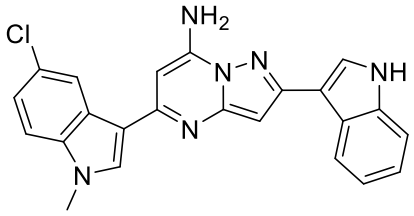

Yield: 30%; light yellow crystals; m.p.: 157°C; IR (cm^{-1}): 3447-3393 (NH_2), 3275 (NH); ^{1}H NMR (400 MHz, DMSO-d_6) δ: 3.89 (s, 3H, CH_3), 6.41 (s, 1H, pyrimidine-CH), 6.75 (s, 1H, pyrazole-CH), 7.10 - 7.20 (m, 2H), 7.25 (dd, *J* = 8.7, 2.2 Hz, 1H), 7.44 (d, *J* = 7.5 Hz, 1H), 7.46 (s, 2H, NH_2, exchangeable with D_2O), 7.55 (d, *J* = 8.7 Hz, 1H), 7.99 (d, *J* = 2.6 Hz, 1H), 8.12 (s, 1H), 8.55 (d, *J* = 7.4 Hz, 1H), 8.61 (d, *J* = 2.1 Hz, 1H), 11.40 (s, 1H, NH, exchangeable with D_2O); ^{13}C NMR (101 MHz, DMSO-d_6) δ: 33.51 (q), 83.24 (d, pyrimidine-CH), 90.43 (d, pyrazole-CH), 109.87 (s), 111.98 (d), 112.34 (d), 114.09 (s), 120.13 (d), 121.63 (d), 122.07 (d), 122.21 (d), 122.48 (d), 125.54 (s), 125.58 (s), 125.73 (d), 127.24 (s), 132.66 (d), 136.47 (s), 137.07 (s), 147.69 (s), 150.17 (s), 152.35 (s), 153.97 (s); *Anal.* Calculated for $C_{23}H_{17}ClN_6$ (MW: 412,88): C, 66.91; H, 4.15; N, 20.36%. Found: C, 66.97; H, 4.13; N, 20.39%.

5-(1*H*-indol-3-yl)-2-(1-methyl-1*H*-indol-3-yl)pyrazolo[1,5-*a*]pyrimidin-7-amine (16j):

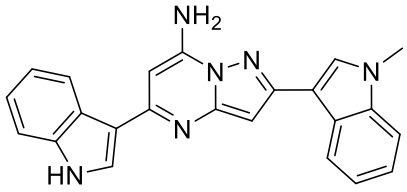

Yield: 60%; creamy white solid; m.p.: 267-268°C; IR (cm^{-1}): 3422-3292 (NH_2), 3244-3179 (NH); ^{1}H NMR (400 MHz, DMSO-d_6) δ: 3.88 (s, 3H, CH_3), 6.52 (s, 1H, pyrimidine-CH), 6.63 (s, 1H, pyrazole-CH), 7.13 - 7.21 (m, 3H), 7.22 - 7.27 (m, 1H), 7.41 (s, 2H, NH_2, exchangeable with D_2O), 7.44 - 7.48 (m, 1H), 7.50 (d, *J* = 8.2 Hz, 1H), 7.96 (s, 1H), 8.01 - 8.04 (m, 1H), 8.52 (d, *J* = 7.5 Hz, 1H), 8.57 (d, *J* = 8.0 Hz, 1H), 11.56 (s, 1H, NH, exchangeable with D_2O); ^{13}C NMR (101 MHz, DMSO-d_6) δ: 33.16

(q), 83.82 (d, pyrimidine-CH), 90.04 (d, pyrazole-CH), 109.05 (s), 110.29 (d), 112.36 (d), 115.50 (s), 120.33 (d), 120.51 (d), 122.19 (3xd), 122.68 (d), 125.83 (s), 125.90 (s), 127.15 (d), 129.65 (d), 137.49 (s), 137.52 (s), 147.60 (s), 150.32 (s), 151.78 (s), 154.91 (s); *Anal.* Calculated for $C_{23}H_{18}N_6$ (MW: 378,44): C, 73.00; H, 4.79; N, 22.21%. Found: C, 73.15; H, 4.83; N, 22.25%.

5-(5-methoxy-1*H*-indol-3-yl)-2-(1-methyl-1*H*-indol-3-yl)pyrazolo[1,5-*a*]pyrimidin-7-amine (16k):

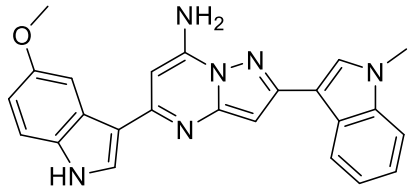

Yield 30%; light yellow solid; m.p.: 165-166°C; IR (cm^{-1}): 3437-3393 (NH_2), 3256 (NH); ^{1}H NMR (400 MHz, DMSO-d_6) δ: 3.85 (s, 3H, CH_3), 3.87 (s, 3H, OCH_3), 6.48 (s, 1H, pyrimidine-CH), 6.62 (s, 1H, pyrazole-CH), 6.84 (d, *J* = 8.8 Hz, 1H), 7.17 (t, *J* = 7.4 Hz, 1H), 7.24 (t, *J* = 7.5 Hz, 1H), 7.35 (d, *J* = 8.8 Hz, 1H), 7.36 (s, 2H, NH_2, exchangeable with D_2O), 7.49 (d, *J* = 7.9 Hz, 1H), 7.96 (s, 1H), 7.97 (s, 1H), 8.06 (s, 1H), 8.55 (d, *J* = 7.9 Hz, 1H), 11.41 (s, 1H, NH, exchangeable with D_2O); ^{13}C NMR (101 MHz, DMSO-d_6) δ: 33.16 (q), 55.90 (q), 83.58 (d, pyrimidine-CH), 90.05 (d, pyrazole-CH), 104.48 (d), 109.08 (s), 110.28 (d), 111.96 (d), 112.88 (d), 115.16 (s), 120.30 (d), 122.16 (d), 122.66 (d), 125.91 (s), 126.37 (s), 127.65 (d), 129.66 (d), 132.63 (s), 137.52 (s), 147.55 (s), 150.31 (s), 151.73 (s), 154.63 (s), 155.05 (s); *Anal.* Calculated for $C_{24}H_{20}N_6O$ (MW: 408,47): C, 70.57; H, 4.94; N, 20.58%. Found: C, 70.62; H, 4.91; N, 20.62%.

5-(5-bromo-1*H*-indol-3-yl)-2-(1-methyl-1*H*-indol-3-yl)pyrazolo[1,5-*a*]pyrimidin-7-amine (16l):

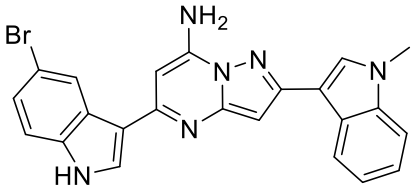

Yield: 37%; light yellow solid; m.p.: 177-178°C; IR (cm^{-1}): 3447-3360 (NH_2), 3186 (NH); ^{1}H NMR (300 MHz, DMSO-d_6) δ: 3.87 (s, 3H, CH_3), 6.47 (s, 1H, pyrimidine-CH), 6.71 (s, 1H, pyrazole-CH), 7.18 (t, *J* = 7.3 Hz, 1H), 7.25 (t, *J* = 7.0 Hz, 1H), 7.31 (dd, *J* = 8.6, 1.7 Hz, 1H), 7.44 (d, *J* = 8.5 Hz,

1H), 7.46 (s, 2H, NH_2, exchangeable with D_2O), 7.49 (d, *J* = 8.0 Hz, 1H), 7.97 (s, 1H), 8.10 (d, *J* = 2.4 Hz, 1H), 8.58 (d, *J* = 7.7 Hz, 1H), 8.75 (s, 1H), 11.75 (s, 1H, NH, exchangeable with D_2O); ^{13}C NMR (101 MHz, DMSO-d_6) δ: 33.19 (q), 83.54 (d), 90.34 (d), 109.05 (s), 110.27 (d), 113.30 (s), 114.32 (d), 115.09 (s), 120.33 (d), 122.18 (d), 122.67 (d), 124.50 (d), 124.73 (d), 125.91 (s), 127.62 (s), 128.49 (d), 129.72 (d), 136.20 (s), 137.54 (s), 147.66 (s), 150.21 (s), 151.89 (s), 154.36 (s); *Anal.* Calculated for $C_{23}H_{17}BrN_6$ (MW: 457.34): C, 60.40; H, 3.75; N, 18.38%. Found: C, 60.46; H, 3.79; N, 18.41%.

5-(5-fluoro-1*H*-indol-3-yl)-2-(1-methyl-1*H*-indol-3-yl)pyrazolo[1,5-*a*]pyrimidin-7-amine (16m):

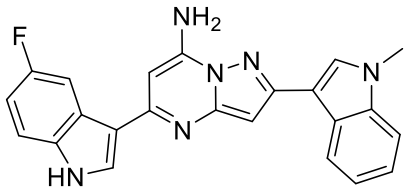

Yield: 57%; creamy white solid; m.p.: 263-264°C; IR (cm^{-1}):3420-3307 (NH_2), 3146 (NH); ^1H NMR (400 MHz, DMSO-d_6) δ: 3.87 (s, 3H, CH_3), 6.47 (s, 1H, pyrimidine-CH), 6.66 (s, 1H, pyrazole-CH), 7.03 (td, *J* = 9.0, 2.4 Hz, 1H), 7.17 (t, *J* = 7.4 Hz, 1H), 7.24 (t, *J* = 7.6 Hz, 1H), 7.40 (s, 2H, NH_2, exchangeable with D_2O), 7.43 - 7.47 (m, 1H), 7.49 (d, *J* = 8.4 Hz, 1H), 7.95 (s, 1H), 8.11 (s, 1H), 8.27 (d, *J* = 10.7 Hz, 1H), 8.55 (d, *J* = 7.9 Hz, 1H), 11.65 (s, 1H, NH, exchangeable with D_2O); ^{13}C NMR (101 MHz, DMSO-d_6) δ: 33.17 (q), 83.46 (d), 90.22 (d), 106.99 (d, $J_{C4\text{-}F}$ = 24.4 Hz), 109.04 (s), 110.28 (d), 110.40 (d, $J_{C6\text{-}F}$ = 23.2 Hz), 113.31 (d, $J_{C7\text{-}F}$ = 9.9 Hz), 115.53 (d, $J_{C7a\text{-}F}$ = 3.5 Hz), 120.33 (d), 122.19 (d), 122.64 (d), 125.91 (s), 126.19 (d, $J_{C3a\text{-}F}$ = 10.8 Hz), 128.91 (d), 129.64 (d), 134.14 (s), 137.53 (s), 147.63 (s), 150.27 (s), 151.81 (s), 154.57 (s), 158.08 (d, $J_{C5\text{-}F}$ = 231.9 Hz); *Anal.* Calculated for $C_{23}H_{17}FN_6$ (MW: 396.43): C, 69.69; H, 4.32; N, 21.20%. Found: C, 69.73; H, 4.38; N, 21.27%.

5-(5-chloro-1*H*-indol-3-yl)-2-(1-methyl-1*H*-indol-3-yl)pyrazolo[1,5-*a*]pyrimidin-7-amine (16n):

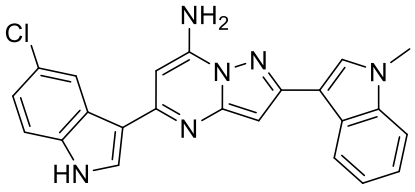

Yield: 34%; light yellow solid; m.p.: 245-246°C; IR (cm^{-1}): 3460-3354 (NH_2), 3144 (NH); ^1H NMR (400 MHz, DMSO-d_6) δ: 3.88 (s, 3H, CH_3), 6.47 (s, 1H, pyrimidine-CH), 6.70 (s, 1H, pyrazole-CH), 7.17 (dd, *J* = 9.5, 1.6 Hz, 1H), 7.20 (dd, *J* = 3.2, 1.6 Hz, 1H), 7.25 (ddd, *J* = 8.2, 7.1, 1.2 Hz, 1H), 7.43 (s, 2H, NH_2, exchangeable with D_2O), 7.48 (d, *J* = 5.5 Hz, 1H), 7.50 (d, *J* = 5.0 Hz, 1H), 7.96 (s, 1H), 8.11 (d, *J* = 2.8 Hz, 1H), 8.57 (d, *J* = 7.8 Hz, 1H), 8.59 (d, *J* = 1.9 Hz, 1H), 11.74 (s, 1H, NH, exchangeable with D_2O); ^{13}C NMR (101 MHz, DMSO-d_6) δ: 33.19 (q), 83.50 (d), 90.31 (d), 109.03 (s), 110.29 (d), 113.87 (d), 115.15 (s), 120.34 (d), 121.48 (d), 122.20 (2xd), 122.69 (d), 125.20 (s), 125.89 (s), 126.95 (s), 128.68 (d), 129.72 (d), 135.96 (s), 137.53 (s), 147.66 (s), 150.22 (s), 151.88 (s), 154.38 (s); *Anal.* Calculated for $C_{23}H_{17}ClN_6$ (MW: 412.88): C, 66.91; H, 4.15; N, 20.36%. Found: C, 66.96; H, 4.20; N, 20.41%.

5-(5-methoxy-1-methyl-1*H*-indol-3-yl)-2-(1-methyl-1*H*-indol-3-yl)pyrazolo[1,5-*a*]pyrimidin-7-amine (16o):

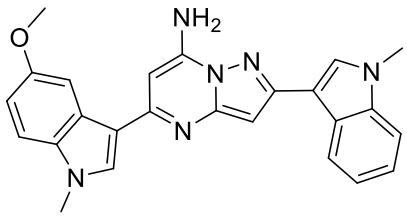

Yield: 51%: creamy white solid; m.p.: 267-268°C; IR (cm^{-1}): 3360-3277 (NH_2); ^1H NMR (400 MHz, DMSO-d_6) δ: 3.85 (s, 3H, CH_3), 3.86 (s, 3H, CH_3), 3.87 (s, 3H, OCH_3), 6.43 (s, 1H, pyrimidine-CH), 6.60 (s, 1H, pyrazole-CH), 6.90 (dd, *J* = 8.9, 2.5 Hz, 1H), 7.15 - 7.20 (m, 1H), 7.24 (ddd, *J* = 8.2, 7.1, 1.3 Hz, 1H), 7.39 (s, 2H, NH_2, exchangeable with D_2O), 7.40 (d, *J* = 8.8 Hz, 1H), 7.49 (d, *J* = 8.1 Hz, 1H), 7.96 (s, 1H), 7.99 (s, 1H), 8.06 (d, *J* = 2.4 Hz, 1H), 8.55 (d, *J* = 7.5 Hz, 1H); ^{13}C NMR (101 MHz, DMSO-d_6) δ: 33.17 (q), 33.42 (q), 55.94 (q), 83.41 (d), 90.01 (d), 104.66 (d), 109.06 (s), 110.29 (d), 111.32 (d), 111.89 (d), 113.95 (s), 120.30 (d), 122.17 (d), 122.65 (d), 125.90 (s), 126.72 (s), 129.69 (d), 131.72 (d), 133.27 (s), 137.52 (s), 147.58 (s), 150.29 (s), 151.77 (s), 154.65 (s), 154.91 (s); *Anal.* Calculated for $C_{25}H_{22}N_6O$ (MW: 422.49): C, 71.07; H, 5.25; N, 19.89%. Found: C, 71.13; H, 5.28; N, 19.94%.

5-(5-bromo-1-methyl-1*H*-indol-3-yl)-2-(1-methyl-1*H*-indol-3-yl)pyrazolo[1,5-*a*]pyrimidin-7-amine (16p):

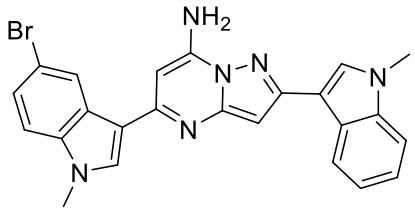

Yield: 45%; yellow crystals; m.p.: 277-278°C; IR (cm^{-1}): 3447-3391 (NH_2); ^1H NMR (400 MHz, DMSO-d_6) δ: 3.87 (s, 3H, CH_3), 3.89 (s, 3H, CH_3), 6.42 (s, 1H, pyrimidine-CH), 6.68 (s, 1H, pyrazole-CH), 7.15 - 7.20 (m, 1H), 7.22 - 7.27 (m, 1H), 7.37 (dd, *J* = 8.7, 2.0 Hz, 1H), 7.45 (s, 2H, NH_2, exchangeable with D_2O), 7.49 (d, *J* = 5.5 Hz, 1H), 7.51 (d, *J* = 6.1 Hz, 1H), 7.96 (s, 1H), 8.10 (s, 1H), 8.55 (d, *J* = 7.8 Hz, 1H), 8.74 (d, *J* = 1.9 Hz, 1H); ^{13}C NMR (101 MHz, DMSO-d_6) δ: 33.18 (q), 33.48 (q), 83.42 (d), 90.34 (d), 109.05 (s), 110.28 (d), 112.80 (d), 113.69 (s), 114.06 (s), 120.33 (d), 122.19 (d), 122.65 (d), 124.59 (d), 124.77 (d), 125.92 (s), 127.88 (s), 129.73 (d), 132.53 (d), 136.73 (s), 137.56 (s), 147.71 (s), 150.21 (s), 151.94 (s), 153.98 (s); *Anal.* Calculated for $C_{24}H_{19}BrN_6$ (MW: 471.36): C, 61.16; H, 4.06; N, 17.83%. Found: C, 61.23; H, 4.23; N, 17.91%.

5-(5-fluoro-1-methyl-1*H*-indol-3-yl)-2-(1-methyl-1*H*-indol-3-yl)pyrazolo[1,5-*a*]pyrimidin-7-amine (16q):

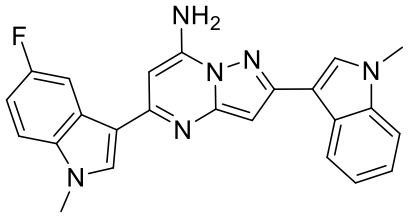

Yield: 42%; light yellow solid; m.p.: 301,6-302,1°C; IR (cm^{-1}): 3489-3381 (NH_2); ^1H NMR (400 MHz, DMSO-d_6) δ: 3.87 (s, 3H, CH_3), 3.89 (s, 3H, CH_3), 6.43 (s, 1H, pyrimidine-CH), 6.65 (s, 1H, pyrazole-CH), 7.10 (td, *J* = 9.1, 2.4 Hz, 1H), 7.17 (t, *J* = 7.4 Hz, 1H), 7.24 (t, *J* = 7.5 Hz, 1H), 7.41 (s, 2H, NH_2, exchangeable with D_2O), 7.49 (d, *J* = 8.3 Hz, 1H), 7.52 (dd, *J* = 9.1, 4.8 Hz, 1H), 7.94 (s, 1H), 8.12 (s, 1H), 8.27 (dd, *J* = 10.6, 2.3 Hz, 1H), 8.54 (d, *J* = 7.8 Hz, 1H); ^{13}C NMR (101 MHz, DMSO-d_6) δ: 33.16 (q), 33.58 (q), 83.32 (d), 90.21 (d), 107.17 (d, J_{C4-F} = 25.0 Hz), 109.03 (s), 110.28 (d), 110.40 (d, J_{C6-F} = 24.0 Hz), 111.86 (d, J_{C7-F} = 9.5 Hz), 114.36 (d, J_{C7a-F} = 4.4 Hz), 120.33 (d), 122.19 (d), 122.63 (d), 125.91 (s), 126.51 (d, J_{C3a-F} = 10.8 Hz), 129.65 (d), 132.89 (d), 134.73 (s), 137.54 (s), 147.67 (s), 150.26 (s), 151.85 (s), 154.19 (s), 158.34 (d, J_{C5-F} = 232.4 Hz); *Anal.* Calculated for $C_{24}H_{19}FN_6$ (MW: 410.46): C, 70.23; H, 4.67; N, 20.48%. Found: C, 70.26; H, 4.70; N, 20.51%.

5-(5-chloro-1-methyl-1*H*-indol-3-yl)-2-(1-methyl-1*H*-indol-3-yl)pyrazolo[1,5-*a*]pyrimidin-7-amine (16r):

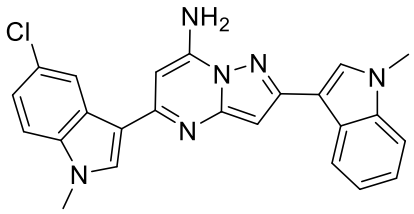

Yield: 40%; light yellow solid; m.p.: 291-292°C; IR (cm^{-1}): 3383-3310 (NH_2); ^{1}H NMR (400 MHz, DMSO-d_6) δ: 3.87 (s, 3H, CH_3). 3.89 (s, 3H, CH_3), 6.42 (s, 1H, pyrimidine-CH), 6.68 (s, 1H, pyrazole-CH), 7.15 - 7.20 (m, 1H), 7.23 (dd, *J* = 8.6, 1.6 Hz, 1H), 7.26 (t, *J* = 1.9 Hz, 1H), 7.44 (s, 2H, NH_2, exchangeable with D_2O), 7.49 (d, *J* = 8.1 Hz, 1H), 7.55 (d, *J* = 8.7 Hz, 1H), 7.95 (s, 1H), 8.12 (s, 1H), 8.55 (d, *J* = 7.8 Hz, 1H), 8.59 (d, *J* = 2.1 Hz, 1H); ^{13}C NMR (101 MHz, DMSO-d_6) δ: 33.18 (q), 33.51 (q), 83.39 (d), 90.31 (d), 109.03 (s), 110.28 (d), 112.35 (d), 114.11 (s), 116.49 (s), 120.34 (d), 121.57 (d), 122.20 (2xd), 122.65 (d), 125.60 (s), 125.91 (s), 127.22 (s), 129.71 (d), 132.70 (d), 136.49 (s), 137.54 (s), 147.70 (s), 150.22 (s), 151.93 (s); *Anal.* Calculated for $C_{24}H_{19}ClN_6$ (MW: 426.91): C, 67.52; H, 4.49; N, 19.69%. Found: C, 67.55; H, 4.52; N, 19.65%.

2-(5-chloro-1-methyl-1*H*-indol-3-yl)-5-(1*H*-indol-3-yl)pyrazolo[1,5-*a*]pyrimidin-7-amine (16s):

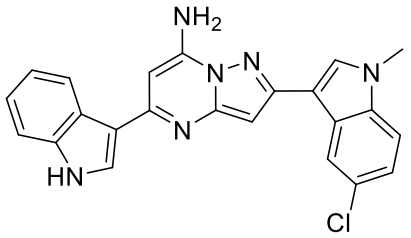

Yield: 48%; light yellow crystals; m.p.: 260-261°C; IR (cm^{-1}): 3451-3389 (NH_2), 3309 (NH); ^{1}H NMR (300 MHz, DMSO-d_6) δ: 3.88 (s, 3H, CH_3). 6.53 (s, 1H, pyrimidine-CH), 6.63 (s, 1H, pyrazole-CH), 7.18 (p, *J* = 6.9 Hz, 1H), 7.24 (dd, *J* = 8.7, 2.0 Hz, 1H), 7.47 (dd, *J* = 5.9, 3.3 Hz, 1H), 7.50 (s, 2H, NH_2, exchangeable with D_2O), 7.54 (d, *J* = 8.8 Hz, 1H), 8.04 (d, *J* = 2.6 Hz, 1H), 8.05 (s, 1H), 8.49 - 8.55 (m, 1H), 8.59 (d, *J* = 2.0 Hz, 1H), 11.57 (s, 1H, NH, exchangeable with D_2O); ^{13}C NMR (101 MHz, DMSO-d_6) δ: 33.40 (q), 83.96 (d), 90.07 (d), 108.93, 111.99 (d), 112.36 (d), 115.51 (s), 120.51 (d), 121.63 (d), 122.11 (d), 122.20 (d), 122.25 (d), 125.40 (s), 125.84 (s), 126.70 (s), 127.16 (d), 131.30 (d), 136.07 (s), 137.50 (s), 147.72 (s), 150.40 (s), 151.24 (s), 155.03 (s); *Anal.* Calculated for $C_{23}H_{17}ClN_6$ (MW: 412.88): C, 66.91; H, 4.15; N, 20.36%. Found: C, 66.97; H, 4.22; N, 20.40%.

2-(5-chloro-1-methyl-1*H*-indol-3-yl)-5-(1-methyl-1*H*-indol-3-yl)pyrazolo[1,5-*a*]pyrimidin-7-amine (16t):

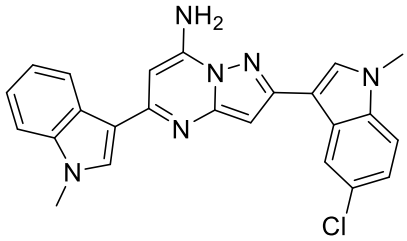

Yield: 44%; creamy white solid; m.p.: 289-289.5°C; IR (cm^{-1}): 3480-3372 (NH_2); ^1H NMR (300 MHz, DMSO-d_6) δ: 3.88 (s, 3H, CH_3). 3.89 (s, 3H, CH_3), 6.50 (s, 1H, pyrimidine-CH), 6.63 (s, 1H, pyrazole-CH), 7.18 - 7.25 (m, 2H), 7.27 (t, *J* = 3.9 Hz, 1H), 7.51 (d, *J* = 6.6 Hz, 1H), 7.52 (s, 2H, NH_2, exchangeable with D_2O), 7.53 (d, *J* = 8.2 Hz, 1H), 8.06 (d, *J* = 2.3 Hz, 2H), 8.53 (d, *J* = 7.0 Hz, 1H), 8.60 (d, *J* = 1.9 Hz, 1H); ^{13}C NMR (101 MHz, DMSO-d_6) δ: 33.27 (q), 33.39 (q), 83.84 (d), 90.05 (d), 108.92 (s), 110.67 (d), 111.99 (d), 114.50 (s), 120.77 (d), 121.62 (d), 122.25 (2xd), 122.29 (d), 125.40 (s), 126.20 (s), 126.70 (s), 131.32 (2xd), 136.08 (s), 137.96 (s), 147.76 (s), 150.39 (s), 151.30 (s), 154.64 (s); *Anal.* Calculated for $C_{24}H_{19}ClN_6$ (MW: 426.91): C, 67.52; H, 4.49; N, 19.69%. Found: C, 67.57; H, 4.53; N, 19.72%.

General procedure for the synthesis of 1-methyl-7-azaindoles (34a,c):

To a cold solution of appropriate 7-azaindole (**35a,c**) (2.5 mmol) in anhydrous toluene (25 ml), potassium *tert*-butoxide (*t*-BuOK) (0.38 g, 3.4 mmol) and TDA-1 (1 or 2 drops) were added. After stirring for overnight, methyl iodide (2.5 mmol, 0.2 ml) was added dropwise to the reaction mixture. Then, the resulting suspension was stirred at room temperature for 1-2 hours. After the solvent was removed in vacuo, the resulting residue was treated with water (15 ml) and extracted with DCM (3 × 15 ml), dried (Na_2SO_4) and evaporated under reduced pressure. The product obtained was further purified by column chromatography, using DCM/EtOAc (9/1) as eluent.

1-Methyl-7-azaindole (34a):

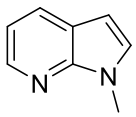

Yield: 96%; yellow oil; ^{1}H NMR (200 MHz, $CDCl_3$) δ: 3.87 (3H, s, CH_3), 6.43 (d, *J* = 3.4 Hz, 1H, H-3), 7.03 (dd, *J* = 7.8, 4.8 Hz, 1H, H-5), 7.15 (d, *J* = 3.4 Hz, 1H, H-2), 7.88 (dd, *J* = 7.8, 1.5 Hz, 1H, H-4), 8.33 (d, *J* = 4.8 Hz, 1H, H-6); ^{13}C NMR (50 MHz, DMSO-d_6) δ: 31.1 (q), 99.1 (d), 115.3 (d), 120.4 (s), 128.6 (d), 128.9 (d), 142.6 (d), 148.7 (s); *Anal*. Calculated for $C_8H_8N_2$ (MW: 132.16): C, 72.70; H, 6.10; N, 21.20%. Found: C, 72.65; H, 6.24; N, 21.45%.

5-Bromo-1-methyl-7-azaindole (34c):

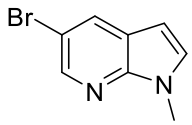

Yield: 85%; brown solid; m.p.: 62–63 °C; ^{1}H NMR (200 MHz, DMSO-d_6) δ: 3.83 (3H, s, CH_3), 6.44 (d, *J* = 3.4 Hz, 1H, H-3), 7.60 (d, *J* = 3.4 Hz, 1H, H-2), 8.21 (d, *J* = 2.1 Hz, 1H, H-4), 8.33 (d, *J* = 2.1 Hz, 1H, H-6); ^{13}C NMR (50 MHz, DMSO-d_6) δ: 31.0 (q), 98.5 (d), 110.7 (s), 121.7 (s), 130.3 (d), 131.8 (d), 142.2 (d), 145.7 (s); *Anal.* Calculated for $C_8H_7BrN_2$ (MW: 211.06): C, 45.53; H, 3.34; N, 13.27%. Found: C, 45.38; H, 3.24; N, 13.45%.

General procedure for the synthesis of 3-(1-methyl-7-azaindol-3-yl)-3-oxopropanenitriles (33a,c):

A solution of cyanoacetic acid (7 mmol) and acetic anhydride (Ac_2O) (7 ml) was heated to 85 °C for 10 minutes. Then appropriate 1-methyl-7-azaindole (**34a,c**) (7 mmol) was added to this solution and heating was continuing at 85°C for 3 - 8 hours (the progress of the reaction was monitored by TLC). After completion the reaction mixture was left to cool and was poured into water and ice. It was extracted with ethyl acetate (3 × 15 ml), dried (Na_2SO_4), evaporated under reduced pressure and was further purified by column chromatography, using cyclohexane/ethyl acetate as eluent to obtain the desired products (**33a,c**).

3-(1-methyl-7-azaindol-3-yl)-3-oxopropanenitrile (33a):

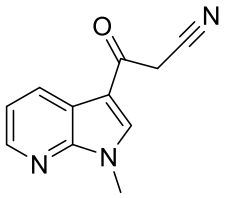

Yield: 35%; yellow solid; m.p.: 209.6-210.3°C; IR (cm^{-1}): 2255 (CN), 1653 (CO); ^{1}H NMR (300 MHz, DMSO-d_6) δ: 3.90 (s, 3H, CH_3). 4.50 (s, 2H, CH_2), 7.34 (dd, J = 7.7, 4.8 Hz, 1H, H-5), 8.43 (t, J = 6.0 Hz, 2H, H-4, H-6), 8.58 (s, 1H, H-2); ^{13}C NMR (75 MHz, DMSO-d_6) δ: 29.39 (t), 31.73 (q), 111.72 (s), 116.10 (s), 117.83 (s), 118.85 (d), 129.66 (d), 138.80 (d), 144.55 (d), 148.01 (s), 182.79 (s); *Anal.* Calculated for $C_{11}H_9N_3O$ (MW: 199,21): C, 66.32; H, 4.55; N, 21.09%. Found: C, 66.41; H, 4.57; N, 21.13%.

3-(5-bromo-1-methyl-7-azaindol-3-yl)-3-oxopropanenitrile (33c):

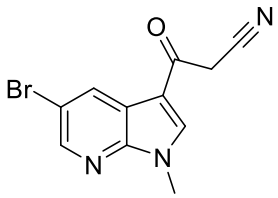

Yield: 46%; light yellow solid; m.p.: 238.6-239.6°C; IR (cm^{-1}): 2257 (CN), 1653 (CO); ^{1}H NMR (300 MHz, DMSO-d_6) δ: 3.87 (s, 3H, CH_3). 4.51 (s, 2H, CH_2), 8.47 (d, J = 2.1 Hz, 1H, H-4), 8.49 (d, J = 2.1 Hz, 1H, H-6), 8.62 (s, 1H, H-2); ^{13}C NMR (75 MHz, DMSO-d_6) δ: 29.97 (t) 32.40 (q), 111.59 (s), 114.74 (s), 116.33 (s), 119.70 (s), 131.69 (d), 140.41 (d), 145.15 (d), 146.90 (s), 183.28 (s); *Anal.* Calculated for $C_{11}H_8BrN_3O$ (MW: 278,11): C, 47.51; H, 2.90; N, 15.11%. Found: C, 47.57; H, 2.93; N, 15.15%.

General procedure for the synthesis of 2-(1*H*-indol-3-yl)-5-(1-methyl-7-azaindol-3-yl)pyrazolo[1,5-*a*]pyrimidin-7-amines (17a-t):

To a mixture of appropriate 3-(1-methyl-7-azaindol-3-yl)-3-oxopropanenitrile (**33a,c**) (0.5 mmol) and appropriate 3-(1*H*-indol-3-yl)-1*H*-pyrazol-5-amine (**27a-e**,**28a-e**) (0.5 mmol) in anhydrous *n*-butanol (*n*-BuOH) (8 ml) *p*-toluenesulfonic acid monohydrate (PTSA·H_2O) (2.5 mmol) was added. The reaction mixture was stirred to 90°C for 12 - 48 hours (the progress of the reaction was monitored by TLC). After completion the reaction mixture was left to cool, and the obtained precipitate was filtered

off. Solid was neutralised by adding a few drops of saturated aqueous solution of sodium hydrogencarbonate ($NaHCO_3$) and water (20 ml), extracted with ethyl acetate (3 × 20 ml), dried (Na_2SO_4) and evaporated under reduced pressure. The product obtained was further purified by column chromatography, using dichloromethane or dichloromethane/methanol as eluent.

2-(1*H*-indol-3-yl)-5-(1-methyl-7-azaindol-3-yl)pyrazolo[1,5-*a*]pyrimidin-7-amine (17a):

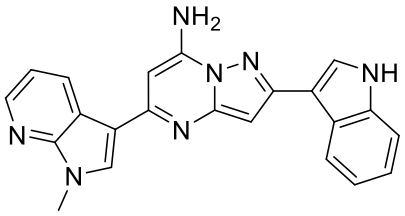

Yield: 47%; creamy white solid; m.p.: 344-345°C; IR (cm^{-1}): 3433-3375 (NH_2), 3244 (NH); ^{1}H NMR (400 MHz, DMSO-d_6) δ: 3.92 (s, 3H, CH_3). 6.47 (s, 1H, pyrimidine-CH), 6.70 (s, 1H, pyrazole-CH), 7.11 - 7.20 (m, 2H), 7.26 (dd, *J* = 7.9, 4.6 Hz, 1H), 7.45 (dd, *J* = 7.0, 1.1 Hz, 1H), 7.48 (s, 2H, NH_2, exchangeable with D_2O), 7.98 (d, *J* = 2.6 Hz, 1H), 8.24 (s, 1H), 8.35 (dd, *J* = 4.6, 1.6 Hz, 1H), 8.54 (d, *J* = 7.1 Hz, 1H), 8.84 (dd, *J* = 7.9, 1.6 Hz, 1H), 11.41 (s, 1H, NH, exchangeable with D_2O); ^{13}C NMR (101 MHz, DMSO-d_6) δ: 31.62 (q), 83.23 (d), 90.38 (d), 109.83 (s), 112.01 (d), 113.08 (s), 117.14 (d), 118.63 (s), 120.15 (d), 122.09 (d), 122.42 (d), 125.57 (s), 125.70 (d), 130.65 (d), 131.02 (d), 137.08 (s), 143.55 (d), 147.76 (s), 148.59 (s), 150.25 (s), 152.35 (s), 153.86 (s); *Anal.* Calculated for $C_{22}H_{17}N_7$ (MW: 379,43): C, 69.64; H, 4.52; N, 25.84%. Found: C, 69.69; H, 4.57; N, 25.82%.

5-(5-bromo-1-methyl-7-azaindol-3-yl)-2-(1*H*-indol-3-yl)pyrazolo[1,5-*a*]pyrimidin-7-amine (17b):

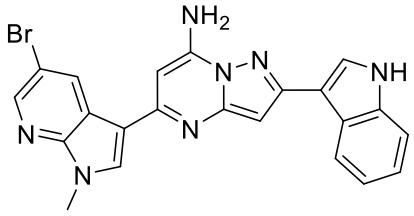

Yield 42%; yellow solid; m.p.: 308-309°C; IR (cm^{-1}): 3445 (NH_2), 3231 (NH); ^{1}H NMR (400 MHz, DMSO-d_6) δ: 3.90 (s, 3H, CH_3). 6.43 (s, 1H, pyrimidine-CH), 6.77 (s, 1H, pyrazole-CH), 7.11 - 7.21 (m, 2H), 7.44 (d, *J* = 7.8 Hz, 1H), 7.52 (s, 2H, NH_2, exchangeable with D_2O), 7.98 (d, *J* = 2.5 Hz, 1H), 8.32 (s, 1H), 8.42 (d, *J* = 2.3 Hz, 1H), 8.55 (d, *J* = 7.9 Hz, 1H), 9.03 (d, *J* = 2.3 Hz, 1H), 11.40 (s, 1H, NH, exchangeable with D_2O); ^{13}C NMR (101 MHz, DMSO-d_6) δ: 31.86 (q), 82.97 (d), 90.62

(d), 109.79 (s), 112.00 (d), 112.56 (s), 112.58 (s), 120.16 (d), 120.26 (s), 122.10 (d), 122.46 (d), 125.53 (s), 125.78 (d), 132.57 (d), 132.62 (d), 137.07 (s), 143.58 (d), 147.03 (s), 147.83 (s), 150.12 (s), 152.48 (s), 153.25 (s); *Anal.* Calculated for $C_{22}H_{16}BrN_7$ (MW: 458,32): C, 57.65; H, 3.52; N, 21.39%. Found: C, 57.68; H, 3.57; N, 21.43%.

2-(5-methoxy-1*H*-indol-3-yl)-5-(1-methyl-7-azaindol-3-yl)pyrazolo[1,5-*a*]pyrimidin-7-amine (17c):

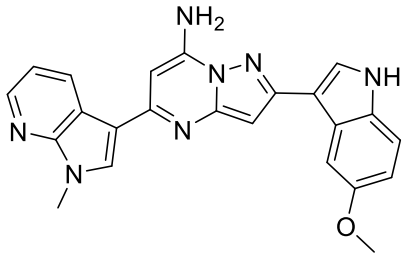

Yield 58%; light yellow solid; m.p.: 285-286°C; IR (cm^{-1}): 3474 (NH_2), 3271 (NH); ^{1}H NMR (400 MHz, DMSO-d_6) δ: 3.88 (s, 3H, CH_3). 3.92 (s, 3H, OCH_3), 6.48 (s, 1H, pyrimidine-CH), 6.68 (s, 1H, pyrazole-CH), 6.82 (dd, *J* = 8.8, 2.5 Hz, 1H), 7.27 (dd, *J* = 7.9, 4.6 Hz, 1H), 7.34 (d, *J* = 8.8 Hz, 1H), 7.45 (s, 2H, NH_2, exchangeable with D_2O), 7.92 (dd, *J* = 7.8, 2.6 Hz, 2H), 8.25 (s, 1H), 8.35 (dd, *J* = 4.6, 1.6 Hz, 1H), 8.84 (dd, *J* = 7.9, 1.6 Hz, 1H), 11.29 (s, 1H, NH, exchangeable with D_2O); ^{13}C NMR (101 MHz, DMSO-d_6) δ: 31.64 (q), 56.06 (q), 83.28 (d), 90.39 (d), 103.96 (d), 109.57 (s), 112.21 (d), 112.68 (d), 113.05 (s), 117.15 (d), 118.61 (s), 125.92 (s), 126.31 (d), 130.65 (d), 131.03 (d), 132.21 (s), 143.56 (d), 147.75 (s), 148.58 (s), 150.27 (s), 152.46 (s), 153.80 (s), 154.52 (s); *Anal.* Calculated for $C_{23}H_{19}N_7O$ (MW: 409,45): C, 67.47; H, 4.68; N, 23.95%. Found: C, 67.51; H, 4.73; N, 23.99%.

5-(5-bromo-1-methyl-7-azaindol-3-yl)-2-(5-methoxy-1*H*-indol-3-yl)pyrazolo[1,5-*a*]pyrimidin-7-amine (17d):

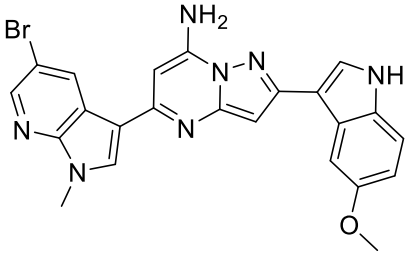

Yield 50%; creamy white solid; m.p.: 302-303°C; IR (cm^{-1}): 3456-3373 (NH_2), 3273-3196 (NH); ^1H NMR (400 MHz, DMSO-d_6) δ: 3.89 (s, 3H, CH_3). 3.91 (s, 3H, CH_3), 6.44 (s, 1H, pyrimidine-CH), 6.77 (s, 1H, pyrazole-CH), 6.82 (dd, *J* = 8.8, 2.5 Hz, 1H), 7.34 (d, *J* = 8.8 Hz, 1H), 7.51 (s, 2H, NH_2, exchangeable with D_2O), 7.93 (d, *J* = 2.1 Hz, 1H), 7.95 (d, *J* = 2.5 Hz, 1H), 8.34 (s, 1H), 8.43 (d, *J* = 2.3 Hz, 1H), 9.03 (d, *J* = 2.3 Hz, 1H), 11.30 (s, 1H, NH, exchangeable with D_2O); ^{13}C NMR (101 MHz, DMSO-d_6) δ: 31.88 (q), 56.08 (q), 83.00 (d), 90.62 (d), 104.04 (d), 109.52 (s), 112.20 (d), 112.56 (2xs), 112.66 (d), 120.22 (s), 125.87 (s), 126.43 (d), 132.19 (s), 132.52 (d), 132.65 (d), 143.58 (d), 147.01 (s), 147.82 (s), 150.14 (s), 152.60 (s), 153.20 (s), 154.52 (s); *Anal.* Calculated for $C_{23}H_{18}BrN_7O$ (MW: 488,35): C, 56.57; H, 3.72; N, 20.08%. Found: C, 56.52; H, 3.75; N, 20.13%.

2-(5-bromo-1*H*-indol-3-yl)-5-(1-methyl-7-azaindol-3-yl)pyrazolo[1,5-*a*]pyrimidin-7-amine (17e):

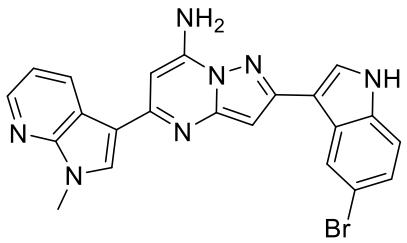

Yield 49%; light yellow solid; m.p.: 321,6-322,6°C; IR (cm^{-1}): 3447 (NH_2), 3244 (NH); ^1H NMR (400 MHz, DMSO-d_6) δ: 3.91 (s, 3H, CH_3). 6.47 (s, 1H, pyrimidine-CH), 6.69 (s, 1H, pyrazole-CH), 7.26 (dd, *J* = 6.2, 2.9 Hz, 1H), 7.28 (dd, *J* = 6.9, 1.7 Hz, 1H), 7.41 (d, *J* = 8.6 Hz, 1H), 7.56 (s, 2H, NH_2, exchangeable with D_2O), 8.05 (d, *J* = 2.6 Hz, 1H), 8.25 (s, 1H), 8.35 (dd, *J* = 4.6, 1.6 Hz, 1H), 8.66 (d, *J* = 1.8 Hz, 1H), 8.83 (dd, *J* = 7.9, 1.6 Hz, 1H), 11.63 (s, 1H, NH, exchangeable with D_2O); ^{13}C NMR (101 MHz, DMSO-d_6) δ: 31.64 (q), 83.34 (d), 90.45 (d), 109.64 (s), 112.99 (s), 113.15 (s), 114.04 (d), 117.16 (d), 118.61 (s), 124.28 (d), 124.80 (d), 127.06 (s), 127.35 (d), 130.64 (d), 131.06 (d), 135.79 (s), 143.56 (d), 147.88 (s), 148.58 (s), 150.28 (s), 151.77 (s), 153.95 (s); *Anal.* Calculated for $C_{22}H_{16}BrN_7$ (MW: 458,32): C, 57.65; H, 3.52; N, 21.39%. Found: C, 57.68; H, 3.55; N, 21.42%.

2-(5-bromo-1*H*-indol-3-yl)-5-(5-bromo-1-methyl-7-azaindol-3-yl)pyrazolo[1,5-*a*]pyrimidin-7-amine (17f):

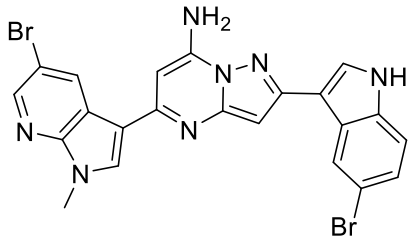

Yield 42%; creamy white solid; m.p.: 304,6-305,6°C; IR (cm^{-1}): 3453-3360 (NH_2), 3208 (NH); ^1H NMR (400 MHz, DMSO-d_6) δ: 3.91 (s, 3H, CH_3). 6.44 (s, 1H, pyrimidine-CH), 6.79 (s, 1H, pyrazole-CH), 7.29 (dd, *J* = 8.6, 2.0 Hz, 1H), 7.42 (d, *J* = 8.6 Hz, 1H), 7.62 (s, 2H, NH_2, exchangeable with D_2O), 8.06 (d, *J* = 2.6 Hz, 1H), 8.34 (s, 1H), 8.43 (d, *J* = 2.3 Hz, 1H), 8.68 (d, *J* = 1.9 Hz, 1H), 9.03 (d, *J* = 2.3 Hz, 1H), 11.64 (s, 1H, NH, exchangeable with D_2O); ^{13}C NMR (101 MHz, DMSO-d_6) δ: 31.88 (q), 83.08 (d), 90.70 (d), 109.62 (s), 112.52 (s), 112.58 (s), 113.17 (s), 114.03 (d), 120.24 (s), 124.31 (d), 124.82 (d), 127.03 (s), 127.43 (d), 132.54 (d), 132.67 (d), 135.79 (s), 143.59 (d), 147.03 (s), 147.95 (s), 150.16 (s), 151.91 (s), 153.35 (s); *Anal.* Calculated for $C_{22}H_{15}Br_2N_7$ (MW: 537,22): C, 49.19; H, 2.81; N, 18.25%. Found: C, 49.23; H, 2.89; N, 18.31%.

2-(5-fluoro-1*H*-indol-3-yl)-5-(1-methyl-7-azaindol-3-yl)pyrazolo[1,5-*a*]pyrimidin-7-amine (17g):

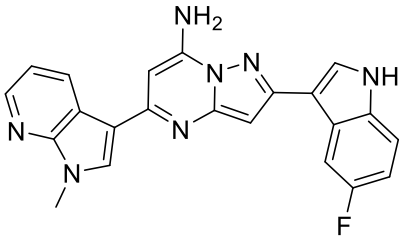

Yield: 29%; light yellow needles; m.p.: 315-316°C; IR (cm^{-1}): 3462 (NH_2), 3244 (NH); ^1H NMR (400 MHz, DMSO-d_6) δ: 3.91 (s, 3H, CH_3), 6.45 (s, 1H, pyrimidine-CH), 6.69 (d, *J* = 1.1 Hz, 1H, pyrazole-CH), 7.01 (td, *J* = 9.1, 2.6 Hz, 1H), 7.26 (dd, *J* = 7.9, 4.6 Hz, 1H), 7.43 (dd, *J* = 8.8, 4.6 Hz, 1H), 7.57 (s, 2H, NH_2, exchangeable with D_2O), 8.07 (d, *J* = 2.4 Hz, 1H), 8.25 (s, 1H), 8.34 (dd, *J* = 4.7, 1.7 Hz, 1H), 8.35 (d, *J* = 1.5 Hz, 1H), 8.81 - 8.84 (m, 1H), 11.52 (s, 1H, NH, exchangeable with D_2O); ^{13}C NMR (101 MHz, DMSO-d_6) δ: 31.63 (s). 83.21 (s), 90.11 (s), 107.28 (d, $J_{C4\text{-}F}$ = 23.8 Hz), 110.13 (d, $J_{C7a\text{-}F}$ = 4.9 Hz), 110.32 (d, $J_{C6\text{-}F}$ = 26.1 Hz), 112.84 (d, $J_{C7\text{-}F}$ = 8.8 Hz), 113.04 (s), 117.15 (s), 118.62 (s), 125.67 (d, $J_{C3a\text{-}F}$ = 10.7 Hz), 127.71 (s), 130.64 (s), 131.04 (s), 133.75 (s), 143.55 (s), 147.84 (s), 148.58 (s), 150.27 (s), 152.02 (s), 153.92 (s), 158.07 (d, $J_{C5\text{-}F}$ = 231.1 Hz); *Anal.* Calculated for $C_{22}H_{16}FN_7$ (MW: 397,42): C, 66.49; H, 4.06; N, 24.67%. Found: C, 66.52; H, 4.22; N, 24.69%.

5-(5-bromo-1-methyl-7-azaindol-3-yl)-2-(5-fluoro-1*H*-indol-3-yl)pyrazolo[1,5-*a*]pyrimidin-7-amine (17h):

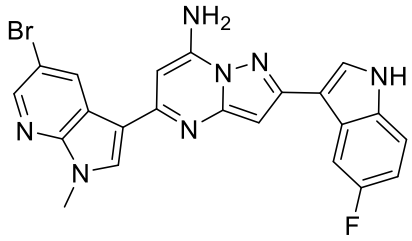

Yield: 45%; creamy white solid; m.p.: 319-320°C; IR (cm^{-1}): 3447 (NH_2), 3186 (NH); ^1H NMR (400 MHz, DMSO-d_6) δ: 3.90 (s, 3H, CH_3), 6.42 (s, 1H, pyrimidine-CH), 6.77 (s, 1H, pyrazole-CH), 7.01 (td, *J* = 9.2, 2.6 Hz, 1H), 7.43 (dd, *J* = 8.8, 4.6 Hz, 1H), 7.62 (s, 2H, NH_2, exchangeable with D_2O), 8.07 (d, *J* = 2.6 Hz, 1H), 8.33 (s, 1H), 8.31 - 8.38 (m, 1H), 8.42 (d, *J* = 2.2 Hz, 1H), 9.02 (d, *J* = 2.3 Hz, 1H), 11.51 (s, 1H, NH, exchangeable with D_2O); ^{13}C NMR (101 MHz, DMSO-d_6) δ: 31.87 (q). 82.94 (d), 90.36 (d), 107.30 (d, J_{C4-F} = 23.8 Hz), 110.09 (d, J_{C7a-F} = 4.3 Hz), 110.33 (d, J_{C6-F} = 27.2 Hz), 112.55 (2xs), 112.92 (d, J_{C7-F} = 9.7 Hz), 120.24 (s), 125.64 (d, J_{C3a-F} = 11.2 Hz), 127.77 (d), 132.56 (d), 132.64 (d), 133.73 (s), 143.57 (d), 147.02 (s), 147.90 (s), 150.13 (s), 152.14 (s), 153.31 (s), 158.08 (d, J_{C5-F} = 231.9 Hz); *Anal.* Calculated for $C_{22}H_{15}BrFN_7$ (MW: 476,31): C, 55.48; H, 3.17; N, 20.58%. Found: C, 55.53; H, 3.23; N, 20.60%.

2-(5-chloro-1*H*-indol-3-yl)-5-(1-methyl-7-azaindol-3-yl)pyrazolo[1,5-*a*]pyrimidin-7-amine (17i):

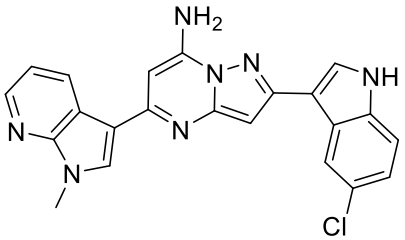

Yield: 24%; yellow solid; m.p.: 315-316°C; IR (cm^{-1}): 3441-3368 (NH_2), 3244 (NH); ^1H NMR (400 MHz, DMSO-d_6) δ: 3.91 (s, 3H, CH_3), 6.47 (s, 1H, pyrimidine-CH), 6.70 (s, 1H, pyrazole-CH), 7.17 (dd, *J* = 8.6, 2.1 Hz, 1H), 7.26 (dd, *J* = 7.9, 4.6 Hz, 1H), 7.46 (d, *J* = 8.6 Hz, 1H), 7.57 (s, 2H, NH_2, exchangeable with D_2O), 8.07 (d, *J* = 2.5 Hz, 1H), 8.25 (s, 1H), 8.35 (dd, *J* = 4.6, 1.6 Hz, 1H), 8.56 (d, *J* = 2.0 Hz, 1H), 8.83 (dd, *J* = 7.9, 1.6 Hz, 1H), 11.62 (s, 1H, NH, exchangeable with D_2O); ^{13}C

NMR (101 MHz, DMSO-d_6) δ: 31.64 (q), 83.31 (d), 90.38 (d), 109.74 (s), 113.01 (s), 113.55 (d), 117.16 (d), 118.61 (s), 121.44 (d), 122.23 (d), 125.07 (s), 126.42 (s), 127.51 (d), 130.64 (d), 131.06 (d), 135.56 (s), 143.56 (d), 147.87 (s), 148.57 (s), 150.28 (s), 151.82 (s), 153.95 (s); *Anal.* Calculated for $C_{22}H_{16}ClN_7$ (MW: 413,87): C, 63.85; H, 3.90; N, 23.69%. Found: C, 63.82; H, 3.88; N, 23.63%.

5-(5-bromo-1-methyl-7-azaindol-3-yl)-2-(5-chloro-1*H*-indol-3-yl)pyrazolo[1,5-*a*]pyrimidin-7-amine (17j):

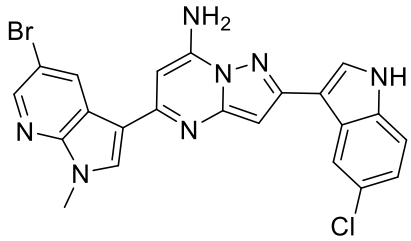

Yield: 35%; light yellow solid; m.p.: 317-318°C; IR (cm^{-1}): 3447-3366 (NH_2), 3283 (NH); ^{1}H NMR (400 MHz, DMSO-d_6) δ: 3.90 (s, 3H, CH_3). 6.43 (s, 1H, pyrimidine-CH), 6.78 (s, 1H, pyrazole-CH), 7.16 (dd, *J* = 8.6, 2.1 Hz, 1H), 7.45 (d, *J* = 8.6 Hz, 1H), 7.62 (s, 2H, NH_2, exchangeable with D_2O), 8.07 (d, *J* = 2.6 Hz, 1H), 8.33 (s, 1H), 8.42 (d, *J* = 2.3 Hz, 1H), 8.57 (d, *J* = 2.1 Hz, 1H), 9.02 (d, *J* = 2.3 Hz, 1H), 11.61 (s, 1H, NH, exchangeable with D_2O); ^{13}C NMR (101 MHz, DMSO-d_6) δ: 31.87 (q), 83.05 (d), 90.63 (d), 109.71 (s), 112.52 (s), 112.57 (s), 113.54 (d), 120.24, 121.46 (d), 122.24 (d), 125.08 (s), 126.38 (s), 127.58 (d), 132.54 (d), 132.67 (d), 135.55 (s), 143.58 (d), 147.03 (s), 147.95 (s), 150.16 (s), 151.94 (s), 153.34 (s); *Anal.* Calculated for $C_{22}H_{15}BrClN_7$ (MW: 492,77): C, 53.62; H, 3.07; N, 19.90%. Found: C, 53.65; H, 3.13; N, 19.95%.

2-(1-methyl-1*H*-indol-3-yl)-5-(1-methyl-7-azaindol-3-yl)pyrazolo[1,5-*a*]pyrimidin-7-amine (17k):

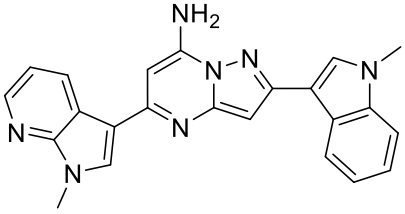

Yield: 39%; white needles; m.p.: 330-331°C; IR (cm^{-1}): 3447 (NH_2); ^{1}H NMR (400 MHz, DMSO-d_6) δ: 3.87 (s, 3H, CH_3), 3.91 (s, 3H, CH_3), 6.47 (s, 1H, pyrimidine-CH), 6.64 (s, 1H, pyrazole-CH), 7.18

(t, *J* = 7.4 Hz, 1H), 7.23 (d, *J* = 8.2 Hz, 1H), 7.27 (dd, *J* = 7.9, 4.6 Hz, 1H), 7.48 (s, 2H, NH_2, exchangeable with D_2O), 7.49 (d, *J* = 8.0 Hz, 1H), 7.96 (s, 1H), 8.25 (s, 1H), 8.35 (dd, *J* = 4.6, 1.5 Hz, 1H), 8.55 (d, *J* = 7.9 Hz, 1H), 8.83 (d, *J* = 7.9 Hz, 1H); ^{13}C NMR (101 MHz, DMSO-d_6) δ: 31.62 (q), 33.16 (q), 83.32 (d), 90.23 (d), 108.96 (s), 110.30 (d), 113.05 (s), 117.15 (d), 118.61 (s), 120.35 (d), 122.20 (d), 122.65 (d), 125.90, 129.72 (d), 130.64 (d), 131.05 (d), 137.54 (s), 143.56 (d), 147.76 (s), 148.60 (s), 150.27 (s), 151.94 (s), 153.90 (s); *Anal.* Calculated for $C_{23}H_{19}N_7$ (MW: 393,45): C, 70.21; H, 4.87; N, 24.92%. Found: C, 70.25; H, 4.88; N, 24.98%.

5-(5-bromo-1-methyl-7-azaindol-3-yl)-2-(1-methyl-1*H*-indol-3-yl)pyrazolo[1,5-*a*]pyrimidin-7-amine (17l):

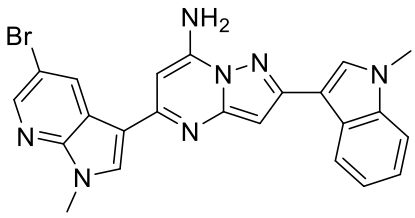

Yield: 34%; white solid; m.p.: 297.3-297.6°C; IR (cm^{-1}): 3447 (NH_2); ^{1}H NMR (400 MHz, DMSO-d_6) δ: 3.87 (s, 3H, CH_3). 3.90 (s, 3H, CH_3), 6.43 (s, 1H, pyrimidine-CH), 6.71 (s, 1H, pyrazole-CH), 7.17 (t, *J* = 7.1 Hz, 1H), 7.22 - 7.27 (m, 1H), 7.49 (d, *J* = 8.1 Hz, 1H), 7.53 (s, 2H, NH_2, exchangeable with D_2O), 7.96 (s, 1H), 8.33 (s, 1H), 8.42 (d, *J* = 2.2 Hz, 1H), 8.56 (d, *J* = 7.7 Hz, 1H), 9.02 (d, *J* = 2.2 Hz, 1H); ^{13}C NMR (101 MHz, DMSO-d_6) δ: 31.86 (q), 33.20 (q), 83.08 (d), 90.49 (d), 108.93 (s), 110.31 (d), 112.57 (2xs), 120.23 (s), 120.36 (d), 122.21 (d), 122.65 (d), 129.77 (d), 132.52 (d), 132.67 (d), 137.54 (s), 143.59 (d), 147.04 (s), 147.83 (s), 150.15 (s), 152.05 (s), 153.28 (s), 155.05 (s); *Anal*. Calculated for $C_{23}H_{18}BrN_7$ (MW: 472,35): C, 58.48; H, 3.84; N, 20.76%. Found: C, 58.44; H, 3.80; N, 20.73%.

2-(5-methoxy-1-methyl-1*H*-indol-3-yl)-5-(1-methyl-7-azaindol-3-yl)pyrazolo[1,5-*a*]pyrimidin-7-amine (17m):

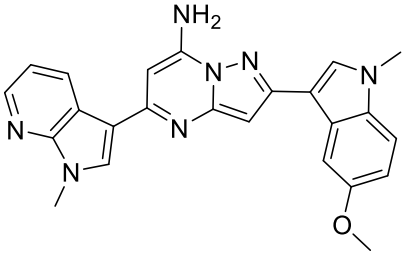

Yield: 47%; light yellow solid; m.p.: 273-274°C; IR (cm^{-1}): 3437 (NH_2); ^1H NMR (300 MHz, DMSO-d_6) δ: 3.84 (s, 3H, CH_3). 3.89 (s, 3H, CH_3), 3.92 (s, 3H, OCH_3), 6.49 (s, 1H, pyrimidine-CH), 6.63 (s, 1H, pyrazole-CH), 6.89 (dd, *J* = 8.8, 2.4 Hz, 1H), 7.27 (dd, *J* = 7.9, 4.6 Hz, 1H), 7.40 (d, *J* = 8.9 Hz, 1H), 7.45 (s, 2H, NH_2, exchangeable with D_2O), 7.91 (s, 1H), 7.92 (d, *J* = 2.4 Hz, 1H), 8.26 (s, 1H), 8.36 (dd, *J* = 4.6, 1.5 Hz, 1H), 8.84 (dd, *J* = 7.9, 1.5 Hz, 1H); ^{13}C NMR (101 MHz, DMSO-d_6) δ: 31.63 (q), 33.32 (q), 56.14 (q), 83.40 (d), 90.25 (d), 104.28 (d), 108.53 (s), 111.09 (d), 112.19 (d), 113.06 (s), 117.14 (d), 118.60 (s), 126.28 (s), 130.20 (d), 130.61 (d), 131.04 (d), 132.89 (s), 143.56 (d), 147.75 (s), 148.60 (s), 150.30 (s), 152.06 (s), 153.84 (s), 154.79 (s); *Anal.* Calculated for $C_{24}H_{21}N_7O$ (MW: 423,48): C, 68.07; H, 5.00; N, 23.15%. Found: C, 68.15; H, 5.21; N, 23.27%.

5-(5-bromo-1-methyl-7-azaindol-3-yl)-2-(5-methoxy-1-methyl-1*H*-indol-3-yl)pyrazolo[1,5-*a*]pyrimidin-7-amine (17n):

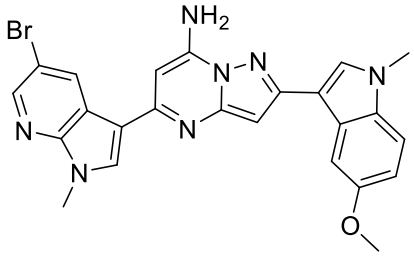

Yield: 39%; white solid; m.p.: 249-249,7°C; IR (cm^{-1}): 3420 (NH_2); ^1H NMR (300 MHz, DMSO-d_6) δ: 3.84 (s, 3H, CH_3). 3.89 (s, 3H, CH_3), 3.91 (s, 3H, OCH_3), 6.45 (s, 1H, pyrimidine-CH), 6.71 (s, 1H, pyrazole-CH), 6.89 (dd, *J* = 8.8, 2.3 Hz, 1H), 7.40 (d, *J* = 8.9 Hz, 1H), 7.50 (s, 2H, NH_2, exchangeable with D_2O), 7.91 (s, 1H), 7.93 (d, *J* = 2.3 Hz, 1H), 8.34 (s, 1H), 8.43 (d, *J* = 2.1 Hz, 1H), 9.02 (d, *J* = 2.2 Hz, 1H); ^{13}C NMR (101 MHz, DMSO-d_6) δ: 31.87 (q), 33.35 (q), 56.18 (q), 83.22 (d), 90.46 (d), 104.37 (d), 108.47 (s), 111.08 (d), 112.19 (d), 112.50 (s), 112.58 (s), 120.19 (s), 126.25 (s), 130.31 (d), 132.44 (d), 132.70 (d), 132.89 (s), 143.61 (d), 147.04 (s), 147.86 (s), 150.04 (s), 152.22 (s), 153.12 (s), 154.81 (s); *Anal.* Calculated for $C_{24}H_{20}BrN_7O$ (MW: 502,38): C, 57.38; H, 4.01; N, 19.52%. Found: C, 57.42; H, 4.15; N, 19.58%.

2-(5-bromo-1-methyl-1*H*-indol-3-yl)-5-(1-methyl-7-azaindol-3-yl)pyrazolo[1,5-*a*]pyrimidin-7-amine (17o):

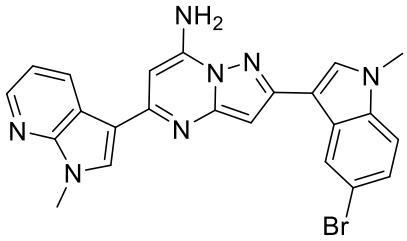

Yield: 46%; yellow solid; m.p.: 310.6-311.6°C; IR (cm^{-1}): 3447 (NH_2); ^1H NMR (400 MHz, DMSO-d_6) δ: 3.87 (s, 3H, CH_3). 3.91 (s, 3H, CH_3), 6.48 (s, 1H, pyrimidine-CH), 6.63 (s, 1H, pyrazole-CH), 7.26 (dd, *J* = 7.9, 4.6 Hz, 1H), 7.35 (dd, *J* = 8.7, 2.0 Hz, 1H), 7.49 (d, *J* = 8.7 Hz, 1H), 7.57 (s, 2H, NH_2, exchangeable with D_2O), 8.03 (s, 1H), 8.25 (s, 1H), 8.35 (dd, *J* = 4.6, 1.6 Hz, 1H), 8.68 (d, *J* = 1.9 Hz, 1H), 8.82 (dd, *J* = 7.9, 1.6 Hz, 1H); ^{13}C NMR (101 MHz, DMSO-d_6) δ: 31.64 (q), 33.40 (q), 83.43 (d), 90.29 (d), 108.71 (s), 112.50 (d), 112.97 (s), 113.50 (s), 117.17 (d), 118.59 (s), 124.47 (d), 124.86 (d), 127.28 (s), 130.62 (d), 131.10 (d), 131.26 (d), 136.29 (s), 143.56 (d), 147.88 (s), 148.58 (s), 150.31 (s), 151.37 (s), 153.99 (s); *Anal.* Calculated for $C_{23}H_{18}BrN_7$ (MW: 472,35): C, 58.48; H, 3.84; N, 20.76%. Found: C, 58.54; H, 3.89; N, 20.82%.

2-(5-bromo-1-methyl-1*H*-indol-3-yl)-5-(5-bromo-1-methyl-7-azaindol-3-yl)pyrazolo[1,5-*a*]pyrimidin-7-amine (17p):

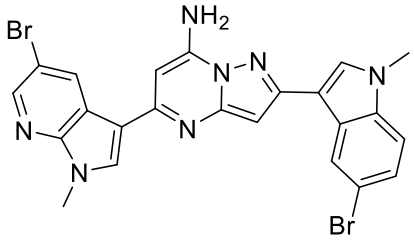

Yield: 46%; yellow needles; m.p.: 307-308°C; IR (cm^{-1}): 3447 (NH_2); ^1H NMR (400 MHz, DMSO-d_6) δ: 3.87 (s, 3H, CH_3). 3.90 (s, 3H, CH_3), 6.44 (s, 1H, pyrimidine-CH), 6.72 (s, 1H, pyrazole-CH), 7.35 (dd, *J* = 8.7, 2.0 Hz, 1H), 7.49 (d, *J* = 8.7 Hz, 1H), 7.62 (s, 2H, NH_2, exchangeable with D_2O), 8.03 (s, 1H), 8.33 (s, 1H), 8.42 (d, *J* = 2.3 Hz, 1H), 8.68 (d, *J* = 1.9 Hz, 1H), 9.01 (d, *J* = 2.3 Hz, 1H); ^{13}C NMR (101 MHz, DMSO-d_6) δ: 31.87 (q), 33.42 (q), 83.26 (d), 90.58 (d), 108.72 (s), 112.51 (d), 112.55 (s), 112.59 (s), 113.52 (s), 120.22 (s), 124.45 (d), 124.88 (d), 127.28, 131.31 (d), 132.49 (d),

132.70 (d), 136.31 (s), 143.59 (d), 147.04 (s), 147.96 (s), 150.21 (s), 151.49 (s), 153.38 (s); *Anal.* Calculated for $C_{23}H_{17}Br_2N_7$ (MW: 551,25): C, 50.11; H, 3.11; N, 17.79%. Found: C, 50.18; H, 3.21; N, 17.85%.

2-(5-fluoro-1-methyl-1*H*-indol-3-yl)-5-(1-methyl-7-azaindol-3-yl)pyrazolo[1,5-*a*]pyrimidin-7-amine (17q):

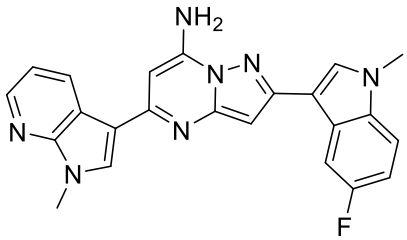

Yield: 35%; yellow needles; m.p.: 322-323°C; IR (cm^{-1}): 3447 (NH_2); ^{1}H NMR (400 MHz, DMSO-d_6) δ: 3.87 (s, 3H, CH_3). 3.91 (s, 3H, CH_3), 6.46 (s, 1H, pyrimidine-CH), 6.62 (s, 1H, pyrazole-CH), 7.08 (td, J = 9.2, 2.6 Hz, 1H), 7.26 (dd, J = 7.9, 4.6 Hz, 1H), 7.50 (dd, J = 8.9, 4.5 Hz, 1H), 7.58 (s, 2H, NH_2, exchangeable with D_2O), 8.05 (s, 1H), 8.25 (s, 1H), 8.33 - 8.39 (m, 2H), 8.82 (dd, J = 7.9, 1.5 Hz, 1H); ^{13}C NMR (101 MHz, DMSO-d_6) δ: 31.63 (q), 33.48 (q), 83.28 (d), 89.93 (d), 107.57 (d, $J_{C4\text{-}F}$ = 23.9 Hz), 109.07 (d, $J_{C7a\text{-}F}$ = 4.4 Hz), 110.37 (d, $J_{C6\text{-}F}$ = 26.1 Hz), 111.45 (d, $J_{C7\text{-}F}$ = 8.6 Hz), 113.00 (s), 117.16 (d), 118.60 (s), 124.58 (s), 125.96 (d, $J_{C3a\text{-}F}$ = 10.7 Hz), 130.63 (d), 131.08 (d), 131.55 (d), 134.31 (s), 143.56 (d), 147.83 (s), 148.57 (s), 150.28 (s), 150.36 (s), 152.78 (d, $J_{C5\text{-}F}$ = 235.7 Hz); *Anal.* Calculated for $C_{23}H_{18}FN_7$ (MW: 411,44): C, 67.14; H, 4.41; N, 23.83%. Found: C, 67.22; H, 4.46; N, 23.79%.

5-(5-bromo-1-methyl-7-azaindol-3-yl)-2-(5-fluoro-1-methyl-1*H*-indol-3-yl)pyrazolo[1,5-*a*]pyrimidin-7-amine (17r):

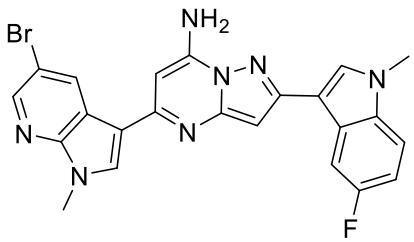

Yield: 35%; yellow needles; m.p.: 333,5-334,5°C; IR (cm^{-1}): 3431-3310 (NH_2); ^1H NMR (400 MHz, DMSO-d_6) δ: 3.87 (s, 3H, CH_3). 3.90 (s, 3H, CH_3), 6.43 (s, 1H, pyrimidine-CH), 6.71 (s, 1H, pyrazole-CH), 7.08 (td, *J* = 9.2, 2.6 Hz, 1H), 7.51 (dd, *J* = 8.9, 4.5 Hz, 1H), 7.65 (s, 2H, NH_2, exchangeable with D_2O), 8.05 (s, 1H), 8.34 (s, 1H), 8.38 (dd, *J* = 10.2, 2.6 Hz, 1H), 8.43 (d, *J* = 2.3 Hz, 1H), 9.02 (d, *J* = 2.3 Hz, 1H); ^{13}C NMR (101 MHz, DMSO-d_6) δ: 31.87 (q). 33.52 (q), 83.03 (d), 90.20 (d), 107.58 (d, *J* = 23.5 Hz), 109.04 (d, *J* = 4.4 Hz), 110.38 (d, *J* = 26.9 Hz), 111.47 (d, *J* = 10.1 Hz), 112.51 (s), 112.57 (s), 120.21 (s), 125.92 (d, *J* = 10.7 Hz), 131.60 (d), 132.52 (d), 132.69 (d), 134.30 (s), 143.58 (d), 147.01 (s), 147.90 (s), 150.16 (s), 151.72 (s), 153.34 (s), 158.32 (d, *J* = 232.3 Hz); *Anal.* Calculated for $C_{23}H_{17}BrFN_7$ (MW: 490,34): C, 56.34; H, 3.49; N, 20.00%. Found: C, 56.40; H, 3.52; N, 20.15%.

2-(5-chloro-1-methyl-1*H*-indol-3-yl)-5-(1-methyl-7-azaindol-3-yl)pyrazolo[1,5-*a*]pyrimidin-7-amine (17s):

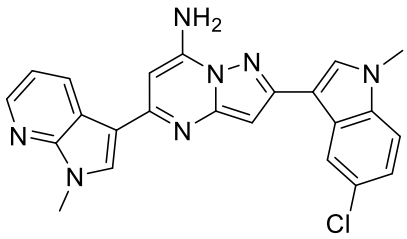

Yield: 30%; yellow solid; m.p.: 300.7-301.2°C; IR (cm^{-1}): 3368 (NH_2); ^1H NMR (400 MHz, DMSO-d_6) δ: 3.88 (s, 3H, CH_3). 3.92 (s, 3H, CH_3), 6.48 (s, 1H, pyrimidine-CH), 6.63 (s, 1H, pyrazole-CH), 7.24 (dd, *J* = 8.7, 2.1 Hz, 1H), 7.27 (dd, *J* = 7.9, 4.7 Hz, 1H), 7.53 (d, *J* = 8.7 Hz, 1H), 7.57 (s, 2H, NH_2, exchangeable with D_2O), 8.05 (s, 1H), 8.25 (s, 1H), 8.35 (dd, *J* = 4.6, 1.6 Hz, 1H), 8.57 (d, *J* = 2.1 Hz, 1H), 8.82 (dd, *J* = 7.9, 1.6 Hz, 1H); ^{13}C NMR (101 MHz, DMSO-d_6) δ: 31.63 (q), 33.41 (q), 83.48 (d), 90.26 (d), 108.84 (s), 112.01 (d), 113.05 (s), 117.15 (d), 118.61 (s), 121.58 (d), 122.27 (d), 125.43 (s), 126.70 (s), 130.60 (d), 131.07 (d), 131.37 (d), 136.09 (s), 143.57 (d), 147.89 (s), 148.62 (s), 150.33 (s), 151.40 (s), 154.00 (s); *Anal.* Calculated for $C_{23}H_{18}ClN_7$ (MW: 427,90): C, 64.56; H, 4.24; N, 22.91%. Found: C, 64.63; H, 4.28; N, 22.98%.

5-(5-bromo-1-methyl-7-azaindol-3-yl)-2-(5-chloro-1-methyl-1*H*-indol-3-yl)pyrazolo[1,5-*a*]pyrimidin-7-amine (17t):

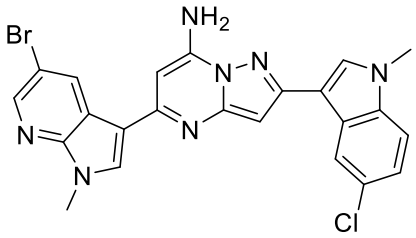

Yield: 32%; light beige solid; m.p.: 297.8-298.1°C; IR (cm^{-1}): 3447 (NH_2); ^1H NMR (400 MHz, DMSO-d_6) δ: 3.87 (s, 3H, CH_3). 3.90 (s, 3H, CH_3), 6.44 (s, 1H, pyrimidine-CH), 6.72 (s, 1H, pyrazole-CH), 7.23 (dd, *J* = 8.7, 2.1 Hz, 1H), 7.53 (d, *J* = 8.7 Hz, 1H), 7.62 (s, 2H, NH_2, exchangeable with D_2O), 8.04 (s, 1H), 8.33 (s, 1H), 8.42 (d, *J* = 2.2 Hz, 1H), 8.57 (d, *J* = 2.1 Hz, 1H), 9.01 (d, *J* = 2.3 Hz, 1H); ^{13}C NMR (101 MHz, DMSO-d_6) δ: 31.87 (q), 33.44 (q), 83.26 (d), 90.50 (d), 108.80 (s), 112.01 (d), 112.53 (s), 112.58 (s), 120.22 (s), 121.59 (d), 122.29 (d), 125.45 (s), 126.66 (s), 131.45 (d), 132.48 (d), 132.70 (d), 136.09 (s), 143.60 (d), 147.05 (s), 147.97 (s), 150.17 (s), 151.53 (s), 153.34 (s); *Anal.* Calculated for $C_{23}H_{17}BrClN_7$ (MW: 506,79): C, 54.51; H, 3.38; N, 19.35%. Found: C, 54.58; H, 3.42; N, 19.39%.

General procedure for the synthesis of 1-benzyl-7-azaindole (36) [84,85]:

Following a literature procedure [86]: a solution of 7-azaindole **35a** (17 mmol) in anhydrous tetrahydrofuran (10 ml) was cooled down to 0 ºC under nitrogen atmosphere and sodium hydride (20.4 mmol, 60% oil dispersion) was added in portions. The reaction mixture was stirred at room temperature for 1 hour, benzyl bromide (20.4 mmol) was added dropwise, and the reaction mixture was stirred for 3 hours. After completion of the reaction, it was quenched with water and ice (10 ml) and was extracted with ethyl acetate (3 x 20 ml). The combined organic layer was dried over Na_2SO_4, and the solvent was removed under reduced pressure. The product was purified by column chromatography using cyclohexane/ethyl acetate as eluent.

1-benzyl-7-azaindole (36):

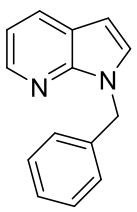

Yield: 58%; yellow solid; m.p.: 38 °C; ^1H NMR (400 MHz, $CDCl_3$) δ: 5.54 (s, 2H, CH_2), 6.51(d, *J* = 3.2 Hz, 1H, H-3), 7.09-7.34 (m, 7H, Ar-H, H-5, H-2), 7.95 (dd, *J* = 1.6, 6.4 Hz, 1H, H-4), 8.37 (d, *J*

= 1.6 Hz, 1H, H-6); ^{13}C NMR (100 MHz, $CDCl_3$) δ: 47.7 (t), 100.0 (d), 115.8 (d), 120.4 (s), 127.4 (dx2), 127.5 (d), 127.8 (dx2), 128.6 (d), 128.7 (d), 137.7 (s), 142.9 (d), 147.7 (s); *Anal.* Calculated for $C_{14}H_{12}N_2$ (MW: 208,26): C, 80.74; H, 5.81; N, 13.45%. Found: C, 80.72; H, 5.80; N, 13.47%.

General procedure for the synthesis of 3-(1-benzyl-7-azaindol-3-yl)-3-oxopropanenitrile (37):

A solution of cyanoacetic acid (5 mmol) and acetic anhydride (Ac_2O) (5 ml) was heated to 85 °C for 10 minutes. 1-benzyl-7-azaindole **36** (5 mmol) was added to this solution and heating was continued overnight. The reaction mixture was cooled and was poured into water and ice. It was extracted with ethyl acetate (3 × 15 ml), dried (Na_2SO_4), evaporated under reduced pressure and was further purified by column chromatography, using cyclohexane/ethyl acetate as eluent.

3-(1-benzyl-7-azaindol-3-yl)-3-oxopropanenitrile (37):

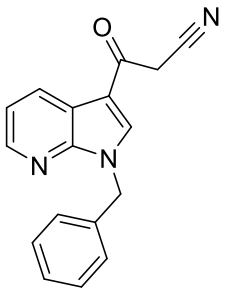

Yield: 45%; yellow solid; m.p.: 195-196°C; IR (cm^{-1}): 2256 (CN), 1654 (CO); ^{1}H NMR (400 MHz, DMSO-d_6) δ: 4.54 (s, 2H, CH_2CN), 5.56 (s, 2H, CH_2Ph), 7.29 (dd, *J* = 8.1, 4.3 Hz, 1H, H-5), 7.32-7.37 (m, 5H, Ar-H), 8.42 (dd, *J* = 4.7, 1.6 Hz, 1H, H-6), 8.46 (dd, *J* = 7.9, 1.6 Hz, 1H, H-4), 8.72 (s, 1H, H-2); ^{13}C NMR (101 MHz, DMSO-d_6) δ: 29.96 (t), 48.45 (t), 112.84 (s), 116.50 (s), 118.35 (s), 119.55 (d), 128.04 (dx2), 128.25 (d), 129.15 (dx2), 130.35 (d), 137.49 (s), 138.36 (d), 145.25 (d), 148.08 (s), 183.57 (s); *Anal.* Calculated for $C_{17}H_{13}N_3O$ (MW: 275,31): C, 74.17; H, 4.76; N, 15.26%. Found: C, 74.25; H, 4.70; N, 15.28%.

General procedure for the synthesis of 5-(1-benzyl-7-azaindol-3-yl)-2-(1*H*-indol-3-yl)pyrazolo[1,5-*a*]pyrimidin-7-amine (18a-d) and 5-(1-benzyl-7-azaindol-3-yl)-2-(1-methyl-1*H*-indol-3-yl)pyrazolo[1,5-*a*]pyrimidin-7-amine (18e-h):

To a mixture of 3-(1-benzyl-7-azaindol-3-yl)-3-oxopropanenitrile **37** (0.5 mmol) and appropriate 3-(1*H*-indol-3-yl)-1*H*-pyrazol-5-amine (**27,28**) in anhydrous *n*-butanol (*n*-BuOH) (8 ml) *p*-toluenesulfonic acid monohydrate (PTSA·H_2O) (2.5 mmol) was added. The reaction mixture was stirred to 90°C for 12 - 30 hours (the progress of the reaction was monitored by TLC). After completion the reaction mixture was left to cool, and the obtained precipitate was filtered off. Solid was neutralised by adding a few drops of saturated aqueous solution of sodium hydrogencarbonate ($NaHCO_3$) and water (20 ml), extracted with ethyl acetate (3 × 20 ml), dried (Na_2SO_4) and evaporated under reduced pressure. The product obtained was further purified by column chromatography, using dichloromethane or dichloromethane/methanol as eluent.

5-(1-benzyl-7-azaindol-3-yl)-2-(1*H*-indol-3-yl)pyrazolo[1,5-*a*]pyrimidin-7-amine (18a):

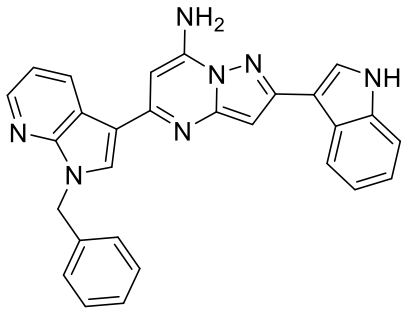

Yield: 61%; creamy white solid; m.p.: 229-230°C; IR (cm^{-1}): 3447 (NH_2), 3308-3184 (NH); ^{1}H NMR (400 MHz, DMSO-d_6) δ: 5.58 (s, 2H, CH_2), 6.48 (s, 1H, pyrimidine-CH), 6.71 (s, 1H, pyrazole-CH), 7.11-7.15 (m, 1H), 7.15-7.20 (m, 1H), 7.26-7.31 (m, 2H), 7.33 (d, *J* = 3.3 Hz, 2H), 7.34 (s, 2H), 7.45 (d, *J* = 7.8 Hz, 1H), 7.47 (s, 2H, NH_2, exchangeable with D_2O), 7.98 (s, 1H), 8.35 (s, 1H), 8.36 (dd, *J* = 4.6, 1.5 Hz, 1H), 8.54 (d, *J* = 7.5 Hz, 1H), 8.85 (d, *J* = 7.9 Hz, 1H), 11.41 (s, 1H, NH exchangeable with D_2O); ^{13}C NMR (101 MHz, DMSO-d_6) δ: 47.87 (t), 83.40 (d), 90.43 (d), 109.80 (s), 112.01 (d), 113.81 (s), 117.47 (d), 118.69 (s), 120.16 (d), 122.09 (d), 122.41 (d), 125.56 (s), 125.73 (dx3), 127.98 (dx2), 129.08 (d), 129.96 (d), 130.83 (d), 137.08 (s), 138.52 (s), 143.82 (d), 147.80 (s), 148.25 (s), 150.24 (s), 152.40 (s), 153.65 (s); *Anal.* Calculated for $C_{28}H_{21}N_7$ (MW: 455,53): C, 73.83; H, 4.65; N, 21.52%. Found: C, 73.88; H, 4.60; N, 21.57%.

5-(1-benzyl-7-azaindol-3-yl)-2-(5-methoxy-1*H*-indol-3-yl)pyrazolo[1,5-*a*]pyrimidin-7-amine (18b):

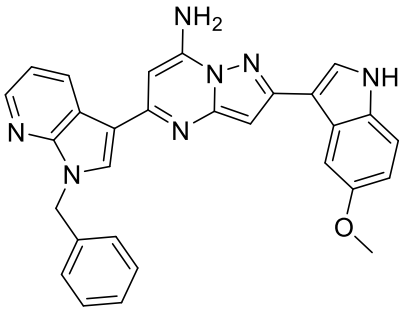

Yield: 62%; white solid; m.p.: 179-179.5°C; IR (cm^{-1}): 3426 (NH_2), 3292-3171 (NH); ^1H NMR (400 MHz, DMSO-d_6) δ: 3.88 (s, 3H, OCH_3), 5.58 (s, 2H, CH_2), 6.49 (s, 1H, pyrimidine-CH), 6.69 (s, 1H, pyrazole-CH), 6.82 (d, *J* = 8.8 Hz, 1H), 7.23-7.33 (m, 3H), 7.34 (d, *J* = 4.2 Hz, 2H), 7.35 (s, 2H), 7.42 (s, 2H, NH_2, exchangeable with D_2O), 7.92 (dd, *J* = 7.1, 2.4 Hz, 2H), 8.34 (s, 1H), 8.36 (dd, *J* = 4.6, 1.4 Hz, 1H), 8.85 (dd, *J* = 7.9, 1.1 Hz, 1H), 11.28 (s, 1H, NH, exchangeable with D_2O); ^{13}C NMR (101 MHz, DMSO-d_6) δ: 47.88 (t), 56.10 (q), 83.52 (d), 90.46 (d), 104.01 (d), 109.57 (s), 112.22 (d), 112.67 (d), 113.85 (s), 117.45 (d), 118.68 (s), 125.96 (s), 126.28 (d), 128.01 (dx3), 129.08 (dx2), 129.91 (d), 130.79 (d), 132.25 (s), 138.49 (s), 143.82 (d), 147.78 (s), 148.28 (s), 150.29 (s), 152.51 (s), 153.60 (s), 154.56 (s); *Anal.* Calculated for $C_{29}H_{23}N_7O$ (MW: 485,55): C, 71.74; H, 4.77; N, 20.19%. Found: C, 71.79; H, 4.70; N, 20.23%.

5-(1-benzyl-7-azaindol-3-yl)-2-(5-bromo-1*H*-indol-3-yl)pyrazolo[1,5-*a*]pyrimidin-7-amine (18c):

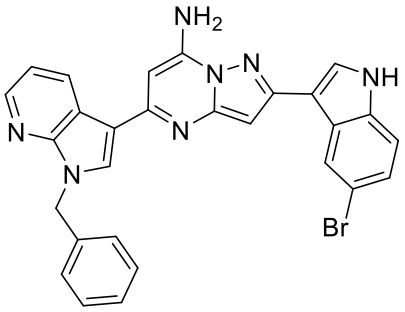

Yield: 41%; creamy white solid; m.p.: 196.5-197.5°C; IR (cm^{-1}): 3416 (NH_2), 3296 (NH); ^1H NMR (400 MHz, DMSO-d_6) δ: 5.59 (s, 2H, CH_2), 6.50 (s, 1H, pyrimidine-CH), 6.70 (s, 1H, pyrazole-CH), 7.25-7.37 (m, 7H), 7.42 (d, *J* = 8.6 Hz, 1H), 7.52 (s, 2H, NH_2, exchangeable with D_2O), 8.05 (d, *J* = 2.5 Hz, 1H), 8.34 (s, 1H), 8.37 (dd, *J* = 4.6, 1.6 Hz, 1H), 8.66 (s, 1H), 8.85 (dd, *J* = 7.9, 1.5 Hz, 1H), 11.61 (s, 1H, NH, exchangeable with D_2O); ^{13}C NMR (101 MHz, DMSO-d_6) δ: 47.88 (t), 83.55 (d), 90.52 (d), 109.63, 113.15 (s), 113.76 (s), 114.04 (d), 117.48 (d), 118.68 (s), 124.27 (d), 124.80 (d), 127.08 (s), 127.34 (dx3), 127.99 (dx2), 129.08 (d), 129.99 (d), 130.80 (d), 135.81 (s), 138.50 (s),

143.83 (d), 147.91 (s), 148.25 (s), 150.29 (s), 151.82 (s), 153.75 (s); *Anal.* Calculated for $C_{28}H_{20}BrN_7$ (MW: 534,42): C, 62.93; H, 3.77; N, 18.35%. Found: C, 62.97; H, 3.79; N, 18.38%.

5-(1-benzyl-7-azaindol-3-yl)-2-(5-chloro-1*H*-indol-3-yl)pyrazolo[1,5-*a*]pyrimidin-7-amine (18d):

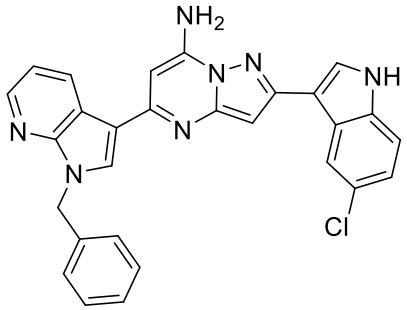

Yield: 40%; creamy white solid; m.p.: 198.6-199.6°C; IR (cm^{-1}): 3447-3420 (NH_2), 3292 (NH); ^1H NMR (400 MHz, DMSO-d_6) δ: 5.58 (s, 2H, CH_2), 6.48 (s, 1H, pyrimidine-CH), 6.70 (s, 1H, pyrazole-CH), 7.17 (dd, *J* = 8.6, 2.1 Hz, 1H), 7.25-7.32 (m, 2H), 7.33 (d, *J* = 2.9 Hz, 2H), 7.34 (s, 2H), 7.46 (d, *J* = 8.6 Hz, 1H), 7.55 (s, 2H, NH_2, exchangeable with D_2O), 8.06 (d, *J* = 2.5 Hz, 1H), 8.34 (s, 1H), 8.36 (dd, *J* = 4.6, 1.6 Hz, 1H), 8.55 (d, *J* = 2.0 Hz, 1H), 8.84 (dd, *J* = 7.9, 1.6 Hz, 1H), 11.61 (s, 1H, NH, exchangeable with D_2O); ^{13}C NMR (101 MHz, DMSO-d_6) δ: 47.87 (t), 83.51 (d), 90.44 (d), 109.72 (s), 113.55 (d), 113.76 (s), 117.47 (d), 118.68 (s), 121.42 (d), 122.22 (d), 125.07 (s), 126.42 (s), 127.50 (dx3), 127.98 (dx2), 129.08 (d), 129.99 (d), 130.80 (d), 135.56 (s), 138.50 (s), 143.83 (d), 147.91 (s), 148.24 (s), 150.28 (s), 151.85 (s), 153.74 (s); *Anal.* Calculated for $C_{28}H_{20}ClN_7$ (MW: 489,97): C, 68.64; H, 4.11; N, 20.01%. Found: C, 68.68; H, 4.16; N, 20.12%.

5-(1-benzyl-7-azaindol-3-yl)-2-(1-methyl-1*H*-indol-3-yl)pyrazolo[1,5-*a*]pyrimidin-7-amine (18e):

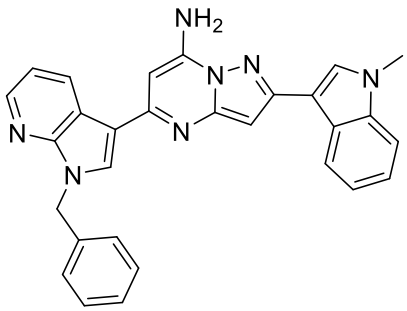

Yield: 51%; white solid; m.p.: 284-285°C; IR (cm^{-1}): 3420 (NH_2); ^1H NMR (400 MHz, DMSO-d_6) δ: 3.87 (s, 3H, CH_3), 5.58 (s, 2H, CH_2), 6.48 (s, 1H, pyrimidine-CH), 6.64 (s, 1H, pyrazole-CH), 7.17 (t, *J* = 7.4 Hz, 1H), 7.22-7.31 (m, 3H), 7.33 (d, *J* = 3.6 Hz, 2H), 7.34 (s, 2H), 7.48 (s, 2H, NH_2, exchangeable with D_2O), 7.50 (s, 1H), 7.96 (s, 1H), 8.35 (s, 1H), 8.36 (dd, *J* = 4.7, 1.6 Hz, 1H), 8.55 (d, *J* = 7.8 Hz, 1H), 8.84 (dd, *J* = 7.9, 1.6 Hz, 1H); ^{13}C NMR (101 MHz, DMSO-d_6) δ: 33.16 (q), 47.87 (t), 83.49 (d), 90.28 (d), 108.93 (s), 110.30 (d), 113.78 (s), 117.48 (d), 118.67 (s), 120.36 (d), 122.21 (d), 122.64 (d), 125.88 (s), 127.99 (dx3), 129.08 (dx2), 129.74 (d), 130.00 (d), 130.80 (d), 137.54 (s), 138.51 (s), 143.82 (d), 147.79 (s), 148.25 (s), 150.26 (s), 151.99 (s), 153.68 (s); *Anal.* Calculated for $C_{29}H_{23}N_7$ (MW: 469,55): C, 74.18; H, 4.94; N, 20.88%. Found: C, 74.23; H, 4.92; N, 20.91%.

5-(1-benzyl-7-azaindol-3-yl)-2-(5-methoxy-1-methyl-1*H*-indol-3-yl)pyrazolo[1,5-*a*]pyrimidin-7-amine (18f):

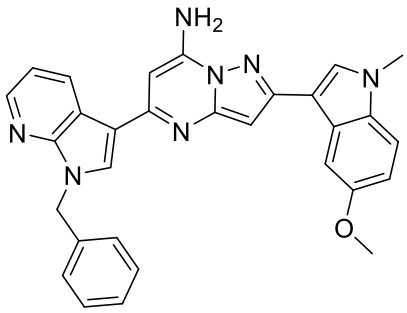

Yield: 47%; creamy white solid; m.p.: 222.7-223.7°C; IR (cm^{-1}): 3377 (NH_2); ^1H NMR (400 MHz, DMSO-d_6) δ: 3.83 (s, 3H, CH_3), 3.89 (s, 3H, OCH_3), 5.58 (s, 2H, CH_2), 6.50 (s, 1H, pyrimidine-CH), 6.63 (s, 1H, pyrazole-CH), 6.88 (dd, *J* = 8.8, 2.5 Hz, 1H), 7.26-7.32 (m, 2H), 7.34 (d, *J* = 4.5 Hz, 2H), 7.35 (s, 2H), 7.39 (d, *J* = 8.9 Hz, 1H), 7.44 (s, 2H, NH_2, exchangeable with D_2O), 7.90 (s, 1H), 7.92 (d, *J* = 2.3 Hz, 1H), 8.35 (s, 1H), 8.37 (dd, *J* = 4.6, 1.5 Hz, 1H), 8.85 (d, *J* = 7.9 Hz, 1H); ^{13}C NMR (101 MHz, DMSO-d_6) δ: 33.31 (q), 47.88 (t), 56.11 (q), 83.57 (d), 90.29 (d), 104.22 (d), 108.49 (s), 111.10 (d), 112.22 (d), 113.79 (s), 117.47 (d), 118.66 (s), 126.25 (s), 128.02 (dx3), 129.09 (dx2), 129.98 (d), 130.22 (d), 130.78 (d), 132.86 (s), 138.50 (s), 143.83 (d), 147.79 (s), 148.24 (s), 150.30 (s), 152.12 (s), 153.63 (s), 154.78 (s); *Anal.* Calculated for $C_{30}H_{25}N_7O$ (MW: 499,58): C, 72.13; H, 5.04; N, 19.63; O, 3.20%. Found: C, 72.17; H, 5.14; N, 19.71; O, 3.25%.

5-(1-benzyl-7-azaindol-3-yl)-2-(5-bromo-1-methyl-1*H*-indol-3-yl)pyrazolo[1,5-*a*]pyrimidin-7-amine (18g):

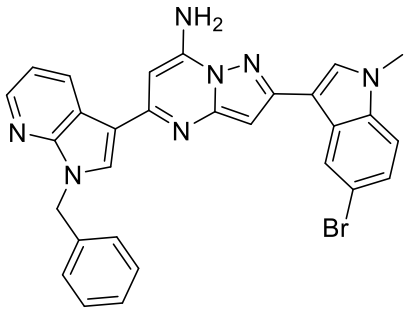

Yield: 49%; creamy white solid; m.p.: 208.8-209°C; IR (cm^{-1}): 3385 (NH_2); ^1H NMR (400 MHz, DMSO-d_6) δ: 3.87 (s, 3H, CH_3), 5.58 (s, 2H, CH_2), 6.50 (s, 1H, pyrimidine-CH), 6.64 (s, 1H, pyrazole-CH), 7.26-7.31 (m, 2H), 7.33 (d, *J* = 3.2 Hz, 2H), 7.34 (s, 2H), 7.36 (d, *J* = 1.9 Hz, 1H), 7.48 (d, *J* = 8.7 Hz, 1H), 7.55 (s, 2H, NH_2, exchangeable with D_2O), 8.02 (s, 1H), 8.35 (s, 1H), 8.36 (dd, *J* = 4.6, 1.4 Hz, 1H), 8.67 (d, *J* = 1.8 Hz, 1H), 8.84 (dd, *J* = 7.9, 1.5 Hz, 1H); ^{13}C NMR (101 MHz, DMSO-d_6) δ: 33.39 (q), 47.88 (t), 83.64 (d), 90.35 (d), 108.69 (s), 112.50 (d), 113.51 (s), 113.73 (s), 117.49 (d), 118.66 (s), 124.45 (d), 124.87 (d), 127.29 (s), 128.00 (dx3), 129.08 (dx2), 130.03 (d), 130.78 (d), 131.26 (d), 136.30 (s), 138.49 (s), 143.83 (d), 147.92 (s), 148.24 (s), 150.31 (s), 151.42 (s), 153.79 (s); *Anal.* Calculated for $C_{29}H_{22}BrN_7$ (MW: 548,45): C, 63.51; H, 4.04; N, 17.88%. Found: C, 63.55; H, 4.11; N, 17.89%.

5-(1-benzyl-7-azaindol-3-yl)-2-(5-chloro-1-methyl-1*H*-indol-3-yl)pyrazolo[1,5-*a*]pyrimidin-7-amine (18h):

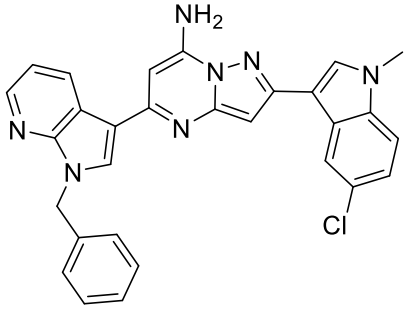

Yield: 34%; yellow solid; m.p.: 189.2-189.5°C; IR (cm^{-1}): 3431 (NH_2); ^1H NMR (400 MHz, DMSO-d_6) δ: 3.87 (s, 3H, CH_3), 5.58 (s, 2H, CH_2), 6.49 (s, 1H, pyrimidine-CH), 6.63 (s, 1H, pyrazole-CH), 7.23 (dd, *J* = 8.7, 2.1 Hz, 1H), 7.27-7.31 (m, 2H), 7.33 (d, *J* = 3.0 Hz, 2H), 7.34 (s, 2H), 7.53 (d, *J* = 8.7 Hz, 1H), 7.56 (s, 2H, NH_2, exchangeable with D_2O), 8.04 (s, 1H), 8.34 (s, 1H), 8.36 (dd, *J* = 4.6,

1.6 Hz, 1H), 8.56 (d, *J* = 2.0 Hz, 1H), 8.83 (dd, *J* = 7.9, 1.6 Hz, 1H); ^{13}C NMR (101 MHz, DMSO-*d*$_6$) δ: 33.40 (q), 47.88 (t), 83.64 (d), 90.29 (d), 108.80 (s), 112.01 (d), 113.77 (s), 117.48 (d), 118.67 (s), 121.59 (d), 122.28 (d), 125.43 (s), 126.67 (s), 128.00 (dx3), 129.08 (dx2), 130.00 (d), 130.76 (d), 131.39 (d), 136.08 (s), 138.49 (s), 143.83 (d), 147.91 (s), 148.26 (s), 150.31 (s), 151.44 (s), 153.78 (s); *Anal.* Calculated for $C_{29}H_{22}ClN_7$ (MW: 503,99): C, 69.11; H, 4.40; N, 19.45%. Found: C, 69.17; H, 4.45; N, 19.51%.

General procedure to prepare solution of cyanoacetyl chloride (41):

To a mixture of cyanoacetic acid (21 mmol) in anhydrous dichloromethane (DCM) (25 ml), under nitrogen atmosphere, anhydrous DMF (0.03 ml) was added. The reaction mixture was stirred and cooled to 0 °C, and oxalyl chloride (21 mmol) was added dropwise. After 5 minutes, the cooling bath was removed, and the mixture was stirred for 2 hours at room temperature. This solution was used without further purification for the next step.

General procedure for the synthesis of 3-oxo-3-(7-azaindol-3-yl)propanenitrile (38):

A solution of aluminium chloride ($AlCl_3$) (21 mmol) in anhydrous dichloromethane (DCM) (25 ml), under nitrogen atmosphere, was stirred at room temperature for 5 minutes. 7-azaindole **35** (4.2 mmol) was added, the mixture was stirred at room temperature for 1.5 hours. The reaction mixture was cooled to 0 °C, and freshly prepared solution of cyanoacetyl chloride (21 mmol) in DCM was added dropwise. The cooling bath was removed, and the reaction mixture was heated under reflux overnight. The reaction was quenched with methanol (10 ml), and the solvent was removed in vacuo. The resulting residue was neutralised by adding saturated aqueous solution of sodium hydrogencarbonate ($NaHCO_3$), extracted with water (20 ml) and ethyl acetate (3 × 20 ml), dried (Na_2SO_4) and evaporated under reduced pressure. The product obtained was further purified by column chromatography, using dichloromethane/methanol as eluent.

3-oxo-3-(7-azaindol-3-yl)propanenitrile (38):

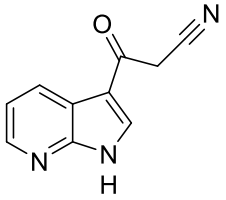

Yield: 10%; orange solid; m.p.: 274-275 °C; IR (cm^{-1}): 3122 (NH), 2253 (CN), 1636 (CO); ^{1}H NMR (400 MHz, DMSO-*d*$_6$) δ: 4.52 (s, 2H, CH_2), 7.29 (dd, *J* = 7.9, 4.7 Hz, 1H, H-5), 8.36 (dd, *J* = 4.7, 1.6

Hz, 1H, H-6), 8.43 (dd, *J* = 7.9, 1.7 Hz, 1H, H-4), 8.52 (s, 1H, H-2), 12.69 (s, 1H, NH, exchangeable with D_2O); ^{13}C NMR (101 MHz, DMSO-d_6) δ: 29.76 (t), 113.60 (s), 116.60 (s), 117.97 (s), 119.02 (d), 129.89 (d), 136.26 (d), 145.19 (d), 149.44 (s), 183.72 (s); *Anal.* Calculated for $C_{10}H_7N_3O$ (MW: 185,19): C, 64.86; H, 3.81; N, 22.69%. Found: C, 64.89; H, 3.88; N, 22.59%.

Procedure leading to the synthesis of undesirable reaction products 1-(7-azaindol-1-yl)ethan-1-one (39) and 3-oxo-3-(7-azaindol-1-yl)propanenitrile (40):

A solution of cyanoacetic acid (7 mmol) and acetic anhydride (Ac_2O) (7 ml) was heated to 85 °C for 10 minutes. 7-azaindole **35** (7 mmol) was added to this solution and heating continued at 85°C. After 15 minutes the reaction is completed, and it was left to cool and was poured into water and ice. It was extracted with ethyl acetate (3 × 15 ml), dried (Na_2SO_4), evaporated under reduced pressure and was further purified by column chromatography, using cyclohexane/ethyl acetate as eluent. The reaction did not provide the desired 3-oxo-3-(7-azaindol-3-yl)propanenitrile **38** but two undesirable reaction products **39,40**.

1-(7-azaindol-1-yl)ethan-1-one (39) [87]**:**

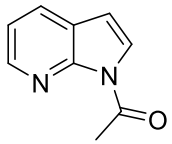

Yield 36%; white needles; m.p.: 63-65°C; ^1H NMR (300 MHz, DMSO-d_6) δ: 2.98 (s, 3H, CH_3), 6.79 (d, *J* = 4.1 Hz, 1H, H-3), 7.32 (dd, *J* = 7.8, 4.8 Hz, 1H, H-5), 8.00 (d, *J* = 4.1 Hz, 1H, H-2), 8.09 (dd, *J* = 7.8, 1.4 Hz, 1H, H-4), 8.39 - 8.42 (m, 1H, H-6); ^{13}C NMR (101 MHz, $CDCl_3$) δ: 25.8 (q), 105.7 (d), 118.6 (d), 123.7 (s), 125.4 (d), 129.3 (d), 143.8 (d), 147.8 (s), 169.1 (s); *Anal.* Calculated for $C_9H_8N_2O$ (MW: 160,18): C, 67.49; H, 5.03; N, 17.49%. Found: C, 67.42; H, 4.97; N, 17.52%.

3-oxo-3-(7-azaindol-1-yl)propanenitrile (40):

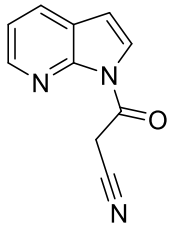

Yield: 18%; beige solid; m.p.: 42-45°C; ^{1}H NMR (300 MHz, DMSO-d_6) δ: 5.11 (s, 2H, CH_2), 6.88 (d, *J* = 4.0 Hz, 1H, H-3), 7.37 (dd, *J* = 7.6, 5.0 Hz, 1H, H-5), 8.01 (d, *J* = 4.1 Hz, 1H, H-2), 8.12 (d, *J* = 7.8 Hz, 1H, H-4), 8.42 (d, *J* = 4.7 Hz, 1H, H-6); *Anal.* Calculated for $C_{10}H_7N_3O$ (MW: 185,19): C, 64.86; H, 3.81; O, 8.64%. Found: C, 64.75; H, 3.91; O, 8.50%. Compound **40** was characterized only by ^{1}H NMR spectra due to its poor stability.

General procedure for the synthesis of 1-(benzenesulfonyl)-7-azaindole (43) [88]**:**

7-azaindole **35** (17 mmol) was dissolved in dry tetrahydrofuran THF (17 ml) under nitrogen, cooled to 0°C, and sodium hydride NaH (18.7 mmol, 60% oil dispersion) was added in portions. Then the mixture was stirred for an additional hour at room temperature. Benzenesulfonyl chloride (17 mmol) was added dropwise, the mixture was stirred overnight. After completion, the reaction mixture was left to cool, and was poured into water and ice. The obtained precipitate was filtered off and further purified by column chromatography, using cyclohexane/ethyl acetate as eluent.

1-(benzenesulfonyl)-7-azaindole (43) [89–91]**:**

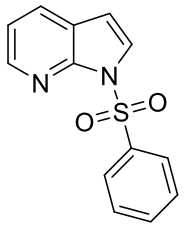

Yield: 58%; white crystals; m.p.: 129°C; ^{1}H NMR (300 MHz, DMSO-d_6) δ: 6.83 (d, *J* = 4.0 Hz, 1H, H-3), 7.29 (dd, *J* = 7.9, 4.8 Hz, 1H, H-5), 7.61 (t, *J* = 7.6 Hz, 2H, ArH), 7.71 (t, *J* = 7.4 Hz, 1H, ArH), 7.91 (d, *J* = 4.0 Hz, 1H, H-2), 8.05 (dd, *J* = 7.9, 1.2 Hz, 1H, H-4), 8.14 – 8.07 (m, 2H, ArH), 8.36 (d, *J* = 4.7 Hz, 1H, H-6); ^{13}C NMR (75 MHz, $CDCl_3$) δ: 105.5, 119.0, 123.0, 126.5, 128.0 (x2), 129.1 (x2), 129.9, 134.1, 138.3, 144.7 (x2); *Anal.* Calculated for $C_{13}H_{10}N_2O_2S$ (MW: 258,30): C, 60.45; H, 3.90; N, 10.85%. Found: C, 60.39; H, 3.95; N, 10.83%.

General procedure for the synthesis of 7-azaindole-3-carbohydrazides (46a-c):

Appropriate carboxylic acid **48** (3.1 mmol) was stirred at room temperature with thionyl chloride (68 mmol), then the reaction mixture was heated under reflux for three hours. The reaction mixture was cooled and the excess of thionyl chloride ($SOCl_2$) was distilled off. The resulting solid was recrystallized from aqueous ethanol, dissolved in absolute alcohol (5 ml) and heated under reflux with hydrazine hydrate (18.6 mmol) to give 7-azaindole-3-carbohydrazide. The product was then recrystallized from aqueous ethanol.

7-azaindole-3-carbohydrazide (46a):

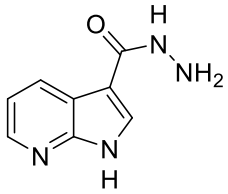

Yield: 70%; white solid; m.p.: 118°C; IR (cm^{-1}): 3242 (NH_2), 2972 (NH), 2889 (NH), 1681 (CO); ^1H NMR (200 MHz, DMSO-d_6) δ: 7.16-7.29 (m, 1H), 8.14 (s, 1H), 8.18-8.36 (m, 1H), 8.40-8.44 (m, 1H), 9.41-10.58 (br s, 2H, NH_2), 10.96 (br s, 1H, NH), 12.50-12.52 (br s, 1H, NH); ^{13}C NMR (50 MHz, DMSO-d_6) δ: 105.23 (s), 117.57 (d), 118.07 (s), 128.87 (d), 130.11 (d), 144.10 (d), 148.31 (s), 163.66 (s); *Anal.* Calculated for $C_8H_8N_4O$ (MW: 176,18): C, 54.54; H, 4.58; N, 31.80%. Found: C, 54.25; H, 4.68; N, 31.78%.

1-methyl-7-azaindole-3-carbohydrazide (46b):

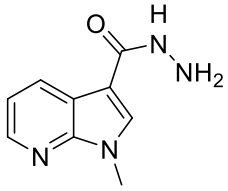

Yield: 90%; white solid; m.p.: 109°C; IR (cm^{-1}): 3252 (NH_2), 2972 (NH), 1682 (CO); ^1H NMR (200 MHz, DMSO-d_6) δ: 3.91 (s, 3H, CH_3), 7.25-7.31 (dd, J = 4.7, 7.9 Hz, 1H), 8.27 (s, 1H), 8.37-8.46 (m, 2H), 10.39-10.90 (br s, 2H, NH_2), 11.52 (br s, H, NH); ^{13}C NMR (50 MHz, DMSO-d_6) δ: 31.42 (q),

105.12 (s), 117.53 (d), 118.59 (s), 129.32 (d), 132.76 (d), 143.69 (d), 147.27 (s), 162.55 (s); *Anal.* Calculated for $C_9H_{10}N_4O$ (MW: 190,21): C, 56.83; H, 5.30; N, 29.46%. Found: C, 56.79; H, 5.42; N, 29.51%.

5-bromo-1-methyl-7-azaindole-3-carbohydrazide (46c):

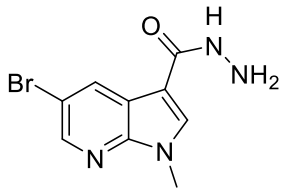

Yield: 70%; white solid; m.p.: 130°C; IR (cm^{-1}): 3310 (NH_2), 3148 (NH), 1684 (CO); ^1H NMR (200 MHz, DMSO-d_6) δ: 3.84 (s, 3H, CH_3), 4.40 (NH_2), 8.17 (s, 1H), 8.42 (d, *J* = 2.2 Hz, 1H), 8.58 (d, *J* = 2.3 Hz, 1H), 9.40 (br s, H, NH); *Anal.* Calculated for $C_9H_9BrN_4O$ (MW: 269,10): C, 40.17; H, 3.37; N, 20.82%. Found: C, 40.17; H, 3.37; N, 20.82%.

General procedure for the synthesis of *N*'-(1-methyl-1*H*-indole-3-carbonyl)-7-azaindole-3-carbohydrazides (45a-h):

To a solution of the proper acid **47a-d** (2 mmol) in dimethylformamide (10 ml), 1-ethyl-3(3-dimethylaminopropyl)carbodiimide (2 mmol), hydroxylbenzotriazole (2 mmol) and diisopropylethylamine (4 mmol) were added. The reaction was stirred for 1 hour at room temperature or heated at 60°C. Then, the proper hydrazine **46a-c** (4 mmol) was added and the reaction mixture was heated at 60° for 4-24 hours or under reflux for 1-6 hours. Once cooled, ice was added and the formed precipitate was filtered off and recrystallized in diethyl ether to afford the pure compounds.

***N*'-(1-methyl-1*H*-indole-3-carbonyl)-7-azaindole-3-carbohydrazide (45a):**

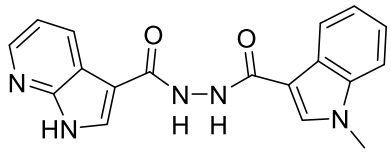

Yield: 50%; brown solid; m.p.: 182°C; IR (cm^{-1}): 3447 (NH), 3366 (NH), 3229 (NH), 1558 (CO), 1541 (CO); ^1H NMR (200 MHz, DMSO-d_6) δ: 3.87 (s, 3H, CH_3), 7.18 (dd, *J* = 10.0, 5.2 Hz, 1H), 7.19

– 7.22 (m, 1H), 7.22 – 7.28 (m, 1H), 7.53 (d, *J* = 8.2 Hz, 1H), 8.11 (s, 1H), 8.15 (d, *J* = 7.9 Hz, 1H), 8.25 – 8.32 (m, 2H), 8.44 (d, *J* = 6.7 Hz, 1H), 9.83 (br s, H, NH), 9.94 (br s, H, NH), 12.21 (br s, H, NH); ^{13}C NMR (101 MHz, DMSO-d_6) δ: 33.56 (q), 107.18 (s), 107.86 (s), 110.81 (d), 117.57 (d), 119.08 (s), 119.85 (s), 121.34 (d), 121.55 (d), 122.63 (d), 126.24 (s), 127.12 (s), 128.96 (d), 129.66 (d), 132.56 (d), 137.15 (s), 144.16 (d), 148.85 (s); *Anal.* Calculated for $C_{18}H_{15}N_5O_2$ (MW: 333,35): C, 64.86; H, 4.54; N, 21.01%. Found C, 64.71; H, 4.50; N, 21.22%.

1-methyl-*N*'-(1-methyl-1*H*-indole-3-carbonyl)-7-azaindole-3-carbohydrazide (45b):

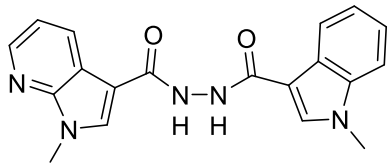

Yield: 80%; brown solid; m.p.: 159°C; IR (cm^{-1}): 3228 (2 NH), 1653 (CO), 1636 (CO); ^{1}H NMR (200 MHz, DMSO-d_6) δ: 3.88 (s, 3H, CH_3), 3.91 (s, 3H, CH_3), 7.15-7.29 (m, 3H), 7.52-7.56 (d, *J* = 8 Hz, 1H), 8.13 (s, 1H), 8.15-8.18 (d, *J* = 7.3 Hz, 1H), 8.31 (s, 1H), 8.36-8.39 (dd, *J* = 1.4, 4.6 Hz, 1H), 8.45-8.49 (dd, *J* = 1.4, 7.9 Hz, 1H), 9.87 (br s, H, NH), 9.98 (br s, H, NH); ^{13}C NMR (50 MHz, DMSO-d_6) δ: 31.36 (q), 33.08 (q), 106.19 (s), 107.32 (sx2), 110.34 (d), 117.25 (d), 118.78 (s), 120.86 (dx2), 121.05 (d), 122.13 (d), 126.62 (s), 129.41 (d), 132.14 (d), 136.62 (s), 143.51 (d), 147.35 (s), 163.56 (s); *Anal.* Calculated for $C_{19}H_{17}N_5O_2$ (MW: 347,38): C, 65.69; H, 4.93; N, 20.16%. Found C, 65.57; H, 4.81; N, 20.10%.

***N*'-(5-fluoro-1-methyl-1*H*-indole-3-carbonyl)-1-methyl-7-azaindole-3-carbohydrazide (45c):**

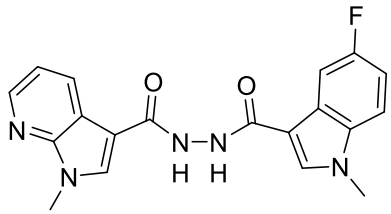

Yield: 85%; brown solid; m.p.: 172°C; IR (cm^{-1}): 3184 (NH), 3119 (NH), 1576 (CO), 1526 (CO); ^{1}H NMR (200 MHz, DMSO-d_6) δ: 3.89 (s, 3H, CH_3), 3.91 (s, 3H, CH_3), 7.07-7.17 (td, *J* = 2.4, 9.2 Hz, 1H), 7.22-7.29 (dd, *J* = 4.7, 7.9 Hz, 1H), 7.54-7.61 (dd, *J* = 4.3, 8.9 Hz, 1H), 7.80-7.86 (dd, *J* = 2.3, 10 Hz, 1H), 8.19 (s, 1H), 8.31 (s, 1H), 8.36-8.38 (d, *J* = 4.6 Hz, 1H), 8.44-8.48 (d, *J* = 7.5 Hz, 1H),

9.93 (br s, H, NH), 9.99 (br s, H, NH); *Anal.* Calculated for $C_{19}H_{16}FN_5O_2$ (MW: 365,37): C, 62.46; H, 4.41; N, 19.17%. Found: C, 62.40; H, 4.37; N, 19.22%.

<u>*N*'-(5-bromo-1-methyl-1*H*-indole-3-carbonyl)-1-methyl-7-azaindole-3-carbohydrazide (45d):</u>

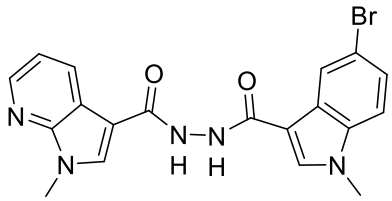

Yield: 88%; white solid; m.p.: 169°C; IR (cm^{-1}): 3184 (2 NH), 1647 (CO), 1578 (CO); ^{1}H NMR (200 MHz, DMSO-d_6) δ: 3.88 (s, 3H, CH_3), 3.91 (s, 3H, CH_3), 7.22-7.29 (dd, *J* = 4.7, 7.8 Hz, 1H), 7.36-7.41 (dd, *J* = 1.7, 8.8 Hz, 1H), 7.52-7.57 (d, *J* = 8.7 Hz, 1H), 8.17 (s, 1H), 8.31 (s, 2H), 8.36-8.39 (d, *J* = 4.6 Hz, 1H), 8.44-8.48 (d, *J* = 7.8 Hz, 1H), 9.96 (br s, H, NH), 9.99 (br s, H, NH); ^{13}C NMR (50 MHz, DMSO-d_6) δ: 31.36 (q), 33.32 (q), 106.13 (s), 106.94 (s), 112.62 (d), 113.83 (s), 117.26 (d), 118.78 (s), 123.15 (d), 124.67 (d), 128.28 (s), 129.40 (d), 132.20 (d), 133.32 (d), 135.43 (s), 143.51 (d), 147.33 (s), 163.51 (s), 163.67 (s); *Anal.* Calculated for $C_{19}H_{16}BrN_5O_2$ (MW: 426,27): C, 53.54; H, 3.78; N, 16.43%. Found: C, 53.50; H, 3.74; N, 16.33%.

<u>5-bromo-1-methyl-*N*'-(1-methyl-1*H*-indole-3-carbonyl)-7-azaindole-3-carbohydrazide (45e):</u>

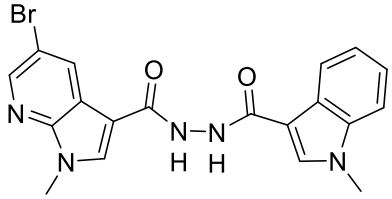

Yield: 80%; white solid; m.p.: 175°C; IR (cm^{-1}): 3354 (NH), 3254 (NH), 1558 (CO), 1541 (CO); ^{1}H NMR (200 MHz, DMSO-d_6) δ: 3.88 (s, 3H, CH_3), 3.91 (s, 3H, CH_3), 7.15-7.30 (m, 2H), 7.52-7.56 (d, *J* = 7.6 Hz, 1H), 8.13 (s, 1H), 8.13-8.18 (d, *J* = 9.0 Hz, 1H), 8.37 (s, 1H), 8.45-8.46 (d, *J* = 2.2 Hz, 1H), 8.60-8.61 (d, *J* = 2.2 Hz, 1H), 9.91-9.96 (br s, 2H, 2NH); ^{13}C NMR (50 MHz, DMSO-d_6) δ: 31.61 (q), 33.08 (q), 105.83 (s), 107.22 (s), 110.35 (d), 112.70 (s), 120.29 (s), 120.87 (d), 121.02 (d), 122.14 (d), 126.59 (s), 131.10 (d), 132.11 (d), 133.84 (d), 136.62 (s), 143.65 (d), 145.82 (s), 162.26 (s), 163.09 (s); *Anal.* Calculated for $C_{19}H_{16}BrN_5O_2$ (MW: 426,27): C, 53.54; H, 3.78; N, 16.43%. Found: C, 53.50; H, 3.81; N, 16.39%.

5-bromo-*N*'-(5-bromo-1-methyl-1*H*-indole-3-carbonyl)-1-methyl-7-azaindole-3-carbohydrazide (45f):

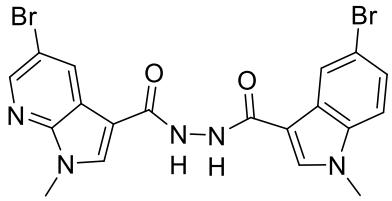

Yield: 82%; white solid; m.p.: 168°C; IR (cm^{-1}): 3244 (2 NH), 1730 (2 CO); ^{1}H NMR (200 MHz, DMSO-d_6) δ: 3.89 (s, 3H, CH_3), 3.91 (s, 3H, CH_3), 7.07-7.17 (td, *J* = 2.6, 9.2 Hz, 1H), 7.23-7.29 (dd, *J* = 4.7, 7.9 Hz, 1H), 7.54-7.61 (dd, *J* = 4.5, 8.9 Hz, 1H), 7.81-7.87 (dd, *J* = 2.5, 10 Hz, 1H), 8.20 (s, 1H), 8.35-8.38 (dd, *J* = 1.5, 4.7 Hz, 1H), 8.44-8.49 (dd, *J* = 1.5, 7.9 Hz, 1H), 9.93 (br s, H, NH), 10.0 (br s, H, NH); ^{13}C NMR (50 MHz, DMSO-d_6) δ: 31.36 (q), 33.42 (q), 105.45 (d), 105.94 (d), 117.27 (d), 129.38 (d), 132.17 (d), 133.61 (d), 143.53 (d); *Anal.* Calculated for $C_{19}H_{15}Br_2N_5O_2$ (MW: 505,17): C, 45.17; H, 2.99; N, 13.86%. Found C, 45.12; H, 2.88; N, 13.80%.

5-bromo-*N*'-(5-fluoro-1-methyl-1*H*-indole-3-carbonyl)-1-methyl-7-azaindole-3-carbohydrazide (45g):

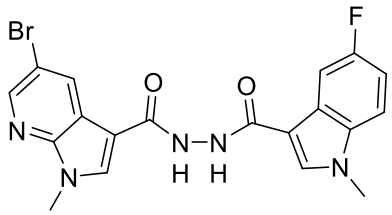

Yield: 85%; brown solid; m.p.: 189°C; IR (cm^{-1}): 3420 (NH), 3312 (NH), 1653 (CO), 1616 (CO); ^{1}H NMR (200 MHz, DMSO-d_6) δ: 3.89 (s, 3H, CH_3), 3.90 (s, 3H, CH_3), 7.07-7.17 (td, *J* = 2.5, 9.2 Hz, 1H), 7.55-7.61 (dd, *J* = 4.5, 8.9 Hz, 1H), 7.79-7.86 (dd, *J* = 2.4, 10.0 Hz, 1H), 8.19 (s, 1H), 8.36 (s, 1H), 8.45-8.46 (d, *J* = 2.2 Hz, 1H), 8.59-8.60 (d, *J* = 2.1 Hz, 1H), 9.96 (br s, H, NH), 10.08 (br s, H, NH); *Anal.* Calculated for $C_{19}H_{15}BrFN_5O_2$ (MW: 444,26): C, 51.37; H, 3.40; N, 15.76%. Found: C, 51.30; H, 3.47; N, 15.79%.

***N*'-(5-methoxy-1-methyl-1*H*-indole-3-carbonyl)-1-methyl-7-azaindole-3-carbohydrazide (45h):**

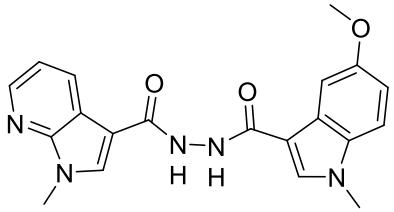

Yield: 88%; white solid; m.p.: 198°C; IR (cm^{-1}): 3231-3101 (2 NH), 1624 (CO), 1541 (CO); ^{1}H NMR (200 MHz, DMSO-d_6) δ: 3.77 (s, 3H, CH_3), 3.84 (s, 3H, CH_3), 3.91 (s, 3H, OCH_3), 6.85-6.91 (dd, *J* = 2.4, 8.9 Hz, 1H), 7.23-7.29 (dd, *J* = 4.7, 7.8 Hz, 1H), 7.42-7.46 (d, *J* = 8.9 Hz, 1H), 7.66-7.67 (d, *J* = 2.3 Hz, 1H), 8.06 (s, 1H), 8.30 (s, 1H), 8.36-8.38 (d, *J* = 4.5 Hz, 1H), 8.45-8.48 (d, *J* = 6.9 Hz, 1H), 9.82 (br s, H, NH), 9.94 (br s, H, NH); ^{13}C NMR (50 MHz, DMSO-d_6) δ: 31.36 (q), 32.23 (q), 55.17 (q), 102.49 (d), 111.19 (d), 112.21 (d), 117.27 (d), 129.40 (d), 132.11 (d), 132.23 (d), 143.51 (d); *Anal.* Calculated for $C_{20}H_{19}N_5O_3$ (MW: 377,40): C, 63.65; H, 5.07; N, 18.56%. Found: C, 63.55; H, 5.21; N, 18.60%.

General procedure for the synthesis of *N'*-benzoyl-7-azaindole-3-carbohydrazides (51a-d):

To a solution of the proper acid **48** (2 mmol) in dimethylformamide (10 ml), 1-ethyl-3(3-dimethylaminopropil)carbodiimide (2 mmol), hydroxylbenzotriazole (2 mmol) and diisopropylethylamine (4 mmol) were added. The reaction was stirred for 1 hour at room temperature or heated at 60°C. Then, the proper hydrazine **49** (4 mmol) was added and the reaction mixture was heated at 60° for 4-24 hours or under reflux for 1-6 hours. Once cooled, ice was added and the formed precipitate was filtered off and recrystallized in diethyl ether to afford the pure compounds.

***N'*-benzoyl-7-azaindole-3-carbohydrazide (51a):**

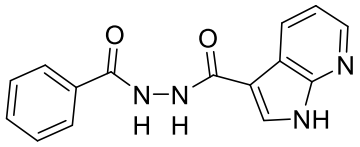

Yield: 92%; white solid; m.p.: 170°C; IR (cm^{-1}): 3454 (NH), 3377 (NH), 3221 (NH), 1636 (CO), 1558 (CO); ^{1}H NMR (200 MHz, DMSO-d_6) δ: 7.22 (dd, *J* = 7.5, 4.8 Hz, 1H), 7.57 (t, *J* = 8.0 Hz, 3H), 7.95 (d, *J* = 6.8 Hz, 2H), 8.30 (s, 2H), 8.45 (d, *J* = 7.6 Hz, 1H), 10.11 (br s, H, NH), 10.44 (br s, H, NH), 12.27 (br s, H, NH); ^{13}C NMR (50 MHz, DMSO-d_6) δ: 107.08 (s), 117.18 (d), 118.52 (s), 127.41 (dx2), 128.48 (dx2), 128.60 (d), 129.13 (d), 131.76 (d), 132.69 (s), 143.73 (d), 148.31 (s), 163.49 (s),

166.09 (s); *Anal.* Calculated for $C_{15}H_{12}N_4O_2$ (MW: 280,29): C, 64.28; H, 4.32; N, 19.99%. Found C, 64.32; H, 4.45; N, 19.80%.

<u>*N*'-benzoyl-1-methyl-7-azaindole-3-carbohydrazide (51b):</u>

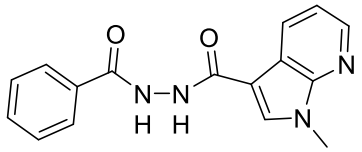

Yield: 94%; white solid; m.p.: 174°C; IR (cm^{-1}): 3219 (2 NH), 1663 (CO), 1636 (CO); ^{1}H NMR (200 MHz, DMSO-d_6) δ: 3.91 (s, 3H, CH_3), 7.27 (s, 1H), 7.55 (d, J = 6.2 Hz, 3H), 7.94 (d, J = 5.4 Hz, 2H), 8.30 (s, 1H), 8.37 (s, 1H), 8.45 (d, J = 6.1 Hz, 1H), 10.12 (br s, H, NH), 10.44 (br s, H, NH); *Anal.* Calculated for $C_{16}H_{14}N_4O_2$ (MW: 294,31): C, 65.30; H, 4.79; N, 19.04%. Found C, 65.41; H, 4.82; N, 19.00%.

<u>*N*'-benzoyl-5-bromo-7-azaindole-3-carbohydrazide (51c):</u>

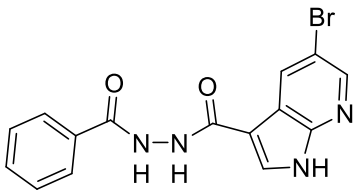

Yield: 92%; white solid; m.p.: 205°C; IR (cm^{-1}): 3458 (NH), 3184 (NH), 3098 (NH), 1628 (CO), 1558 (CO); ^{1}H NMR (200 MHz, DMSO-d_6) δ: 7.69 – 7.52 (m, 3H), 7.99 (d, J = 6.6 Hz, 2H), 8.40 (s, 1H),. 8.45 (s, 1H), 8.64 (d, J = 2.1 Hz, 1H), 10.23 (br s, H, NH), 10.50 (br s, H, NH), 12.58 (br s, H, NH); ^{13}C NMR (50 MHz, DMSO-d_6) δ: 106.82 (s), 112.52 (s), 120.01 (s), 120.21 (s), 127.41 (dx2), 128.48 (dx2), 130.32 (d), 130.89 (d), 131.79 (d), 132.63 (s), 143.88 (d), 146.72 (s), 166.09 (s); *Anal.* Calculated for $C_{15}H_{11}BrN_4O_2$ (MW: 359,18): C, 50.16; H, 3.09; N, 15.60%. Found C, 50.26; H, 3.21; N, 15.64%.

<u>*N*'-benzoyl-5-bromo-1-methyl-7-azaindole-3-carbohydrazide (51d):</u>

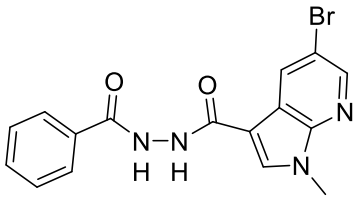

Yield: 95%; white solid; m.p.: 180°C; IR (cm^{-1}): 3221 (NH), 3098 (NH), 1707 (CO), 1629 (CO); ^1H NMR (200 MHz, DMSO-d_6) δ: ^1H NMR (200 MHz, DMSO-d_6) δ: 3.91 (s, 3H, CH_3), 7.56 (d, J = 7.5 Hz, 2H), 7.94 (d, J = 7.4 Hz, 3H), 8.36 (s, 1H), 8.47 (s, 1H), 8.59 (s, 1H), 10.21 (br s, H, NH), 10.47 (br s, H, NH); *Anal.* Calculated for $C_{16}H_{13}BrN_4O_2$ (MW: 373,21): C, 51.49; H, 3.51; N, 15.01%. Found C, 51.55; H, 3.61; N, 15.23%.

General procedure for the synthesis of-[5-(1-methyl-1*H*-indol-3-yl)-1,3,4-oxadiazol-2-yl]-7-azaindoles (19a-g):

The solution of the proper intermediate **45** (0.81 mmol) in phosphoryl chloride (5.4 ml) was heated at 45 °C overnight or under reflux for 3-6 hours. Once cooled, the reaction mixture was evaporated in vacuo and extracted with a saturated solution of sodium hydrogen carbonate (3 x 30 ml) and ethyl acetate (3 x 30 ml). The organic layers were evaporated in vacuo and dried with sodium sulphate. The resulting crude material was purified in column using dichloromethane/methanol 99:1 as eluent.

3-[5-(1-methyl-1*H*-indol-3-yl)-1,3,4-oxadiazol-2-yl]-7-azaindole (19a):

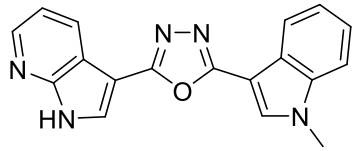

Yield 75%; white solid; m.p.: 302-303°C; IR (cm^{-1}): 3117 (NH); ^1H NMR (200 MHz, DMSO-d_6) δ: 3.93 (s, 3H, CH_3), 7.28 – 7.32 (m, 2H), 7.32 – 7.37 (m, 2H), 8.20 – 8.23 (m, 1H), 8.29 (s, 1H), 8.37 (d, J = 2.4 Hz, 1H), 8.41 (dd, J = 4.7, 1.6 Hz, 1H), 8.53 (dd, J = 7.9, 1.6 Hz, 1H), 12.57 (s, 1H, NH); ^{13}C NMR (50 MHz, DMSO-d_6) δ: 33.55 (q), 99.12 (s), 99.21 (s), 111.30 (d), 117.02 (s), 117.90 (d), 121.02 (d), 121.87 (d), 123.30 (d), 124.92 (s), 128.52 (d), 129.19 (d), 132.11 (d), 137.51 (s), 144.87 (d), 149.18 (s), 159.54 (s), 160.25 (s); *Anal.* Calculated for $C_{18}H_{13}N_5O$ (MW: 315,34): C, 68.56; H, 4.16; N, 22.21%. Found: C, 68.59; H, 4.21; N, 22.15%.

1-methyl-3-[5-(1-methyl-1*H*-indol-3-yl)-1,3,4-oxadiazol-2-yl]-7-azaindole (19b):

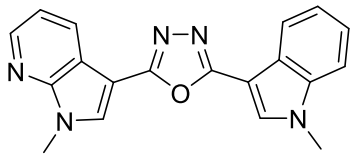

Yield 86%; white solid, m.p.: 238-239°C; ^{1}H NMR (200 MHz, DMSO-d_6) δ: 3.94 (s, 3H, CH_3), 3.96 (s, 3H, CH_3), 7.37-7.51 (m, 3H), 7.61-7.65 (d, *J* = 8.1 Hz, 1H), 8.19-8.23 (d, *J* = 7.3 Hz, 1H,), 8.30 (s, 1H), 8.45-8.55 (m, 3H); *Anal.* Calculated for $C_{19}H_{15}N_5O$ (MW: 329,36): C, 69.29; H, 4.59; N, 21.26%. Found: C, 71.29; H, 4.69; N, 21.20%.

3-[5-(5-fluoro-1-methyl-1*H*-indol-3-yl)-1,3,4-oxadiazol-2-yl]-1-methyl-7-azaindole (19c):

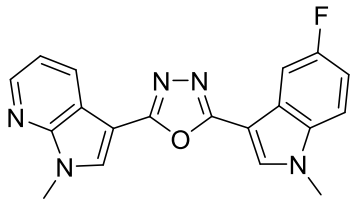

Yield 85%; white solid; m.p.: 265-268°C; ^{1}H NMR (200 MHz, DMSO-d_6) δ: 3.97 (s, 6H, 2 CH_3), 7.24-7.28 (d, *J* = 8.8 Hz, 1H), 7.35-7.42 (dd, *J* = 5.1, 7.6 Hz, 1H), 7.65-7.71 (dd, *J* = 4.4, 8.9 Hz, 1H), 7.85-7.90 (d, *J* = 9.4 Hz, 1H), 8.39 (s, 1H), 8.46-8.48 (d, *J* = 4.0 Hz, 1H), 8.53 - 8.56 (d, *J* = 7.1 Hz, 2H); *Anal.* Calculated for $C_{19}H_{14}FN_5O$ (MW: 347,35): C, 65.70; H, 4.06; N, 20.16%. Found: C, 65.75; H, 4.13; N, 20.26%.

3-[5-(5-bromo-1-methyl-1*H*-indol-3-yl)-1,3,4-oxadiazol-2-yl]-1-methyl-7-azaindole (19d):

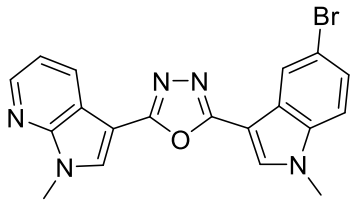

Yield 86%; white solid; m.p.: 277-278°C; ^{1}H NMR (200 MHz, DMSO-d_6) δ: 3.95 (s, 3H, CH_3), 3.97 (s, 3H, CH_3), 7.38 (dd, *J* = 4.7, 7.8 Hz, 1H), 7.49 (dd, *J* =1.8, 8.7 Hz, 1H), 7.64 (d, *J* = 8.8 Hz, 1H), 8.31 (d, *J* = 1.7 Hz, 1H), 8.37 (s, 1H), 8.47 (d, *J* = 2.9 Hz, 2H), 8.54 (dd, *J* = 7.9, 1.2 Hz, 1H); *Anal.*

Calculated for $C_{19}H_{14}BrN_5O$ (MW: 408,26): C, 55.90; H, 3.46; N, 17.15%. Found: C, 55.87; H, 3.51; N, 17.27%.

5-bromo-1-methyl-3-[5-(1-methyl-1*H*-indol-3-yl)-1,3,4-oxadiazol-2-yl]-7-azaindole (19e):

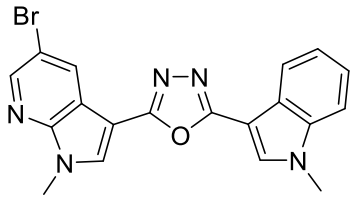

Yield 78%; white solid; m.p.:244-246°C; ^{1}H NMR (200 MHz, DMSO-d_6) δ: 3.95 (s, 6H, 2 CH_3), 7.32-7.40 (m, 2H), 7.61-7.65 (dd, *J* = 2.1, 6.1 Hz, 1H), 8.17-8.22 (m, 1H), 8.29 (s, 1H), 8.53-8.54 (d, *J* = 2.3 Hz, 2H), 8.61-8.62 (d, *J* = 2.2 Hz, 1H); *Anal.* Calculated for $C_{19}H_{14}BrN_5O$ (MW: 408,26): C, 55.90; H, 3.46; N, 17.15%. Found: C, 55.81; H, 3.57; N, 17.23%.

5-bromo-3-[5-(5-bromo-1-methyl-1*H*-indol-3-yl)-1,3,4-oxadiazol-2-yl]-1-methyl-7-azaindole (19f):

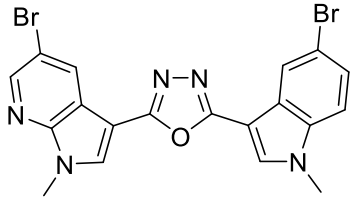

Yield 90%; white solid; m.p.: 275°C; ^{1}H NMR (200 MHz, DMSO-d_6) δ: 3.96 (s, 6H, 2CH_3), 7.50 (d, *J* = 8.6 Hz, 1H), 7.65 (d, *J* = 8.5 Hz, 1H), 8.31 (s, 1H), 8.37 (s, 1H), 8.55 (s, 2H), 8.62 (s, 1H); *Anal.* Calculated for $C_{19}H_{13}Br_2N_5O$ (MW: 487,16): C, 46.85; H, 2.69; N, 14.38%. Found: 46.93; H, 2.75; N, 14.52%.

5-bromo-3-[5-(5-fluoro-1-methyl-1*H*-indol-3-yl)-1,3,4-oxadiazol-2-yl]-1-methyl-7-azaindole (19g):

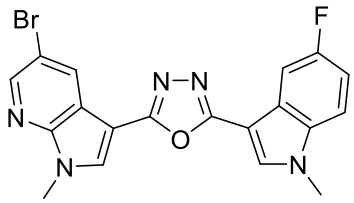

Yield 45%; beige solid m.p.: 310-311°C; ^{1}H NMR (200 MHz, DMSO-d_6) δ: 3.97 (s, 6H, 2 CH_3), 7.24 (td, *J* = 9.2, 2.3 Hz, 1H), 7.69 (dd, *J* = 9.0, 4.3 Hz, 1H), 7.88 (dd, *J* = 9.5, 2.5 Hz, 1H), 8.40 (s, 1H), 8.54 – 8.60 (m, 3H); *Anal.* Calculated for $C_{19}H_{13}BrFN_5O$ (MW: 426,25): C, 53.54; H, 3.07; N, 16.43%. Found: C, 53.45; H, 3.16; N, 16.51%.

General procedure for the synthesis of-3-[5-(1-methyl-1*H*-indol-3-yl)-1,3,4-thiadiazol-2-yl]-7-azaindoles (21a-h)

To a solution of the proper intermediate **45** (0.38 mmol) in pyridine (15 ml), the Lawesson's reagent (0.41 mmol), was added and the reaction mixture was heated at 45°C overnight or under reflux for 3-6 hours. The mixture was evaporated in vacuo and the crude material was purified in chromatography column using dichloromethane/methanol 99:1 as eluent.

3-[5-(1-methyl-1*H*-indol-3-yl)-1,3,4-thiadiazol-2-yl]-7-azaindole (21a):

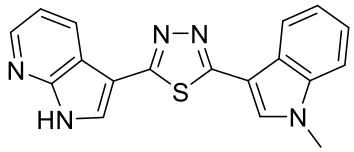

Yield 78%; beige solid; m.p.: 244-246°C; IR (cm^{-1}): 3171 (NH); ^{1}H NMR (200 MHz, DMSO-d_6) δ: 3.94 (s, 3H, CH_3), 7.28 – 7.39 (m, 3H), 7.60 (t, *J* = 9.3 Hz, 1H), 8.18 – 8.23 (m, 1H), 8.30 (s, 1H), 8.36 – 8.42 (m, 2H), 8.53 (dd, *J* = 7.9, 1.5 Hz, 1H), 12.58 (s, 1H, NH); ^{13}C NMR (50 MHz, DMSO-d_6) δ: 33.56 (q), 99.11 (s), 99.20 (s), 111.32 (d), 117.02 (s), 117.91 (d), 121.02 (d), 121.88 (d), 123.31 (d), 124.92 (s), 128.54 (d), 129.19 (d), 132.13 (d), 137.51 (s), 144.88 (d), 149.19 (s), 159.54 (s), 160.25 (s); *Anal.* Calculated for $C_{18}H_{13}N_5S$ (MW: 331,40): C, 65.24; H, 3.95; N, 21.13%. Found: C, 65.41; H, 3.71; N, 21.32%.

1-methyl-3-[5-(1-methyl-1*H*-indol-3-yl)-1,3,4-thiadiazol-2-yl]-7-azaindole (21b):

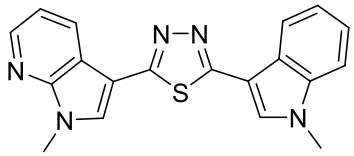

Yield 99%; white solid; m.p.: 244-246°C; ^{1}H NMR (200 MHz, DMSO-d_6) δ: 3.91 (s, 3H, CH_3), 3.93 (s, 3H, CH_3), 7.25-7.41 (m, 3H), 7.60 (d, *J* = 6.7 Hz, 1H), 8.22 (s, 1H), 8.27 (dd, *J* = 6.1, 2.1 Hz, 1H), 8.40 (s, 1H), 8.44 (d, *J* = 4.5 Hz, 1H), 8.61 (d, *J* = 7.6 Hz, 1H); *Anal.* Calculated for $C_{19}H_{15}N_5S$ (MW: 345,42): C, 66.07; H, 4.38; N, 20.28%. Found C, 66.23; H, 4.42; N, 20.33; S, 9.35%.

3-[5-(5-bromo-1-methyl-1*H*-indol-3-yl)-1,3,4-thiadiazol-2-yl]-1-methyl-7-azaindole (21c):

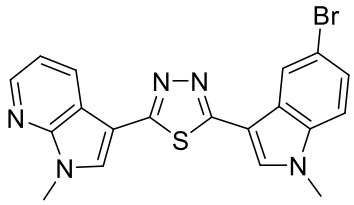

Yield 78%; beige solid; m.p.: 292-293°C; ^{1}H NMR (200 MHz, DMSO-d_6) δ: 3.96 (s, 3H, CH_3), 3.97 (s, 3H, CH_3), 7.36-7.42 (dd, *J* =4.5, 7.8 Hz, 1H), 7.47-7.52 (dd, *J* =1.8, 8.8 Hz, 1H), 7.63-7.71 (m, 1H), 8.29-8.32 (m, 1H), 8.38 (s, 1H), 8.44-8.56 (m, 3H); *Anal.* Calculated for $C_{19}H_{14}BrN_5S$ (MW: 424,32): C, 53.78; H, 3.33; N, 16.51%. Found C, 53.81; H, 3.40; N, 16.72%.

3-[5-(5-fluoro-1-methyl-1*H*-indol-3-yl)-1,3,4-thiadiazol-2-yl]-1-methyl-7-azaindole (21d):

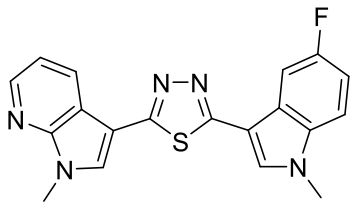

Yield 60%; white solid; m.p.:240-242°C; ^{1}H NMR (200 MHz, DMSO-d_6) δ: 3.92 (s, 3H, CH_3), 3.93 (s, 3H, CH_3), 7.16-7.26 (td, *J* = 2.5, 9.2, 9.2 Hz, 1H), 7.33-7.39 (dd, *J* = 4.7, 7.9 Hz, 1H), 7.61-7.67 (dd, *J* = 4.5, 8.9 Hz, 1H), 7.94-8.00 (dd, *J* = 2.5, 9.8 Hz, 1H), 8.29 (s, 1H), 8.41 (s, 1H), 8.42-8.46 (dd, *J* = 1.5, 4.7 Hz, 1H), 8.58-8.62 (dd, *J* = 1.5, 7.9 Hz, 1H); *Anal.* Calculated for $C_{19}H_{14}FN_5S$ (MW: 363,41): C, 62.80; H, 3.88; N, 19.27%. Found: C, 62.89; H, 3.67; N, 19.31%.

3-[5-(5-methoxy-1-methyl-1*H*-indol-3-yl)-1,3,4-thiadiazol-2-yl]-1-methyl-7-azaindole (21e):

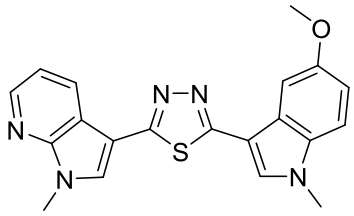

Yield 60%; white solid; m.p.:199-200°C; ^{1}H NMR (200 MHz, DMSO-d_6) δ: 3.87 (s, 3H, CH_3), 3.90 (s, 3H, CH_3), 3.95 (s, 3H, OCH_3), 6.93-7.00 (dt, *J* = 2.9, 5.8 Hz, 1H), 7.31-7.40 (dt, *J* = 7.9, 3.9 Hz, 1H), 7.47-7.54 (dd, *J* = 5.8, 8.9 Hz, 1H), 7.64-7.77 (m, 1H), 8.12-8.21 (m, 1H), 8.37-8.63 (m, 3H); *Anal.* Calculated for $C_{20}H_{17}N_5OS$ (MW: 375,45): C, 63.98; H, 4.56; N, 18.65%. Found C, 63.98; H, 4.56; N, 18.65%.

5-bromo-1-methyl-3-[5-(1-methyl-1*H*-indol-3-yl)-1,3,4-thiadiazol-2-yl]-7-azaindole (21f):

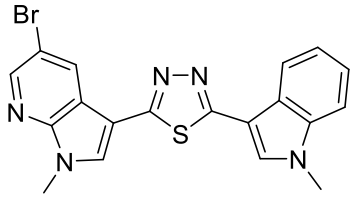

Yield 70%; beige solid; m.p.: 232-233°C; ^{1}H NMR (200 MHz, DMSO-d_6) δ: 3.91 (s, 3H, CH_3), 3.95 (s, 3H, CH_3), 7.29-7.38 (m, 2H), 7.58-7.64 (m, 1H), 8.23-8.30 (m, 2H), 8.47 (s, 1H), 8.51-8.55 (dd, *J* = 2.2, 5.4 Hz, 1H,), 8.73-8.74 (d, *J* = 2.2 Hz, 1H); *Anal.* Calculated for $C_{19}H_{14}BrN_5S$ (MW: 424,32): C, 53.78; H, 3.33; N, 16.51%. Found C, 53.81; H, 3.40; N, 16.62%.

5-bromo-3-[5-(5-bromo-1-methyl-1*H*-indol-3-yl)-1,3,4-thiadiazol-2-yl]-1-methyl-7-azaindole (21g):

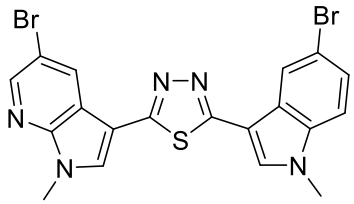

Yield 50%; beige solid m.p.: 275-276°C; ^{1}H NMR (200 MHz, DMSO-d_6) δ: 3.91 (s, 3H, CH_3). 3.95 (s, 3H, CH_3), 7.39 – 7.52 (m, 1H), 7.61 (t, *J* = 7.4 Hz, 1H), 8.28 (s, 1H), 8.35 (s, 1H), 8.52 (t, *J* = 5.6

Hz, 2H), 8.60 (d, *J* = 2.1 Hz, 1H); *Anal.* Calculated for $C_{19}H_{13}Br_2N_5S$ (MW: 503,22): C, 45.35; H, 2.60; N, 13.92%. Found C, 45.45; H, 2.65; N, 13.99%.

5-bromo-3-[5-(5-fluoro-1-methyl-1*H*-indol-3-yl)-1,3,4-thiadiazol-2-yl]-1-methyl-7-azaindole (21h):

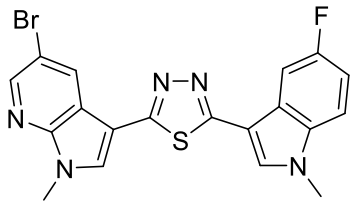

Yield 80%; white solid; m.p.: 290-291°C; ^{1}H NMR (200 MHz, DMSO-d_6) δ: 3.90 (s, 3H, CH_3), 3.94 (s, 3H, CH_3), 7.16-7.25 (m, 1H), 7.59-7.68 (m, 1H), 7.81-7.97 (qd, *J* = 2.3, 9.5 Hz, 1H), 8.28 (s, 1H), 8.45-8.59 (m, 3H); *Anal.* Calculated for $C_{19}H_{13}BrFN_5S$ (MW: 442,31): C, 51.59; H, 2.96; N, 15.83%. Found C, 51.78; H, 2.85; N, 15.89%.

General procedure for the synthesis of-(5-phenyl-1,3,4-oxadiazol-2-yl)-7-azaindoles (20a-d):

The solution of the proper intermediate **51** (0.81 mmol) in phosphoryl chloride (5.4 ml) was heated at 45 °C overnight or under reflux for 3-6 hours. Once cooled, the reaction mixture was evaporated in vacuo and extracted with a saturated solution of sodium hydrogen carbonate (3 x 30 ml) and ethyl acetate (3 x 30 ml). The organic layers were evaporated in vacuo and dried with sodium sulphate. The resulting crude material was purified in column using dichloromethane/methanol 99:1 as eluent.

3-(5-phenyl-1,3,4-oxadiazol-2-yl)-7-azaindole (20a):

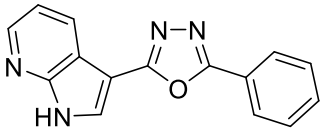

Yield 70%; white solid; m.p.272-274°C; IR (cm^{-1}): 3111 (NH); ^{1}H NMR (200 MHz, DMSO-d_6) δ:7.34 (dd, *J* = 7.9, 4.7 Hz, 1H), 7.62-7.68 (m, 3H), 8.15 (dd, *J* = 6.5, 3.0 Hz, 2H), 8.42 (dd, *J* = 4.6, 1.4 Hz, 1H), 8.51 (dd, *J* = 9.7, 1.8 Hz, 2H), 12.68 (s, 1H, NH); *Anal.* Calculated for $C_{15}H_{10}N_4O$ (MW: 262,27): C, 68.69; H, 3.84; N, 21.36%. Found C, 68.78; H, 3.90; N, 21.61%.

1-methyl-3-(5-phenyl-1,3,4-oxadiazol-2-yl)-7-azaindole (20b):

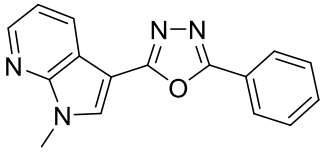

Yield 75%; white solid; m.p.: 200-201°C; ^{1}H NMR (200 MHz, DMSO-d_6) δ: 3.96 (s, 3H, CH_3), 7.38 (dd, *J* = 4.7, 7.9 Hz, 1H), 7.62 - 7.67 (m, 3H), 8.11 (d, *J* = 3.4 Hz, 1H), 8.15 (d, *J* = 2.2 Hz, 1H), 8.47 (d, *J* = 4.7 Hz, 1H), 8.52 (dd, *J* = 7.9, 1.4 Hz, 1H), 8.56 (s, 1H); *Anal.* Calculated for $C_{16}H_{12}N_4O$ (MW: 276,30): C, 69.55; H, 4.38; N, 20.28%. Found C, 69.66; H, 4.51; N, 20.41%.

5-bromo-3-(5-phenyl-1,3,4-oxadiazol-2-yl)-7-azaindole (20c):

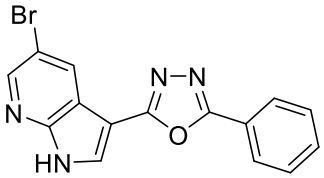

Yield 55%; beige solid; m.p.: 275-276°C; IR (cm^{-1}): 3112 (NH); ^{1}H NMR (200 MHz, DMSO-d_6) δ: 7.64 (d, *J* = 2.2 Hz, 3H), 8.12 (d, *J* = 3.6 Hz, 2H), 8.53 (dd, *J* = 10.2, 7.7 Hz, 3H), 12.91 (s, 1H, NH); *Anal.* Calculated for $C_{15}H_9BrN_4O$ (MW: 341,17): C, 52.81; H, 2.66; N, 16.42%. Found C, 52.85; H, 2.60; N, 16.40%.

5-bromo-1-methyl-3-(5-phenyl-1,3,4-oxadiazol-2-yl)-7-azaindole (20d):

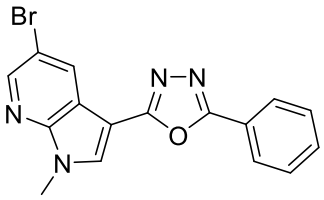

Yield 60%; white solid; m.p.: 235-236°C; ^{1}H NMR (200 MHz, DMSO-d_6) δ: 3.95 (s, 3H, CH_3), 7.67 (s, 3H), 8.13 (s, 2H), 8.56 (s, 1H), 8.62 (d, *J* = 5.0 Hz, 2H); *Anal.* Calculated for $C_{16}H_{11}BrN_4O$ (MW: 355,20): C, 54.10; H, 3.12; N, 15.77%. Found C, 54.10; H, 3.12; N, 15.77%.

General procedure for the synthesis of-3-[5-(1-methyl-1*H*-indol-3-yl)-1,3,4-thiadiazol-2-yl]-7-azaindoles (22a-d):

To a solution of the proper intermediate **51** (0.38 mmol) in pyridine (15 ml), the Lawesson's reagent (0.41 mmol), was added and the reaction mixture was heated at 45°C overnight or under reflux for 3-6 hours. The mixture was evaporated in vacuo and the crude material was purified in chromatography column using dichloromethane/methanol 99:1 as eluent.

3-(5-phenyl-1,3,4-thiadiazol-2-yl)-7-azaindole (22a):

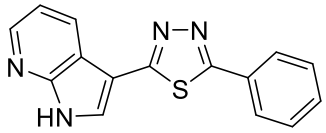

Yield: 78%; white solid; m.p.: 248-249°C; IR (cm^{-1}): 3111 (NH); ^{1}H NMR (200 MHz, DMSO-d_6) δ: 7.29-7.35 (dd, *J* = 4.7, 7.9 Hz, 1H), 7.57-7.58 (d, *J* = 2.7 Hz, 2H), 7.60 (s, 1H), 7.98-8.03 (m, 2H), 8.38-8.39 (d, *J* = 1.4 Hz, 1H), 8.41 (s, 1H), 8.57-8.61 (dd, *J* = 1.4, 7.9 Hz, 1H), 12.56 (s, 1H, NH); ^{13}C NMR (50 MHz, DMSO-d_6) δ: 105.06 (s), 116.68 (s), 117.53 (d), 127.45 (dx2), 129.00 (d), 129.45 (dx2), 129.58 (d), 129.74 (s), 130.99 (d), 144.39 (d), 148.78 (s), 162.47 (s), 164.45 (s); *Anal.* Calculated for $C_{15}H_{10}N_4S$ (MW: 278,33): C, 64.73; H, 3.62; N, 20.13%. Found C, 64.80; H, 3.91; N, 20.25%.

1-methyl-3-(5-phenyl-1,3,4-thiadiazol-2-yl)-7-azaindole (22b):

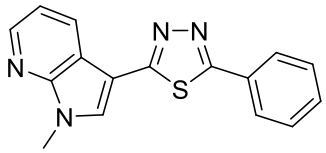

Yield: 95%; white solid; m.p.:190-191°C; ^{1}H NMR (200 MHz, DMSO-d_6) δ: 3.91 (s, 3H, CH_3), 7.57-7.60 (t, *J* = 3.2 Hz, 3H), 7.69-7.70 (d, *J* = 2.1 Hz, 1H), 7.99-8.06 (m, 2H), 8.51-8.52 (d, *J* = 2.2 Hz, 1H), 8.54 (s, 1H), 8.70-8.71 (d, *J* = 2.2 Hz, 1H). ^{13}C NMR (50 MHz, DMSO-d_6) δ: 31.61 (q), 103.36 (s), 112.98 (s), 118.39 (s), 127.51 (dx2), 129.47 (dx2), 130.97 (d), 131.15 (d), 131.57 (d), 134.44 (d), 144.36 (d), 146.14 (s), 161.60 (s), 164.73 (s); *Anal.* Calculated for $C_{16}H_{12}N_4S$ (MW: 292,36): C, 65.73; H, 4.14; N, 19.16%. Found C, 65.65; H, 4.20; N, 19.31%.

5-bromo-3-(5-phenyl-1,3,4-thiadiazol-2-yl)-7-azaindole (22c):

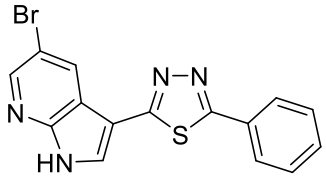

Yield: 60%; white solid; m.p.: 307-308°C; IR (cm^{-1}): 3111 (NH); ^{1}H NMR (200 MHz, DMSO-d_6) δ: 7.57-7.60 (t, *J* = 3.2 Hz, 3H), 7.98-7.99 (d, *J* = 2.5 Hz, 1H), 8.01-8.02 (d, *J* = 3.5 Hz, 1H), 8.46-8.47 (d, *J* = 2.2 Hz, 1H), 8.49 (s, 1H), 8.72-8.73 (d, *J* = 2.2 Hz, 1H), 12.68 (s, 1H, NH); ^{13}C NMR (50 MHz, DMSO-d_6) δ: 104.70 (s), 112.69 (s), 118.28 (s), 127.48 (dx2), 129.47 (dx2), 129.62 (s), 130.84 (d), 131.09 (d), 131.29 (d), 144.49 (d), 147.18 (s), 161.97 (s), 164.75 (s); *Anal.* Calculated for $C_{15}H_9BrN_4S$ (MW: 357,23): C, 50.43; H, 2.54; N, 15.68%. Found C, 50.49; H, 2.40; N, 15.77%.

5-bromo-1-methyl-3-(5-phenyl-1,3,4-thiadiazol-2-yl)-7-azaindole (22d):

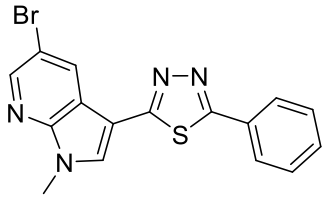

Yield: 82%; beige solid; m.p.: 187-188°C; ^{1}H NMR (200 MHz, DMSO-d_6) δ: 3.92 (s, 3H, CH_3), 7.58-7.61 (t, *J* = 3.3 Hz, 3H), 7.99-8.00 (d, *J* = 2.5 Hz, 1H), 8.03-8.04 (d, *J* = 3.3 Hz, 1H), 8.53-8.54 (d, *J* = 2.3 Hz, 1H), 8.57 (s, 1H), 8.72-8.73 (d, *J* = 2.2 Hz, 1H); *Anal.* Calculated for $C_{16}H_{11}BrN_4S$ (MW: 371,26): C, 51.76; H, 2.99; N, 15.09%. Found C, 51.70; H, 2.79; N, 15.25%.

5.2 Biology

5.2.1 *In vitro* viability assay

Cytotoxic activity of derivatives **19,20,21,22** against seven PDAC cell lines was determined by the sulforhodamine B (SRB) chemosensitivity assay. The sulforhodamine B (SRB), a pink anionic amino xanthene protein dye with two sulfonic groups, has been used to the quantification of cellular proteins content of adherent cultures. Its distribution and its ability to bind biological components, such as cellular proteins, within and between biological cell (histochemistry) is like that of related dyes, such as Coomassie brilliant blue154, naphthol yellow S154, and bromophenol blue160, which are widely used as protein stains. The SRB assay is based on the property of SRB, which binds stoichiometrically, by electrostatic complex formation, to basic amino acid residues of proteins under mild acidic conditions and then can be extracted using basic conditions. This molecule is UV active, and the quantification of the dye bound to the cells at 490 or 540 nm, provides an estimate of total protein mass, which is related to number of viable cells. In other words, the greater the number of viable cells, the greater the amount of dye responsible for a more intense colour and greater absorption capacity.

Optimized cell numbers (3000-5000 cells/well) were seeded into 96 wells flat bottom plates in 100 µl of cell line specific medium. After a 24 hours pre-incubation period at 37°C and 5.0% CO_2, cells of the test plate were treated with the compounds at screening concentrations and incubated at 37°C for 72 hours. After the treatment, cells were fixed with 25 µl of cold 50% trichloroacetic acid (TCA) for each well and incubated for at least 60 minutes at 4 °C. Afterwards plates were washed five times with demi-water and left to dry for at least 1 hour. Then, the plates were stained with 50 µl of 0.4% SRB solution in 1% acetic acid for 15 minutes. The excess stain was rinsed off by placing the plates under running 1% acetic acid and allowed to dry at room temperature for at least 2 hours. SRB staining was rinsed with 150 µl tris(hydroxymethyl)aminomethane solution pH= 8.8 (TRIS-base), and the OD (optical density) was read at 490 nm. Each assay was performed in triplicate as three independent experiments. The comparison of the average optical density of the growth in control wells with that in the sample wells allowed estimating the cell growth percentage, using the following equation:

$$Cell\ Growth = \frac{\text{mean ODcompound} - \text{mean ODday zero plate}}{\text{mean ODcontrol cells} - \text{mean ODday zero plate}} * 100$$

The results obtained were adjusted by the day zero plate (wells containing cells growing for only 24 hours) and normalized by the control cells (wells with untreated cells) to obtain the rate of viable cells.

5.2.2 Cell cycle analysis

Cell cycle stage was analyzed by flow cytometry. Optimized numbers of cells (5 x 10^5 cells/ml) were seeded in 6-well plates. After an overnight incubation at 37 °C, the cells were treated with the compound **19b**, at two concentrations (2 μM and 4-fold IC_{50}) and incubated for 24 hours. After treatment, the cells were harvested by trypsinization (250 μl trypsine-EDTA/well), incubated until the cells detached, re-suspended using the same medium used for culture, collected in FAC tubes, and washed with 1.5 ml PBS (phosphate-buffered saline). The samples were then centrifuged to form a pellet (5 minutes at 1500 rpm). These pellets were fixed in 1 ml of ice-cold 70% ethanol, drop by drop during vortex, and placed in the refrigerator at 4°C overnight. Dopo overnight cells were washed twice with PBS, centrifuged (5 minutes at 1500 rpm), re-suspended in 50 μl of RNase (100 μg/ml) and incubated for 30 minutes at 37 °C. Finally, 200 μl of propidium iodide solution (PI, 50 μg/ml) was added, and the cells distribution in the various phases of the cell cycle was analyzed in a FACS (Fluorescence Activated Cell Sorting) Calibur instrument.

PI is an interlayer that selectively binds nucleic acids. It also acts as a synthetic dye characterized by a low fluorescence (red-orange). The PI is in fact able to establish a stable bond with the DNA, intercalating between two pairs of adjacent bases, with a stoichiometry of one dye per 4–5 base pairs of DNA. Once the dye is bound to nucleic acids, it increases twenty-thirty times, compared to the free dye, its quantum fluorescence efficiency. The PI is therefore an excellent fluorescent "marker" of the double helix nucleic acids, thus providing information on the amount of DNA content in the cells, in relation to the emitted fluorescence intensity (the higher the DNA content, the greater the fluorescence). It is known that the DNA content varies according to the phase of the cycle in which a cell is located. In particular, the G2 phase and mitosis (M) have double amount of DNA compared to the G1 phase, while during the DNA synthesis phase (S phase), the cell has a quantity of DNA intermediate between the content in G1 and G2. This technique allows to analyze the cells percentage in the various phases of the cell cycle (G0/G1, S and G2/M), as well as to evaluate possible blocks.

5.2.3 *In vitro* wound healing assay

Cell migration was assessed using a Scratch wound healing assay. Optimized numbers of cells (3-5 x 10^4 cells/well) were seeded in a 96-well plate, to form confluent monolayer. Subsequently, a scratch was performed in each well with a 96-pin scratcher (Figure 34b), allowing the formation of uniform scratches. The detached cell after the scratch induction were removed. Immediately after this passage, cells were cultured for 24 hours in complete medium with each compound (4-fold IC_{50}) for experimental wells or without any drug for the control wells, incubated at 37 °C and 5.0% CO_2. Pictures were taken with an optical microscope at different time points (0, 4, 8, 20 and 24 hours; Figure 34a) and analyzed with the Scratch Assay 6.2 software DCILabs (Digital Cell Imaging Labs, Keerbergen, Belgium). The migration assay was performed in technical and biological triplicates.

The migration percentage was calculated using the following equation:

$$\%\, Migration = \frac{\text{wound width at T} = 0 \; - \; \text{wound width at T} = \text{X}}{\text{wound width at T} = 0} * 100$$

6. REFERENCES:

[1] T. Irie, M. Sawa, 7-Azaindole: A Versatile Scaffold for Developing Kinase Inhibitors, Chem Pharm Bull (Tokyo). 66 (2018) 29–36. https://doi.org/10.1248/cpb.c17-00380.

[2] R. Kannaiyan, D. Mahadevan, A comprehensive review of protein kinase inhibitors for cancer therapy, Expert Rev Anticancer Ther. 18 (2018) 1249–1270. https://doi.org/10.1080/14737140.2018.1527688.

[3] Z. Gagic, D. Ruzic, N. Djokovic, T. Djikic, K. Nikolic, In silico Methods for Design of Kinase Inhibitors as Anticancer Drugs, Front Chem. 7 (2020) 873. https://doi.org/10.3389/fchem.2019.00873.

[4] J.D.R. Knight, B. Qian, D. Baker, R. Kothary, Conservation, Variability and the Modeling of Active Protein Kinases, PLoS One. 2 (2007) 982. https://doi.org/10.1371/journal.pone.0000982.

[5] R. Roskoski, Properties of FDA-approved small molecule protein kinase inhibitors: A 2020 update, Pharmacol Res. 152 (2020) 104609. https://doi.org/10.1016/j.phrs.2019.104609.

[6] R. Roskoski Jr., Properties of FDA-approved small molecule protein kinase inhibitors: A 2022 update, Pharmacol Res. 175 (2022) 106037. https://doi.org/10.1016/j.phrs.2021.106037.

[7] Z. Zhang, L. Bu, J. Luo, J. Guo, Targeting protein kinases benefits cancer immunotherapy, Biochimica et Biophysica Acta (BBA) - Reviews on Cancer. 1877 (2022) 188738. https://doi.org/10.1016/j.bbcan.2022.188738.

[8] C.C. Ayala-Aguilera, T. Valero, Á. Lorente-Macías, D.J. Baillache, S. Croke, A. Unciti-Broceta, Small Molecule Kinase Inhibitor Drugs (1995–2021): Medical Indication, Pharmacology, and Synthesis, J Med Chem. 65 (2022) 1047–1131. https://doi.org/10.1021/acs.jmedchem.1c00963.

[9] X. Gong, M. Hu, J. Liu, G. Kim, J. Xu, A. McKee, T. Palmby, R.A. de Claro, L. Zhao, Decoding kinase-adverse event associations for small molecule kinase inhibitors, Nat Commun. 13 (2022) 4349. https://doi.org/10.1038/s41467-022-32033-5.

[10] K.S. Bhullar, N.O. Lagarón, E.M. McGowan, I. Parmar, A. Jha, B.P. Hubbard, H.P.V. Rupasinghe, Kinase-targeted cancer therapies: progress, challenges and future directions, Mol Cancer. 17 (2018) 48. https://doi.org/10.1186/s12943-018-0804-2.

[11] P. Wu, T.E. Nielsen, M.H. Clausen, Small-molecule kinase inhibitors: an analysis of FDA-approved drugs, Drug Discov Today. 21 (2016) 5–10. https://doi.org/10.1016/j.drudis.2015.07.008.

[12] J.Y. Jeon, A. Sparreboom, S.D. Baker, Kinase Inhibitors: The Reality Behind the Success, Clin Pharmacol Ther. 102 (2017) 726–730. https://doi.org/10.1002/cpt.815.

[13] A. v. Danilov, S. Hu, B. Orr, K. Godek, L.M. Mustachio, D. Sekula, X. Liu, M. Kawakami, F.M. Johnson, D.A. Compton, S.J. Freemantle, E. Dmitrovsky, Dinaciclib Induces Anaphase Catastrophe in Lung Cancer Cells via Inhibition of Cyclin-Dependent Kinases 1 and 2, Mol Cancer Ther. 15 (2016) 2758–2766. https://doi.org/10.1158/1535-7163.MCT-16-0127.

[14] R. Roskoski, Cyclin-dependent protein serine/threonine kinase inhibitors as anticancer drugs, Pharmacol Res. 139 (2019) 471–488. https://doi.org/10.1016/j.phrs.2018.11.035.

[15] R. Roskoski, Properties of FDA-approved small molecule protein kinase inhibitors, Pharmacol Res. 144 (2019) 19–50. https://doi.org/10.1016/j.phrs.2019.03.006.

[16] S.M. Pham, J. Kankanala, J.D. Pettigrew, C.P. Miller, Pujala Brahmam, B. Bhatt, V. Kumar, A.K. Nayak, A.S. Shete, S. Soni, Heterocyclic compounds as kinase inhibitors. Patent WO2022236257A1, n.d.

[17] B. Jiang, E.S. Wang, K.A. Donovan, Y. Liang, E.S. Fischer, T. Zhang, N.S. Gray, Development of Dual and Selective Degraders of Cyclin-Dependent Kinases 4 and 6, Angewandte Chemie International Edition. 58 (2019) 6321–6326. https://doi.org/10.1002/anie.201901336.

[18] A. Ammazzalorso, M. Agamennone, B. de Filippis, M. Fantacuzzi, Development of CDK4/6 Inhibitors: A Five Years Update, Molecules. 26 (2021) 1488. https://doi.org/10.3390/molecules26051488.

[19] N.J. Vogelzang, B. George, N. Ashenbramer, W.J. Edenfield, D. Richards, M.E. Gross, G.D. Fine, P. Martinez, Abstract CT191: Phase 1, first-in-human, dose-escalation study of oral TP-1287, a cyclin dependent kinase 9 (CDK9) inhibitor, in patients (pts) with advanced solid tumors (ASTs), Cancer Res. 82 (2022) CT191–CT191. https://doi.org/10.1158/1538-7445.AM2022-CT191.

[20] S. Rajput, N. Khera, Z. Guo, J. Hoog, S. Li, C.X. Ma, Inhibition of cyclin dependent kinase 9 by dinaciclib suppresses cyclin B1 expression and tumor growth in triple negative breast cancer, Oncotarget. 7 (2016) 56864–56875. https://doi.org/10.18632/oncotarget.10870.

[21] D. Parry, T. Guzi, F. Shanahan, N. Davis, D. Prabhavalkar, D. Wiswell, W. Seghezzi, K. Paruch, M.P. Dwyer, R. Doll, A. Nomeir, W. Windsor, T. Fischmann, Y. Wang, M. Oft, T. Chen, P. Kirschmeier, E.M. Lees, Dinaciclib (SCH 727965), a Novel and Potent Cyclin-Dependent Kinase Inhibitor, Mol Cancer Ther. 9 (2010) 2344–2353. https://doi.org/10.1158/1535-7163.MCT-10-0324.

[22] I. Gojo, M. Sadowska, A. Walker, E.J. Feldman, S.P. Iyer, M.R. Baer, E.A. Sausville, R.G. Lapidus, D. Zhang, Y. Zhu, Y.-M. Jou, J. Poon, K. Small, R. Bannerji, Clinical and laboratory studies of the novel cyclin-dependent kinase inhibitor dinaciclib (SCH 727965) in acute leukemias, Cancer Chemother Pharmacol. 72 (2013) 897–908. https://doi.org/10.1007/s00280-013-2249-z.

[23] P. Ghia, L. Scarfò, S. Perez, K. Pathiraja, M. Derosier, K. Small, C. McCrary Sisk, N. Patton, Efficacy and safety of dinaciclib vs ofatumumab in patients with relapsed/refractory chronic lymphocytic leukemia, Blood. 129 (2017) 1876–1878. https://doi.org/10.1182/blood-2016-10-748210.

[24] L. Meijer, E. Raymond, Roscovitine and Other Purines as Kinase Inhibitors. From Starfish Oocytes to Clinical Trials, Acc Chem Res. 36 (2003) 417–425. https://doi.org/10.1021/ar0201198.

[25] M. Malumbres, M. Barbacid, Cell cycle, CDKs and cancer: a changing paradigm, Nat Rev Cancer. 9 (2009) 153–166. https://doi.org/10.1038/nrc2602.

[26] L. le Roy, A. Letondor, C. le Roux, A. Amara, S. Timsit, Cellular and Molecular Mechanisms of R/S-Roscovitine and CDKs Related Inhibition under Both Focal and Global Cerebral Ischemia: A Focus on Neurovascular Unit and Immune Cells, Cells. 10 (2021) 104. https://doi.org/10.3390/cells10010104.

[27] W. DePinto, X.-J. Chu, X. Yin, M. Smith, K. Packman, P. Goelzer, A. Lovey, Y. Chen, H. Qian, R. Hamid, Q. Xiang, C. Tovar, R. Blain, T. Nevins, B. Higgins, L. Luistro, K. Kolinsky, B. Felix, S. Hussain, D. Heimbrook, In vitro and in vivo activity of R547: a potent and selective cyclin-dependent kinase inhibitor currently in phase I clinical trials, Mol Cancer Ther. 5 (2006) 2644–2658. https://doi.org/10.1158/1535-7163.MCT-06-0355.

[28] R. Wijnen, C. Pecoraro, D. Carbone, H. Fiuji, A. Avan, G.J. Peters, E. Giovannetti, P. Diana, Cyclin Dependent Kinase-1 (CDK-1) Inhibition as a Novel Therapeutic Strategy against Pancreatic Ductal Adenocarcinoma (PDAC), Cancers (Basel). 13 (2021) 4389. https://doi.org/10.3390/cancers13174389.

[29] M. Zhang, L. Zhang, R. Hei, X. Li, H. Cai, X. Wu, Q. Zheng, C. Cai, CDK inhibitors in cancer therapy, an overview of recent development., Am J Cancer Res. 11 (2021) 1913–1935.

[30] P. Chen, N. v. Lee, W. Hu, M. Xu, R.A. Ferre, H. Lam, S. Bergqvist, J. Solowiej, W. Diehl, Y.-A. He, X. Yu, A. Nagata, T. VanArsdale, B.W. Murray, Spectrum and Degree of CDK Drug Interactions

Predicts Clinical Performance, Mol Cancer Ther. 15 (2016) 2273–2281. https://doi.org/10.1158/1535-7163.MCT-16-0300.

[31] S. Sofi, U. Mehraj, H. Qayoom, S. Aisha, A. Almilaibary, M. Alkhanani, M.A. Mir, Targeting cyclin-dependent kinase 1 (CDK1) in cancer: molecular docking and dynamic simulations of potential CDK1 inhibitors, Medical Oncology. 39 (2022) 133. https://doi.org/10.1007/s12032-022-01748-2.

[32] U. Asghar, A.K. Witkiewicz, N.C. Turner, E.S. Knudsen, The history and future of targeting cyclin-dependent kinases in cancer therapy, Nat Rev Drug Discov. 14 (2015) 130–146. https://doi.org/10.1038/nrd4504.

[33] T. Ettl, D. Schulz, R.J. Bauer, The Renaissance of Cyclin Dependent Kinase Inhibitors, Cancers (Basel). 14 (2022) 293. https://doi.org/10.3390/cancers14020293.

[34] G. Augello, M.R. Emma, A. Cusimano, A. Azzolina, G. Montalto, J.A. McCubrey, M. Cervello, The Role of GSK-3 in Cancer Immunotherapy: GSK-3 Inhibitors as a New Frontier in Cancer Treatment, Cells. 9 (2020) 1427. https://doi.org/10.3390/cells9061427.

[35] S. Frame, P. Cohen, R.M. Biondi, A Common Phosphate Binding Site Explains the Unique Substrate Specificity of GSK3 and Its Inactivation by Phosphorylation, Mol Cell. 7 (2001) 1321–1327. https://doi.org/10.1016/S1097-2765(01)00253-2.

[36] I. Khan, M.A. Tantray, M.S. Alam, H. Hamid, Natural and synthetic bioactive inhibitors of glycogen synthase kinase, Eur J Med Chem. 125 (2017) 464–477. https://doi.org/10.1016/j.ejmech.2016.09.058.

[37] P. Wadhwa, P. Jain, H.R. Jadhav, Glycogen Synthase Kinase 3 (GSK3): Its Role and Inhibitors, Curr Top Med Chem. 20 (2020) 1522–1534. https://doi.org/10.2174/1568026620666200516153136.

[38] L. Ding, D.D. Billadeau, Glycogen synthase kinase-3β: a novel therapeutic target for pancreatic cancer, Expert Opin Ther Targets. 24 (2020) 417–426. https://doi.org/10.1080/14728222.2020.1743681.

[39] A. Vulpetti, P. Crivori, A. Cameron, J. Bertrand, M.G. Brasca, R. D'Alessio, P. Pevarello, Structure-Based Approaches to Improve Selectivity: CDK2−GSK3β Binding Site Analysis, J Chem Inf Model. 45 (2005) 1282–1290. https://doi.org/10.1021/ci0500280.

[40] A.P. Saraswati, S.M. Ali Hussaini, N.H. Krishna, B.N. Babu, A. Kamal, Glycogen synthase kinase-3 and its inhibitors: Potential target for various therapeutic conditions, Eur J Med Chem. 144 (2018) 843–858. https://doi.org/10.1016/j.ejmech.2017.11.103.

[41] J.E. Gray, J.R. Infante, L.H. Brail, G.R. Simon, J.F. Cooksey, S.F. Jones, D.L. Farrington, A. Yeo, K.A. Jackson, K.H. Chow, M.J. Zamek-Gliszczynski, H.A. Burris, A first-in-human phase I dose-escalation, pharmacokinetic, and pharmacodynamic evaluation of intravenous LY2090314, a glycogen synthase kinase 3 inhibitor, administered in combination with pemetrexed and carboplatin, Invest New Drugs. 33 (2015) 1187–1196. https://doi.org/10.1007/s10637-015-0278-7.

[42] D.A. Rizzieri, S. Cooley, O. Odenike, L. Moonan, K.H. Chow, K. Jackson, X. Wang, L. Brail, G. Borthakur, An open-label phase 2 study of glycogen synthase kinase-3 inhibitor LY2090314 in patients with acute leukemia, Leuk Lymphoma. 57 (2016) 1800–1806. https://doi.org/10.3109/10428194.2015.1122781.

[43] S. Russi, A. Sgambato, A.M. Bochicchio, P. Zoppoli, M. Aieta, A.M.L. Capobianco, V. Ruggieri, E. Zifarone, G. Falco, S. Laurino, CHIR99021, trough GSK-3β Targeting, Reduces Epithelioid Sarcoma Cell Proliferation by Activating Mitotic Catastrophe and Autophagy, Int J Mol Sci. 22 (2021) 11147. https://doi.org/10.3390/ijms222011147.

[44] T.L. Mathuram, V. Ravikumar, L.M. Reece, S. Karthik, C.S. Sasikumar, K.M. Cherian, Tideglusib induces apoptosis in human neuroblastoma IMR32 cells, provoking sub-G0/G1 accumulation and ROS

generation, Environ Toxicol Pharmacol. 46 (2016) 194–205. https://doi.org/10.1016/j.etap.2016.07.013.

[45] L. Serenó, M. Coma, M. Rodríguez, P. Sánchez-Ferrer, M.B. Sánchez, I. Gich, J.M. Agulló, M. Pérez, J. Avila, C. Guardia-Laguarta, J. Clarimón, A. Lleó, T. Gómez-Isla, A novel GSK-3β inhibitor reduces Alzheimer's pathology and rescues neuronal loss in vivo, Neurobiol Dis. 35 (2009) 359–367. https://doi.org/10.1016/j.nbd.2009.05.025.

[46] W. Mai, K. Kawakami, A. Shakoori, S. Kyo, K. Miyashita, K. Yokoi, M. Jin, T. Shimasaki, Y. Motoo, T. Minamoto, Deregulated GSK3β Sustains Gastrointestinal Cancer Cells Survival by Modulating Human Telomerase Reverse Transcriptase and Telomerase, Clinical Cancer Research. 15 (2009) 6810–6819. https://doi.org/10.1158/1078-0432.CCR-09-0973.

[47] L.T. Pierce, M.M. Cahill, H.J. Winfield, F.O. McCarthy, Synthesis and identification of novel indolo[2,3-a]pyrimido[5,4-c]carbazoles as a new class of anti-cancer agents, Eur J Med Chem. 56 (2012) 292–300. https://doi.org/10.1016/j.ejmech.2012.08.002.

[48] A. Carbone, B. Parrino, P. Barraja, V. Spanò, G. Cirrincione, P. Diana, A. Maier, G. Kelter, H.H. Fiebig, Synthesis and antiproliferative activity of 2,5-bis(3′-Indolyl) pyrroles, analogues of the marine alkaloid nortopsentin, Mar Drugs. 11 (2013) 643–654. https://doi.org/10.3390/md11030643.

[49] P. Diana, A. Carbone, P. Barraja, A. Martorana, O. Gia, L. DallaVia, G. Cirrincione, 3,5-Bis(3′-indolyl)pyrazoles, analogues of marine alkaloid nortopsentin: Synthesis and antitumor properties, Bioorg Med Chem Lett. 17 (2007) 6134–6137. https://doi.org/10.1016/j.bmcl.2007.09.042.

[50] P. Diana, A. Carbone, P. Barraja, A. Montalbano, A. Martorana, G. Dattolo, O. Gia, L.D. Via, G. Cirrincione, Synthesis and antitumor properties of 2,5-bis(3′-indolyl)thiophenes: Analogues of marine alkaloid nortopsentin, Bioorg Med Chem Lett. 17 (2007) 2342–2346. https://doi.org/10.1016/j.bmcl.2007.01.065.

[51] Q. Zhou, A.F. Phoa, R.H. Abbassi, M. Hoque, T.A. Reekie, J.S. Font, R.M. Ryan, B.W. Stringer, B.W. Day, T.G. Johns, L. Munoz, M. Kassiou, Structural Optimization and Pharmacological Evaluation of Inhibitors Targeting Dual-Specificity Tyrosine Phosphorylation-Regulated Kinases (DYRK) and CDC-like kinases (CLK) in Glioblastoma, J Med Chem. 60 (2017) 2052–2070. https://doi.org/10.1021/acs.jmedchem.6b01840.

[52] K. Nelms, R. Natoli, B. Schwartz, Methods of treating ocular disorders, 2017.

[53] J. Tsai, J.T. Lee, W. Wang, J. Zhang, H. Cho, S. Mamo, R. Bremer, S. Gillette, J. Kong, N.K. Haass, K. Sproesser, L. Li, K.S.M. Smalley, D. Fong, Y.-L. Zhu, A. Marimuthu, H. Nguyen, B. Lam, J. Liu, I. Cheung, J. Rice, Y. Suzuki, C. Luu, C. Settachatgul, R. Shellooe, J. Cantwell, S.-H. Kim, J. Schlessinger, K.Y.J. Zhang, B.L. West, B. Powell, G. Habets, C. Zhang, P.N. Ibrahim, P. Hirth, D.R. Artis, M. Herlyn, G. Bollag, Discovery of a selective inhibitor of oncogenic B-Raf kinase with potent antimelanoma activity, Proceedings of the National Academy of Sciences. 105 (2008) 3041–3046. https://doi.org/10.1073/pnas.0711741105.

[54] D.R. Motati, R. Amaradhi, T. Ganesh, Azaindole therapeutic agents, Bioorg Med Chem. 28 (2020) 115830. https://doi.org/10.1016/j.bmc.2020.115830.

[55] T. Al-Warhi, A.M. el Kerdawy, N. Aljaeed, O.E. Ismael, R.R. Ayyad, W.M. Eldehna, H.A. Abdel-Aziz, G.H. Al-Ansary, Synthesis, Biological Evaluation and In Silico Studies of Certain Oxindole–Indole Conjugates as Anticancer CDK Inhibitors, Molecules. 25 (2020) 2031. https://doi.org/10.3390/molecules25092031.

[56] T. Adon, D. Shanmugarajan, H.Y. Kumar, CDK4/6 inhibitors: a brief overview and prospective research directions, RSC Adv. 11 (2021) 29227–29246. https://doi.org/10.1039/D1RA03820F.

[57] A. K. Rathi, R. Syed, V. Singh, H.-S. Shin, R. v. Patel, Kinase Inhibitor Indole Derivatives as Anticancer Agents: A Patent Review, Recent Pat Anticancer Drug Discov. 12 (2017) 55–72. https://doi.org/10.2174/1574892811666161003112119.

[58] A. Kumar, V. Rajendran, R. Sethumadhavan, R. Purohit, AKT Kinase Pathway: A Leading Target in Cancer Research, The Scientific World Journal. 2013 (2013) 1–6. https://doi.org/10.1155/2013/756134.

[59] B.J. Greber, J.M. Perez-Bertoldi, K. Lim, A.T. Iavarone, D.B. Toso, E. Nogales, The cryoelectron microscopy structure of the human CDK-activating kinase, Proceedings of the National Academy of Sciences. 117 (2020) 22849–22857. https://doi.org/10.1073/pnas.2009627117.

[60] V. Kumar, S. Parate, G. Thakur, G. Lee, H.-S. Ro, Y. Kim, H.J. Kim, M.O. Kim, K.W. Lee, Identification of CDK7 Inhibitors from Natural Sources Using Pharmacoinformatics and Molecular Dynamics Simulations, Biomedicines. 9 (2021) 1197. https://doi.org/10.3390/biomedicines9091197.

[61] S. Hu, J.J. Marineau, N. Rajagopal, K.B. Hamman, Y.J. Choi, D.R. Schmidt, N. Ke, L. Johannessen, M.J. Bradley, D.A. Orlando, S.R. Alnemy, Y. Ren, S. Ciblat, D.K. Winter, A. Kabro, K.T. Sprott, J.G. Hodgson, C.C. Fritz, J.P. Carulli, E. di Tomaso, E.R. Olson, Discovery and Characterization of SY-1365, a Selective, Covalent Inhibitor of CDK7, Cancer Res. 79 (2019) 3479–3491. https://doi.org/10.1158/0008-5472.CAN-19-0119.

[62] E. Panagiotou, G. Gomatou, I.P. Trontzas, N. Syrigos, E. Kotteas, Cyclin-dependent kinase (CDK) inhibitors in solid tumors: a review of clinical trials, Clinical and Translational Oncology. 24 (2022) 161–192. https://doi.org/10.1007/s12094-021-02688-5.

[63] H. Liang, J. Du, R.M. Elhassan, X. Hou, H. Fang, Recent progress in development of cyclin-dependent kinase 7 inhibitors for cancer therapy, Expert Opin Investig Drugs. 30 (2021) 61–76. https://doi.org/10.1080/13543784.2021.1850693.

[64] J.J. Marineau, K.B. Hamman, S. Hu, S. Alnemy, J. Mihalich, A. Kabro, K.M. Whitmore, D.K. Winter, S. Roy, S. Ciblat, N. Ke, A. Savinainen, A. Wilsily, G. Malojcic, R. Zahler, D. Schmidt, M.J. Bradley, N.J. Waters, C. Chuaqui, Discovery of SY-5609: A Selective, Noncovalent Inhibitor of CDK7, J Med Chem. 65 (2022) 1458–1480. https://doi.org/10.1021/acs.jmedchem.1c01171.

[65] H. Nakano, T. Hasegawa, H. Kojima, T. Okabe, T. Nagano, Design and Synthesis of Potent and Selective PIM Kinase Inhibitors by Targeting Unique Structure of ATP-Binding Pocket, ACS Med Chem Lett. 8 (2017) 504–509. https://doi.org/10.1021/acsmedchemlett.6b00518.

[66] D. Carbone, B. Parrino, S. Cascioferro, C. Pecoraro, E. Giovannetti, V. di Sarno, S. Musella, G. Auriemma, G. Cirrincione, P. Diana, 1,2,4-Oxadiazole Topsentin Analogs with Antiproliferative Activity against Pancreatic Cancer Cells, Targeting GSK3β Kinase, ChemMedChem. 16 (2021) 537–554. https://doi.org/10.1002/cmdc.202000752.

[67] C. Pecoraro, B. Parrino, S. Cascioferro, A. Puerta, A. Avan, G.J. Peters, P. Diana, E. Giovannetti, D. Carbone, A New Oxadiazole-Based Topsentin Derivative Modulates Cyclin-Dependent Kinase 1 Expression and Exerts Cytotoxic Effects on Pancreatic Cancer Cells, Molecules. 27 (2021) 19. https://doi.org/10.3390/molecules27010019.

[68] V. Spanò, A. Attanzio, S. Cascioferro, A. Carbone, A. Montalbano, P. Barraja, L. Tesoriere, G. Cirrincione, P. Diana, B. Parrino, Synthesis and antitumor activity of new thiazole nortopsentin analogs, Mar Drugs. 14 (2016). https://doi.org/10.3390/md14120226.

[69] P. Diana, A. Carbone, P. Barraja, A. Montalbano, B. Parrino, A. Lopergolo, M. Pennati, N. Zaffaroni, G. Cirrincione, Synthesis and Antitumor Activity of 3-(2-Phenyl-1,3-thiazol-4-yl)-1H-indoles and 3-

(2-Phenyl-1,3-thiazol-4-yl)-1H-7-azaindoles, ChemMedChem. 6 (2011) 1300–1309. https://doi.org/10.1002/cmdc.201100078.

[70] A. Carbone, M. Pennati, B. Parrino, A. Lopergolo, P. Barraja, A. Montalbano, V. Spanò, S. Sbarra, V. Doldi, M. de Cesare, G. Cirrincione, P. Diana, N. Zaffaroni, Novel 1H-pyrrolo[2,3-b]pyridine derivative nortopsentin analogues: Synthesis and antitumor activity in peritoneal mesothelioma experimental models, J Med Chem. 56 (2013) 7060–7072. https://doi.org/10.1021/jm400842x.

[71] B. Parrino, A. Attanzio, V. Spanò, S. Cascioferro, A. Montalbano, P. Barraja, L. Tesoriere, P. Diana, G. Cirrincione, A. Carbone, Synthesis, antitumor activity and CDK1 inhibiton of new thiazole nortopsentin analogues, Eur J Med Chem. 138 (2017) 371–383. https://doi.org/10.1016/j.ejmech.2017.06.052.

[72] S. di Franco, B. Parrino, M. Gaggianesi, V.D. Pantina, P. Bianca, A. Nicotra, L.R. Mangiapane, M. lo Iacono, G. Ganduscio, V. Veschi, O.R. Brancato, A. Glaviano, A. Turdo, I. Pillitteri, L. Colarossi, S. Cascioferro, D. Carbone, C. Pecoraro, M.E. Fiori, R. de Maria, M. Todaro, I. Screpanti, G. Cirrincione, P. Diana, G. Stassi, CHK1 inhibitor sensitizes resistant colorectal cancer stem cells to nortopsentin, IScience. 24 (2021) 102664. https://doi.org/10.1016/j.isci.2021.102664.

[73] R.M. Abdel-Motaleb, A.-M.A.-S. Makhloof, H.M. Ibrahim, M.H. Elnagdi, Studies with azoles and benzoazoles: A novel simple approach for synthesis of 3-functionally substituted 3-acylindoles, J Heterocycl Chem. 44 (2007) 109–114. https://doi.org/10.1002/jhet.5570440119.

[74] M. Krasavin, I. Konstantinov, Minimizing Side Reactions in Classical Pyrazole Synthesis from β - Oxonitriles: The Use of Acetylhydrazine, Lett Org Chem. 5 (2008) 594–598. https://doi.org/10.2174/157017808785982266.

[75] R. Vadlakonda, R. Nerella, S. Vijaya Srinivas, Synthesis and cytotoxic evaluation of novel azaindole derivatives, Rasayan Journal of Chemistry. 10 (2017) 1316–1322. https://doi.org/10.7324/rjc.2017.1041914.

[76] K. QUINT, M. TONIGOLD, P. di FAZIO, R. MONTALBANO, S. LINGELBACH, F. RÜCKERT, B. ALINGER, M. OCKER, D. NEUREITER, Pancreatic cancer cells surviving gemcitabine treatment express markers of stem cell differentiation and epithelial-mesenchymal transition, Int J Oncol. 41 (2012) 2093–2102. https://doi.org/10.3892/ijo.2012.1648.

[77] S. Cascioferro, G.L. Petri, B. Parrino, D. Carbone, N. Funel, C. Bergonzini, G. Mantini, H. Dekker, D. Geerke, G.J. Peters, G. Cirrincione, E. Giovannetti, P. Diana, Imidazo[2,1-b] [1,3,4]thiadiazoles with antiproliferative activity against primary and gemcitabine-resistant pancreatic cancer cells, Eur J Med Chem. 189 (2020) 112088. https://doi.org/10.1016/j.ejmech.2020.112088.

[78] M. Amrutkar, I. Gladhaug, Pancreatic Cancer Chemoresistance to Gemcitabine, Cancers (Basel). 9 (2017) 157. https://doi.org/10.3390/cancers9110157.

[79] R.A. Fryer, B. Barlett, C. Galustian, A.G. Dalgleish, Mechanisms underlying gemcitabine resistance in pancreatic cancer and sensitisation by the iMiD lenalidomide., Anticancer Res. 31 11 (2011) 3747–56.

[80] P. Diana, A. Carbone, P. Barraja, G. Kelter, H.H. Fiebig, G. Cirrincione, Synthesis and antitumor activity of 2,5-bis(3′-indolyl)-furans and 3,5-bis(3′-indolyl)-isoxazoles, nortopsentin analogues, Bioorg Med Chem. 18 (2010) 4524–4529. https://doi.org/10.1016/j.bmc.2010.04.061.

[81] J. Slätt, I. Romero, J. Bergman, Cyanoacetylation of Indoles, Pyrroles and Aromatic Amines with the Combination Cyanoacetic Acid and Acetic Anhydride, Synthesis (Stuttg). 2004 (2004) 2760–2765. https://doi.org/10.1055/s-2004-831164.

[82] A.M.F. Oliveira-Campos, A.M. Salaheldin, F.A.A. Paz, L.M. Rodrigues, Synthesis of 3-indolylazoles and meridianin derivatives from indolyl enaminonitriles, Arkivoc. 2011 (2011) 121–133. https://doi.org/10.3998/ark.5550190.0012.b11.

[83] M. Venkatanarayana, P.K. Dubey, A facile cyanoacetylation of indoles with cyanocetic acid and propionic anhydride, 2013.

[84] P.Y. Choy, C.P. Lau, F.Y. Kwong, Palladium-Catalyzed Direct and Regioselective C−H Bond Functionalization/Oxidative Acetoxylation of Indoles, J Org Chem. 76 (2011) 80–84. https://doi.org/10.1021/jo101584k.

[85] Alfred.K.K. Fung, L.-J. Yu, M.S. Sherburn, M.L. Coote, Atom Transfer Radical Polymerization-Inspired Room Temperature (sp3)C–N Coupling, J Org Chem. 86 (2021) 9723–9732. https://doi.org/10.1021/acs.joc.1c01029.

[86] J.K. Laha, R.A. Bhimpuria, M.K. Hunjan, Intramolecular Oxidative Arylations in 7-Azaindoles and Pyrroles: Revamping the Synthesis of Fused N-Heterocycle Tethered Fluorenes, Chemistry - A European Journal. 23 (2017) 2044–2050. https://doi.org/10.1002/chem.201604192.

[87] C. G. Bochet, C. Helgen, Pyridine-derived Heterocycles as Potential Photoacylating Reagents, Heterocycles. 67 (2006) 797–805. https://doi.org/10.3987/COM-05-S(T)72.

[88] T. Beckers, A. Sellmer, E. Eichhorn, H. Pongratz, C. Schächtele, F. Totzke, G. Kelter, R. Krumbach, H.-H. Fiebig, F.-D. Böhmer, S. Mahboobi, Novel inhibitors of epidermal growth factor receptor: (4-(Arylamino)-7H-pyrrolo[2,3-d]pyrimidin-6-yl)(1H-indol-2-yl)methanones and (1H-indol-2-yl)(4-(phenylamino)thieno[2,3-d]pyrimidin-6-yl)methanones, Bioorg Med Chem. 20 (2012) 125–136. https://doi.org/10.1016/j.bmc.2011.11.023.

[89] E. Desarbre, S. Coudret, C. Meheust, J.-Y. Mérour, Synthesis of 2-Substituted-1H-pyrrolo[2,3-b]pyridines: Preparation of 7-azaolivacine analogue and 7-azaindolopyridopyrimidine derivatives, Tetrahedron. 53 (1997) 3637–3648. https://doi.org/10.1016/S0040-4020(97)00107-5.

[90] S. Komoriya, S. Kobayashi, K. Osanai, T. Yoshino, T. Nagata, N. Haginoya, Y. Nakamoto, A. Mochizuki, T. Nagahara, M. Suzuki, T. Shimada, K. Watanabe, Y. Isobe, T. Furugoori, Design, synthesis, and biological activity of novel factor Xa inhibitors: Improving metabolic stability by S1 and S4 ligand modification, Bioorg Med Chem. 14 (2006) 1309–1330. https://doi.org/10.1016/j.bmc.2005.09.056.

[91] C.B. Baltus, R. Jorda, C. Marot, K. Berka, V. Bazgier, V. Kryštof, G. Prié, M.-C. Viaud-Massuard, Synthesis, biological evaluation and molecular modeling of a novel series of 7-azaindole based tri-heterocyclic compounds as potent CDK2/Cyclin E inhibitors, Eur J Med Chem. 108 (2016) 701–719. https://doi.org/10.1016/j.ejmech.2015.12.023.

7. SUPPORTING INFORMATION

7.1 Representative cell cycle spectra

a **b**

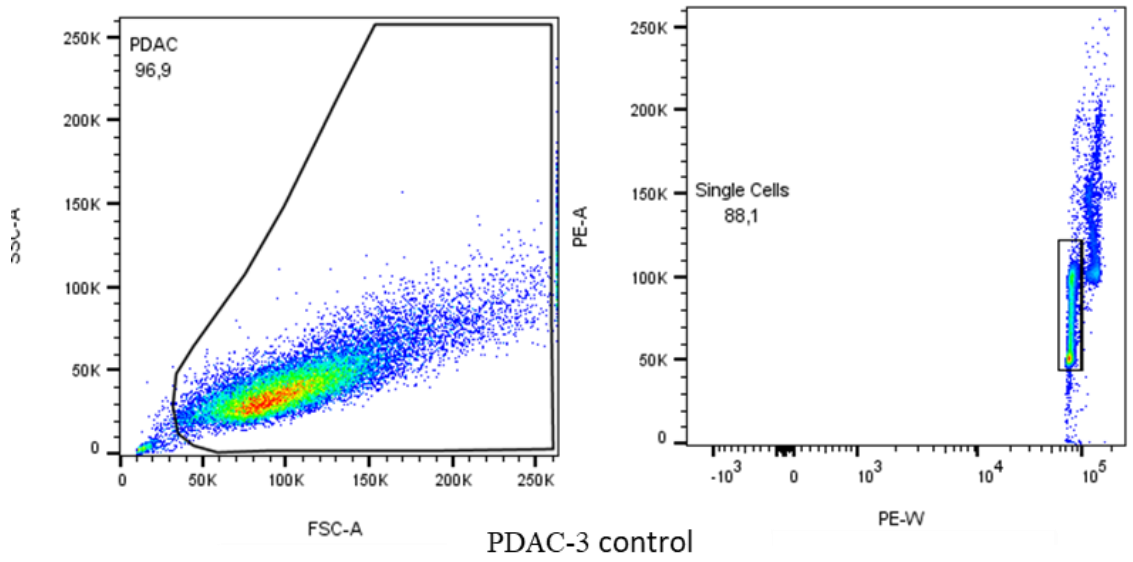

c

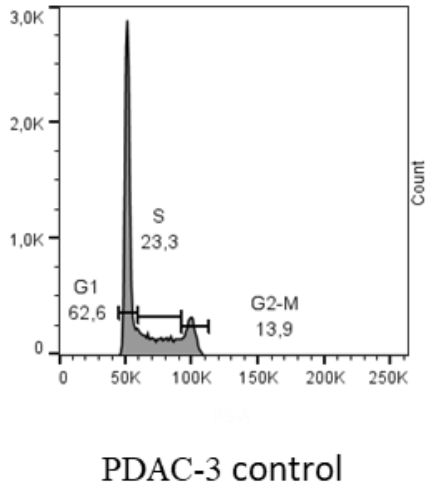

Figure 35. Flow cytometry analysis of the PDAC-3 cell cycle after 24 hours: untreated cells (negative control). (a) Tumor cells are identified on a forward scatter (FSC, X-axis) versus side scatter (SSC, Y-axis) plot and gated to exclude debris which is found in the lower left corner. (b) The color of each point represents the density of events at the corresponding intensity values. (c) Representative DNA fluorescence histogram of PI-stained cells: their fluorescence is determined on a linear fluorescence scale reported on X-axis, whilst cell count is reported on Y-axis. The cell cycle fitting algorithm is used to separate the population into G1, S, and G2 phases of the cell cycle.

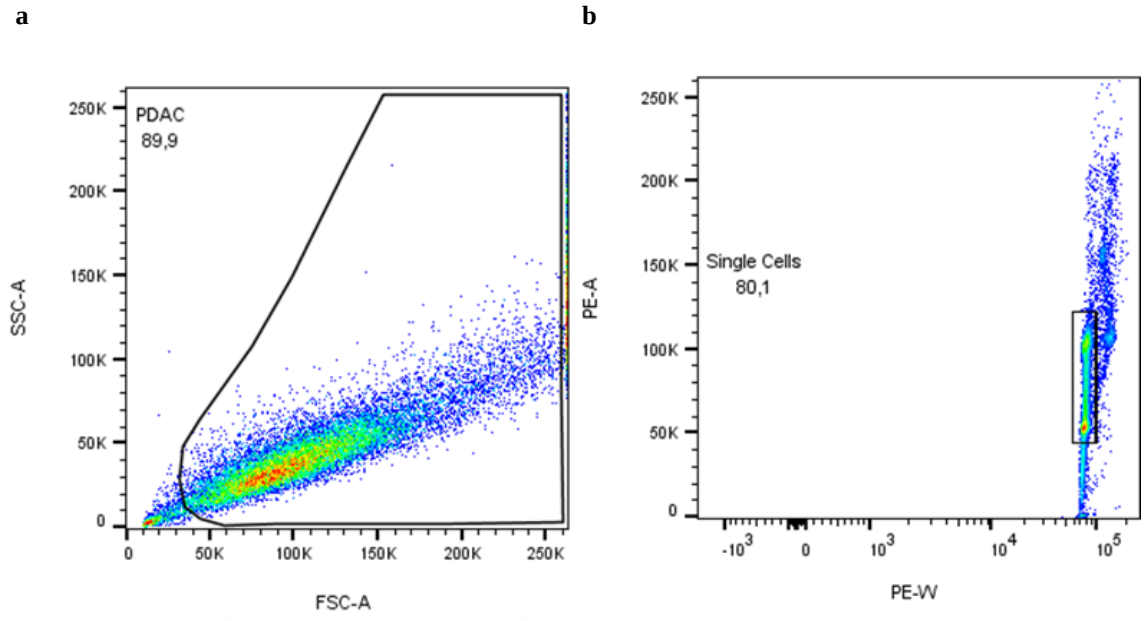

Figure 36. Flow cytometry analysis of the PDAC-3 cell cycle after 24 hours: cells after treatment with the compound **19b** at concentration of 2 µM. (a) Tumor cells are identified on a forward scatter (FSC, X-axis) versus side scatter (SSC, Y-axis) plot and gated to exclude debris which is found in the lower left corner. (b) The color of each point represents the density of events at the corresponding intensity values. (c) Representative DNA fluorescence histogram of PI-stained cells: their fluorescence is determined on a linear fluorescence scale reported on X-axis, whilst cell count is reported on Y-axis. The cell cycle fitting algorithm is used to separate the population into G1, S, and G2 phases of the cell cycle.

a **b**

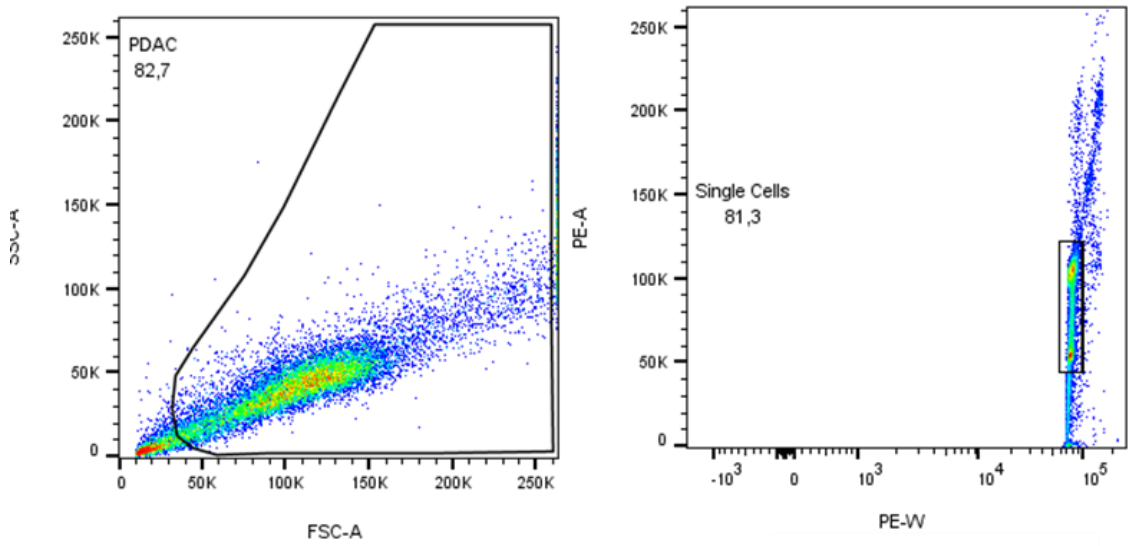

PDAC-3 4xIC$_{50}$ compound **19b**

c

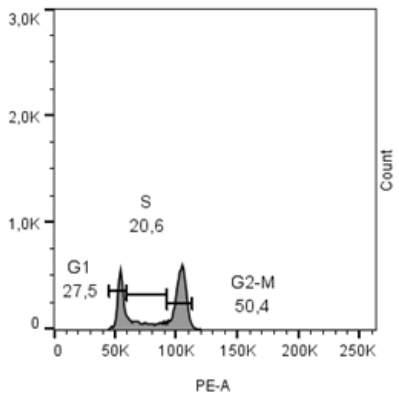

PDAC-3 4xIC$_{50}$ compound **19b**

Figure 37. Flow cytometry analysis of the PDAC-3 cell cycle after 24 hours: cells after treatment with the compound **19b** at concentration of 4 x IC$_{50}$. (a) Tumor cells are identified on a forward scatter (FSC, X-axis) versus side scatter (SSC, Y-axis) plot and gated to exclude debris which is found in the lower left corner. (b) The color of each point represents the density of events at the corresponding intensity values. (c) Representative DNA fluorescence histogram of PI-stained cells: their fluorescence is determined on a linear fluorescence scale reported on X-axis, whilst cell count is reported on Y-axis. The cell cycle fitting algorithm is used to separate the population into G1, S, and G2 phases of the cell cycle.

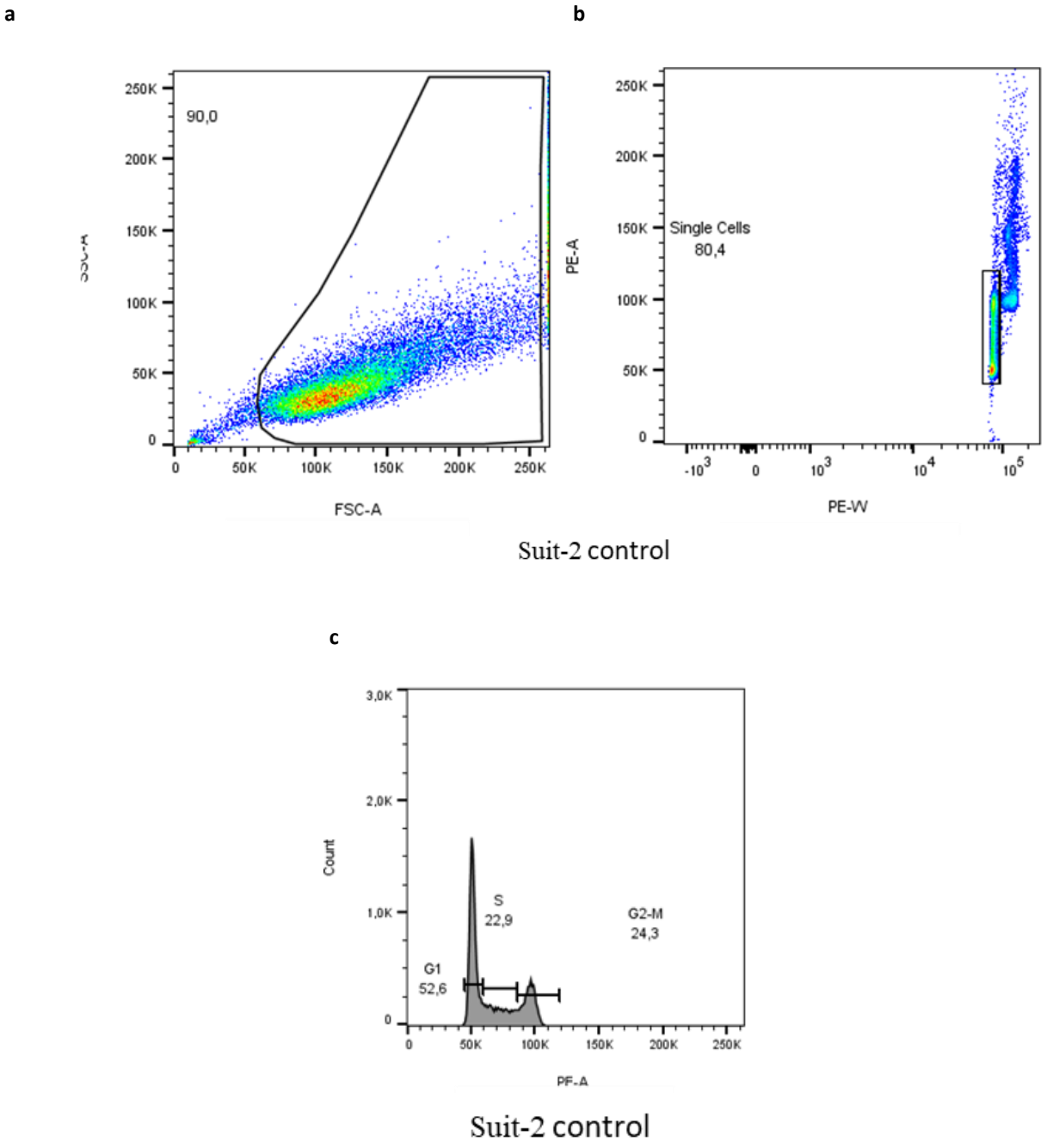

Figure 38. Flow cytometry analysis of the Suit-2 cell cycle after 24 hours: untreated cells (negative control). (a) Tumor cells are identified on a forward scatter (FSC, X-axis) versus side scatter (SSC, Y-axis) plot and gated to exclude debris which is found in the lower left corner. (b) The color of each point represents the density of events at the corresponding intensity values. (c) Representative DNA fluorescence histogram of PI-stained cells: their fluorescence is determined on a linear fluorescence scale reported on X-axis, whilst cell count is reported on Y-axis. The cell cycle fitting algorithm is used to separate the population into G1, S, and G2 phases of the cell cycle.

a **b**

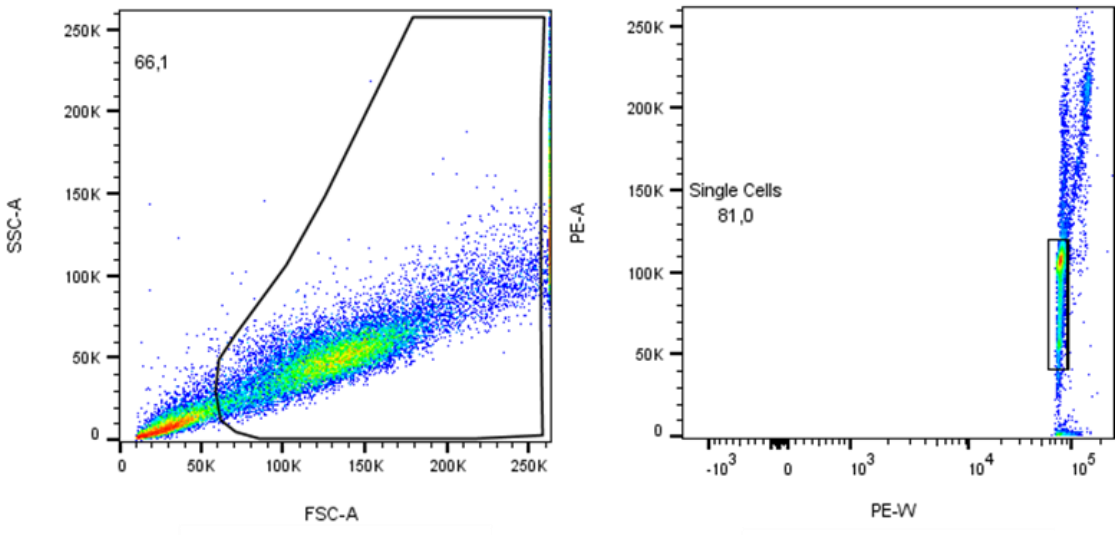

Suit-2 2µM compound **19b**

c

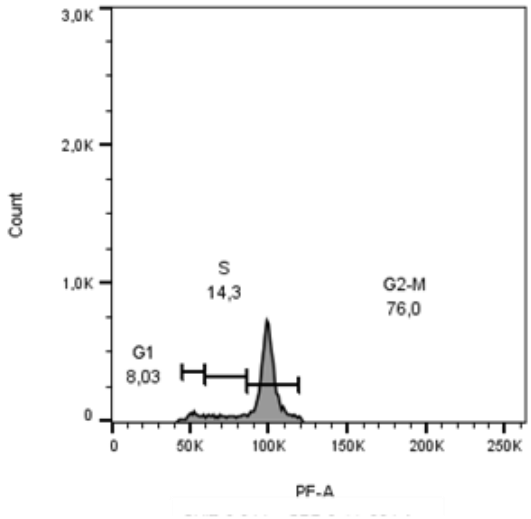

Suit-2 2µM compound **19b**

Figure 39. Flow cytometry analysis of the Suit-2 cell cycle after 24 hours: cells after treatment with the compound **19b** at concentration of 2 µM. (a) Tumor cells are identified on a forward scatter (FSC, X-axis) versus side scatter (SSC, Y-axis) plot and gated to exclude debris which is found in the lower left corner. (b) The color of each point represents the density of events at the corresponding intensity values. (c) Representative DNA fluorescence histogram of PI-stained cells: their fluorescence is determined on a linear fluorescence scale reported on X-axis, whilst cell count is reported on Y-axis. The cell cycle fitting algorithm is used to separate the population into G1, S, and G2 phases of the cell cycle.

a **b**

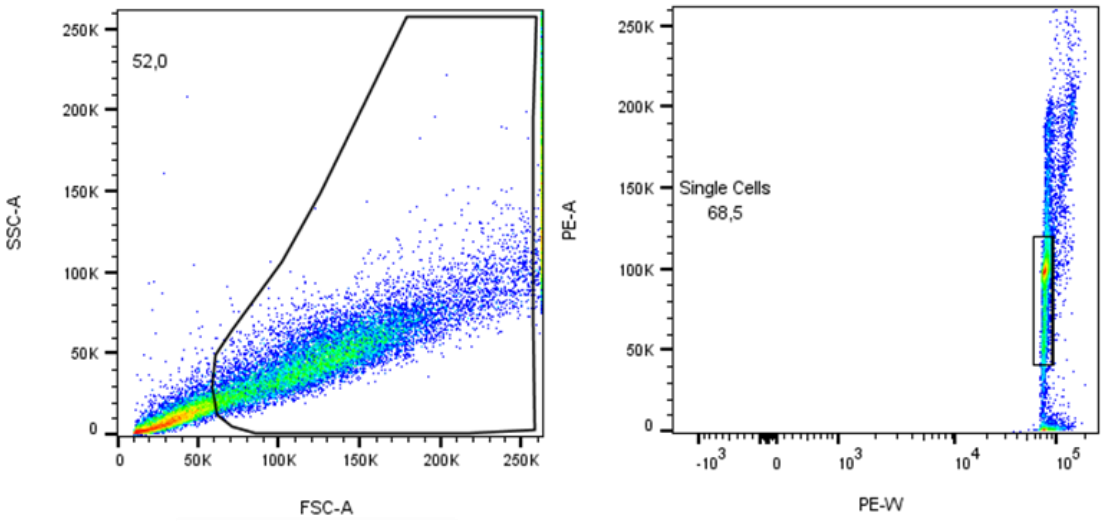

Suit-2 4xIC$_{50}$ compound **19b**

c

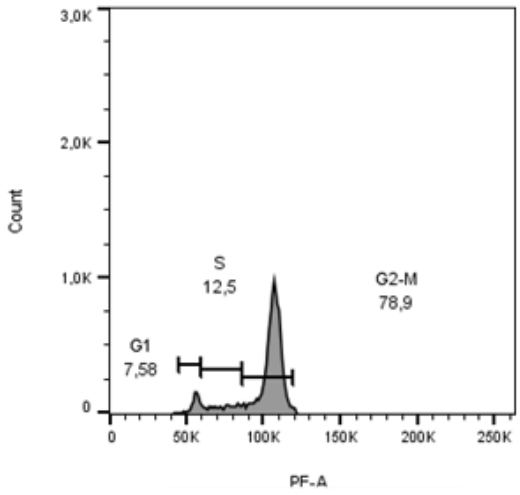

Suit-2 4xIC$_{50}$ compound **19b**

Figure 40. Flow cytometry analysis of the Suit-2 cell cycle after 24 hours: cells after treatment with the compound **19b** at concentration of 4 x IC$_{50}$. (a) Tumor cells are identified on a forward scatter (FSC, X-axis) versus side scatter (SSC, Y-axis) plot and gated to exclude debris which is found in the lower left corner. (b) The color of each point represents the density of events at the corresponding intensity values. (c) Representative DNA fluorescence histogram of PI-stained cells: their fluorescence is determined on a linear fluorescence scale reported on X-axis, whilst cell count is reported on Y-axis. The cell cycle fitting algorithm is used to separate the population into G1, S, and G2 phases of the cell cycle.